Department of Biotechnology e Biosciences

PhD program in BIOLOGY AND BIOTECHNOLOGIES - Cycle XXX

Curriculum in MORPHO-FUNCTIONAL BIOLOGY

FROM CELLS TO EMBRYOS:
IN VITRO MODELS FOR NANOTOXICOLOGY

SAIBENE MELISSA

798752

Tutor: Dr. Bonfanti Patrizia

Co-tutor: Dr. Serchi Tommaso

Coordinator: Prof. Vanoni Marco Ercole

ACADEMIC YEAR 2016/2017

Summary

During the last decades, we are witnessing the explosion of the nanotechnologies, which have developed with the aim of manipulating matter in the nanoscale dimension. According to The International Standard Organization (ISO) "Nanoparticles indicate nano-objects with the three external dimensions ranging from 1 to 100 nm" (ISO TS27687/2008).

This Innovative and unknown nanomaterials (NMs) have been brought on the market continuously, resulting in a massive human and environmental exposure. NM market seems nowadays constantly growing and in the vast NM catalogue, metal-based NPs represent one of the most widely used categories in industrial applications, globally produced in thousands of tons per year.

The introduction of these previously-unknown materials into the environment implies the generation of new ecological relationships among living and non-living systems with unpredictable scenarios for the long-term effects on both human and environmental health.

The main route of human exposure is represented by inhalation. NPs characterized by their small size (less than 100 nm) are able to reach the alveoli site, the latest part of our air way tract. The capability of NMs to deposit into alveoli, is the reason why considerer human lung toxicological studies mandatory.

About the environmental exposure, NPs are considered as a new class of pollutants especially for the aquatic habitats always considered as a sink for wastes. In the light of this, nanotoxicology studies have become fundamental for assessing the adverse effects of NPs on the aquatic organisms.

The main physico-chemical properties that characterize NMs are ascribable to their size, shape, surface charge and coating agents. NM size and shape contribute significantly to their interaction with cells, however, functional groups on the NP surface are the primary dictators of many important nanomaterial properties, such as solubility and macromolecule and cell surface interactions.

The knowledge of how cells interact with NPs and how their physico-chemical properties are relevant to toxic effects is of great importance in the perspective of proposing and supporting the development of a Safe-by-Design (SbD) approach for safer NP production.

The use of several models with different level of complexity allows to obtain a more complete and well-described characterization of NP behavior. Different *in vitro* models with increasing complexity have been proposed in this thesis for a complete assessment: a simple alveolar monoculture, a novel 3D tetraculture alveolar model and a whole developing organism, *Xenopus laevis* early embryos. Monoculture systems are the most commonly models used for the first screening of chemical and particle effects. In particular, the A549 Human Alveolar Adenocarcinoma Cell Line is an established model of Type II alveolar epithelium widely used to performe lung toxicity experiments.

In the last years, numerous 3D *in vitro* lung models have been proposed to perform predictive toxicological inhalation studies. These models, more or less complex, mimic the tissue organization trying to modulate the response of human lung tissue better than a monoculture.

Xenopus laevis, a South African Clawed Amphibian, is a classical model for embryological studies, also suitable for aquatic toxicology assessment in the standardized procedure called Frog Embryo Teratogenenis Assay – FETAX (ASTM 1998). FETAX is conducted on fertilized *Xenopus* mid-blastula stage over the organogenesis period, representing an excellent development toxicity alert test, alternative to Mammals to predict the teratogenic potential of a compound with an accuracy of about 80%.

The thesis starts with a brief introduction regarding the Nanotechnologies, the Nanoparticle physico-chemical properties and the *in vitro* models used in different studies. After that, the manuscript proposes four different chapters regarding different cases of study. First, it will address the toxicological effects

of three different shaped nZnO on a simple monoculture of A549 cells (Chapter 1 – paper in preparation); then the focus will place on the effects of AuNPs on a complex 3D *in vitro* alveolar model (Chapter 2 – paper in preparation). The complexity of the models will increase passing on a whole developing organism, *Xenopus laevis*; on this model the effects on embryos of several nZnOs (Chapter 3 – Bonfanti *et al.*, 2015) and differently coated AgNPs (Chapter 4 – Colombo *et al.*, 2017) will be discuss.

Finally, all the results obtained during the three years of PhD will be gather together and discussed.

Our findings highlighted how the NP physico-chemical properties can affect the bio-interactions between particles and all the models proposed. In a SbD approach, the selection of particular physico-chemical properties could be the first way in order to obtain safer nanomaterials. In all the presented studies, the shape is taken into account to describe the effects of NPs, metal-oxides (nZnO) and metal-based (AuNPs and AgNPs).

In particular, the cubical form of nZnO seems to be the most safe for the A549 cell line monoculture compared to the round and rod-like counterpart.

Concerning the AuNPs, we can observe clear shape-dependent effects, with GNSs as the most effective on the tetraculture alveolar model. In addition, this model resulted perfectly suitable for nanotoxicological studies.

In *Xenopus laevis*, not only the shape, but also the coating agents were taken into account. ZnONPs differing in size, shape and polymeric surface coating targeted the same organ (intestine) and shared similar mode of action but we cannot find out precisely which property mainly drives the bio-interaction between NPs and embryos. Considering only the shape, anyway, we can affirm that the round-small nZnO resulted more embryotoxic than the big-rod-like counterparts.

Comparing BPEI-coated or citrate-coated AgNPs, we found that the positively charged BPEI-coated AgNPs induced severe effects on embryo development

posing teratogenic hazard, interacting with and disrupting embryo tissues, intestine in particular. Taken together the results of this thesis highlight that all the models result suitable for nanotoxicological studies representing in different ways useful tools to describe the effects of metal oxide and metal-based NPs.

Introduction

The explosion of Nanotechnologies

During the last decades we witness the explosion of the nanotechnology field. Innovative and unknown nanomaterials (NMs) were brought on the market continuously, creating a massive human and environmental exposure to these materials.

NM market seems nowadays continuously growing. For example, Metal Oxide nanoparticles (MeONPs) are widely used in cosmetics and sunscreens, while the market for gold nanoparticles is expected to exceed $8 billion by 2022, with major revenues generated in the electronics and medical diagnostics sectors. (Gold Nanoparticles Market, https://www.gminsights.com/ industry-analysis/gold-nanoparticles-market.)

In the vast NM catalogue, metal-based NPs represent one of the more widely-used categories in industrial applications and they are globally produced in thousands of tons per year (Bondarenko *et al.*, 2013).

NM extensive applications including cosmetics, personal care products, electronics, drug delivery systems, paints, sportswear and more entail workers and consumers growing exposure (Vance *et al.*, 2015). In this way, enhance our knowledge about the effects of new NMs is mandatory to orient safe nanotech future development.

The explosion of the nanotech revolution implies that new and previously-unknown materials are introduced into the environment generating new ecological relationships among living and non-living systems with unpredictable scenarios for the long-term effects on both human and environmental health.

The main route of human exposure is represented by inhalation. NPs characterized by their small size (less than 100 nm) are able to reach the alveoli site, latest part of our air way tract. The capability of NMs to deposit into the alveoli is the reason why consider human lung toxicological studies mandatory.

About the environmental exposure, NPs are considered as a new class of pollutants especially for the aquatic habitats always considered as a sink for wastes. In the light of this, relevant became the nanotoxicology studies on the adverse effects of NPs on the aquatic organisms.

Trying to fill the gap between the use of NMs and the possible health and environmental risks, the nanotoxicology discipline has the mission to unravel the toxicological properties of the huge number of NMs already employed and to orient safe nanotech future development.

From a toxicological point of view NP small size is a fundamental aspect. Decreasing the particle dimension brings unavoidably the increase of the surface area and consequently also allows a greater proportion of its atoms or molecules to be displayed on the surface rather than the interior of the material (Nel *et al.*, 2006).

Nanoparticles and their physico-chemical properties

The International Standard Organization (ISO) proposed a definition of NPs: "Nanoparticles indicate nano-objects with the three external dimensions ranging from 1 to 100 nm" (ISO TS27687/2008).

The main physico-chemical properties that characterize NMs are ascribable to their size, shape, surficial charge and coating agents.

Since the research and development in NP field started, the chemistry community continuously is developing rigorous methodologies to control size, shape, and surface structure for a large number of functional materials (Talapin and Shevchenko, 2016).

Among physico-chemical properties, size represent the most relevant. NP dimension places NMs in the transitional zone between individual atoms or molecules and the corresponding bulk materials. This can modify the physico-

chemical properties of the material, first raise the surface/volume ratio, as well as create the opportunity for increased uptake and interaction with biological tissues. This combination of effects can generate adverse biological effects in living cells that would not otherwise be possible with the same material in the larger form (Nel *et al.*, 2006).

The bio-interactions between NPs and cells are a critical aspect in many fields of NM application, such as phototherapy (El-Sayed *et al.*, 2006; West and Halas, 2003), imaging (Weissleder, 2006), and specially drug/gene delivery (Panyam and Labhasetwar, 2003; Whitehead *et al.*, 2009). Clearly, many applications require the NP capability to cross cell membrane in order to reach their cytosolic or nuclear targets. However, crossing cell membranes is inherently challenging due to the nature of the lipid bilayer which originated, from an evolutionary point of view, to protect the cell. Nonetheless, many NMs have demonstrated an ability to successfully overcome cell membranes (Verma and Stellacci, 2010).

The internalization of NMs in cells is not only influenced by a large number of physical and chemical properties of the specific NP, but also by the circumstances in the exposure medium of the cells (Kettler *et al.*, 2014).

The size and shape of NPs has been found to greatly influence their cellular uptake and can have implications in NP toxicity (Verma and Stellacci, 2010).

However, functional groups on the NP surface are the primary dictators of many important nanomaterial properties, such as solubility and macromolecule and cell surface interactions. Typically, incubation of NMs with cells in culture media results in adsorption of serum proteins on their surface that induce the entry of nanoparticles into cells by receptor-mediated endocytosis (Khan *et al.*, 2007).

Surfaces of NPs that are in contact with a biological milieu are in a dynamic exchange with biomolecules such as proteins and lipids (Lynch 2009).

However, in many applications, such as the use of antibacterial NMs, generating nanoparticles that do not interact with cell membranes or other biological macromolecules is also desirable (Verma and Stellacci, 2010).

The knowledge of how cells interact with NPs and the toxic effects of NMs related to their physico-chemical properties results relevant to propose and support the development and the production of safer NPs in the light of a Safe-by-Design (SbD) approach.

SbD approaches, indeed, aim at addressing risks of new technologies like nanotechnology already in the design phase to eliminate or at least reduce toxicological risks (van de Poel & Robaey, 2017).

1. Size

Several bio-interaction between cells and NPs including endocytosis, cellular uptake, and efficiency of particle processing in the endocytic pathway are strictly correlated to NP size (Aillon *et al.*, 2009; Nel *et al.*, 2006).

Generally, size dependent toxicity can be attributed to NP ability to enter the biological systems (Loyric *et al.*, 2005) and then modify or damage the structure of various macromolecules (Aggarwal *et al.*, 2009), interfering with crucial biological functions.

These evidences were evaluated by several authors employing numerous cell types, several culture conditions and different times of exposure (Yin *et al.*, 2005; Hu *et al.*, 2007). For instance, previous studies highlight that particle uptake by non-phagocytic cells shows a clear trend: uptake increases with particle size to an optimum around 50 nm and decreases for larger particles (Chithrani and Chan, 2007; Chithrani *et al.*, 2006; Jiang *et al.*, 2008; Osaki *et al.*, 2004; Rejman *et al.*, 2004; Wang *et al.*, 2010).

2. Shape

Regarding the toxicity dependent on NP shape numerous are the data reported in the literature considering various NMs such as carbon nanotubes, silica, allotropies, nickel, gold, and titanium nanomaterials (Chithrani *et al.*, 2006; Hamilton *et al.*, 2006; Ispas *et al.*, 2009; Petersen and Nelson, 2010). It has been observed that endocytosis of spherical NPs is easier and faster as compared to rod-shaped or fibre-like NPs (Champion and Mitragotri, 2006).

The uptake of rod-shaped gold NPs with citric acid ligands and their spherical counterparts into HeLa cells has been compared by Chithrani *et al.* (2006). They found that gold nanoparticles entered the cells via the receptor mediated endocytosis pathway and that the larger rods with one dimension of more than 50 nm were taken up less than the smaller rods with a length of 40 nm; this could be due to a slowdown of the receptor mediated endocytosis because the larger contact area of rod-shaped NPs with cellular membrane led to a reduction in available receptor binding sites.

3. Surface Charge

Third property taken into account is the surface charge of NPs that plays a key role in the bio-interactions.

Zero surface charges, either by neutral surface groups (e.g., hydroxyl groups) or by zwitterionic ligands, have been shown to lead to low cellular uptake compared with charged particles (Allen *et al.*, 1991; He *et al.*, 2010; Heath *et al.*, 1985; Patil *et al.*, 2007; Raz *et al.*, 1981).

This is due to the low NP affinity toward the overall negatively charged cell membrane (Kettler *et al.*, 2014). High charges prevent agglomeration, particles with a low zeta potential tend to aggregate, lowering their uptake rate (Hanaor *et al.*, 2012; Zhao and Wang, 2012a). When positive and negative surface charges

were directly compared, setting other properties, positively charged particles were shown to be taken up by non-phagocytes more favorably than negatively charged particles (Harush-Frenkel *et al.*, 2007; He *et al.*, 2010).

Studies have also reported the uptake of negatively charged NPs into cells, despite their repulsion by the negatively charged membrane. Positively charged NPs, however, are most effective in crossing cell-membrane barriers and localizing in the cytosol or nucleus. Studies examining the interaction of positively charged NPs have shown that regardless of the type of particle, cationic particles penetrate cell membranes, which may contribute to the observed cytotoxicity with such particles (Verma and Stellacci, 2010).

As the interactions of NPs with the biological systems are largely influenced by their surface charge, researchers have employed various amendments to shield or modulate their surface characteristics so as to reduce their toxic effects (Gatoo *et al.*, 2014).

4. Coating Agents

Surface coating could give to NPs aspects such as magnetic, electric, and optical properties and chemical reactivity (Gupta and Gupta, 2005; Yin *et al.*, 2007) and alter the pharmacokinetics, distribution, accumulation, and toxicity of NPs compared to the non-coated counterpart.

However, it is possible to take advantage of surface coating employing it to reduce NP toxicity. In general, surface coating can mitigate or eliminate the adverse effects of NPs (Gatoo *et al.*, 2014). In particular, proper surface coating can lead to stabilization of NPs as well as elude the release of toxic ions from nanomaterials (Kirchner *et al.*, 2005).

To this purpose, commonly Polyethylene Glycol (PEG; $HO–(CH_2–CH_2–O)n–H$) is used. PEG is hydrophilic and flexible polymer able to resist protein adhesion;

surfaces covered with PEG have been shown to be biocompatible because this polymer's properties yield nonimmunogenicity, nonantigenicity, and protein rejection (Alcantar *et al.*, 2000).

Nanoparticles with neutral surface coatings, such as PEG, resist interaction with cells and consequently display minimal internalization, if none at all. In pegylated NPs, the molecular architecture of PEG on the nanoparticle surface is a key determinant of nanoparticle–cell interactions.

In all the cases of study presented in this manuscript the main NP features above described (size, shape, surface charge and coating agent) will be taken into account, even if the NM used are not the same and tested on different *in vitro* models.

Nanoparticles: cases of study

1. Zinc Oxide Nanoparticles

Nano-Zinc Oxide (nZnO) is the Nano Metal Oxide (NMeO) most abundantly produced after the Nano Titanium Dioxide (nTiO$_2$, Bondarenko *et al.*, 2013). It is a NM suitable for a wide range of applications in particular for its UV-protective and antibacterial capacities (Nohynek *et al.*, 2010). Moreover, nZnO is considered a good stabilizer agent and it has been promoted its use in food, cosmetic and other consumer products, for instance paints.

The wide uses of nZnO place this NMeO as one of the prioritized NM to be considered for regulation, confirmed also by the abundant literature available about its toxicological effects. Many studies investigated nZnO effects on human cells and laboratory mammals, pointing out the relevant cytotoxic and inflammatory potency of this NM (Pandurangan and Kim, 2015).

NZnO is known to work as antimicrobial agent thanks to its capability of producing Reactive Oxygen Species (ROS) when in contact with water (Applerot

et al., 2009; Perelshtein, 2015; Zhang *et al.*, 2006). ROS-induced oxidative changes to cell structures stand at the base of the bacterial killing effect, but are also widely involved in the NP-mediated cytotoxicity in eukaryotic cells. Several NM characteristics can indeed culminate in ROS generation, which is currently the best-developed paradigm for NP toxicity (Nel *et al.*, 2006; Nel *et al.*, 2009). Several papers report the effects of nZnO on human cell lines. NZnO induced cytotoxicity in cell lines such as HepG2, A549, BEASB-2 (Asharani *et al.*, 2008; Pati *et al.*, 2016; Roszak *et al.*, 2016; Saptarshi *et al.*, 2015; Sharma *et al.*, 2014) and the dissolution of the ZnO NPs with the consequent release of Zn^{2+} is considered one of the main cause of its cell toxicity. However, the response after exposure to this NM depends largely on the cell type and not only on the NP physico-chemical properties

The adverse effects after nZnO exposure were reported also in different aquatic organisms (Ates *et al.*, 2015; Skjolding *et al.*, 2014). Several papers attributed to nZnO a heavy acute toxic effect on different ecologically-relevant groups, such as algae, bacteria and crustaceans (Aruoja *et al.*, 2009; Blinova *et al.*, 2010; Heinlaan *et al.*, 2008; Santo *et al.*, 2014).

Regarding the Vertebrates, nZnO seems to cause adverse effects on Zebrafish, both embryos and adults (Bai *et al.*, 2010; Brun *et al.*, 2014; Xiong *et al.*, 2011; Zhu *et al.*, 2009) and on the Amphibian *Xenopus laevis* (Bacchetta *et al.*, 2012; Nations *et al.*, 2011a; Nations *et al.*, 2011b).

In this work, eight different ZnO NPs are taken into account (Chapter 1 and 3). They differ in terms of size, shape and coating agent.

Table I – ZnO NPs

Name	Size (nm)*	Shape	Coating Agent*	Commercial Products	Reference (Chapter
S-nZnO		Round	/	Sigma Aldrich	1
C-nZnO		Elliptical	/	Not Commercial - Sonochemically prepared	1
bZnO or R-nZnO	334 ± 208	Rod-like	/	Tecstar	3 and 1
PVP-bZnO		Rod-like	PVP	Tecstar	3
PEG-bZnO		Rod-like	PEG	Tecstar	3
sZnO	63 ± 29	Round	/	Tecstar	3
PVP-sZnO		Round	PVP	Tecstar	3
PEG-sZnO		Round	PEG	Tecstar	3

* size information obtained by different analysis, Transmission Electron Microscope (TEM) or Dynamic Light Scattering (DLS)
** coating agents: polyvinylpyrrolidone (PVP10K) and polyethylene glycol (PEG400)
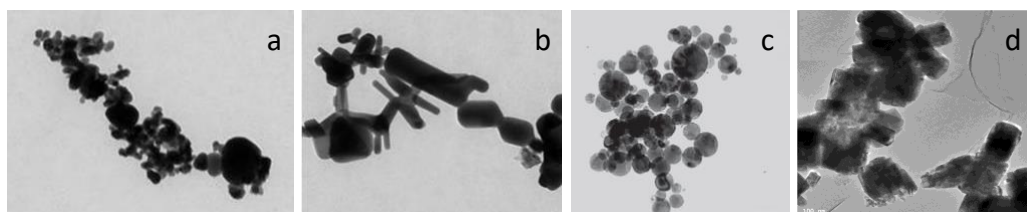
Fig. 1: images of nZNOs used in this work. Respectively: s-nZnO, b-nZnO or R-nZnO, S-nZnO and C-nZnO

The effects of nZnOs were evaluated on two different *in vitro* models, for human and environmental exposure: Human Alveolar Adenocarcinoma Cells, A549 line, (Chapter 1) and *Xenopus laevis* embryos (Chapter 3).

2. Gold Nanoparticles

Among the nanomaterials, gold is with no doubts one of the most used, having its first medical application dating back to several centuries ago (Dreaden *et al.*, 2012; Dykman and Khlebtsov, 2012). Gold NPs (AuNPs) are largely used in biomedical application, due especially to their biocompatibility (Fytianos *et al.*, 2015).

Gold in its bulk form has long been considered an inert, nontoxic, bio-compatible, noble metal with some therapeutic (and even medicinal) properties. However, when the size of the typical objects decreases into nanoscopic dimensions

(nanometer dimensions), gold behaves very differently than in bulk and its safety as a promising material for biomedical applications is no longer unquestionable and many important concerns regarding the risk to humans have been raised. The a priori assumption that gold nanoparticles are intrinsically bio-compatible must be rejected (Fratoddi *et al.*, 2014).

When reduced to the nanoscale in the form of spheres, cages, stars or rods, and functionalized by different molecular coatings, this metal seems particularly attractive for the development of a plenty of innovative diagnostic and therapeutic processes, which take advantage of its extraordinary properties. Indeed, the range of uses of AuNPs in current medical and biological research is extremely broad and include diagnostics, therapy, prophylaxis and hygiene (Dykman and Khlebtsov, 2012). However, their possible toxicity is still an open issue (Di Bucchianico 2015) so much that some authors discussed the effects of AuNPs from a toxicological point of view (Pan *et al.*, 2007; Sabella *et al.*, 2014; Sung *et al.*, 2011; Villiers *et al.*, 2010; Zhang *et al.*, 2009).

Studies available in literature are specially focused on the uptake and bio-interaction of AuNPs on monoculture (Chithrani *et al.*, 2006); few are the publications reporting the effects on more complex system as co-culture models (Braakhuis *et al.*, 2016b).

Table II – Au NPs

Name	Size (nm)*	Shape	Coating Agent**	Commercial Products	Reference (Chapter
GNPs	61.33 ± 0.34	Round	PEG	/	2
GNRs	8.44 ± 6.4 x 68.3 ± 10.3	Rod-like	PEG	/	2
GNSs	63.43 ± 2.35	Star-like	PEG	/	2

* *size information obtained by different analysis, Transmission Electron Microscope (TEM) or Dynamic Light Scattering (DLS)*
** *coating agents: polyethylene glycol (PEG)*
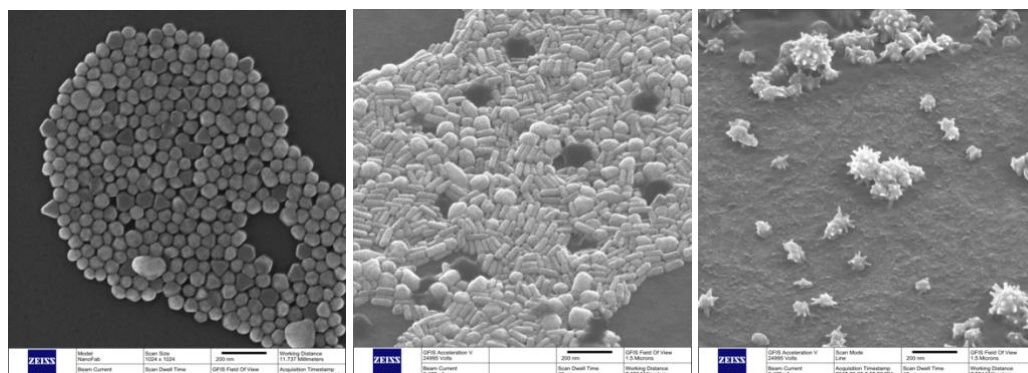
Fig.2: images of AuNPs, used in this work, obtained with ORION-Helium Ion Microscope (HIM). GNPs, GNRs and GNSs respectively

The AuNPs used in this study have been prepared endotoxin-free, suitable for biological application, ensuring solubility in water and stability in biologically relevant media. The set of Pegylated AuNPs with comparable size (around 60 nm) included Gold Nano Spheres (GNPs), Gold Nano Rods (GNRs) and Gold Nano Stars (GNSs) were used to exposed a complex 3D Tetraculture Alveolar Model (Chapter 4).

3. Silver Nanoparticles

Based on the most recent nanotechnology consumer product inventories, silver represents the most frequently used NM. Indeed, out of the 1814 consumer products listed, 435 contain Silver nanoparticles (AgNPs), accounting for 24% of the already marketed nanomaterials (Vance *et al.*, 2015).

AgNPs are so widely used for their high efficacy as antibacterial agents and their relevant catalytic and conductivity activity. Especially the antimicrobial properties make this NM suitable for healthcare products, textile industry and food sector (in particular food packaging).

Due to the numerous applications, AgNPs are easily released into the aquatic environment, as reported in several studies (Benn and Westerhoff, 2008; Geranio

et al., 2009; Kaegi *et al.*, 2010). According to the studies on the Predicted Environmental Concentration (PEC), AgNPs are pointed out as the most hazardous NM, posing serious concerns toward environmental health and thus deserving careful future evaluation (Gottschalk *et al.*, 2013).

AgNPs, indeed, are highly toxic not only to bacteria, but also to yeasts, algae, crustaceans and mammalian cells, within a range of concentrations comparable to the ones having bactericidal effects (Bondarenko *et al.*, 2013).

There is evidence that the toxicity was crucially dependent on both Ag^+ dissolved from particles and NP size. Focusing on the dissolution, it was determined to be the leading mechanism driving cell toxicity (Le Ouay and Stellacci, 2015). Indeed, comparable toxicity was seen in cells and organisms exposed to Ag^+ (Hadrup and Lam, 2014; Kim *et al.*, 2011; Kim and Ryu, 2013; Lubick, 2008; Singh and Ramarao, 2012; van Aerle *et al.*, 2013; Volker *et al.*, 2015; Yang *et al.*, 2012; Zhao and Wang, 2012b).

Xiu *et al.* (2012) proposed that the environmental impact of AgNPs may be mitigated mainly modulating ions release. This modulation can be achieved reducing particle oxidation, limiting oxygen availability and varying NP size and/or surface coating.

These considerations highlighted, again, how the modification of NP surface properties may influence the biological responses, opening up the possibility to engineer NPs by a SbD approach.

Although copious toxicity studies on AgNPs adverse effects are available, the reproductive and developmental effects are not extensively contemplated.

For example, in Zebrafish, AgNPs have been proved to be embryotoxic at concentrations of 1-50 mg/L. The effects were seen to be dependent on size: smaller are the NPs, greater were the effects observed (Bar-Ilan *et al.*, 2009; Browning *et al.*, 2013); however, the main mode of action remains not completely clarified. Other data in exposed Zebrafish embryos support the

hypothesis that the effects on gene expression are mainly caused by dissolved silver ions (van Aerle *et al.*, 2013).

Table III– Ag NPs

Name	Size (nm)*	Shape	Coating Agent**	Commercial Products	Reference (Chapter)
BPEI-AgNPs	10.2 ± 2.0	Round	BPEI	NanoComposix	4
Cit-AgNPs	10.3 ± 2.0	Round	Cit	NanoComposix	4

* size information obtained by Transmission Electron Microscope (TEM), NanoComposix data
** coating agents: branched polyethylenimine (BPEI) and citrate (Cit)

Using the standard Frog Embryo Teratogenesis Assay – *Xenopus*, FETAX (ASTM, 1998) two commercially differently coated AgNPs and Silver Nitrate (AgNO$_3$) as ionic control have been comparatively tested. Part of this work aims to understand if and how differently surface coated AgNPs and the surface charge, may induce developmental toxicity (Chapter 4).
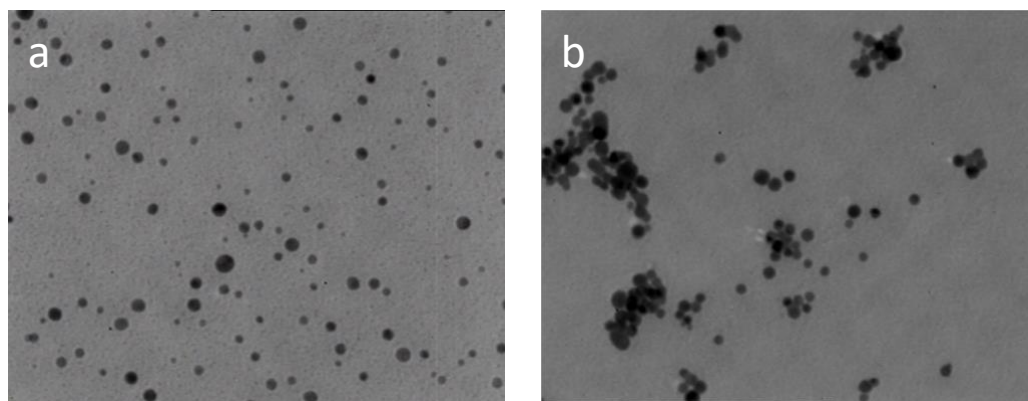
Fig.3: Transmission Electron Microscope (TEM) images of AgNPs used in this work, on the left the BPEI coated AgNPs, while on the right side the citrate coated AgNPS

In vitro models suitable for Nanotoxicology

Generally, toxicological studies shaped on the description of human adverse effects are performed *in vivo*. Nevertheless, the discussion arisen in the last years regarding the use of laboratory animals culminate in the even more spreading of

the proposal so-called 3R strategy: Replacement, Reduction and Refinement (Russel and Burch, 1959).

In the light of this, the request of alternative methods has been increased specially bringing the reduction and the refinement of *in vivo* experiments.

Here, three different *in vitro* models have been proposed to perform Nanotoxicological studies. From a simple cell monoculture (A549, Chapter 1), a novel 3D alveolar model tetraculture (Chapter 2) and to a whole developing organism (*Xenopus laevis* embryos, Chapter 3 and 4) including thus not only human toxicology but also aquatic toxicology.

The innovation of this work is the evaluation of the NP bio-interactions, taking into account their main physico-chemical properties, with *in vitro* models characterized by different level of complexity, different circumstances in the exposure and different experimental conditions; all these aspects allow to obtain a complete and wide assessment of NP toxicity.

1. Human Exposure

The main route of human exposure is represented by inhalation. Our respiratory system is specialized and designed for gas exchanging between blood and atmospheres. The air way tract is divided in the upper and lower tract. The upper tract is composed by nasal cavity, pharynx and larynx; in the lower part are present bronchi, bronchioles and alveoli. Focusing on the lower air way tract, bronchi and bronchioles have the function to conduct the air to the alveoli. The alveolar sacs represent the last and thinner barrier between air and organism. Here takes place the gas exchanging.

As previously mentioned, NPs characterized by their small size (less than 100 nm) are able to reach the alveoli site, latest part of the air way tract (Fig. 4).
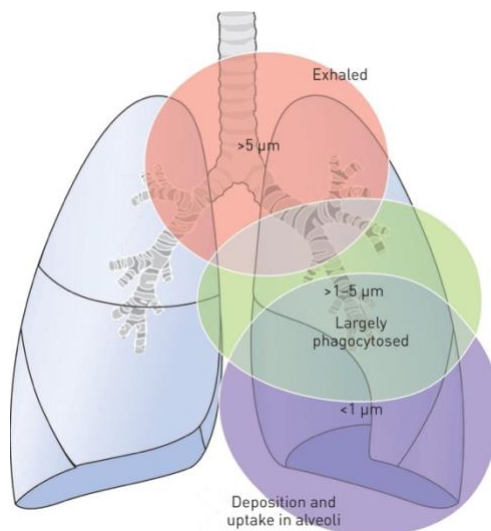
Fig. 4: schematic representation of the size-dependent deposition of inhaled particles in the human air ways. From van Rijt et al., (2014)

Here most of them are able to cross the air-blood barrier and reach other target organs such as hearth, pancreas, kidney and spleen (Yacobi *et al.*, 2011). In addition, there are evidences that inhaled particles can cause lung diseases (Inoue *et al.*, 2006; Pietropaoli *et al.*, 2004) and passing through the blood circulatory system they can bring to damages at the cardiovascular level (Donaldson *et al.*, 2005; Geiser *et al.*, 2005; Schulz *et al.*, 2005).

Since the pulmonary system is the most involved in the interaction with particles, mandatory becomes to perform lung toxicological studies.

Inhalation studies were commonly performed in an *in vivo* situation with the advantages of reconstituting organ- and organism-levels functions (Secondo *et al.*, 2017). Nevertheless, the use of 3D *in vitro* models represents a valid and efficient alternative to predict the acute toxicity effects of inhaled substances on our health (de Souza Carvalho *et al.*, 2014; Müller *et al.*). Indeed, Secondo *et al.* (2017) recently compared studies of *in vivo* and *in vitro* exposure observing that the responses in term of cytotoxicity and inflammation were similar.

Concerning the human exposure, two *in vitro* models are proposed. The first one is a simple monoculture of Human Alveolar Adenocarcinoma Cell Line (A549, Chapter 1), while the second system is a complex 3D Alveolar model (Chapter 2).

1.1 Human Alveolar Adenocarcinoma Cell Line, A549 Monoculture

Monoculture systems are the most commonly models used to assess the effects of chemical and particles. Several are the cell lines used for that purpose, e.g. Calu-3, BEAS-2B, A549.

The A549 Human Alveolar Adenocarcinoma Cell Line is an established model of Type II alveolar epithelium widely used to performed lung toxicity experiments (Foster *et al.*, 1998). Numerous are the studies reporting the effects of different chemicals, not only particles, on this cell line.

As reported by Foster *et al.*, (1998), A549 cells have many important biological properties of Type II alveolar cells, as membrane bound inclusions that resemble lamellar bodies, distinct polarization, tight junctions and extensive cytoplasmic extensions. However, it is not still clear if these cells have the capability to express thigh junction. Some authors suggested that A549 cells did not express zonula occludens-1 (Elbert *et al.*, 1999), while other researchers (Rothen-Rutishauser *et al.*, 2008) have shown that A549 cells are able to create a barrier and generate Trans Epithelial Electrical Resistance (TEER), which is a good requisite for the development of an intact epithelium characterized also by the presence of thigh junctions (Agu and Ugwoke, 2011; Geys *et al.*, 2006).

It is clear that using a single cell line is a simplification of a complex system as the lung is, but a monoculture system is an easy, fast and anyway valid model for screening the effects of certain chemicals and particles.

The monoculture of A549 cells was choosen to describe the effects of three different shaped nZnOs (Chapter 2).

1.2 Innovative 3D Tetraculture Alveolar Model

In the last years, numerous 3D *in vitro* lung models have been proposed to assess predictive toxicological inhalation studies. These models, more or less complex, mimic the tissue organization trying to modulate the response of the human lung tissue (Blank *et al.*, 2006; Braakhuis *et al.*, 2016a; Kimlin *et al.*, 2013; Klein *et al.*, 2013; Rothen-Rutishauser *et al.*, 2005) better than a monoculture.

Since it is already known that different cells communicate continuously with each other, testing NPs toxicity on monoculture could be not enough to predict their behavior on the whole organ. For example, the presence of epithelial cells, as A549 cells, or cells belonging to the immune system such as macrophages entails a different response of the system. In a previous work, Klein *et al.* (2013) demonstrated the different response of a mono-, bi- and tetra-culture after the same exposure conditions.

The *in vitro* models could be composed by one or more cell lines, in submerged or in air-liquid-interface (ALI) conditions. 3D models including more than one cell lines, relevant lung cell lines, exposed in air-liquid-interface (ALI) condition gives a significant contribute to better characterize the effects of inhaled particles (de Souza Carvalho *et al.*, 2014) compared to a submerged condition.

The ALI condition seems more sensitive and realistic than the submerged state, even with comparable doses of exposure. The ALI condition is more realistic because in the air ways, in alveoli particularly, no medium or liquid phase is present, except for a thin layer of surfactant (Bitterle *et al.*, 2006; Herzog *et al.*; Holder and Marr, 2013; Lenz *et al.*, 2013; Raemy *et al.*, 2012; Stoehr *et al.*, 2015). The presence of Cell Culture Medium (CCM) could generally change NP properties such as dimension (formation of agglomeration) or could bring the formation of a massive protein corona modifying the surface of NPs (Holder *et al.*, 2008). For this reason, it is not possible to determine exactly the doses used and the quantity of NPs able to reach cells in the wells. In other terms, the ALI

condition mimics better the inhalation situation. Several papers report this as suggested by (Mülhopt *et al.*, 2016) review.

The combination of ALI condition and nebulization of NPs simulate the inhalation of NPs able to reach the alveoli compartment.

Several systems are available to expose cells cultured in ALI condition to nebulized compound and suspensions. Among these systems, there is the VitroCell® Cloud System.

As above-mentioned, VitroCell® Cloud System allowed exposing cells cultured at the air/liquid interface directly to nebulized NP suspensions (known concentration – homogeneous deposition). This system has been specifically designed for dose-controlled and spatially uniform deposition of aerosols from liquids and suspensions. In this way is possible the screening of inhaled drugs and to perform toxicity tests of inhaled substances including nanoparticle suspensions.

The tetraculture alveolar model used in this study has been proposed by Klein *et al.*, (2011). The model is composed by the following cell lines: endothelial cells (EA.hy296), epithelial cells (A549), mast cells (HMC-1) and macrophage-like cells (differentiated THP-1 cells); cells were grown on Transwell inserts and exposed to nebulized AuNP suspensions using the VitroCell® Cloud System at ALI condition (Chapter 2).

In the system the tri-culture of epithelial cells (A549), mast cells (HMC-1) and macrophages-like cells (differentiated THP-1) are placed onto the porous membrane (porous dimeter 1 µm) on the apical side of the insert and the endothelial cells (EA.hy926) are located on the basolateral side of the same insert membrane (Fig. 5). This arrangement allowed to better mimic the *in vivo* anatomy of the alveolar region compared to previous version of the model (Alfaro-Moreno *et al.*, 2008) in which not only the insert membrane, but also a layer of CCM separated the triculture from the endothelial layer.

Day 0

Seeding of EA.hy 926 cells on the basolateral side of the Transwell insert
→ 2.4 x 10^5 cells/cm^2

Seeding of A549 cells in Transwell inserts
→ 1.2 x 10^5 cells/cm^2

Day 3

Stimulation of THP-1 cells with 20 ng/ml PMA over night

Day 4

Seeding of differentiated THP-1 cells
→ 2.4 x 10^5 cells/cm^2

Seeding HMC-1 cells
→ 1.2 x 10^5 cells/cm^2

Switch to ALI conditions for 24 hrs once THP-1 and HMC-1 cells attached

Day 5

System ready for exposure to particles or chemicals via Vitrocell chamber

Aerosol chamber

⬜ : A549 cells   : HMC-1 cells   : Differentiated THP-1 cells   ⬭ : EA.hy 926 cells

● : NPs   ⊔ : Cultivation well   ⊔ : Transwell™ insert   ▮ : Culture medium   ▬ : Surfactant

Fig. 5: Tetraculture alveolar model proposed by Klein et al. (2013)

Peculiarity of our experimental design is also the ALI condition in which cells were maintained before, during and after the nebulization.

ALI exposure avoids the interaction between NPs and CCM, preventing eventually surface modification or the formation of a massive protein corona. It is already established that CCM, as the biological fluid, has the ability to modify the NP surface, modifying at the same time their toxicological potency (de Souza Carvalho *et al.*, 2014; Fleischer and Payne, 2014). Due to the main modifications occurring in submerged condition is not possible to determine exactly the doses used and the quantity of NPs able to reach cells. In other terms, the ALI condition mimics better the inhalation situation (Mulphot *et al.*, 2016).

This study, for the first time, describes the effects of three different shaped AuNPs on a complex 3D in vitro lung model (Chapter 2). The complexity of the

model represents a good compromise for predicting NP inhalation effects. The AuNPs were indeed nebulized by the VitroCell® Cloud System at ALI condition, the best combination to characterize an inhalation exposure.

2. Aquatic Toxicology

NPs can enter the aquatic environment during their life cycle increasing the risk for the aquatic organisms (Baun *et al.*, 2008; Blinova *et al.*, 2010; Federici *et al.*, 2007; Kasemets *et al.*, 2009).

In this environmental compartment, the behavior and the fate of NPs remain unclear and it is well known that their state of aggregation and their consequent settlement to sediments depend on the hydrodynamic properties of NPs (Gregory 2006), making prediction of these phenomena almost unreliable.

The aquatic environments, more than other habitats, are the ecosystem most at risk of exposure to pollutants representing a sink for these wastes (Scown *et al.*, 2010). Since NPs are considered a new class of pollutants, relevant became the nanotoxicology studies on the aquatic organisms.

2.1 Frog Embryo Teratogenenis Assay Xenopus – FETAX

In this work, the aquatic model taken into account is *Xenopus laevis*, a South African Clawed Amphibian. *X. laevis* is a classical model for embryological studies following the standardized procedure called Frog Embryo Teratogenesis Assay – FETAX (ASTM, 1998). FETAX is a 96-hours whole embryo developmental toxicity test. This assay is well suited for aquatic toxicology assessment and represent an excellent alternative to teratogenesis studies on Mammals.

FETAX is widely used to screen the teratogenic potential of environmental contaminants and pharmaceuticals (Bonfanti *et al.*, 2004; Chae *et al.*, 2015; Fort and Paul, 2002; Williams *et al.*, 2015) and only recently it has been applied in

nanotoxicology to assess the interference of NMs with embryonic development(Bacchetta *et al.*, 2012; Nations *et al.*, 2011b). Moreover, *Xenopus* embryos can offer the opportunity to study the interaction of nanoparticles with embryonic tissues.

Embryogenesis can be considered as one of the most sensitive life stages, since even small perturbations occurring during can affect the entire life of an organism (Colombo *et al.*, 2017).

Unlike some of the other teratogenesis screens that use cell or organ cultures, the frog embryo is an intact developing system which undergoes events (e.g., cleavage, gastrulation, organogenesis) comparable to those of other vertebrates, including mammals (Dumont 1983).

As Dumont (1983) suggested, this model has been considered attractive and suitable for several reason. First of all, the FETAX assay is rapid, routinely the end points are reached within 96 h post fertilization (p.f.) and all the developmental stages are well described by Niewkoop and Faber (1975); the test is quite cheap and the protocol is simple. From a single test is possible to obtain a large number of embryos.

Additionally, the embryos are completely functional organisms, at the end of the test (96 h p.f.) they are motile so assessment of the functional state of the nervous and muscular systems can be made by simple observations of swimming ability. Finally, the end points are easy to recognize and score; in particular the following parameters are routinely used: growth retardation in terms of embryo length, mortality and malformation rate (Fig. 6).

FETAX

ENDPOINTS:
Growth Retardation – Mortality – Malformations

STAGE 8 (5 hours pf)

STAGE 46 (96 hr pf)

CONVENTIONAL EXPOSURE (stages 8-46)
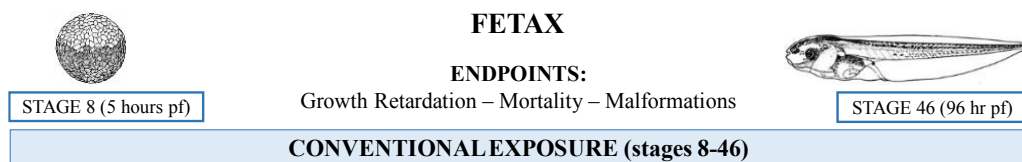
Fig. 6: Experimental design of FETAX – scheme regarding the time of exposure. In the conventional test the exposure starts at the stage of blastula (5 hours post-fertilization) and ends after 96 hours post-fertilization at the tadpole stage; all the developmental stages of Xenopus laevis have been described by Nieuwkoop and Faber (1975). After 96 hr p.f. the endpoints taken into account are: Growth Retardation, Mortality and Malformations.

About the route of exposure to NPs, it has been suggested that for this organism the ingestion could be the most probable. Indeed, in previous studies (Bacchetta *et al.*, 2014; Bacchetta *et al.*, 2012) it has been shown that the main affected organ is the gut. In particular, smallest ZnONPs tested were more effective in inducing severe histopathological effects at the gut mucosa level, with the epithelium severely eroded (Bacchetta *et al.*, 2014).

In the present work (Chapter 3 and 4), the intestine resulted to be again the target organ of the NPs and the abnormal gut coiling was the principal malformation recorded. Nevertheless, embryo histopathological screening and gut ultrastructural analysis revealed only a slight alteration of intestinal mucosa, ascribable to detachment between adjacent cells and from basal lamina (Chapter 3) or abnormalities at the abdominal level of the embryos where severe oedemas were coupled with irregular gut coiling (Chapter 4).

In experiments different from conventional FETAX, embryos were exposed to NPs during two different developmental windows, before and after the opening of the stomodeum (Fig. 7). This particular exposure allows us to demonstrate clearly the hypothesis that ingestion is the main exposure route to NPs, and translocation through the intestinal barrier the main uptake mechanism.

Indeed, *Xenopus laevis* embryos become susceptible to NPs with the acquisition of grazing behavior following the stomodeum opening. By this route, suspended

particles in the liquid column and aggregated NPs deposited on the bottom of Petri dish were ingested and able to reach gut lumen.

FETAX

ENDPOINTS:
Growth Retardation – Mortality – Malformations

| STAGE 8 (5 hours pf) | STAGE 39 (56 hr 30 minpf) | STAGE 46 (96 hr pf) |

| FIRST EXPOSURE WINDOW: <u>BEFORE</u> STOMODEUM OPENING (stages 8-39) | SECOND EXPOSURE WINDOW: <u>AFTER</u> STOMODEUM OPENING (stages 39-46) |

Fig. 7: Experimental design of FETAX modified version – scheme regarding the time of exposure. Two different developmental windows were choosed: from the stage 8 to stage 39, before the stomodeum opening and from the stage 39 untill the stage 46 after the stomodeum opening. All the developmental stages of Xenopus laevis have been described by Nieuwkoop and Faber (1975). After 96 hr pf the endpoints taken into account are: Growth Retardation, Mortality and Malformations.
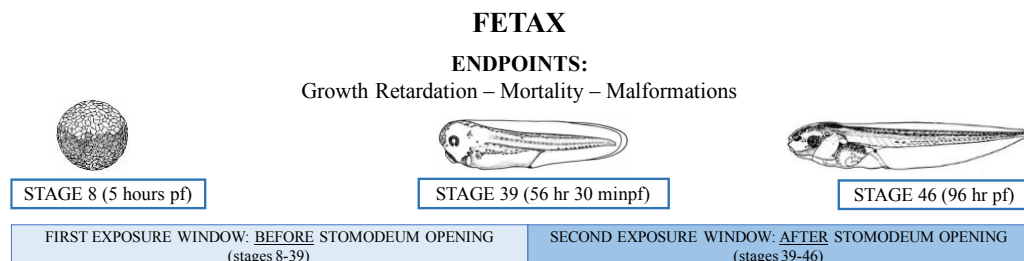
In this work, using the conventional and the modified FETAX were evaluated the adverse effect of several NPs, nZnOs (Chapter 3) and AgNPs (Chapter 4).

References

Aggarwal, P., Hall, J.B., McLeland, C.B., Dobrovolskaia, M.A., McNeil, S.E., 2009. Nanoparticle interaction with plasma proteins as it relates to particle biodistribution, biocompatibility and therapeutic efficacy. Adv Drug Deliv Rev 61, 428-437.

Agu, R.U., Ugwoke, M.I., 2011. In vitro and in vivo testing methods for respiratory drug delivery. Expert Opin Drug Deliv 8, 57-69.

Aillon, K.L., Xie, Y., El-Gendy, N., Berkland, C.J., Forrest, M.L., 2009. Effects of nanomaterial physicochemical properties on in vivo toxicity. Adv Drug Deliv Rev 61, 457-466.

Alcantar, N.A., Aydil, E.S., Israelachvili, J.N., 2000. Polyethylene glycol-coated biocompatible surfaces. J Biomed Mater Res 51, 343-351.

Alfaro-Moreno, E., Nawrot, T.S., Vanaudenaerde, B.M., Hoylaerts, M.F., Vanoirbeek, J.A., Nemery, B., Hoet, P.H., 2008. Co-cultures of multiple cell types mimic pulmonary cell communication in response to urban PM10. Eur Respir J 32, 1184-1194.

Allen, T.M., Austin, G.A., Chonn, A., Lin, L., Lee, K.C., 1991. Uptake of liposomes by cultured mouse bone marrow macrophages: influence of liposome composition and size. Biochim Biophys Acta 1061, 56-64.

Applerot, G., Lipovsky, A., Dror, R., Perkas, N., Nitzan, Y., Lubart, R., Gedanken, A., 2009. Enhanced Antibacterial Activity of Nanocrystalline ZnO Due to Increased ROS-Mediated Cell Injury. Advanced Functional Materials 19, 842-852.

Aruoja, V., Dubourguier, H.C., Kasemets, K., Kahru, A., 2009. Toxicity of nanoparticles of CuO, ZnO and TiO2 to microalgae Pseudokirchneriella subcapitata. Sci Total Environ 407, 1461-1468.

Asharani, P.V., Lian Wu, Y., Gong, Z., Valiyaveettil, S., 2008. Toxicity of silver nanoparticles in zebrafish models. Nanotechnology 19, 255102.

Ates, M., Arslan, Z., Demir, V., Daniels, J., Farah, I.O., 2015. Accumulation and toxicity of CuO and ZnO nanoparticles through waterborne and dietary exposure of goldfish (Carassius auratus). Environ Toxicol 30, 119-128.

Bacchetta, R., Moschini, E., Santo, N., Fascio, U., Del Giacco, L., Freddi, S., Camatini, M., Mantecca, P., 2014. Evidence and uptake routes for Zinc oxide nanoparticles through the gastrointestinal barrier in Xenopus laevis. Nanotoxicology 8, 728-744.

Bacchetta, R., Santo, N., Fascio, U., Moschini, E., Freddi, S., Chirico, G., Camatini, M., Mantecca, P., 2012. Nano-sized CuO, TiO(2) and ZnO affect Xenopus laevis development. Nanotoxicology 6, 381-398.

Bai, J., Zhong, X., Jiang, S., Huang, Y., Duan, X., 2010. Graphene nanomesh. Nat Nanotechnol 5, 190-194.

Bar-Ilan, O., Albrecht, R.M., Fako, V.E., Furgeson, D.Y., 2009. Toxicity assessments of multisized gold and silver nanoparticles in zebrafish embryos. Small 5, 1897-1910.

Baun, A., Hartmann, N.B., Grieger, K., Kusk, K.O., 2008. Ecotoxicity of engineered nanoparticles to aquatic invertebrates: a brief review and recommendations for future toxicity testing. Ecotoxicology 17, 387-395.

Benn, T.M., Westerhoff, P., 2008. Nanoparticle silver released into water from commercially available sock fabrics. Environ Sci Technol 42, 4133-4139.

Bitterle, E., Karg, E., Schroeppel, A., Kreyling, W.G., Tippe, A., Ferron, G.A., Schmid, O., Heyder, J., Maier, K.L., Hofer, T., 2006. Dose-controlled exposure of A549 epithelial cells at the air-liquid interface to airborne ultrafine carbonaceous particles. Chemosphere 65, 1784-1790.

Blank, F., Rothen-Rutishauser, B.M., Schurch, S., Gehr, P., 2006. An optimized in vitro model of the respiratory tract wall to study particle cell interactions. J Aerosol Med 19, 392-405.

Blinova, I., Ivask, A., Heinlaan, M., Mortimer, M., Kahru, A., 2010. Ecotoxicity of nanoparticles of CuO and ZnO in natural water. Environ Pollut 158, 41-47.

Bondarenko, O., Juganson, K., Ivask, A., Kasemets, K., Mortimer, M., Kahru, A., 2013. Toxicity of Ag, CuO and ZnO nanoparticles to selected environmentally relevant test organisms and mammalian cells in vitro: a critical review. Arch Toxicol, vol. 87, Berlin/Heidelberg, pp. 1181-1200.

Bonfanti, P., Colombo, A., Orsi, F., Nizzetto, I., Andrioletti, M., Bacchetta, R., Mantecca, P., Fascio, U., Vailati, G., Vismara, C., 2004. Comparative teratogenicity of Chlorpyrifos and Malathion on Xenopus laevis development. Aquatic Toxicology 70, 189-200.

Braakhuis, H.M., Giannakou, C., Peijnenburg, W.J., Vermeulen, J., van Loveren, H., Park, M.V., 2016a. Simple in vitro models can predict pulmonary toxicity of silver nanoparticles. Nanotoxicology 10, 770-779.

Braakhuis, H.M., Oomen, A.G., Cassee, F.R., 2016b. Grouping nanomaterials to predict their potential to induce pulmonary inflammation. Toxicology and Applied Pharmacology 299, 3-7.

Browning, L.M., Lee, K.J., Nallathamby, P.D., Xu, X.H., 2013. Silver nanoparticles incite size- and dose-dependent developmental phenotypes and nanotoxicity in zebrafish embryos. Chem Res Toxicol 26, 1503-1513.

Brun, N.R., Lenz, M., Wehrli, B., Fent, K., 2014. Comparative effects of zinc oxide nanoparticles and dissolved zinc on zebrafish embryos and eleuthero-embryos: importance of zinc ions. Sci Total Environ 476-477, 657-666.

Chae, J.P., Park, M.S., Hwang, Y.S., Min, B.H., Kim, S.H., Lee, H.S., Park, M.J., 2015. Evaluation of developmental toxicity and teratogenicity of diclofenac using Xenopus embryos. Chemosphere 120, 52-58.

Champion, J.A., Mitragotri, S., 2006. Role of target geometry in phagocytosis. Proc Natl Acad Sci U S A 103, 4930-4934.

Chithrani, B.D., Chan, W.C., 2007. Elucidating the mechanism of cellular uptake and removal of protein-coated gold nanoparticles of different sizes and shapes. Nano Lett 7, 1542-1550.

Chithrani, B.D., Ghazani, A.A., Chan, W.C., 2006. Determining the size and shape dependence of gold nanoparticle uptake into mammalian cells. Nano Lett 6, 662-668.

Colombo, A., Saibene, M., Moschini, E., Bonfanti, P., Collini, M., Kasemets, K., Mantecca, P., 2017. Teratogenic hazard of BPEI-coated silver nanoparticles to Xenopus laevis. Nanotoxicology 11, 405-418.

de Souza Carvalho, C., Daum, N., Lehr, C.-M., 2014. Carrier interactions with the biological barriers of the lung: Advanced in vitro models and challenges for pulmonary drug delivery. Advanced Drug Delivery Reviews 75, 129-140.

Donaldson, K., Tran, L., Jimenez, L.A., Duffin, R., Newby, D.E., Mills, N., MacNee, W., Stone, V., 2005. Combustion-derived nanoparticles: A review of their toxicology following inhalation exposure. Part Fibre Toxicol, vol. 2, London, p. 10.

Dreaden, E.C., Alkilany, A.M., Huang, X., Murphy, C.J., El-Sayed, M.A., 2012. The golden age: gold nanoparticles for biomedicine. Chem Soc Rev 41, 2740-2779.

Dykman, L., Khlebtsov, N., 2012. Gold nanoparticles in biomedical applications: recent advances and perspectives. Chem Soc Rev 41, 2256-2282.

El-Sayed, I.H., Huang, X., El-Sayed, M.A., 2006. Selective laser photo-thermal therapy of epithelial carcinoma using anti-EGFR antibody conjugated gold nanoparticles. Cancer Letters 239, 129-135.

Elbert, K.J., Schafer, U.F., Schafers, H.J., Kim, K.J., Lee, V.H., Lehr, C.M., 1999. Monolayers of human alveolar epithelial cells in primary culture for pulmonary absorption and transport studies. Pharm Res 16, 601-608.

Federici, G., Shaw, B.J., Handy, R.D., 2007. Toxicity of titanium dioxide nanoparticles to rainbow trout (Oncorhynchus mykiss): gill injury, oxidative stress, and other physiological effects. Aquat Toxicol 84, 415-430.

Fleischer, C.C., Payne, C.K., 2014. Nanoparticle-cell interactions: molecular structure of the protein corona and cellular outcomes. Acc Chem Res 47, 2651-2659.

Fort, D.J., Paul, R.R., 2002. Enhancing the predictive validity of Frog Embryo Teratogenesis Assay--Xenopus (FETAX). J Appl Toxicol 22, 185-191.

Foster, K.A., Oster, C.G., Mayer, M.M., Avery, M.L., Audus, K.L., 1998. Characterization of the A549 cell line as a type II pulmonary epithelial cell model for drug metabolism. Exp Cell Res 243, 359-366.

Fytianos, K., Rodriguez-Lorenzo, L., Clift, M.J., Blank, F., Vanhecke, D., von Garnier, C., Petri-Fink, A., Rothen-Rutishauser, B., 2015. Uptake efficiency of surface modified gold nanoparticles does not correlate with functional changes and cytokine secretion in human dendritic cells in vitro. Nanomedicine 11, 633-644.

Gatoo, M.A., Naseem, S., Arfat, M.Y., Dar, A.M., Qasim, K., Zubair, S., 2014. Physicochemical properties of nanomaterials: implication in associated toxic manifestations. Biomed Res Int 2014, 498420.

Geiser, M., Rothen-Rutishauser, B., Kapp, N., Schürch, S., Kreyling, W., Schulz, H., Semmler, M., Hof, V.I., Heyder, J., Gehr, P., 2005. Ultrafine Particles Cross Cellular Membranes by Nonphagocytic Mechanisms in Lungs and in Cultured Cells. Environ Health Perspect, vol. 113, pp. 1555-1560.

Geranio, L., Heuberger, M., Nowack, B., 2009. The behavior of silver nanotextiles during washing. Environ Sci Technol 43, 8113-8118.

Geys, J., Coenegrachts, L., Vercammen, J., Engelborghs, Y., Nemmar, A., Nemery, B., Hoet, P.H., 2006. In vitro study of the pulmonary translocation of nanoparticles: a preliminary study. Toxicol Lett 160, 218-226.

Gottschalk, F., Kost, E., Nowack, B., 2013. Engineered nanomaterials in water and soils: a risk quantification based on probabilistic exposure and effect modeling. Environ Toxicol Chem 32, 1278-1287.

Gupta, A.K., Gupta, M., 2005. Synthesis and surface engineering of iron oxide nanoparticles for biomedical applications. Biomaterials 26, 3995-4021.

Hadrup, N., Lam, H.R., 2014. Oral toxicity of silver ions, silver nanoparticles and colloidal silver--a review. Regul Toxicol Pharmacol 68, 1-7.

Hamilton, R.F., Jr., Thakur, S.A., Mayfair, J.K., Holian, A., 2006. MARCO mediates silica uptake and toxicity in alveolar macrophages from C57BL/6 mice. J Biol Chem 281, 34218-34226.

Hanaor, D., Michelazzi, M., Leonelli, C., Sorrell, C.C., 2012. The effects of carboxylic acids on the aqueous dispersion and electrophoretic deposition of ZrO2. Journal of the European Ceramic Society 32, 235-244.

Harush-Frenkel, O., Debotton, N., Benita, S., Altschuler, Y., 2007. Targeting of nanoparticles to the clathrin-mediated endocytic pathway. Biochem Biophys Res Commun 353, 26-32.

He, C., Hu, Y., Yin, L., Tang, C., Yin, C., 2010. Effects of particle size and surface charge on cellular uptake and biodistribution of polymeric nanoparticles. Biomaterials 31, 3657-3666.

Heath, T.D., Lopez, N.G., Papahadjopoulos, D., 1985. The effects of liposome size and surface charge on liposome-mediated delivery of methotrexate-gamma-aspartate to cells in vitro. Biochim Biophys Acta 820, 74-84.

Heinlaan, M., Ivask, A., Blinova, I., Dubourguier, H.C., Kahru, A., 2008. Toxicity of nanosized and bulk ZnO, CuO and TiO2 to bacteria Vibrio fischeri and crustaceans Daphnia magna and Thamnocephalus platyurus. Chemosphere 71, 1308-1316.

Herzog, F., Loza, K., Balog, S., Clift, M.J.D., Epple, M., Gehr, P., Petri-Fink, A., Rothen-Rutishauser, B.

Holder, A.L., Marr, L.C., 2013. Toxicity of silver nanoparticles at the air-liquid interface. Biomed Res Int 2013, 328934.

Inoue, A., Suzuki, T., Fukuhara, T., Maemondo, M., Kimura, Y., Morikawa, N., Watanabe, H., Saijo, Y., Nukiwa, T., 2006. Prospective phase II study of gefitinib for chemotherapy-naive patients with advanced non-small-cell lung cancer with epidermal growth factor receptor gene mutations. J Clin Oncol 24, 3340-3346.

Ispas, C., Andreescu, D., Patel, A., Goia, D.V., Andreescu, S., Wallace, K.N., 2009. Toxicity and developmental defects of different sizes and shape nickel nanoparticles in zebrafish. Environ Sci Technol 43, 6349-6356.

Jiang, W., Kim, B.Y., Rutka, J.T., Chan, W.C., 2008. Nanoparticle-mediated cellular response is size-dependent. Nat Nanotechnol, vol. 3, England, pp. 145-150.

Kaegi, R., Sinnet, B., Zuleeg, S., Hagendorfer, H., Mueller, E., Vonbank, R., Boller, M., Burkhardt, M., 2010. Release of silver nanoparticles from outdoor facades. Environmental Pollution 158, 2900-2905.

Kasemets, K., Ivask, A., Dubourguier, H.C., Kahru, A., 2009. Toxicity of nanoparticles of ZnO, CuO and TiO2 to yeast Saccharomyces cerevisiae. Toxicol In Vitro 23, 1116-1122.

Kettler, K., Veltman, K., van de Meent, D., van Wezel, A., Hendriks, A.J., 2014. Cellular uptake of nanoparticles as determined by particle properties, experimental conditions, and cell type. Environ Toxicol Chem 33, 481-492.

Khan, J.A., Pillai, B., Das, T.K., Singh, Y., Maiti, S., 2007. Molecular effects of uptake of gold nanoparticles in HeLa cells. Chembiochem 8, 1237-1240.

Kim, J., Kim, S., Lee, S., 2011. Differentiation of the toxicities of silver nanoparticles and silver ions to the Japanese medaka (Oryzias latipes) and the cladoceran Daphnia magna. Nanotoxicology 5, 208-214.

Kim, S., Ryu, D.Y., 2013. Silver nanoparticle-induced oxidative stress, genotoxicity and apoptosis in cultured cells and animal tissues. J Appl Toxicol 33, 78-89.

Kimlin, L., Kassis, J., Virador, V., 2013. 3D in vitro tissue models and their potential for drug screening. Expert Opin Drug Discov 8, 1455-1466.

Kirchner, C., Liedl, T., Kudera, S., Pellegrino, T., Munoz Javier, A., Gaub, H.E., Stolzle, S., Fertig, N., Parak, W.J., 2005. Cytotoxicity of colloidal CdSe and CdSe/ZnS nanoparticles. Nano Lett 5, 331-338.

Klein, S.G., Serchi, T., Hoffmann, L., Blömeke, B., Gutleb, A.C., 2013. An improved 3D tetraculture system mimicking the cellular organisation at the alveolar barrier to study the potential toxic effects of particles on the lung. Part Fibre Toxicol, vol. 10, p. 31.

Le Ouay, B., Stellacci, F., 2015. Antibacterial activity of silver nanoparticles: A surface science insight. Nano Today 10, 339-354.

Lenz, A.G., Karg, E., Brendel, E., Hinze-Heyn, H., Maier, K.L., Eickelberg, O., Stoeger, T., Schmid, O., 2013. Inflammatory and oxidative stress responses of an alveolar epithelial cell line to airborne zinc oxide nanoparticles at the air-liquid interface: a comparison with conventional, submerged cell-culture conditions. Biomed Res Int 2013, 652632.

Lubick, N., 2008. Nanosilver toxicity: ions, nanoparticles--or both? Environ Sci Technol 42, 8617.

Mülhopt, S., Dilger, M., Diabaté, S., Schlager, C., Krebs, T., Zimmermann, R., Buters, J., Oeder, S., Wäscher, T., Weiss, C., Paur, H.-R., 2016. Toxicity testing of combustion aerosols at the air–liquid interface with a self-contained and easy-to-use exposure system. Journal of Aerosol Science 96, 38-55.

Müller, L., Gasser, M., Raemy, D.O., Herzog, F., Brandenberger, C., Schmid, O., Gehr, P., Rothen-Rutishauser, B., Clift, M.J.D., - Realistic exposure methods for investigating the interaction of nanoparticles with the lung at the air-liquid interface in vitro. - 30.

Nations, S., Long, M., Wages, M., Canas, J., Maul, J.D., Theodorakis, C., Cobb, G.P., 2011a. Effects of ZnO nanomaterials on Xenopus laevis growth and development. Ecotoxicol Environ Saf 74, 203-210.

Nations, S., Wages, M., Cañas, J.E., Maul, J., Theodorakis, C., Cobb, G.P., 2011b. Acute effects of Fe_2O_3, TiO_2, ZnO and CuO nanomaterials on Xenopus laevis. Chemosphere 83, 1053-1061.

Nel, A., Xia, T., Madler, L., Li, N., 2006. Toxic potential of materials at the nanolevel. Science 311, 622-627.

Nel, A.E., Madler, L., Velegol, D., Xia, T., Hoek, E.M., Somasundaran, P., Klaessig, F., Castranova, V., Thompson, M., 2009. Understanding biophysicochemical interactions at the nano-bio interface. Nat Mater 8, 543-557.

Nohynek, G.J., Antignac, E., Re, T., Toutain, H., 2010. Safety assessment of personal care products/cosmetics and their ingredients. Toxicol Appl Pharmacol 243, 239-259.

Osaki, F., Kanamori, T., Sando, S., Sera, T., Aoyama, Y., 2004. A quantum dot conjugated sugar ball and its cellular uptake. On the size effects of endocytosis in the subviral region. J Am Chem Soc 126, 6520-6521.

Pan, Y., Neuss, S., Leifert, A., Fischler, M., Wen, F., Simon, U., Schmid, G., Brandau, W., Jahnen-Dechent, W., 2007. Size-dependent cytotoxicity of gold nanoparticles. Small 3, 1941-1949.

Pandurangan, M., Kim, D., 2015. In vitro toxicity of zinc oxide nanoparticles: a review. Journal of Nanoparticle Research C7 - 158 17, 1-8.

Panyam, J., Labhasetwar, V., 2003. Biodegradable nanoparticles for drug and gene delivery to cells and tissue. Advanced Drug Delivery Reviews 55, 329-347.

Pati, R., Das, I., Mehta, R.K., Sahu, R., Sonawane, A., 2016. Zinc-Oxide Nanoparticles Exhibit Genotoxic, Clastogenic, Cytotoxic and Actin Depolymerization Effects by Inducing Oxidative Stress Responses in Macrophages and Adult Mice. Toxicol Sci 150, 454-472.

Patil, S., Sandberg, A., Heckert, E., Self, W., Seal, S., 2007. Protein adsorption and cellular uptake of cerium oxide nanoparticles as a function of zeta potential. Biomaterials 28, 4600-4607.

Perelshtein, I., 2015. The influence of the crystalline nature of nano-metal oxides on their antibacterial and toxicity properties. In: Lipovsky, A., Perkas, N., Gedanken, A., Moschini, E., Mantecca, P. (Eds.), vol. 8.

Petersen, E.J., Nelson, B.C., 2010. Mechanisms and measurements of nanomaterial-induced oxidative damage to DNA. Anal Bioanal Chem 398, 613-650.

Pietropaoli, A.P., Frampton, M.W., Hyde, R.W., Morrow, P.E., Oberdorster, G., Cox, C., Speers, D.M., Frasier, L.M., Chalupa, D.C., Huang, L.S., Utell, M.J., 2004. Pulmonary function, diffusing capacity, and inflammation in healthy and asthmatic subjects exposed to ultrafine particles. Inhal Toxicol 16 Suppl 1, 59-72.

Raemy, D.O., Grass, R.N., Stark, W.J., Schumacher, C.M., Clift, M.J., Gehr, P., Rothen-Rutishauser, B., 2012. Effects of flame made zinc oxide particles in human lung cells - a comparison of aerosol and suspension exposures. Part Fibre Toxicol 9, 33.

Raz, A., Bucana, C., Fogler, W.E., Poste, G., Fidler, I.J., 1981. Biochemical, morphological, and ultrastructural studies on the uptake of liposomes by murine macrophages. Cancer Res 41, 487-494.

Rejman, J., Oberle, V., Zuhorn, I.S., Hoekstra, D., 2004. Size-dependent internalization of particles via the pathways of clathrin- and caveolae-mediated endocytosis. Biochem J 377, 159-169.

Rincker, M.J., Clarke, S.L., Eisenstein, R.S., Link, J.E., Hill, G.M., 2005. Effects of iron supplementation on binding activity of iron regulatory proteins and the subsequent effect on growth performance and indices of hematological and mineral status of young pigs. J Anim Sci 83, 2137-2145.

Roszak, J., Catalan, J., Jarventaus, H., Lindberg, H.K., Suhonen, S., Vippola, M., Stepnik, M., Norppa, H., 2016. Effect of particle size and dispersion status on cytotoxicity and genotoxicity of zinc oxide in human bronchial epithelial cells. Mutat Res Genet Toxicol Environ Mutagen 805, 7-18.

Rothen-Rutishauser, B., Blank, F., Muhlfeld, C., Gehr, P., 2008. In vitro models of the human epithelial airway barrier to study the toxic potential of particulate matter. Expert Opin Drug Metab Toxicol 4, 1075-1089.

Rothen-Rutishauser, B.M., Kiama, S.G., Gehr, P., 2005. A three-dimensional cellular model of the human respiratory tract to study the interaction with particles. Am J Respir Cell Mol Biol 32, 281-289.

Sabella, S., Carney, R.P., Brunetti, V., Malvindi, M.A., Al-Juffali, N., Vecchio, G., Janes, S.M., Bakr, O.M., Cingolani, R., Stellacci, F., Pompa, P.P., 2014. A general mechanism for intracellular toxicity of metal-containing nanoparticles. Nanoscale, vol. 6, pp. 7052-7061.

Santo, N., Fascio, U., Torres, F., Guazzoni, N., Tremolada, P., Bettinetti, R., Mantecca, P., Bacchetta, R., 2014. Toxic effects and ultrastructural damages to Daphnia magna of two differently sized ZnO nanoparticles: does size matter? Water Res 53, 339-350.

Saptarshi, S.R., Duschl, A., Lopata, A.L., 2015. Biological reactivity of zinc oxide nanoparticles with mammalian test systems: an overview. Nanomedicine (Lond) 10, 2075-2092.

Scown, T.M., Santos, E.M., Johnston, B.D., Gaiser, B., Baalousha, M., Mitov, S., Lead, J.R., Stone, V., Fernandes, T.F., Jepson, M., van Aerle, R., Tyler, C.R., 2010. Effects of aqueous exposure to silver nanoparticles of different sizes in rainbow trout. Toxicol Sci 115, 521-534.

Secondo, L.E., Liu, N.J., Lewinski, N.A., 2017. Methodological considerations when conducting in vitro, air-liquid interface exposures to engineered nanoparticle aerosols. Crit Rev Toxicol 47, 225-262.

Sharma, V.K., Siskova, K.M., Zboril, R., Gardea-Torresdey, J.L., 2014. Organic-coated silver nanoparticles in biological and environmental conditions: fate, stability and toxicity. Adv Colloid Interface Sci 204, 15-34.

Singh, R.P., Ramarao, P., 2012. Cellular uptake, intracellular trafficking and cytotoxicity of silver nanoparticles. Toxicol Lett 213, 249-259.

Skjolding, L.M., Winther-Nielsen, M., Baun, A., 2014. Trophic transfer of differently functionalized zinc oxide nanoparticles from crustaceans (Daphnia magna) to zebrafish (Danio rerio). Aquat Toxicol 157, 101-108.

Stoehr, L.C., Endes, C., Radauer-Preiml, I., Boyles, M.S., Casals, E., Balog, S., Pesch, M., Petri-Fink, A., Rothen-Rutishauser, B., Himly, M., Clift, M.J., Duschl, A., 2015. Assessment of a panel of interleukin-8 reporter lung epithelial cell lines to monitor the pro-inflammatory response following zinc oxide nanoparticle exposure under different cell culture conditions. Part Fibre Toxicol 12, 29.

Sung, J.H., Ji, J.H., Park, J.D., Song, M.Y., Song, K.S., Ryu, H.R., Yoon, J.U., Jeon, K.S., Jeong, J., Han, B.S., Chung, Y.H., Chang, H.K., Lee, J.H., Kim, D.W., Kelman, B.J., Yu, I.J., 2011. Subchronic inhalation toxicity of gold nanoparticles. Part Fibre Toxicol 8, 16.

Talapin, D.V., Shevchenko, E.V., 2016. Introduction: Nanoparticle Chemistry. Chem Rev 116, 10343-10345.

van Aerle, R., Lange, A., Moorhouse, A., Paszkiewicz, K., Ball, K., Johnston, B.D., de-Bastos, E., Booth, T., Tyler, C.R., Santos, E.M., 2013. Molecular mechanisms of toxicity of silver nanoparticles in zebrafish embryos. Environ Sci Technol 47, 8005-8014.

van Rijt, S.H., Bein, T., Meiners, S., 2014. Medical nanoparticles for next generation drug delivery to the lungs. Eur Respir J, vol. 44. (c)ERS 2014., England, pp. 765-774.

Vance, M.E., Kuiken, T., Vejerano, E.P., McGinnis, S.P., Hochella, M.F., Rejeski, D., Hull, M.S., 2015. Nanotechnology in the real world: Redeveloping the nanomaterial consumer products inventory. Beilstein J Nanotechnol 6, 1769-1780.

Verma, A., Stellacci, F., 2010. Effect of surface properties on nanoparticle-cell interactions. Small 6, 12-21.

Villiers, C., Freitas, H., Couderc, R., Villiers, M.B., Marche, P., 2010. Analysis of the toxicity of gold nano particles on the immune system: effect on dendritic cell functions. J Nanopart Res 12, 55-60.

Volker, C., Kampken, I., Boedicker, C., Oehlmann, J., Oetken, M., 2015. Toxicity of silver nanoparticles and ionic silver: Comparison of adverse effects and potential toxicity mechanisms in the freshwater clam Sphaerium corneum. Nanotoxicology 9, 677-685.

Wang, S.H., Lee, C.W., Chiou, A., Wei, P.K., 2010. Size-dependent endocytosis of gold nanoparticles studied by three-dimensional mapping of plasmonic scattering images. J Nanobiotechnology, vol. 8, p. 33.

Weissleder, R., 2006. Molecular imaging in cancer. Science 312, 1168-1171.

West, J.L., Halas, N.J., 2003. Engineered nanomaterials for biophotonics applications: improving sensing, imaging, and therapeutics. Annu Rev Biomed Eng 5, 285-292.

Whitehead, K.A., Langer, R., Anderson, D.G., 2009. Knocking down barriers: advances in siRNA delivery. Nat Rev Drug Discov 8, 129-138.

Williams, J.R., Rayburn, J.R., Cline, G.R., Sauterer, R., Friedman, M., 2015. Effect of allyl isothiocyanate on developmental toxicity in exposed Xenopus laevis embryos. Toxicology Reports 2, 222-227.

Xiong, D., Fang, T., Yu, L., Sima, X., Zhu, W., 2011. Effects of nano-scale TiO2, ZnO and their bulk counterparts on zebrafish: acute toxicity, oxidative stress and oxidative damage. Sci Total Environ 409, 1444-1452.

Xiu, Z.M., Zhang, Q.B., Puppala, H.L., Colvin, V.L., Alvarez, P.J., 2012. Negligible particle-specific antibacterial activity of silver nanoparticles. Nano Lett 12, 4271-4275.

Yacobi, N.R., Fazllolahi, F., Kim, Y.H., Sipos, A., Borok, Z., Kim, K.-J., Crandall, E.D., 2011. Nanomaterial interactions with and trafficking acrosseffects of air-pollution particles. Air Qual Atmos Health.

Yang, X., Gondikas, A.P., Marinakos, S.M., Auffan, M., Liu, J., Hsu-Kim, H., Meyer, J.N., 2012. Mechanism of silver nanoparticle toxicity is dependent on dissolved silver and surface coating in Caenorhabditis elegans. Environ Sci Technol 46, 1119-1127.

Zhang, L., Jiang, Y., Ding, Y., Povey, M., York, D., 2006. Investigation into the antibacterial behaviour of suspensions of ZnO nanoparticles (ZnO nanofluids). Journal of Nanoparticle Research 9, 479-489.

Zhao, C.M., Wang, W.X., 2012a. Importance of surface coatings and soluble silver in silver nanoparticles toxicity to Daphnia magna. Nanotoxicology 6, 361-370.

Zhao, C.M., Wang, W.X., 2012b. Size-dependent uptake of silver nanoparticles in Daphnia magna. Environ Sci Technol 46, 11345-11351.

Zhu, X., Wang, J., Zhang, X., Chang, Y., Chen, Y., 2009. The impact of ZnO nanoparticle aggregates on the embryonic development of zebrafish (Danio rerio). Nanotechnology 20, 195103.

Chapter 1:

The physico-chemical properties of differently shaped nano-zinc oxides drive their bio-interactions with A549 cells

Melissa Saibene[1], Elisa Moschini[2], Patrizia Bonfanti[1], Anita Colombo[1], Paride Mantecca[1]

[1]*POLARIS Research Centre, DISAT, University of Milano – Bicocca (Italy)*
[2] *Environmental Group, ERIN Department, Luxembourg Institute of Science and Technology (LIST – Luxembourg)*

Paper in preparation

ABSTRACT

The massive production of nano Zinc Oxide (nZnO) and the consequent increase of worker and consumer exposure place this nano-Metal Oxide (nMeO) among the prioritized nanomaterials (NMs) to be considered for toxicological studies.

In this work, the toxic effects induced on human alveolar epithelial cells (A549) by three different forms of nZnO (0 – 30 μg/mL) were compared. The nZnOs used in our study showed the same crystalline phase and size range, but they were different in shape, showing spherical, rod-like and cubic morphologies.

After 24 hours of exposure the effects in term of viability, ROS production, intracellular dissolution and lysosomal activity were evaluated. The spherical form resulted the most cytotoxic, nevertheless all the three forms induced ROS production. The spherical and the rod-like nZnOs in particular dissolved in the intracellular environment bringing to an increase in the lysosomal activity. To better understand the role of nanoparticle (NP) dissolution, cells were also exposed to $ZnSO_4$ (100μM) as positive control.

Our results point out that the NP shape significantly influence the nZnO bio-interaction and toxicity in human epithelial cells Further studies are obviously mandatory also to orient the production of safer nZnOs, which has been proposed as substitute of other more toxic materials in different industrial applications (e.g. antimicrobic coatings).

Keywords: nano Zinc Oxide, A459 cells, bio-interaction, physico-chemical properties, manufacturing process

1. Introduction

The outstanding nanotechnology progress during last decade brought the massive production of new nanomaterials (NMs), involving the unavoidably introduction of unknown compounds into the environment, with unpredictable long-term effect on human and environmental health.

NM extensive applications (including cosmetics, personal care products, electronics, drug delivery systems, paints, sportswear and more) entail worker and consumer growing exposure (Vance *et al.*, 2015). For these reasons, enhancing our knowledge about the effects of new NMs is mandatory to orient nanotechnology towards the development of safer compounds.

Nano Metal Oxides (nMeOs) represent one of the most widely used NM groups in industrial applications and they are globally produced in thousands of tons per year (Bondarenko *et al.*, 2013). In addition, nZnO was the most abundantly produced nMeO After nanosized titanium dioxide ($nTiO_2$) (Bondarenko *et al.*, 2013). Actually it is largely used as stabilizer agent in food, cosmetics and other consumer products, such as paints, and recently, it has attracted a great interest for its UV-protective and antibacterial properties, which make it suitable for a wide range of applications (Nohynek *et al.*, 2010). According to its growing use, nZnO clearly represents one of the prioritized NMs to be considered for regulation, confirmed also by the numerous studies available in literature about its toxicological properties. Many authors investigated nZnO effects on human cells and laboratory mammals, pointing out their relevant cytotoxic and inflammatory potency (Pandurangan and Kim, 2015). Some other papers report data regarding the toxic effects of nZnO on different vertebrate and invertebrate models (Ates *et al.*, 2015; Bonfanti *et al.*, 2015; Brun *et al.*, 2014; Mantecca *et al.*, 2015; Santo *et al.*, 2014; Skjolding *et al.*, 2014).

Interestingly, nZnO probably represents the only NM that has been univocally associated with a human disease, namely the metal fume fever manifested in workers chronically-exposed to welding fume (Gerberding, 2005).

Nano ZnO is known to act as antimicrobial agent thanks to its capability of producing Reactive Oxygen Species (ROS) when in contact with water (Applerot *et al.*, 2009; Perelshtein, 2015; Zhang *et al.*, 2006). ROS-induced oxidative changes to cell structures is at the base of the bacterial killing effect, but are also widely involved in the NP-mediated cytotoxicity in eukaryotic cells. Several NM characteristics can indeed culminate in ROS generation, the currently best-developed paradigm for NP toxicity (Nel *et al.*, 2006; Nel *et al.*, 2009).

The 'nano-bio' interface comprises the dynamic physicochemical interactions, kinetics and thermodynamic exchanges between nanomaterial surfaces and the surfaces of biological components (Nel *et al.*, 2006). Thus, several NP physico-chemical properties govern the bio-interactions between NPs and cells. These bio-interactions are a critical aspect in many fields of NM application, such as phototherapy (El-Sayed *et al.*, 2006; West and Halas, 2003), imaging (Weissleder, 2006), and drug/gene delivery (Panyam and Labhasetwar, 2003; Whitehead *et al.*, 2009). Many applications require that NPs are able to cross cell membrane in order to reach their cytosolic or nuclear target. This capability is a challenge due to the nature of the lipid bilayer which, from an evolutionary point of view, constitutes a barrier to protect the cell. Many nanomaterials have nonetheless demonstrated an ability to successfully penetrate cell membranes (Verma and Stellacci, 2010).

It is almost accepted that the NP physicochemical properties, such as size, shape, surface charge, hydrophilicity, presence of surface functional groups, in combination of the characteristics of the cellular and extracellular matrix are able to influence their uptake (Kettler *et al.*, 2014).

Previous studies highlighted that particle uptake by non-phagocytic cells is strictly dependent on particle size. In particular they observed an increase in NP internalization increasing the particle size (approximatively around 50 nm)) and then a decreases for larger particles (Chithrani and Chan, 2007; Chithrani *et al.*, 2006; Jiang *et al.*, 2008; Osaki *et al.*, 2004; Rejman *et al.*, 2004; Wang *et al.*, 2010). In one of these studies, HeLa cells were used as model to compare the uptake of rod-shaped gold NPs coated with citric acid ligands versus their spherical counterparts (Chithrani *et al.*, 2006). The results demonstrated that small rods with a length of 40 nm were easily taken up by cells compared to rods with one dimension larger than 50 nm suggesting that a wide contact area between NPs and cellular membrane led to a reduction of available binding sites, required for receptor-mediated endocytosis (Chithrani *et al.*, 2006).

In addition to size and shape, another important factor in the bio-interactions between NPs and cells is the NP surface charge. It has been shown that uncharged NPs, either because they present neutral surface groups (e.g., hydroxyl groups) or zwitterionic ligands, has a lower cellular uptake compared to charged particles (Allen *et al.*, 1991; He *et al.*, 2010; Heath *et al.*, 1985; Patil *et al.*, 2007; Raz *et al.*, 1981).

This is due to the low NP affinity toward the overall negatively charged cell membrane (Kettler *et al.*, 2014). It has been shown that high charges prevent agglomeration, while particles with a low zeta potential tend to aggregate, with a decrease in their uptake rate (Hanaor *et al.*, 2012; Zhao and Wang, 2012). When positive and negative surface charges were directly compared, setting other parameters, positively charged particles were shown to be taken up by non-phagocytic-cells more favourably than negatively charged particles (Harush-Frenkel *et al.*, 2007; He *et al.*, 2010).

In this study, the effects and mode of action of three differently shaped nZnOs in human alveolar cells (A549) were investigated.

Cells were exposed for 24 hours to round, rod and cubic shaped nZnO at concentrations from 0 up to 30 µg/mL. The intracellular NP dissolution and ROS production, as well as the lysosomal activity, were also evaluated at sub-cytotoxic concentrations.

2. Material and Methods

2.1 Preparation and characterization of NP suspensions

Spherical nZnO (S-nZnO) was purchased from Sigma Aldrich S.r.l. (Italy), while Rod nZnO (R-nZnO) was provided from TecStar S.r.l. (Campogalliano, Modena, Italy). Cubic nZnO (C-nZnO) was gently provided from the laboratories of the professor Gedanken (Bahr-Ilan University, Israel).

No detailed information are available regarding the process of synthesis to obtain the spherical form; R-nZnO was produced through the gas phase pyrolysis method while C-nZnO was synthesized using the ethanol-based sonochemical ultrasound deposition/process.

Additional details about the characterization of all the particles are available in literature (Bacchetta *et al.* 2014; Bonfanti *et al.* 2015; (Perelshtein *et al.*, 2009).

All the three forms were anyway characterized in term of size and shape by Transmission Electron Microscopy (TEM, Jem Jeol 1220, 80 kV) and Dynamic Light Scattering (DLS, Malvern Zetasizer ZS90). For DLS analysis, the suspensions were prepared in sterile MilliQ water, sonicated, stabilized with BSA and finally diluted in culture medium 1% FBS (OptiMEM).

For the cell exposure, all the NPs were suspended in sterile MilliQ water, sonicated, stabilized with BSA (0,1% as final) and then diluted in culture medium 1% FBS (OptiMEM), to obtain the final working concentrations.

2.2 Cell culture maintenance, seeding and treatments

The human alveolar epithelial cells A549 (American Type Culture Collection, ATCC) were routinely maintained according to (Gualtieri *et al.*, 2009) and normally seeded at the density of 1.8×10^5 c/well.

For the cell viability assay cells were seeded at the density of 1.8×10^5 cell/well in 6 multi-well plates and then exposed for 24 h to NP concentrations ranging from 1 to 30 µg/ml. Untreated cells were used as control. The contribution to cytotoxicity of zinc ions potentially dissolved from NPs was evaluated using $ZnSO_4*7H_2O$ (stock solution of 100µM) as positive control.

All the other experiments were performed using a non-cytotoxic concentration of NPs (15 µg/ml) as determined through the cell viability assay.

For the fluorescence (light) microscopy cells were seeded on sterilized glass coverslips at the density of 1.8×10^5 cell/well in 6 multi-well plates.

For the intracellular Reactive Oxygen Species detection, cells were seeded in 6 multi-well plates.

The reported pictures are representative of three independent experiments.

2.3 Cell viability assay

Cell viability was assessed by MTT assay according to (Mosmann, 1983) with slight modifications after exposing A549 cells to increasing concentrations of nZnOs (0, 10, 15, 20, 22, 25, 30 µg/ml) for 24 h.

After treatment, cells were rinsed with phosphate buffer saline (PBS) and 1 ml MTT (final concentration 0.5 mg/ml) was added for 4 h. The by-product of MTT derived from the cellular metabolism (formazan crystals) was then dissolved with DMSO (1 ml/well). The absorbance of each sample was measured by Multiskan Ascent (Thermo Scientific Inc.) spectrophotometer at 570 nm. Cell viability results were expressed as relative % compared to the

negative control (unexposed cells) and calculated as follow: $(OD_{sample}/OD_{control})$ x 100.

2.4 Measurements of intracellular oxidative stress

The intracellular production of Reactive Oxygen Species (ROS) was assessed by using the fluorescent probes 2'7'- dichlorodihydrofluorescein diacetate (H_2DCFDA). This probe detects several oxygen radicals including hydrogen peroxide, hydroxyl radicals and peroxynitrite.

After exposure to 15 µg/ml nZnOs for 24h, cells were washed once with PBS and incubated for 15 min at 37°C with H_2DCFDA (5 µM); then they were washed with PBS, trypsinated and suspended in PBS. Finally, ROS induced fluorescence was quantified by measuring the intensity of 10,000 events using the flow cytometer EPICS XL-MCL with the 525 nm band pass filter; the results were analysed by the dedicated software (EXPO32 ADC, Beckman–Coulter). The potential nZnO and cell auto-fluorescence was also assessed measuring the fluorescence intensity of exposed and unexposed cells not incubated with H_2DCFDA. These values were subtracted from the fluorescence intensities of the other samples. The experiments were replicated at least three times and results were expressed as mean ± SE. Statistical differences were tested by ANOVA followed by Dunnett's method.

2.5 Assessment of the lysosomal activity

Lysotracker® Red (Molecular Probes) was used to probe functional lysosomes in A549 cells exposed for 24 h to nZnOs at the concentration of 15 µg/ml. After the staining, cells were detached with trypsin, centrifuged and re-suspended in PBS. Lysosomal fluorescence intensity was measured on 10,000 events using the Beckman Coulter Epics XL-MCL equipped with EXPO32 ADC software (Beckman–Coulter), selecting a 525 nm band pass filter. The experiments were

repeated at least three times and the data were reported as mean fluorescence fold-increase compared to negative control.

2.6 Intracellular zinc ion release

Intracellular NP dissolution was investigated by fluorescence detection of free zinc ions in living cells after incubation with FluoZin-3 probe (Life Technologies, Italy), able to permeate the cells and bind the intracellular Zn free ions.

After exposure to nZnOs (15 μg/ml) cells were incubated with 2 μM FluoZin-3 in Opti-MEM medium (10% FBS) for 45 min at 37°C. Subsequently, cells were washed with HBSS 1X (Hank's Balanced Salt 86 Solution, Sigma-Aldrich, Italy) and incubated for additional 30 min in HBSS at 37°C. Finally, cells were detached with trypsin and re-suspended in 500 μl HBSS for the flow-cytometry analysis performed using EPICS XL-MCL equipped with EXPO32 ADC software (Beckman–Coulter; 525 nm band pass filter). Results were expressed as relative fluorescence fold-increase compared to negative control.

2.7 Fluorescence microscopy

Fluorescence microscopy was used to check for the intracellular distribution and potential lysosomal localization of Zn ions. After exposure to nZnOs (15 μg/ml) for 24 h, the cells previously seeded on coverslips, were double stained with FluoZin-3 and Lysotracker® Red (Molecular Probes). Then they were fixed with 4% paraformaldehyde and the coverslips were finally mounted with Prolong Gold Anti-fade mounting medium (Molecular Probes) and observed with a Zeiss Axio Observer Z1 fluorescence microscope. Nuclei were counterstained with DAPI.

3. Results

3.1 NP suspension characterization

The three forms of nZnO used in this study, shown comparable size (< 100 nm), but different shape. Thanks to Transmission Electron Microscope (TEM) analysis it was possible to appreciate this differences (Figure 1). The shapes compared are spherical (S-nZnO), rod-like (R-nZnO) and cubical (C-nZnO).
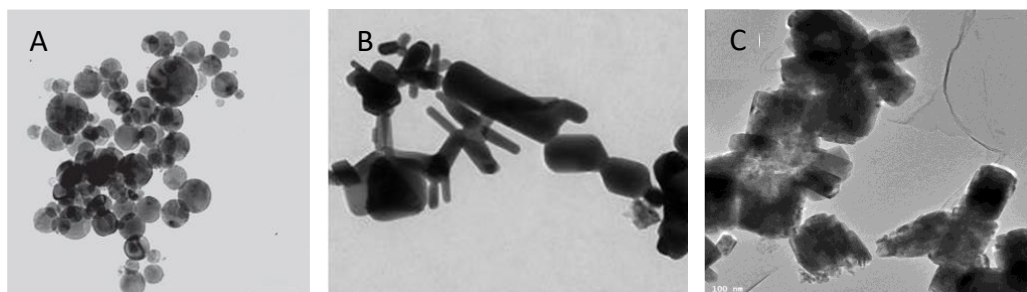
Fig. 1: Transmission Electron Microscope (TEM) pictures of nZnOs, respectively S-nZnO (A, from Bacchetta et al., 2012), R-nZnO (B, from Bonfanti et al., 2015) and C-nZnO (C). The images clearly shown the different shape of NPs.

In order to obtain information regarding the dimension distribution and the surficial charge Dynamic Light Scattering (DLS) analysis were performed (Figure 2).

Table I. Dynamic Light Scattering (DLS) analysis of of hydrodynamic diameter performed after 24 hours of incubation in Cell Culture Medium with 1% BSA, the same working conditions used for cell treatment. C-nZnO. In the table have been reported the values indicated in nm; SD, Standard Deviation and CV, Coefficient of Variation.

nZnO	24 h		
	nm	SD	CV%
C1-nZnO	**224**	13	6
C2-nZnO	**216**	1	0
S-nZnO	**201**	13	6
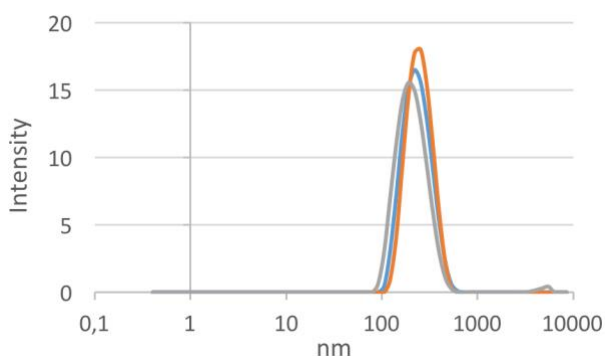
Fig. 2: Dynamic Light Scattering (DLS) analysis of hydrodynamic diameter performed after 24 hours of incubation in Cell Culture Medium with 1% BSA, the same working conditions used for cell treatment. In the graph, Orange: S-nZnO; Blue: R-nZnO; Grey

After 24 hours of incubation in the cell culture medium all the three forms of nZnO showed a similar behaviour forming aggregates around 200 nm.

Table II. Dynamic Light Scattering (DLS) analysis of nZnO Z-potential in MilliQ water, the measurement was performed at time 0 and after 24 hours. SD, Standard Deviation and CV, Coefficient of Variation.

nZnO	0 h			24 h		
	Z-pot	SD	CV%	**Z-pot**	SD	CV%
C1-nZnO	**-28**	1	-4	**-26**	1	-3
C2-nZnO	**-28**	2	-8	**-25**	3	-15
S-nZnO	**-12**	2	-19	**-14**	5	-30

Concerning the surficial charge (Table II), the Zeta-potential was evaluated in Milli-Q water at time 0 and after 24 hours. The nZnOs showed all a negative charge, in both time of evaluation without change in time.

3.2 Cell viability

A549 cell viability was evaluated by MTT assay after exposing cells for 24 h to increasing concentrations (0 – 30 μg/mL) of NPs and Zinc ions (Figure 3).
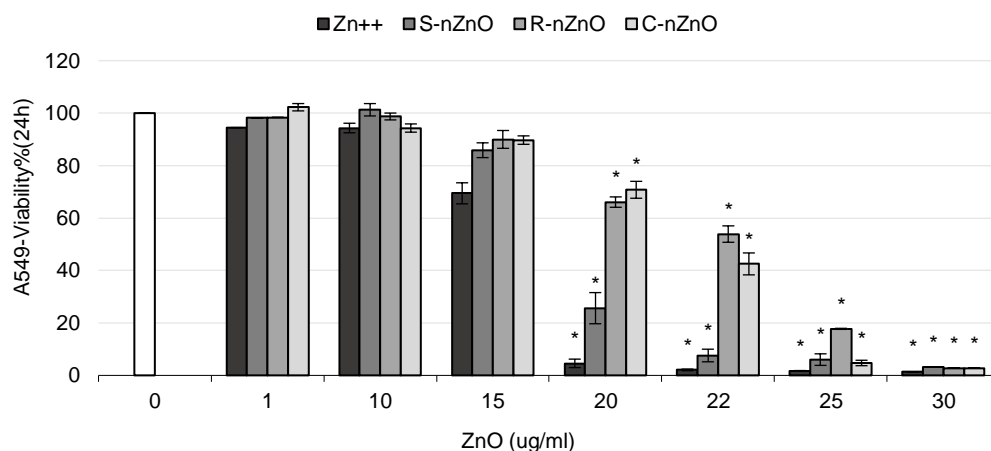
*Fig. 3: Cell viability results (MTT test) of A549 cells exposed for 24 h to increasing concentrations (0-30 μg/mL) of nZnOs and Zn⁺⁺. The results are representative of three independent experiments, except for the concentration of 30 μg/ml. Bars indicate standard error (SE). * Statistically different from control (ANOVA + Dunnett's test, p < 0.05).*

A549 cell viability was evaluated by MTT assay after exposing cells for 24 h to increasing concentrations (0 – 30 μg/mL) of NPs and Zinc ions (Figure 3).

All the three nZnOs and Zinc ions induced a dose-dependent decrease of cell viability, which started to be significant from the dose of 20 μg/mL. In particular, the concentration of 30 μg/mL resulted to be lethal for all the compounds.

Since at the concentration of 15 μg/mL the cell viability was higher than the 85% and comparable among the different NPs (85.86% for S-nZnO, 89.98% for R-nZnO and 89.71% for C-nZnO) this concentration was selected for the further experiments.

3.3 Intracellular oxidative stress

The production of intracellular Reactive Oxygen Species induced by exposing cells to ZnO NPs and zinc ions at the concentration of 15 μg/mL was evaluated. After incubation with 2'7'- dichlorodihydrofluorescein diacetate, (H_2DCFDA) able to react with ROS, the fluorescence intensity was measured by flow

cytometry. All the nZnOs induced a comparable and significant increase in the intracellular ROS levels compared to the negative control (Figure 4).
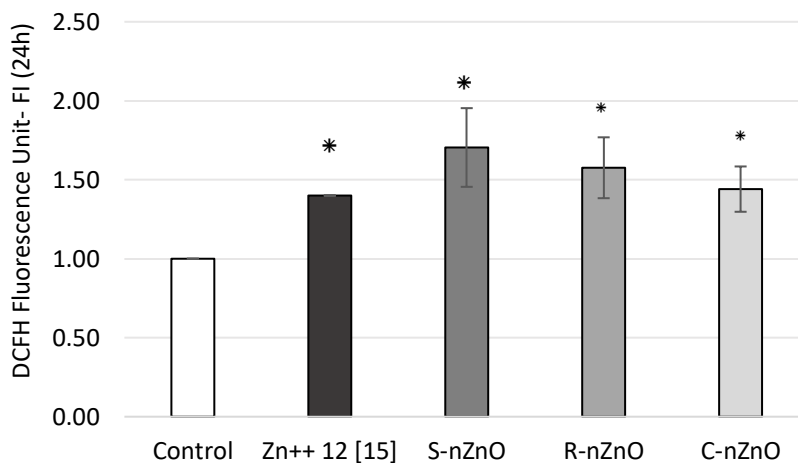
*Fig.4: A549 intracellular ROS production after exposure for 24 h to different nZnOs and Zn^{++} at the concentration of 15 µg/mL. At the end of treatment, cells were incubated with 2'7'-dichlorodihydrofluorescein diacetate (H_2DCFDA). Results are expressed as fluorescence intensity fold increase compared to the control. Data are presented as the mean ± standard error of three independent experiments). * Statistically different from control group (ANOVA + Dunnett's test, $p < 0.05$).*

As in cell viability assay, S-nZnO seems to induce a stronger effect in comparison to R-nZnO and C-nZnO showing an enhanced trend in ROS generation. Zinc ions didn't cause any significant increase in ROS compared to the control.

3.4 Lysosomal functionality

The lysosomal activity was assessed by flow cytometry after incubation of cells with the fluorescent probe Lysotracker® Red. The fluorescence intensity is proportional to the lysosomal activity either in term of functionality and number of lysosomes, conditions that can be affected in case of suffering cells (Figure 5).
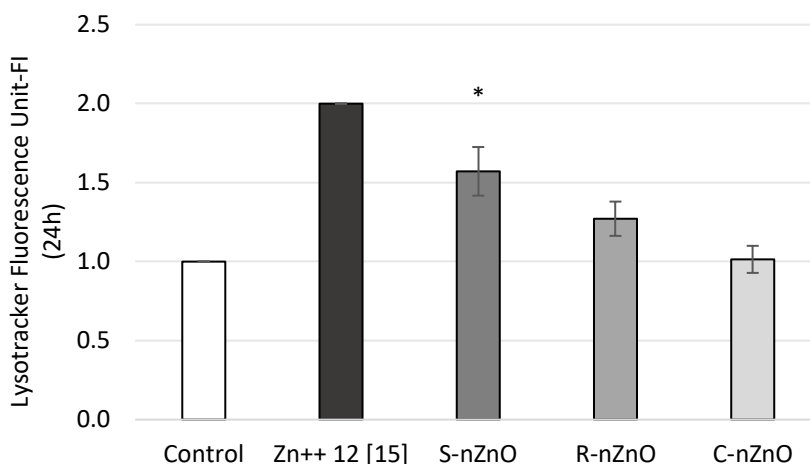
Fig.5: Lysosomal activity in A549 cells exposed for 24 h to different nZnOs and Zn^{++}at the concentration of 15 µg/mL. Results are expressed as increase in fluorescence intensity compared to the control after incubating cells with the fluorescent probe Lysotracker® Red. The results are presented the mean ± standard error of three independent experiments. * Statistically different from control (ANOVA + Dunnett's test, p < 0.05).

After 24 h of exposure to 15 µg/mL of S-nZnO and R-nZnO a significant increase in term of fluorescence intensity was observed (Figure 5). In particular, the lysosomal activity appeared significantly enhanced after treatment with S-nZnO. No significant modulation of lysosomal activity was detected in cells exposed to the C-nZnO.

3.5 NP intracellular dissolution

The Figure 6 shows the intracellular dissolution of ZnO NPs after exposing cells for 24 h to 15 µg/mL of nZnOs. Cells were incubated with FluoZin-3 able to react with the free Zn^{++} ions emitting a fluorescence proportional to the dissolution rate. The spherical and rod-like forms of nZnO dissolved releasing free Zn^{++} ions more than the cubical nano zinc oxide in intracellular environment and between the two the highest dissolution rate was detected for R-nZnO.
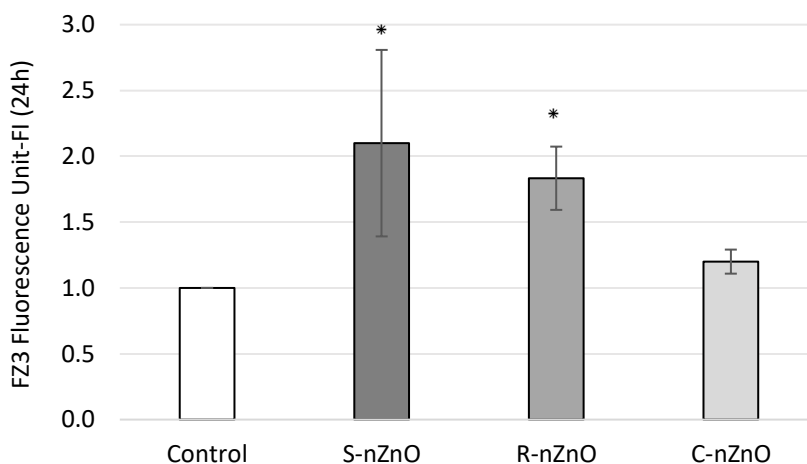
Fig. 6: Intracellular dissolution of nZnOs measured by flow cytometry after incubating cells, exposed for 24 h to 15ug/mL nZnOs, with FluoZin-3. Fluorescence intensity emitted by the probe is proportional to the particle dissolution. The results are representative of three independent experiments. Bars indicate standard error (SE). * Significantly different from control group (ANOVA + Dunnett's test, p < 0.05).

3.6 Fluorescence microscopy

Fluorescence microscopy analysis was performed on control and exposed cells incubated with both the fluorescent probes FluoZin-3 and Lysotracker® Red to check for the cellular distribution of lysosomes and the intracellular dissolved ions (Figure 7).

As is shown in Figure 7 B and C, lysosomes in cells exposed to both the commercial nZnOs appeared bigger compared to unexposed cells. Moreover, a clear co-localization between the red and the green fluorescence found suggesting a potential engulfment of lysosomes combined with NP intralysosomal dissolution after particle internalization through the endocytic process. On the contrary, cells exposed to C-nZnO (Figure 7 D) showed a distribution of lysosomes comparable to the control cells; Zn^{++} resulted more widespread in the cytosol suggesting for a potential but absolutely not significant NP dissolution independent from the lysosomal pathway. These

findings agree with the results obtained from the flow cytometry analysis mentioned above.
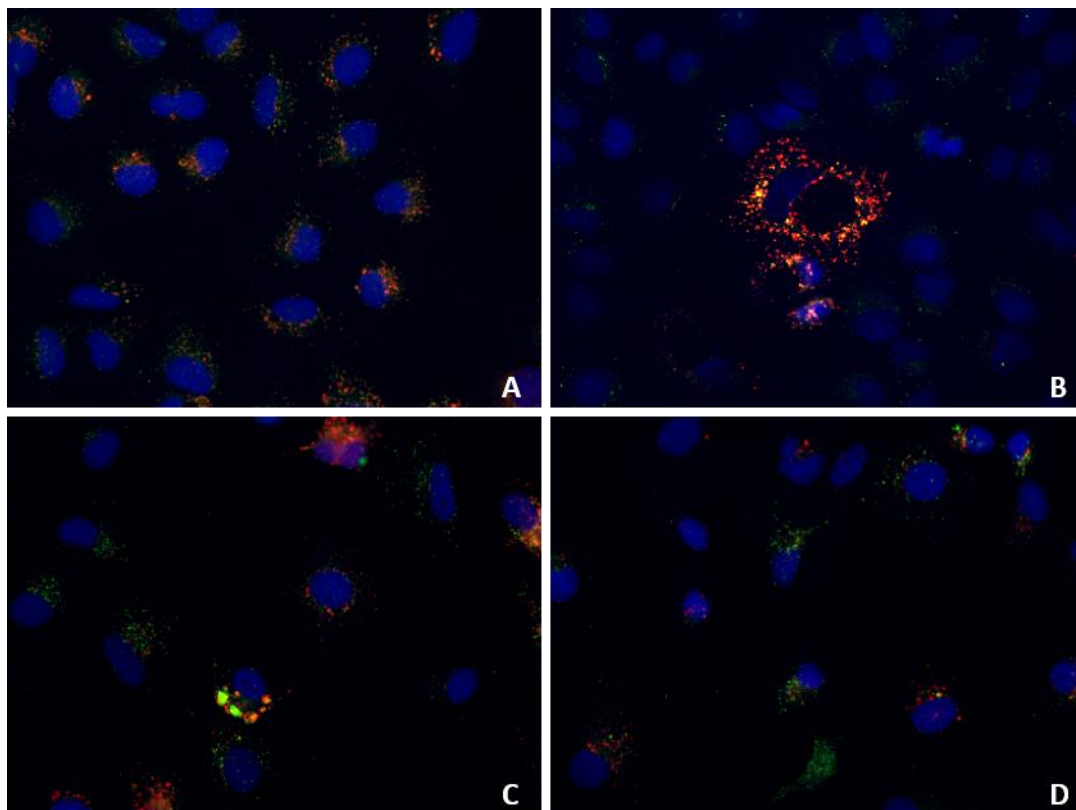
Fig.7: Fluorescence microscopy images of A549 exposed for 24 h to nZnOs at the concentration of 15 µg/mL. Cells were triple stained for intracellular Zn^{++} (FluoZin-3, green), lysosomes (Lysotracker® Red, red) and nuclei (DAPI, blue). A) Unexposed cells; B) S-nZnO-exposed cells; C) R-nZnO-exposed cells; D) C-nZnO-exposed cells. Significant lysosome engulfment was found after treatment with commercial NPs.

4. Discussion

The bio-interactions between NPs and cells are a critical aspect in many fields of application for NMs, such as phototherapy (El-Sayed *et al.*, 2006; West and Halas, 2003), imaging (Weissleder, 2006), and drug/gene delivery (Panyam and Labhasetwar, 2003; Whitehead *et al.*, 2009). Many of these applications require that NPs are able to cross the cell membrane in order to reach the cytosolic or

nuclear targets. However, crossing cell membranes is inherently challenging due to the nature of the lipid bilayer, that works as a barrier to protect the cell functions. Many nanomaterials have nonetheless demonstrated the ability to enter cells (Verma and Stellacci, 2010). Evaluating this capability to cross the membrane and interact with cellular organelles is also an important aspect to highlight the potential cytotoxicity of NPs.

Internalization of NMs in cells is influenced by a large number of physical and chemical properties of the specific NP and the circumstances in the exposure medium of the cells, as size, shape, surface charge, surface functional groups and NP hydrophilicity (Kettler *et al.*, 2014).

Zinc oxide nanoparticles represent one of the most used NMs in emerging applications, mainly because of their antibacterial properties. Besides, safety, toxicity, and their interaction with biological systems are not yet fully understood (Pandurangan and Kim, 2015). In our study, A549 cells were selected as a model to compare the toxic effects induced by three different forms of nZnO. The NPs were comparable in size but different in shape (round, rod-like and cubic). The results obtained indicate that the NP shape significantly modulated the bio-interactions and final cytotoxicity in A549 cell line.

Here we evaluated different parameters, such as intracellular ROS production, lysosomal activity and NP dissolution, after screening cell viability at increasing concentrations of NPs (0 – 30 µg/mL). All the NPs were quite cytotoxic for A549 cells after 24 hours of exposure; in particular S-nZnO induced a significant decrease in cell viability starting from the concentration of 20 µg/mL, while for R-nZnO and C-nZnO the effect started to be significant at 25 µg/mL.

4.1 nZnO exposure induce intracellular ROS production

Intracellular ROS production is known to be a typical cell response to NP treatment (Nel *et al.*, 2006).

After 24 h of exposure all the three nZnOs induced a significant and comparable increase in intracellular ROS production, unlike Zn^{++} ions.

It is interesting to note that ZnO NPs with different shapes induce a similar response in terms of production of ROS into intracellular environmental without inducing high level of cell mortality. Generation of ROS was previously demonstrated to occur in A549 cells exposed to ZnO NPs (Hsiao and Huang, 2011b). In the same paper, it has been shown that the coating of nZnO with TiO_2 moderated its toxicity by reducing the release of zinc ions and decreasing the contact area of the ZnO cores. This suggest that ROS generation by ZnO NPs is mainly due to intracellular Zn^{++} ions release that is independent by the NP shape.

4.2 NP internalization and intracellular dissolution

Previous studies on particle internalization by non-phagocytic cells highlighted that uptake increases with particle size to an optimum of approximately 50 nm and decreases for larger particles (Chithrani and Chan, 2007; Chithrani *et al.*, 2006; Jiang *et al.*, 2008; Osaki *et al.*, 2004; Rejman *et al.*, 2004; Wang *et al.*, 2010). In particular, (Chithrani *et al.*, 2006) found that larger rods with one dimension of more than 50 nm were taken up less than smaller rods with a length of 40 nm because the larger contact area between the rod-shaped NPs and the cellular membrane led to a reduction in available binding sites in Hela cells.

It has been proposed that the mechanism of ZnO nanoparticles toxicity in different cell lines could occur especially in three ways (Pandurangan and Kim, 2015). ZnO nanoparticles can dissolve in the extracellular environment and increase the

intracellular zinc ions level; this increase can reduces the activity of Zn-dependent enzymes and transcription factors (A549, BEAS-2B, and C2C12 cells may undergo this mechanism). In a second mechanism ZnO nanoparticles enter the cells and dissolve in the intracellular region, disrupting the Zn-dependent enzymes and transcription factors (for istance this process can take place in RKO and 3T3-L1 cells). Then, a third mechanism could be that ZnO nanoparticles dissolve in the lysosomes environment that lead to the reduction of pH level; a low pH affects the lysosomal enzymes involving in the protein digestion and increases intra-lysosomal Zn^{++} levels, leading to lysosomal destabilization.

In our study, S-nZnO and R-nZnO seem to dissolve in the intracellular environment releasing Zn^{++}, which partially co-localized with lysosomes as shown in the images obtained by fluorescence microscopy (Fig. 7). In both cases, the number and the size of the lysosomes appeared also increased.

We could hypothesize that the spherical and rod-like nZnOs are abundantly taken up by cells through the classical endocytic pathway, stimulating lysosome production and finally releasing Zn^{++} as a consequence of the NP dissolution in the acidic lysosomal vesicles. Interestingly, the green fluorescence resulted in spot shaped signals, sometimes not completely co-localized with the red fluorescence of healthy lysosomes. This could indicate that the dissolution occurred earlier in those lysosomes affecting their membrane thus compromising the ability of the Lysotracker to stain damaged organelles.

The previous hypothesis could explain also why the cubical nZnO results less toxic than the other ones. Apparently this nanomaterial doesn't dissolve into the lysosomal environment as testified by both confocal and flow cytometry analysis, since the fluorescence measured in C-ZnO was almost comparable to that from control cells. Probably C-nZnO enters cells following some mechanisms different from endocytosis, thus escaping the classical lysosomal-

enhanced Trojan horse mechanism, which has been reported as the main toxicity mechanism displayed by metal-based NPs (Sabella *et al.*, 2014).

5. Conclusion

Our findings highlighted once again how the different NP physico-chemical properties, in this particular case the shape, can affect the bio-interactions between particles and cells, as well as the final toxicity. In a safe-by-design approach, in addition to size, the selection of the NP shape could be the leading point in order to obtain safer nanomaterials. In this study the cubical form of nZnO induced lower levels of oxidative stress in A549 cells, they didn't affect the lysosomal activity and they were not characterised by a strong intracellular dissolution compared to the commercial forms, thus resulting less cytotoxic. Based on our results the cubical shape appeared the less dangerous one. As previously demonstrated (Perelsthein *et al.*, 2015) this sonochemical produced nZnO form also displays very high antibacterial properties, confirming that it is possible to orient the NM production toward processes able to keep the best compromise between safety and efficacy.

Contribution

The candidate elaborated the results and prepared the manuscript.

References

Allen, T.M., Austin, G.A., Chonn, A., Lin, L., Lee, K.C., 1991. Uptake of liposomes by cultured mouse bone marrow macrophages: influence of liposome composition and size. Biochim Biophys Acta 1061, 56-64.

Applerot, G., Lipovsky, A., Dror, R., Perkas, N., Nitzan, Y., Lubart, R., Gedanken, A., 2009. Enhanced Antibacterial Activity of Nanocrystalline ZnO Due to Increased ROS-Mediated Cell Injury. Advanced Functional Materials 19, 842-852.

Ates, M., Arslan, Z., Demir, V., Daniels, J., Farah, I.O., 2015. Accumulation and toxicity of CuO and ZnO nanoparticles through waterborne and dietary exposure of goldfish (Carassius auratus). Environ Toxicol 30, 119-128.

Bondarenko, O., Juganson, K., Ivask, A., Kasemets, K., Mortimer, M., Kahru, A., 2013. Toxicity of Ag, CuO and ZnO nanoparticles to selected environmentally relevant test organisms and mammalian cells in vitro: a critical review. Arch Toxicol 87, 1181-1200.

Bonfanti, P., Moschini, E., Saibene, M., Bacchetta, R., Rettighieri, L., Calabri, L., Colombo, A., Mantecca, P., 2015. Do Nanoparticle Physico-Chemical Properties and Developmental Exposure Window Influence Nano ZnO Embryotoxicity in Xenopus laevis? Int J Environ Res Public Health 12, 8828-8848.

Brun, N.R., Lenz, M., Wehrli, B., Fent, K., 2014. Comparative effects of zinc oxide nanoparticles and dissolved zinc on zebrafish embryos and eleuthero-embryos: importance of zinc ions. Sci Total Environ 476-477, 657-666.

Chithrani, B.D., Chan, W.C., 2007. Elucidating the mechanism of cellular uptake and removal of protein-coated gold nanoparticles of different sizes and shapes. Nano Lett 7, 1542-1550.

Chithrani, B.D., Ghazani, A.A., Chan, W.C., 2006. Determining the size and shape dependence of gold nanoparticle uptake into mammalian cells. Nano Lett 6, 662-668.

El-Sayed, I.H., Huang, X., El-Sayed, M.A., 2006. Selective laser photo-thermal therapy of epithelial carcinoma using anti-EGFR antibody conjugated gold nanoparticles. Cancer Letters 239, 129-135.

Finney, D.J., Probit Analysis: 3d Ed.

Gerberding, J.L., 2005. Protecting health--the new research imperative. JAMA 294, 1403-1406.

Gualtieri, M., Mantecca, P., Corvaja, V., Longhin, E., Perrone, M.G., Bolzacchini, E., Camatini, M., 2009. Winter fine particulate matter from Milan induces morphological and functional alterations in human pulmonary epithelial cells (A549). Toxicol Lett 188, 52-62.

Hanaor, D., Michelazzi, M., Leonelli, C., Sorrell, C.C., 2012. The effects of carboxylic acids on the aqueous dispersion and electrophoretic deposition of ZrO2. Journal of the European Ceramic Society 32, 235-244.

Harush-Frenkel, O., Debotton, N., Benita, S., Altschuler, Y., 2007. Targeting of nanoparticles to the clathrin-mediated endocytic pathway. Biochem Biophys Res Commun 353, 26-32.

He, C., Hu, Y., Yin, L., Tang, C., Yin, C., 2010. Effects of particle size and surface charge on cellular uptake and biodistribution of polymeric nanoparticles. Biomaterials 31, 3657-3666.

Heath, T.D., Lopez, N.G., Papahadjopoulos, D., 1985. The effects of liposome size and surface charge on liposome-mediated delivery of methotrexate-gamma-aspartate to cells in vitro. Biochim Biophys Acta 820, 74-84.

Hsiao, I.L., Huang, Y.J., 2011a. Effects of various physicochemical characteristics on the toxicities of ZnO and TiO nanoparticles toward human lung epithelial cells. Sci Total Environ 409, 1219-1228.

Hsiao, I.L., Huang, Y.J., 2011b. Titanium oxide shell coatings decrease the cytotoxicity of ZnO nanoparticles. Chem Res Toxicol 24, 303-313.

Jiang, W., Kim, B.Y., Rutka, J.T., Chan, W.C., 2008. Nanoparticle-mediated cellular response is size-dependent. Nat Nanotechnol, vol. 3, England, pp. 145-150.

Kettler, K., Veltman, K., van de Meent, D., van Wezel, A., Hendriks, A.J., 2014. Cellular uptake of nanoparticles as determined by particle properties, experimental conditions, and cell type. Environ Toxicol Chem 33, 481-492.

Mantecca, P., Moschini, E., Bonfanti, P., Fascio, U., Perelshtein, I., Lipovsky, A., Chirico, G., Bacchetta, R., Del Giacco, L., Colombo, A., Gedanken, A., 2015. Toxicity Evaluation of a New Zn-Doped CuO Nanocomposite With Highly Effective Antibacterial Properties. Toxicol Sci.

Mosmann, T., 1983. Rapid colorimetric assay for cellular growth and survival: Application to proliferation and cytotoxicity assays. Journal of Immunological Methods 65, 55-63.

Nel, A., Xia, T., Madler, L., Li, N., 2006. Toxic potential of materials at the nanolevel. Science 311, 622-627.

Nel, A.E., Madler, L., Velegol, D., Xia, T., Hoek, E.M., Somasundaran, P., Klaessig, F., Castranova, V., Thompson, M., 2009. Understanding biophysicochemical interactions at the nano-bio interface. Nat Mater 8, 543-557.

Nohynek, G.J., Antignac, E., Re, T., Toutain, H., 2010. Safety assessment of personal care products/cosmetics and their ingredients. Toxicol Appl Pharmacol 243, 239-259.

Osaki, F., Kanamori, T., Sando, S., Sera, T., Aoyama, Y., 2004. A quantum dot conjugated sugar ball and its cellular uptake. On the size effects of endocytosis in the subviral region. J Am Chem Soc 126, 6520-6521.

Pandurangan, M., Kim, D., 2015. In vitro toxicity of zinc oxide nanoparticles: a review. Journal of Nanoparticle Research C7 - 158 17, 1-8.

Panyam, J., Labhasetwar, V., 2003. Biodegradable nanoparticles for drug and gene delivery to cells and tissue. Advanced Drug Delivery Reviews 55, 329-347.

Patil, S., Sandberg, A., Heckert, E., Self, W., Seal, S., 2007. Protein adsorption and cellular uptake of cerium oxide nanoparticles as a function of zeta potential. Biomaterials 28, 4600-4607.

Perelshtein, I., 2015. The influence of the crystalline nature of nano-metal oxides on their antibacterial and toxicity properties. In: Lipovsky, A., Perkas, N., Gedanken, A., Moschini, E., Mantecca, P. (Eds.), vol. 8.

Perelshtein, I., Applerot, G., Perkas, N., Wehrschetz-Sigl, E., Hasmann, A., Guebitz, G.M., Gedanken, A., 2009. Antibacterial properties of an in situ generated and

simultaneously deposited nanocrystalline ZnO on fabrics. ACS Appl Mater Interfaces 1, 361-366.

Raz, A., Bucana, C., Fogler, W.E., Poste, G., Fidler, I.J., 1981. Biochemical, morphological, and ultrastructural studies on the uptake of liposomes by murine macrophages. Cancer Res 41, 487-494.

Rejman, J., Oberle, V., Zuhorn, I.S., Hoekstra, D., 2004. Size-dependent internalization of particles via the pathways of clathrin- and caveolae-mediated endocytosis. Biochem J 377, 159-169.

Sabella, S., Carney, R.P., Brunetti, V., Malvindi, M.A., Al-Juffali, N., Vecchio, G., Janes, S.M., Bakr, O.M., Cingolani, R., Stellacci, F., Pompa, P.P., 2014. A general mechanism for intracellular toxicity of metal-containing nanoparticles. Nanoscale, vol. 6, pp. 7052-7061.

Santo, N., Fascio, U., Torres, F., Guazzoni, N., Tremolada, P., Bettinetti, R., Mantecca, P., Bacchetta, R., 2014. Toxic effects and ultrastructural damages to Daphnia magna of two differently sized ZnO nanoparticles: does size matter? Water Res 53, 339-350.

Skjolding, L.M., Winther-Nielsen, M., Baun, A., 2014. Trophic transfer of differently functionalized zinc oxide nanoparticles from crustaceans (Daphnia magna) to zebrafish (Danio rerio). Aquat Toxicol 157, 101-108.

Vance, M.E., Kuiken, T., Vejerano, E.P., McGinnis, S.P., Hochella, M.F., Rejeski, D., Hull, M.S., 2015. Nanotechnology in the real world: Redeveloping the nanomaterial consumer products inventory. Beilstein J Nanotechnol 6, 1769-1780.

Verma, A., Stellacci, F., 2010. Effect of surface properties on nanoparticle-cell interactions. Small 6, 12-21.

Wang, S.H., Lee, C.W., Chiou, A., Wei, P.K., 2010. Size-dependent endocytosis of gold nanoparticles studied by three-dimensional mapping of plasmonic scattering images. J Nanobiotechnology, vol. 8, p. 33.

Weissleder, R., 2006. Molecular imaging in cancer. Science 312, 1168-1171.

West, J.L., Halas, N.J., 2003. Engineered nanomaterials for biophotonics applications: improving sensing, imaging, and therapeutics. Annu Rev Biomed Eng 5, 285-292.

Whitehead, K.A., Langer, R., Anderson, D.G., 2009. Knocking down barriers: advances in siRNA delivery. Nat Rev Drug Discov 8, 129-138.

Zhang, L., Jiang, Y., Ding, Y., Povey, M., York, D., 2006. Investigation into the antibacterial behaviour of suspensions of ZnO nanoparticles (ZnO nanofluids). Journal of Nanoparticle Research 9, 479-489.

Zhao, C.M., Wang, W.X., 2012. Size-dependent uptake of silver nanoparticles in Daphnia magna. Environ Sci Technol 46, 11345-11351.

Chapter 2:

The use of a complex 3D tetra-culture alveolar model for the study of toxicological effects of nanoparticle (gold suspensions)

Melissa Saibene[1], Sebastien Cambier[2], Tommaso Serchi[2], Elisa Moschini[2], Patrizia Bonfanti[1], Anita Colombo[1], Paride Mantecca[1], Arno C. Gutleb[2]

[1]*Polaris Research Centre, DISAT, University of Milano – Bicocca (Italy)*
[2]*Environmental Group, ERIN Department, Luxembourg Institute of Science and Technology (Luxembourg)*

Paper in preparation

ABSTRACT

In the last decades the advancements of nanotechnologies lead to a massive increase of the engineered nanoparticles in our society and in consumers products, which, in turn, translates in an increased human and environmental exposure to nanomaterials. In the case of humans, inhalation can be considered the main exposure route, reason why lung toxicity studies should be considered a priority. Nanoparticles (NPs, < 100 nm), once inhaled, reach the alveoli, which are the lower part of the human air-ways. Alveoli, which are constituted by a thin barrier between the organism and the atmosphere, represent the first line of defense against airborne threats (e.g. pathogens and particulate matter) and allow for the gas exchange. Unfortunately, NPs are able to cross this barrier, enter the blood stream and reach other organs, exerting systemic effects. Generally, inhalation studies are performed *in vivo* to better mimic the human exposure. Nevertheless, the use of 3D *in vitro* models represents a valid and efficient alternative to predict the acute toxicity effects of inhaled substances on human health.

For the first time, we describe the effects of three different shaped gold nanoparticles (AuNPs) on a complex 3D *in vitro* alveolar tetra-culture model in which cells are maintained at Air-Liquid-Interface (ALI) and exposed to nebulized NP suspension by the VitroCell® Cloud System. The set of Pegylated AuNPs with comparable size included Gold Nano Spheres (GNPs), Gold Nano Rods (GNRs) and Gold Nano Stars (GNSs). 24 hour after exposure, the effects of AuNPs were evaluated in terms of viability, cytotoxicity, inflammatory response and uptake. In addition, the effects of lung surfactant on the AuNPs was evaluated.

Key words: alveolar tetra-culture, in vitro model, gold nanoparticles, nebulized nanoparticle suspension, air-liquid-interface, surfactant

1. Introduction

During the last decades, the increasing use of nanomaterials (NMs) in industrial processes and in consumers' products led to an increased exposure to these innovative materials for both humans and environment. Nowadays, NMs are present into a numerous consumers' products, despite their toxicological potential on human and environmental health still remains an open question (Vance *et al.*, 2015).

Concerning the human exposure, not all the possible exposure routes are considered to be relevant for human toxicity. It is well established that NMs are not able to cross intact epidermis and that the oral uptake is very little and limited to specific NMs (e.g. TiO_2). On the contrary, inhalation route is considered to be extremely relevant for NMs, especially in the occupational exposure scenarios, and, for this reason, lung toxicity studies should be considered a priority.

Depending on the particle dimensions, different tracts of the airways could be interested. Nanoparticles (NPs), which are defined as those particles with all the three external dimensions smaller than 100 nm), are able to reach the alveoli, which are the terminal part of the airways and represent the site of gas exchange (Oberdörster *et al.*, 2005). The alveoli constitute the main barrier between the systemic circulation and ambient air. Upon interaction with the air-blood barrier, NPs have the capability to cross it and reach the systemic circulation, especially when the agglomeration size of NPs is less than 100 nm but > 10 nm (Braakhuis *et al.*). Once the air-blood barrier is passed, NPs can reach other tissues, cause damage, and accumulate in target organs such as hearth, pancreas, kidney and spleen (Yacobi *et al.*, 2011).

Inhalation studies were generally performed *in vivo*, which has the advantage of allowing the direct investigation at organ and organism levels functions (Secondo *et al.*, 2017).

However, the discussion regarding the use of laboratory animals well discussed and summarized in the 3R strategy (Replacement, Reduction and Refinement) proposed by Russel and Burch (1959), place the development and proposal of alternative methods a real challenge to deal with nowadays.

The use of 3D *in vitro* models represents a valid and efficient alternative to predict the acute toxicity of inhaled substances (de Souza Carvalho *et al.*, 2014; Müller *et al.*). Recently, Secondo *et al.* (2017) compared studies *in vivo* and *in vitro* exposure to several NPs (silver, zinc oxide, titanium dioxide and multi-walled carbon nanotubes) observing that the responses in term of cytotoxicity and inflammation were similar.

It is in general well accepted that the introduction and the development of new *in vitro* realistic models could boost the reduction of animals used in toxicological studies, overcoming some ethical issues and decreasing the experimental costs.

However, it is necessary that the *in vitro* models that are to replace the experimental animals provide a certain level of realism and accuracy for the prediction of *in vivo* effects. The organ complexity is difficult to recreate *in vitro*, nevertheless co-culture 3D models represent a good compromise to predict NP inhalation effects.

To better understand the effects of NPs it is important to select the most suitable cell lines and exposure condition for the *in vitro* models. For instance, since NPs are able to reach the deepest lung part (alveoli), it is a good choice to focus the development of alternative *in vitro* models for inhalation nanotoxicology on *in vitro* Air-Liquid-Interface (ALI) alveolar models, making use of alveoli-specific cell lines.

In the last years, numerous 3D *in vitro* lung models have been proposed for inhalation toxicology studies. These models, more or less complex, mimic the tissue organization trying to modulate the response of the human lung tissue

(Blank *et al.*, 2006; Braakhuis *et al.*, 2016a; Kim and Ryu, 2013; Klein *et al.*, 2013; Rothen-Rutishauser *et al.*, 2005).

Since it is well known that different cell types communicate continuously with each other, testing NPs toxicity on monoculture does not seem the best choice, if the aim is to predict NPs toxicity at tissue level. For example, the presence of epithelial cells, e.g. A549 cells, or cells belonging to the immune system such as macrophages bring different response if taken as mono- or co-culture. Indeed, in a previous work, Klein *et al.* (2013) showed different responses of a mono-, bi- and tetra-culture after the same exposure conditions.

In vitro models could be composed by one or more cell lines, in submerged condition or at the ALI. Obviously, a 3D *in vitro* model that includes more than one relevant cell lines and exposed at the ALI provides more realistic conditions for the realistic characterization of the effects of inhaled particles (de Souza Carvalho *et al.*, 2014).

The ALI condition seems more sensitive and realistic than the submerged condition, even with comparable doses of exposure. One major difference between the submerged condition and the ALI condition is that, in "real life", inhaled particles would not encounter any liquid before they deposit on the alveolar membrane, which is covered with lung surfactant. On the contrary, in submerged conditions NPs will be dispersed in cell culture medium (CCM) prior of encountering the cells (Herzog *et al.*, 2013; Holder and Marr, 2013; Lenz *et al.*, 2013; Stoehr *et al.*, 2015).

The presence of CCM will change the NPs' properties, e.g. dimension (formation of aggregates) and will favour the formation of the protein corona modifying the surface of NPs and leading to a modulation of the NPs toxicity (Holder *et al.*, 2008). In other terms, the ALI condition mimics better the inhalation scenario and holds the promise of providing more reliable results (Mülhopt *et al.*, 2016).

The alveolar surface is characterized by the presence of surfactant, a thin layer of surface-active lipid-protein material that protects the cells. Its main function is to reduce the surface tension at the air-liqiuid-interface preventing the lung collapse and favouring the gas exchange. It is approximatively composed by lipids (90%) and protein (10%) (Hidalgo *et al.*, 2015). The large presence of macromolecules in the surfactant could modify the aggregation state of the NPs. For this reason, in our study we decided to characterize NPs, in term of dimension and aggregate formation, after 1 hour of incubation with a lung surfactant (poractant alfa, CUROSURF®, which was kindly provided by Chiesi Pharmaceutic).

Among the most used particles there are the Gold NPs (AuNPs), which find applications in in cosmetic products and in the health field (Vance *et al.*, 2015). Due to their biocompatibility, AuNPs are also the most NPs used in nanomedicine as potential nanocarrier for active principles (drug delivery), as nanosensor, in photothermal therapy or tracking (Fytianos *et al.*, 2015).

In our study, for the first time, the complex 3D *in vitro* alveolar model proposed by Klein *et al.* (2013) is used to assess the toxic potential on the human respiratory system of three different shaped AuNPs. The model is composed by four different cell lines: endothelial cells (EA.hy296), epithelial cells (A549), mast cells (HMC-1) and macrophage-like cells (differentiated THP-1 cells); cells were grown at the ALI on Transwell inserts and exposed to nebulized AuNP suspensions using the VitroCell® Cloud System.

The AuNPs used in this study have been prepared endotoxin-free, suitable for biological application, ensuring solubility in water and stability in biologically relevant media. The set of Pegylated AuNPs with comparable size (around 60 nm) included Gold Nano Spheres (GNPs), Gold Nano Rods (GNRs) and Gold Nano Stars (GNSs). AuNPs were produced within the framework of the FP7 project FutureNanoNeeds, coordinated by Prof. Kenneth Dawson (UCD – Dublin, Ireland).

After 24 hour of exposure viability, cytotoxicity (levels of Lactate Dehydrogenase, LDH), release of Interleukin-8 (IL-8), NP presence and uptake were evaluated.

2. Materials and Methods

2.1 Reagents

All reagents were purchased from Sigma Chemical (Deisenhofen, Germany). Cell culture media and DPBS were purchased from Invitrogen (the Netherlands), fetal bovine serum (FBS Superior) was obtained from Biochrom (Berlin, Germany).

Transwell inserts – Millicell® Hanging Cell Culture Inserts (pore membrane diameter of 1µm) were acquired from Millipore (Merck Chemicals N.V./S.A., Belgium).

Curosurf® (80 mg/mL of phospholipid fraction from porcine lung – poractant alfa) was kindly provided by Chiesi Pharmaceutic (Parma, Italy).

The AuNPs were produced by the Fachbereich Physik laboratory (Philipps University of Marburg, Marburg, 35037, Germany).

AgNPs coated with Citrate were from nanoComposix (40 nm Citrate BioPure™ Silver), while PEG coated AgNPs were produced by Material Research and Technology (MRT Department of the Luxembourg Institute of Science and Technology – LIST).

2.2 NP Synthesis and Characterization

AuNPs were prepared in liquid format, NPs were dispersed in sterile MilliQ water (Talamini *et al.*, 2017). This set of AuNPs included three different shaped NPs: Au-spheres (GNPs), Au-rods (GNRs) and Au-stars (GNSs).

NP suspensions were characterized in MilliQ water and in Curosurf® (data not complete – in preparation) diluted 50 times in DPBS (incubation time: 1 hour).

The observations were performed with the ORION Helium Ion Beam (ORION-HIM, Zeiss) to observe NP shape and aggregation, Transmission Electronic Mycroscope (TEM, Jem Jeol 1400-plus) to obtain information regarding shape and size, Dynamic Light Scattering (DLS, Malvern Zetasizer Nano ZS) in order to characterize our NPs in term of size (hydrodynamic diameter).

NP were also characterized observing their aggregate state and their spectra. Suspensions were prepared in DPBS and Curosurf® (diluted 50 times in DPBS and incubated for 1 hour), then mounted on a microscope slide with Mowiol, covered with a microscope cover slide and observed under the Enhanced Dark Field Microscope (CytoViva®).

2.3 Aerosol Exposure and NP Suspension preparation for Vitrocell® Cloud System

Vitrocell® Cloud System (6-well model) was used to nebulize NP suspensions and expose cells. This system is designed for dose-controlled and spatially uniform deposition of liquid aerosols on cells cultured at the air/liquid interface (ALI) allowing a screening and toxicity testing of inhaled substances including NP suspensions.

System specifically designed for dose-controlled and spatially uniform deposition of aerosols from liquids and suspensions on cells cultured at the air/liquid interface.

NP suspensions were prepared diluting the suspensions in order to obtain concentrations of 0.34 or 1.7 $\mu g/cm^2$ – concentration comparable with a dilution of 0.5 and 1 $\mu g/mL$ in hypothetic submerged condition. The suspensions were diluted with DPBS 0.5X. The same solution used as Negative Control. After 24 hours after exposure the tetracultures were used for further analysis.

Silver Nitrate and Silver NPs (40 nm), coated with Citrate or PEG ($0 - 0.01 - 0.1 - 1$ µg/cm^2, supplementary data) were used as an internal positive control to confirm the efficiency of the tetraculture model in term of viability, cytotoxicity and inflammation (supplementary material).

2.4 Cell Culture

The human cell lines A549 (Lieber *et al.*, 1976), THP-1 (Tsuchyia *et al.*, 1980) and EA.hy926 (Suggs *et al.*, 1986) were obtained from the American Type Culture Collection (Manassas, VA, USA). HMC-1 (Butterfield *et al.*, 1988) cells were kindly provided by J.H. Butterfield, Mayo Clinic (Rochester, MN, USA). As reported in Klein *et al.*, 2013, cells were cultured using different media and they were seeded at specified densities (cells/cm^2) on Millicell® Hanging Cell Culture Inserts (surface area of 4.5 cm^2; 1 µm pore size; high pore density PET membranes for 6-well plates; Millipore) and grown until confluency. Inserts were placed in culture plates (6-well plates; Millipore) with 1.5 mL medium in the upper and 1.5 mL in the lower compartment.

EA.hy926 and A549 cells were grown in T75 flasks and trypsinized twice a week. THP-1 and HMC-1 cells were recovered and count two times per week. Cells were maintained in a humidified atmosphere with 5% CO_2 at 37°C.

2.5 Differentiation THP-1

Human THP-1 cells (human acute monocytic leukemia cell line; Tsuchyia *et al.*, 1980) were grown in RPMI 1640 media containing 10% (v/v) FBS Superior. Differentiation process was achieved resuspending THP-1 cells at 4×10^5 cells/mL in cell culture medium with addition of phorbol-12-myristate-13-acetate (PMA; 20 ng/mL) and incubation at 37°C and 5% CO2 overnight. PMA was prepared as a stock solution (10 mg/mL) in ultrapure absolute ethanol. Stocks

were kept at −20°C in the dark. Differentiated THP-1 cells were rinsed with DPBS and detached by using Accutase in order to harvest them.

2.6 Tetraculture Model

The tetraculture was prepared according to Klein *et al.* (2013). EA.hy 926 endothelial cells were seeded on inverted transwell inserts (2.4×10^5 cells/cm^2; Millipore, 1 μm pore size). After cell attachment on the basolateral side of the transwell insert the plate with the transwell inserts was turned back to its original orientation and A549 cells were seeded inside the transwell (1.2×10^5 cells/cm^2). Epithelial and endothelial cells were grown for three days at 37°C and 5% in a humidified incubator. On day 3 THP-1 cells were stimulated to differentiate into macrophage-like cells by addition of PMA, as previous described. On day 4, Macrophage-like cells and HMC-1 cells were added into the inserts (2.4×10^5 cells/cm^2 and 1.2×10^5 cells/cm^2, respectively) with A549 and EA.hy 926 cells to complete the tetraculture system. The medium for the complete tetraculture contained 1% FBS in order to avoid extensive proliferation of HMC-1 cells. Upon the attachment of Macrophage-like cells and HMC-1 cells, the medium was removed from the upper compartment and the tetraculture was cultivated at the ALI condition for 24 h before the exposure.

2.7 Viability Assay

Tetraculture were exposed to AuNPs, AgNPs and AgNO$_3$ for 24 hours and then basolateral medium was recovered and stored at -20°C to perform further analysis. A working solution of Resazurin (400 μM) was prepared in CCM and 1.5 mL were added in both insert sides (apical and basolateral). The plates containing the inserts were incubated in a humidified atmosphere with 5% CO$_2$ at 37°C for 2 hours. At the end of the incubation 100 or 200 μL of CCM and Resazurin were transfered in a 96 well plate and the fluorescence was read by a

Microplate reader (TECAN), using an excitation wavelength of 530 nm and an emission wavelength of 590 nm. Cell viability was calculated as percentage compared to Negative Control group: [(Sample Fluorescence Intensity/ Negative Control Fluorescence Intensity) *100]. Results are the average of at least three different biological replicate.

2.8 Cytotoxicity Assay

Basolateral medium recovered after 24 hours of treatment with AuNPs and AgNPs were used to perform a cytotoxicity assay measuring the release of Lactate Dehydrogenase (LDH) with CytoTox-ONE™ (Promega), following manufacturer's instruction. For this purpose, 50 µL/ of basolateral surnatant were used. The fluorescence was read by a Microplate reader (TECAN) using an excitation wavelength of 530 nm and an emission wavelength of 590 nm. Cytotoxicity was calculated as a percentage compared to the Maximum Level of LDH Release: [(Sample Fluorescence Intensity – CCM Background)/ (Negative Control Fluorescence Intensity – CCM Background) *100]. Results are the average of at least three different biological replicate.

2.9 Inflammation Response

Inflammatory response was evaluated by quantification of the released Interleukin-8 (IL-8). IL-8 release was measuring by ELISA Assay (ENZO Kit) after 24 hour of exposure to AuNPs, AgNPs. Quantification of IL-8 was performed on XX µL of basolateral surnatant following the kit manufacturer's instruction. The optical density (OD) was read by a Microplate reader (TECAN) at 450 nm. The net OD for each read of the standard was plot against IL-8 known concentration in to obtain a linear correlation curve and calculate the concentration of IL-8 in the samples by interpolation. Concentrations outside the

standard curve were not taken in account. Results are the average of at least three different biological replicate.

2.10 Tetraculture morphology and interaction with NPs.

Cells of both compartments (apical and basolateral) were fixed in Glutaraldehyde (2 % in DPBS) overnight at 4°C after 24 hours of treatment. Glutaraldehyde was removed and the inserts washed with DPBS three times. Then they were post-fixed with a solution of OsO_4 (1% in DPBS) for 1 hour in the dark at 4°C, after that the OsO_4 solution was removed and the inserts washed three times with DPBS. Dehydration of the samples was achieved with increasing concentration of ethanol (30% - 50% - 70% - 90 % - 100%). Dehydrated samples were stored in absolute ethanol until the metallization step. At the end the membranes were detached from the plastic holder, mounted on silica stubs, covered with a Platinum film and observed under the ORION-Helium Ion Microscope (ORION-HIM Zeiss) modified with a Secondary Ion Mass Spectrometer detector (Wirtz *et al.* 2016) (data not shown – in preparation).

2.11 Au-NP Uptake

24 hours after exposure to AuNPs, inserts were gently washed 2 times with DPBS (both apical and basolateral side) to get rid of non-internalized particles from the surface. Then cells were Trypsinazed and recovered with cell culture medium (CCM). After centrifugation, 5 minutes x 150g, CCM was removed and cells were resuspended in DPBS to be counted. A second centrifugation was necessary to compact again the pellet and samples were stored at -20°C until the following step. For sample destruction 200 µL of aqua regia were added onto the cell pellets. Thereby 50 µL HNO3 were added first, lightly swirling the tube until an equal distribution of the HNO_3 throughout the cell pellet is obtained, followed by

adding 150 µL HCl. Then the samples were shaken on a rotating plate for at least 4 hours; after that, 800 µL of 2% HCl were added.

2.12 Global Transcriptomic Analysis

24 hours after exposure, inserts were gently washed to get rid of non-internalized particles from the surface. Using a lysis buffer (Buffer RLT, QIAGEN®) cells were disrupted and recovered. After disruption, recovered material was immediately frozen in liquid Nitrogen and stored at -80°C for few days. mRNA was purified and stored at -80°C until the next step, following the protocol provided with the QIAGEN® – RNA purification kit.

1 µL of each single replicate was checked in term of quantity with the NanoDrop spectrophotometer (Thermo Fisher) and another 1 µL of the same samples was used to verify also the RNA quality by the BioAnalyzer (Agilent Genomics). RNA quality was considered acceptable with RIN values above 9 and quantity higher than 100 ng (data not shown – in preparation).

2.13 Statistical Analysis

Data on tetraculture viability are reported as average percentages compared to the control group plus standard error; statistical analysis were performed by ANOVA followed by the LDS Test.

Data on cytotoxicity and inflammation are reported as mean threshold compared to the control group plus standard error; statistical analysis were performed by ANOVA followed by the LDS Test.

Uptake data (ICP-MS analysis) are reported as mean values ± Standard Error and the statistical analysis were performed by unpaired T-Test.

3. Results

3.1 AuNP suspensions

The suspension analysis by ORION-HIM confirmed the different shape of the three AuNPs used in this work: GNPs, GNRs and GNSs (Figure 1, a-c). The suspensions were also prepared in Surfactant (Curosurf®, Chiesi Pharmaceutic); in the second condition, GNRs and GNSs appeared more aggregate and it was also possible to observe the relevant present of the phospholipids, the major component of the surfactant, on the stub surface (Figure 1, d-e).
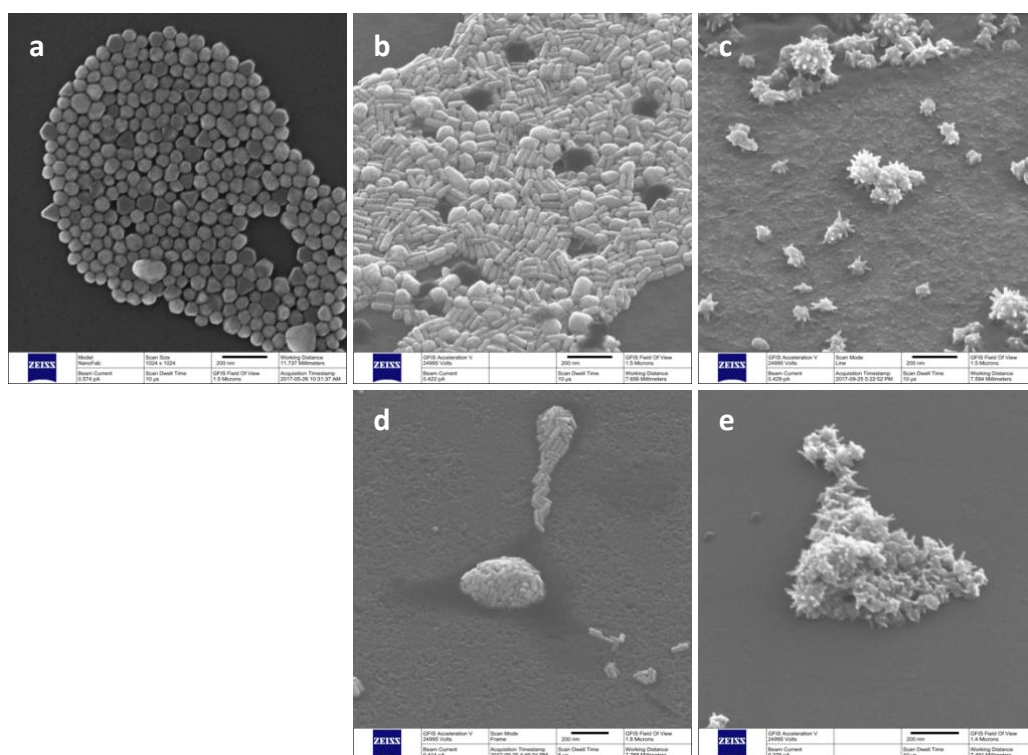
Fig.1: Images of uspensions prepared in MilliQ water (0.5 mg/ml) and the same suspensions incubate 1 hour in Curosurf® diluted with DPBS 0.5X (concentration corresponding to 0.34 or 1.7 µg/cm²) under the ORION-Helium Ion Microscope.

The suspensions were also characterized by TEM and DLS, the following dimensions were calculated: 18.44 ± 6.4 nm for the GNPs, 59.99 ± 7.3 nm for

the GNRs and 63.43 ± 2.35 nm for the GNSs (supplementary materials, Figure S1, S2, S3).

For AuNPs suspensions, a preliminary screening of NP spectra was performed under the Enhanced Dark Field Microscope (CytoViva® - Figure 2). Suspensions were prepared, both in DPBS (Figure 2 a-c, same preparation used for Aerosol Exposure) and in Curosurf® (Figure 2, d-f). The suspensions prepared in DPBS appeared well distributed and disperse, while the suspensions prepared in Curosurf® showed big agglomerates, probably due to the massive presence of phospholipid in the surfactant, as observed also with the ORION-HIM.
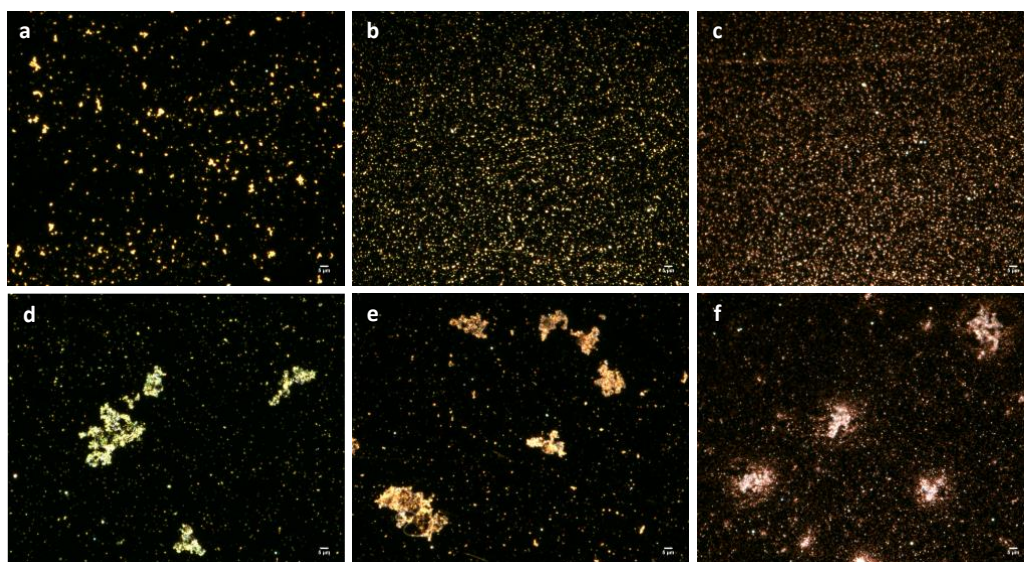
Fig.2: Suspensions prepared in DPBS 0.5X and mounted with Mowiol (a-c) and the same suspensions incubate 1 hour in Curosurf® diluted with DPBS 0.5X (d-f, final concentration corresponding to 0.34 or 1.7 µg/cm²) observed under the CytoViva® microscope (scale bar: 5 µm).

Thanks to the Enhanced Dark Field Microscope (CytoViva® - preliminary data) it was possible also to analyse the GNRs and GNSs spectra (Figure 3). It was clearly confirmed the Au spectrum for the NPs, but, interestingly, the two different shapes showed a slight modification of the peak (Figure 3 a and b).

These little differences are due to different shape of our NPs. The suspensions of GNSs were also observed after incubation (1 hour) with Curosurf® (Figure 3 c). In this case the NP agglomeration caused by the incubation with the surfactant modify the spectra compared to the spectra obtained with the suspensions prepared in DPBS.
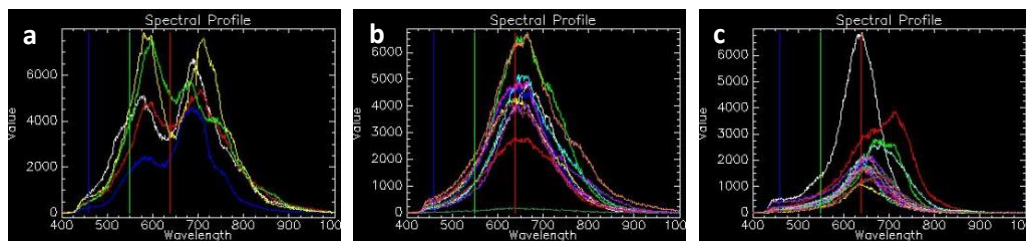
Fig.3: GNR and GNSs spectra. The suspensions were prepared in DPBS 0.5X and mounted with Mowiol (a and b) and the same suspensions of GNSs incubate 1 hour in Curosurf® diluted with DPBS 0.5X (c), final concentration corresponding to 0.34 or 1.7 µg/cm^2) observed under the CytoViva® microscope.

3.2 Tetraculture Viability

The viability of the tetraculture was evaluated incubating cells (both apical and basolateral side) with a solution of Resazurin in CCM (working concentration of 400 µM, from a stock solution of 20 mM) and measuring the fluorescence of the metabolized compound in the aliquot of culture medium recovered.

After 24 hours the triculture (A549, Macrophage-like cells and HMC-1) viability in the apical side showed a significant difference after exposure to GNPs at the concentration of 1.7 µg/cm^2 (Figure 4a). Treatment with the other AgNPs (GNRs and GNRs) at all concentration tested did not result in decrease of cell viability 24 hours after exposure.

Treatment with AgNPs (all shape and concentrations) did not have any significant effect on cell viability on endothelial cells (basolateral compartment) as compared to the negative control (Figure 4b).
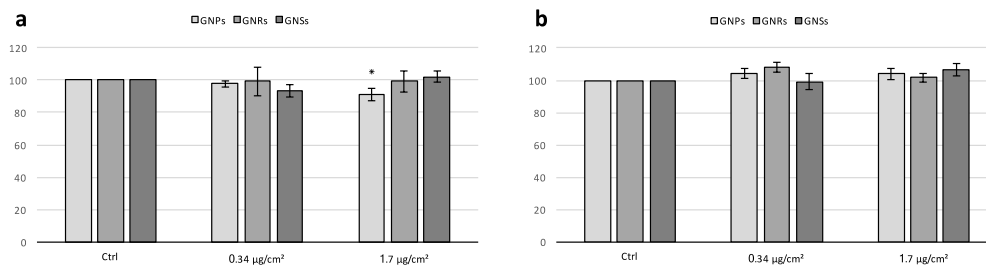
*Fig.4: Histograms showing the tetraculture viability evaluated by measuring the fluorescent signal of the metabolized Resazurin after 24 hours of exposure to AuNPs (0 – 0.34 – 1.7 7 µg/cm²) in the Apical (a) and Basolateral (b) side of the model. * statistically significant increase versus control (p<0.05, ANOVA + Dunn's test).*

To verify the efficiency of the *in vitro* model after exposure to metal NPs, the tetraculture was also exposed to Silver NPs (AgNPs, 40 nm), coated with Citrate or PEG (Cit-AgNPs and PEG-AgNPs, 0 - 0.01 - 0.1 - 1 µg/cm²). In these case significant differences were observed among the control group and exposed tetracultures to 0.1 and 1 µg/cm² Cit-AgNPs and $AgNO_3$ in the basolateral side and only to 0.1 and 1 µg/cm² Cit-AgNPs in the apical compartment (supplementary material, Figure S4).

3.3 Cytotoxicity of AuNPs

In order to evaluate the cytotoxicity of AuNPs, basolateral medium recovered after 24 hours of treatment was used to measure the release of Lactate Dehydrogenase (LDH – Figure 5); when the integrity of the membrane is compromised, after exposure to cytotoxic compound, cells release in the medium this enzyme. LDH is used as a marker for cytotoxicity since it is quite stable and present in every cell. It is possible to observe a significant increase in the level of LDH after the exposure to the highest dose (1.7 µg/cm²) of all AuNPs. In the case of GNSs there was a statistical relevant increase also after the exposure to the lower dose (0.34 µg/cm²) compare to the control group.
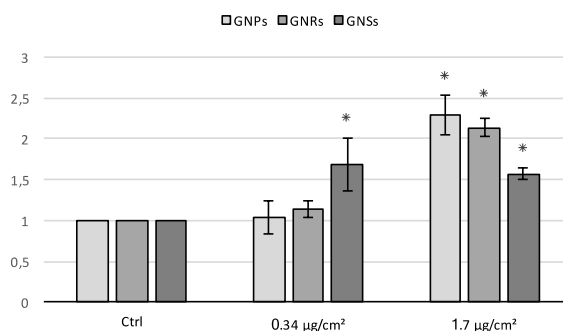
*Fig.5: Histograms showing the levels of LDH (Lactate Dehydrogenase) in the basolateral compartment after 24 hours of exposure to AuNPs (0 – 0.34 – 1.7 7 μg/cm^2) in order to evaluate the cytotoxicity of the treatments. * statistically significant increase versus control (p<0.05, ANOVA + Dunn's test).*

Also in the case of the cytotoxicity parameter the tetraculture was exposed to Cit-AgNPs, PEG-AgNPs and AgNO$_3$ (0 - 0.01 - 0.05 - 0.1 - 0.5 - 1 μg/cm^2); the response is different compared to the AuNP exposure, once again the model shown its efficiency (data not

shown – supplementary material, Figure S5). Surprisingly, while AgNPs induced a higher reduction of cell viability as compared to AuNPs, they also seem to induced less cytotoxicity, indicating a different mechanism of toxicity as than AuNPs.

3.4 Endothelial inflammatory response of tetraculture in the basolateral side

The endothelial inflammatory response was evaluated measuring the release of Interleukin-8 (IL-8) in the basolateral side by performing an ELISA Assay (Figure 6).

The level of IL-8 in the basolateral side increased after exposure to the lower dose (0.34 μg/cm^2) of GNPs and GNSs. No statistically differences were observed after exposure to the highest doses (1.7 μg/cm^2) for any of the tested particles and, in addition, no significant differences were observed after exposure

to both doses of GNRs, while this particle induce significant cytotoxicity after 24 hours of exposure to 1.7 µg/cm².
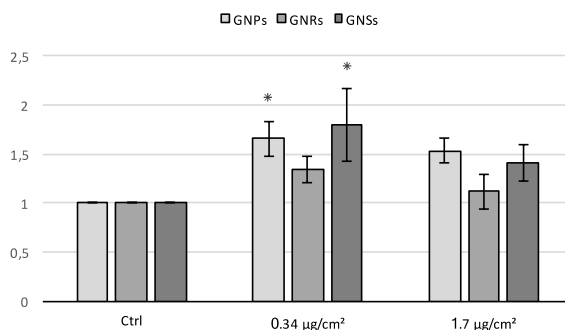
*Fig.6: Histograms showing the levels of Interleukin-8 (IL-8) in the basolateral compartment after 24 hours of exposure to AuNPs (0 – 0.34 – 1.7 7 µg/cm²) to evaluate the inflammation response of the tetraculture. * statistically significant increase versus control (p<0.05, ANOVA + Dunn's test).*

The exposure to AgNPs (0 - 0.01 - 0.05 - 0.1 - 0.5 - 1 µg/cm²) seemed to do not cause an increase of the inflammation level in the basolateral side of the inserts (supplementary material, Figure S6).

3.5 Tetraculture morphology and its bio-interaction with AuNPs

The cells surface was observed under the ORION-HIM to better characterize the interaction between cells and NPs and eventually changes in cell morphology caused by these interactions (data not shown – in preparation).

3.6 AuNP uptake by coculture (A549, Macrophage-like cells and HMC-1) in the apical side and translocation through the model to the endothelial cells in the basolateral side

NP uptake was evaluated measuring the amount of Au in cells by ICP-MS. The apical and basolateral compartment were analysed separately in order to evaluate not only the uptake by the entire tetraculture (given by the sum of Au at the apical

side + the amount at the basolateral side), but also the eventual translocation of NPs in the basolateral compartment (endothelial cells, Fig. 7 b). The amount of gold (pg) was normalized on the number of cells recovered in each insert compartment and it is expressed as picograms of gold per cell (pg/cell).
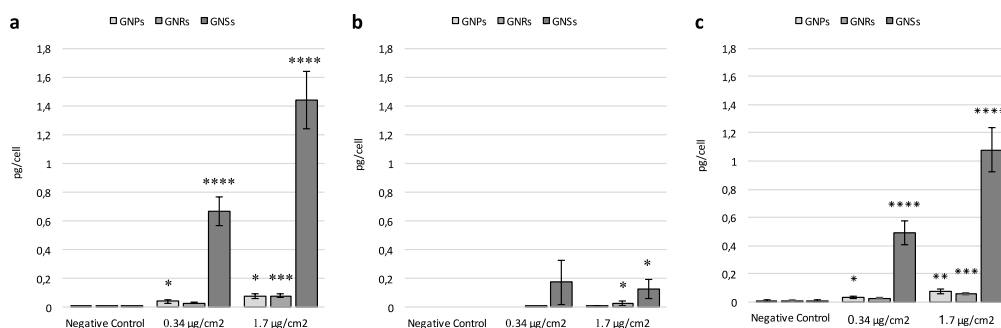
Fig.7: ICP-MS analysis to evaluate the amount of gold in the apical (a), in the basolateral (b) side of the tetraculture model and the total amount considering apical and basolateral sides together (c). The data are expressed in picograms of gold per cell (pg/cell); values under the lower instrument limit of detection were considered as null values, <1.25 ng. Statistical analysis performed by T-Test versus control (* p<0.05; ** p<0.01; *** p<0.001; **** p<0.0001).

In the apical side (Figure 7 a), after 24 hours of exposure to GNPs a significant Au uptake was measured in the after exposure to both doses ($p < 0.05$). Regarding the exposure to GNRs, there is a very significant gold amount only after treatment with the higher dose (1.7 µg/cm^2). After exposure to GNS, we observed a clear dose-dependent uptake: at 0.34 µg/cm^2 we observed an average uptake of 0.665 pg/cell while after exposure to 1.7 µg/cm^2 the uptake increased reaching 1.439 pg/cell, resulting with a very high statistical significance ($p < 0.0001$).

Au was also detected in the basolateral compartment (Figure 7 b), confirming that there is a translocation of GNRs and especially GNSs through the insert membrane and the different cell lines. Au translocation, similarly to uptake, seems to be shape-dependent and dose-dependent. However, the high standard

deviation due to the low amounts detected in the basolateral compartment do not allow to confirm for the dose-dependent relationship in Au translocation.

Then we calculated also the total amount of gold considering all the cells present in the tetra-culture, considering apical and basolateral sides together (Figure 7 c). The graph shows as the trend is completely compared to the data regarding the apical side.

4. Discussion

During the last decades we witnessed the explosion of the nanotechnology field. Nowadays, NMs are present into a numerous consumer product but their toxicological potential on human and environmental health is still an open question (Vance *et al.*, 2015).

Focusing on the human exposure it is well known that the principal route of exposure is represented by inhalation.

NPs are able to reach the alveoli, site of gas exchange and last part of the air way tract representing the thinnest barrier between air and organism (Oberdörster *et al.*, 2005). NPs have the capability to cross the air-blood barrier interacting with alveolar cells (Braakhuis *et al.*, 2016b). Once the air-blood barrier is passed, NPs have the potential to reach some other tissues through the circulatory system and accumulate in target organs such as hearth, pancreas, kidney and spleen (Yacobi *et al.*, 2011).

Inhalation studies were generally performed in *in vivo* condition, to better resemble the real situation of exposure and the organ complexity (Secondo *et al.*, 2017). Nevertheless, the use of 3D *in vitro* models represents a valid and efficient alternative to predict the acute toxicity effects of inhaled substances and particles on our health (de Souza Carvalho *et al.*, 2014; Müller *et al.*, 2011). Additionally, new *in vitro* model, even more complex, could enhance the reduction of

experimental animals used in toxicological studies, overcoming some ethical issues and decreasing the experimental costs. Some different models are available today for the toxicological screening of several compounds, NP suspensions included (Alfaro-Moreno *et al.*, 2008; Blank *et al.*, 2006; Braakhuis *et al.*, 2016a; Kimlin *et al.*, 2013; Rothen-Rutishauser *et al.*, 2005).

AuNPs are known for their biocompatibility and their large use in biomedical application (Fytianos *et al.*, 2015). Studies available in literature are especially regarding the uptake and bio-interaction of AuNPs on monoculture (Chithrani *et al.*, 2006). Only publications are reporting the effects on more complex system as co-culture models (Braakhuis *et al.*, 2016a).

Our study is the first describing the effects of three different shaped AuNPs on a complex 3D *in vitro* alveolar model. The complexity of the model represents a good compromise for predicting NPs' effects upon inhalation. AuNPs were nebulized by the VitroCell® Cloud System at ALI condition, which ensure that no undesired modification is introduced at the NPs' surface due to interaction with media (e.g. CCM) prior of reaching the cells.

The first version of the system used in this study was proposed by Alfaro-Moreno and colleagues (2008). In that model a co-culture of A549, THP-1 and HCM-1 was seeded on the bottom of the well, while the endothelial cells were seeded at the apical side of transwell insert membrane. With this organization, not only the insert membrane, but also a layer of CCM separated the triculture from the endothelial layer. In the modified version (Klein *et al.*, 2011) the same tri-culture is seeded onto the porous membrane on the apical side of the insert and the endothelial cells are placed on the basolateral side of the same insert membrane. This new arrangement allowed to better mimic the *in vivo* anatomy of the alveolar region.

Even so, the model presents the ratio of A549, THP-1 and HMC-1 cells not so close to the physiological situation. The seeding ratios are most likely not

resembling the *in vivo* condition because there might be an overrepresentation of macrophage-like cells (Thorax, 1992) and mast cells (Heard, 1989), compared to endothelial and epithelial cells. The rationale for this seeding ratios is mainly based on methodological arguments. The protocols necessary to study the tetraculture response after exposure require a higher number of cells than the physiological condition. The same happens when applying -omic techniques, such as transcriptomics, that require higher quantities of cells. In order to reduce the technical complexity of such experiments, the authors decided to increase the number of immune cells present in the system (Klein *et al.*, 2013).

ALI exposure avoids the interaction between NPs and CCM, preventing eventually surface modification or the formation of a massive protein corona. It is already established the CCM has the ability to modify the NP surface, modifying at the same time their toxicological potency (de Souza Carvalho *et al.*, 2014; Fleischer and Payne, 2014). The ALI condition mimics better the inhalation situation (Mülhopt *et al.*, 2016).

Additionally, cells cultured at the ALI were expose directly to nebulized NP suspensions with the VitroCell® Cloud System.

VitroCell® Cloud System allowed to expose cells cultured at the air/liquid interface directly to nebulized NP suspensions (known concentration – homogeneous deposition). This system has been specifically designed for dose-controlled and spatially uniform deposition of aerosols from liquids and suspensions. In this way is possible the screening of inhaled drugs and to perform toxicity tests of inhaled substances including nanoparticle suspensions.

The alveoli surface is characterized by the presence of pulmonary surfactant, a thin layer protecting cells and preventing the lung collapse (Hidalgo *et al.*, 2015). Since, in the tetraculture, the alveolar epithelial cells (A549) are able to produce and secrete surfactant (Klein *et al.*, 2017; Klein *et al.*, 2013); we decide to characterize AuNPs after incubation (1 hour) with a surrogate of human lung

surfactant (poractant alfa, CUROSURF®, Chiesi Pharmaceutic). All AuNPs incubated with lung surfactant appeared more aggregate and it was possible to observe the presence of a biological matrix, possibly composed by phospholipids that are the major component of the surfactant, that binds together the NPs (Figure 1, d-f and Figure 2, d-f).

In the lungs, the formation of agglomerate presumably decreases the toxicity of NPs, as they can be more easily uptaken by the macrophages and removed from the alveolar region (Holder *et al.*, 2008).

The most abundant size of air-borne and bacterial pathogens is in the range of 1 to 4 µm. Since the pathogen clearance is the main macrophage function, they better recognise and capture bigger particles than smaller particles (Champion *et al.*, 2008).

Gold NPs use in cosmetic products and health applications (Vance *et al.*, 2015). They also represent the most used NPs in nanomedicine. AuNPs are considered as one of the most promising nanocarriers,

due to their biocompatibility, and they are intended for use in sensing, photothermal therapy, tracking and drug delivery (Fytianos *et al.*, 2015).

The advanced tetraculture *in vitro* alveolar model proposed by Klein *et al.*, (2011) was used in this work to assess for the first time the effects induced by nebulized AuNPs of different shapes on human lungs.

The viability of the model was evaluated incubating cells (both apical and basolateral side) with a solution of Resazurin in CCM; active and viable cells are able to internalize and metabolize this blue dye, which becomes fluorescent. By measuring the fluorescence of the metabolized compound, it is possible to obtain information regarding the cell metabolism, considered as an index of cell viability. Endothelial cells were not affected in term of cell activity and no significant differences could be observed after 24 hours of treatment (Figure 4b).

Instead, in the apical side after exposure to 1.7 μg/cm^2 of GNPs a significant decrease of viable cells was detectable compare to the control group (Figure 4a). The reduced viability indicates that one or maybe more cell lines is affected by the treatment with GNPs. Unfortunately, it is not possible to figure out which cell line is mainly involved in this process. Maybe, the activation of macrophage-like cells, involved in the NPs phagocytosis, and the granulation of the mast cells in response to an inflammatory state (Figure 6) contribute to create a stressful environment for A549 cells. However, in this case one could expect a higher inflammatory status at the 1.7 μg/cm^2 dose and, in parallel, stronger decrease of cell viability at 0.34 μg/cm^2. The decrease in term of viability probably is not observed at the highest dose (1.7 μg/cm^2) because in this case prevail the cytotoxic aspect of all AuNPs (Figure 5). Another possible explanation of absence of decrease of cell viability could be due to a false positive result, due to interferences from the AuNPs, which are fluorescent at similar wavelengths of the resazurin.

Our results demonstrate that AuNPs (GNPs, GNRs and GNSs) exposure, after 24 hours, has the potential to cause cytotoxicity and inflammation.

Cytotoxicity was evaluated in term of release in the CCM of LDH, which is subsequent to damages to the cell membranes. In order to evaluate the cytotoxicity of AuNPs, basolateral medium recovered after 24 hours of treatment was used to measure the release of LDH (Figure 5).

The Lactate Dehydrogenase is an oxidoreductase enzyme involved in the cellular respiration that catalyses the transformation of the pyruvate in to L-Lactate, involving the reduction of NADH to NAD$^+$. This enzyme is ubiquitary and it is quite stable, principally for these reasons LDH is often use as a marker of cytotoxicity. The release in the media of this enzyme is an index of compromised cell membrane and, consequently.

In our experiments, it is possible to observe a significant increase in the level of LDH after the exposure to the highest dose (1.7 µg/cm^2) of all AuNPs. In the case of GNSs there was a relevant statistical increase also after the exposure to the lower dose (0.34 µg/cm^2) compared to the control group.

The high levels of LDH are index of cell death. Unfortunately, it is not possible to distinguish which cell lines are involved in this process and the cytotoxicity can only be considered as a "tissue response".

It is well established that inflammation is the main response after exposure to NPs (Nel *et al.*, 2006; Shrivastava *et al.*, 2016; Srivastava *et al.*, 2012; Yen *et al.*, 2009). IL-8 was chosen to evaluate the inflammatory response of the model. IL-8 is a chemoattractant cytokine produced by a variety of tissue and blood cells. Unlike many other cytokines it has a distinct target specificity for the neutrophil, with only weak effects on other blood cells (Bickel 1993). Many different cells have the ability to produce IL-8 when appropriately stimulated. The expression of IL-8 mRNA and the release of the biologically active cytokine was observed in endothelial cells, fibroblasts from different tissues, keratinocytes, synovial cells, chondrocytes, several types of epithelial cells as well as some tumour cells. Interestingly, even neutrophils can synthesize IL-8, and may thus intensify their own recruitment to sites of inflammation (Baggiolini and Clark-Lewis, 1992).

The inflammatory response maybe is due to the epithelial cells that are suffering after the exposure to AuNPs. The released IL-8 can activate macrophage-like cells, which, in turn, can release additional IL-8 as a response to the inflammatory state. *In vivo,* this mechanism has the physiological function to beckon *in situ* other macrophages and immune cells cells to better react to the treat.

GNRs do not cause decrease in term of viability (both sides of the insert), no release of IL-8 and no cytotoxicity, if not only at the highest dose. Rod-like NP seem not able to cause cell membrane damages. In this case, the dose seems to play a key role in cell response after 24 hours of exposure.

GNSs probably cause serious damages at the cell membrane level with their numerous tips, peculiarity of their star-like shape. Tips can cause physical damages, disrupting the cell membrane during the interaction cell-NPs. Indeed, no differences between the doses of exposure were observed.

Concerning the GNPs, they caused a decreasing of viability and an increasing of cytotoxicity after exposure to the highest dose, while the release of IL-8 was significant only after exposure to 0.34 $\mu g/cm^2$. We can hypothesize that the effects are dose-dependent, the lowest dose bring only an inflammation response that culminate into a decrease of viability and simultaneously a high LDH release increasing.

AuNP uptake, which is the amount of gold internalized by cells, was evaluated by the ICP-MS technique. This technique allowed detecting the amount of the studied element in the samples, in our case Au.

Chu *et al.* (2014) assessed various particles, including large (150 nm) Gold Nano Star (AuNST) and Gold Nano Sphere (AuNSP) in their work. The authors demonstrated that, because of their sharp surface structures, nanostars could readily disrupt the endosomal membranes of human liver carcinoma cells and reside in the cytoplasm for an extended period, irrespective of their surface compositions, charges, materials, and sizes. Alternatively, following endocytosis, nanospheres would reside in the endosomes of the cells under stable conditions, where they would adapt with endosome maturation or be easily excreted by exocytosis.

In one other paper, (Favi *et al.*, 2015) hypothesized that the potential mechanism of cell death by the synthesized AuNSTs is that the nanoparticles enter the cells via endocytosis (Chu *et al.*, 2014), concentrate in the nuclei (Romero *et al.*, 2014) and in the cytoplasm (Chen *et al.*, 2013; Dam *et al.*, 2012), and induce dose-dependent cell death via mechanical damage (Kodiha *et al.*, 2015). Additional AuNST optimization for future research consideration is to synthesize AuNSTs

with controlled size distribution, branch length and number of branched tips, and analysed the effect of these modified AuNST on cells and on native tissue. Controlling the size distribution, branch length, and the number of branched tips of these AuNSTs has the potential to enable further tuning of the optical properties for the AuNSTs for potential medical detection and treatment.

The level of cellular uptake does not simply depend on surface area or charge, but also on the the shape, which is another important factor in determining the level of uptake (Niikura *et al.*, 2013). Comparing rod-like and spherical AuNPs, the first ones were the most efficiently uptaken. This results are in agreement with our data in which comparing only the uptake of GNPs and GNRs, the amount of gold in cells expose to GNRs is higher, compared to the exposure to the spherical counterpart.

(Xie *et al.*, 2017) evaluated the intracellular concentrations of gold by the inductively coupled plasma atomic emission spectrometer (ICP-AES). Shape and time-dependent cellular uptake was observed. The cellular uptake of PEGylated-Gold Nano Triangles (P-GNTs) was the greatest, followed by PEGylated-Gold NanoRods (P-GNRs) and PEGylated-Gold Nano Stars (P-GNSs). Their results suggested that nanoparticle shape played an important role in cellular uptake even if they observed a higher uptake for GNRs than GNSs.

In our experiments, first the apical and the basolateral side of the inserts were considered separately (Figure 7 a and b), then we considered also the compartment together (Figure 7 c). In the apical side, nevertheless represent the side of exposure no significant amount of gold was found in cells after 24 hours of exposure to GNPs and GNRs, as compared to the untreated controls; instead, GNSs were present in the apical tri-culture following a clear dose dependent increasing.

In the basolateral side, we observed a statistically significant amount of gold per cell only after exposure to 1,7 µg/cm^2 GNRs and specially GNSs.

Our study highlighted that Au GNSs are uptaken in a dose-dependent way by epithelial cells. GNPs and GNRs are uptaken at a much lower rate, and, even if Au is above the limit of detection, the observed results are statistically different from the untreated control. This confirms that the is also a shape-dependent effects, with GNSs being uptaken, while Au particles and Au rods are not. Similar observations can be done for translocation from the apical to basolateral compartment. Also in this case a shape-dependent effect observable, with Au nano-starts being translocated much more than particles and rods. However, in this case the dose-dependent relationship could not be confirmed. These results are really interesting because they clarify that there is a distinct translocation of GNSs trough the model and the insert membrane. A further confirmation of the presence intercellular exchange and communication among the different cell lines; once again the model resulted a valid condition to better understand the bio-interaction occurring between NPs and cells.

Looking back also to the LDH release results, we can hypotheses that GNS cytotoxicity is not strictly related to the NPs uptake as we could not observe a dose-dependent increase in cytotoxicity.

Obviously, the presence of four different cell lines hinders the possibility to determine which cell line is the main target in the cytotoxicity or uptake processes.

Nevertheless, despite the contradictory results, previous studies and our own investigations show that the shape of AuNPs is one of the most important aspect involved in NP uptake considering different cell lines and experimental conditions.

In addition, in this work we exposed our model also to AgNPs and $AgNO_3$ (supplementary material – Figure S4, S5 and S6), as expected the model modulated its response in the different conditions. We can clearly affirm that the

model is a suitable and valid approach in the screening of nebulized NP suspension.

5. Conclusion

In our work for the first time the novel and innovative 3D *in vitro* tetra-culture model has been used to study the effects of three differently shaped AuNPs (GNPs, GNRs and GNSs).

The model represents the human alveolar barrier and the cultivation of cells at the ALI is necessary for the exposure to nebulized NP suspensions by the VitroCell Cloud System. This setup ensures a situation similar to the organisation of the alveoli *in vivo*. In addition, to test the model capability to modulate their response to different exposures we assessed also the exposure to AgNPs.

Our results clearly show that the model is perfectly suitable for this kind of studies and how the shape influence the bio-interaction between NP and the tetra-culture, particularly, the star-like AuNPs seems to be the more effective, while the rod-like AuNPs resulted the safest.

6. Supplementary materials

Gold Nano Sphere (GNPs) characterization
Date of preparation: 25-02-2017
Sample storage conditions: Protect from light. It can be stored at room temperature
Shelf life: One year
Format (solid/liquid): Liquid (solution of AuNPs)
For dispersed particles: Particles are dispersed in milli Q water (sterile)
Concentration (molar and weight concentration): 15,4 nM. 1,9 mg/ml.
Particular safety requirements for handling: Startdar lab procedure (wear gloves and protective googles when working on them)
Particle size distribution: 59.99 ± 7.3 nm (core size).
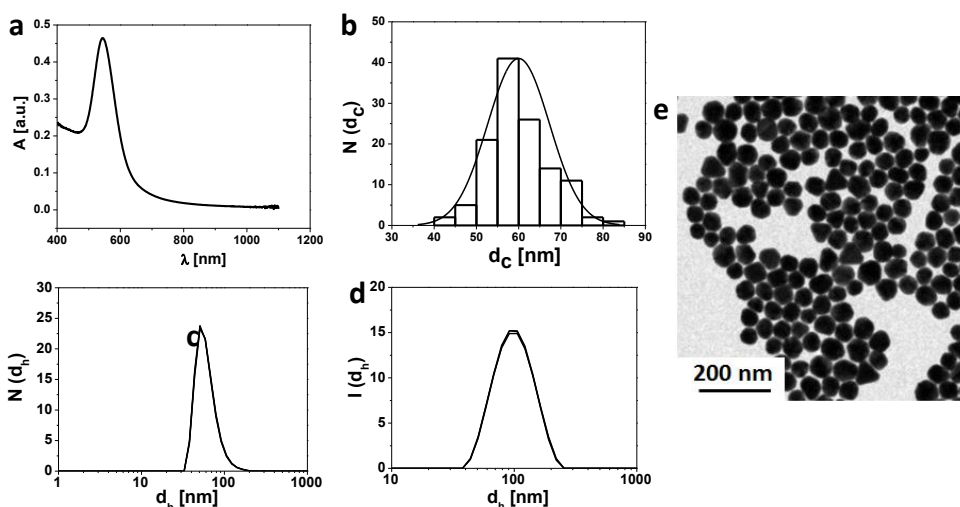
Figure S1: Gold Nano Spheres (GNPs) were prepared in water and coated with polyethyleneglycol (MeO-PEG-SH, M_w= 5 kDa). After that, characterized by UV, DLS and TEM. S1-a, Absorbance spectrum of GNPs; S1-b, core diameter (d_c) size distribution ($N(dc)$) of the GNPs diameter with d_c=59.99 ± 7.3 nm; S1-c, Number distribution ($N(d_h)$) of hydrodynamic diameter (d_{hn}= 61.33 ± 0.34 nm); S1-d, Intensity distribution ($I(d_h)$) of hydrodynamic diameter (d_{hi}=104.2±0.34 nm); S1-e, TEM image of GNPs coated with PEG, the scale bars correspond to 200 nm.

Gold Nano Rods (GNRs) characterization
Date of preparation: 07-02-2017.
Sample storage conditions: It can be stored at room temperature.
Shelf life: 6-12 months.
Format (solid/liquid): Liquid (solution of AuNPs).
For dispersed particles: Particles are dispersed in milli Q water (sterile).

Concentration (molar and weight concentration): 4 nM. 5.3 mg/ml.
Particular safety requirements for handling: Startdar lab procedure (wear gloves and protective googles when working on them).
Particle size distribution: 18.44 ± 6.4 nm (core diameter).
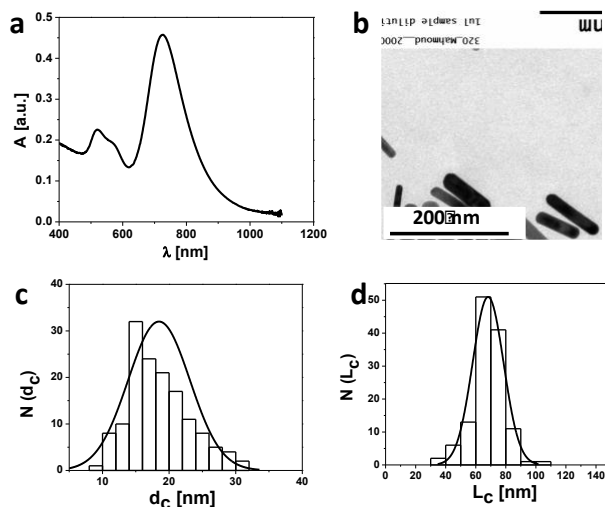
Figure S2: Gold Nano Rods (GNRs) GNRs were prepared in water and coated with polyethyleneglycol (MeO-PEG-SH, M_w= 5 kDa). After that, characterized by UVand TEM. S2-a, Absorbance spectrum of GNRs; S2-b, TEM image of GNRs coated with PEG, the scale bar corresponds to 200 nm; S2-c, core diameter (d_c) size distribution ($N(dc)$) of the GNRs thickness with d_c=18.44 $\pm$ 6.4 nm; S2-d, The core length (L_c) size distribution ($N(L_c)$) of the GNRs length with L_c=68.3 $\pm$ 10.3 nm.

Gold Nano Stars (GNSs) characterization
Date of preparation: 05-02-2017
Sample storage conditions: It can be stored at room temperature.
Shelf life: 3-6 months.
Format (solid/liquid): Liquid (solution of AuNPs).
For dispersed particles: Particles are dispersed in milli Q water (sterile).
Concentration (molar and weight concentration): 3,5 nM. 0,5 mg/ml.
Particular safety requirements for handling: Standar lab procedure (wear gloves and protective googles when working on them).
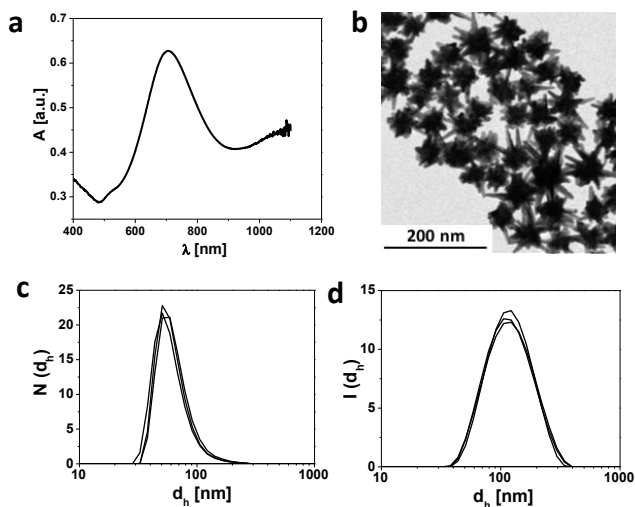
Figure S3: GNS were prepared in water and coated with polyethyleneglycol (HOOC-PEG-SH, M_w= 3 kDa). After that, characterized by UV, DLS and TEM. S3-a, Absorbance spectrum of GNSs; S3-b, TEM image of GNSs coated with PEG, the scale bar corresponds to 200 nm; S3-c, Number distribution (N(d_h)) of hydrodynamic diameter (d_{hn}= 63.43 ± 2.35 nm) and S3-d, Intensity distribution (I (d_h)) of hydrodynamic diameter (d_{hi}= 127.7±1.5) of GNSs.

Tetraculture viability after 24 hours of exposure to AgNPs and AgNO₃
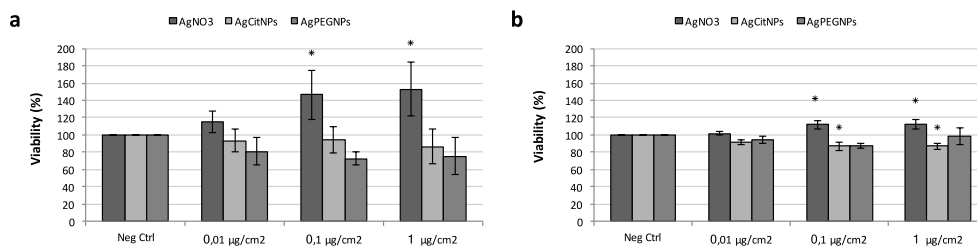
*Figure S4: Fig.4: Histograms showing the tetraculture viability evaluated by measuring the fluorescent signal of the metabolized Resazurin after 24 hours of exposure to AgNPs (0 – 0.01 – 0,1 – 1 µg/cm²) in the Apical (a) and Basolateral (b) side of the model. * statistically significant increase versus control (p<0.05, ANOVA + Dunn's test).*

LDH release after exposure (24 hours) to AgNPs
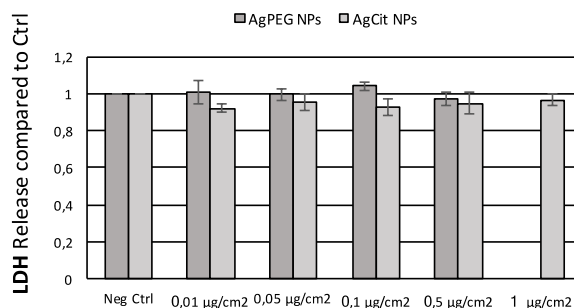
Figure S5: Fig.5: Graph showing the levels of LDH (Lactate Dehydrogenase) in the basolateral compartment after 24 hours of exposure to AgNPs (0 – 0.01 – 0,1 – 1 µg/cm²) in order to evaluate the cytotoxicity of the treatments. No statistically significant differences versus control group (p<0.05, ANOVA + Dunn's test).

Inflammation response (IL-8 level) after 24 hours of exposure to AgNPs
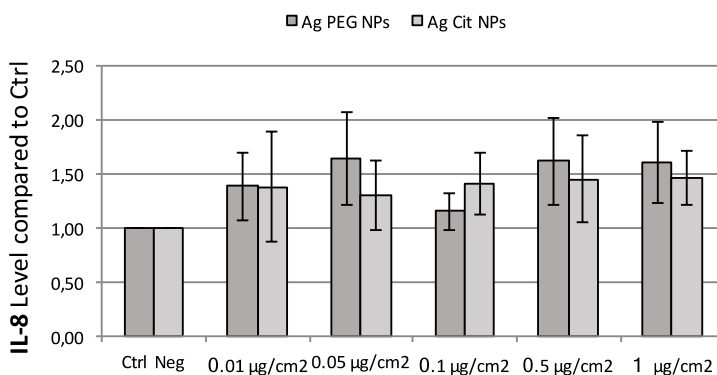
Figure S6: Histogram showing the levels of Interleukin-8 (IL-8) in the basolateral compartment after 24 hours of exposure to AgNPs (0 – 0.01 – 0,1 – 1 µg/cm²) to evaluate the inflammation response of the tetraculture. No statistically significant differences versus control group (p<0.05, ANOVA + Dunn's test).

Contribution

The candidate performed the experiments, preparing and exposing the model for all the analyses. In addition, she prepared the manuscript.

References

Alfaro-Moreno, E., Nawrot, T.S., Vanaudenaerde, B.M., Hoylaerts, M.F., Vanoirbeek, J.A., Nemery, B., Hoet, P.H., 2008. Co-cultures of multiple cell types mimic pulmonary cell communication in response to urban PM10. Eur Respir J 32, 1184-1194.

Baggiolini, M., Clark-Lewis, I., 1992. Interleukin-8, a chemotactic and inflammatory cytokine. FEBS Letters 307, 97-101.

Bitterle, E., Karg, E., Schroeppel, A., Kreyling, W.G., Tippe, A., Ferron, G.A., Schmid, O., Heyder, J., Maier, K.L., Hofer, T., 2006. Dose-controlled exposure of A549 epithelial cells at the air-liquid interface to airborne ultrafine carbonaceous particles. Chemosphere 65, 1784-1790.

Blank, F., Rothen-Rutishauser, B.M., Schurch, S., Gehr, P., 2006. An optimized in vitro model of the respiratory tract wall to study particle cell interactions. J Aerosol Med 19, 392-405.

Braakhuis, H.M., Giannakou, C., Peijnenburg, W.J., Vermeulen, J., van Loveren, H., Park, M.V., 2016a. Simple in vitro models can predict pulmonary toxicity of silver nanoparticles. Nanotoxicology 10, 770-779.

Braakhuis, H.M., Kloet, S.K., Kezic, S., Kuper, F., Park, M.V.D.Z., Bellmann, S., van der Zande, M., Le Gac, S., Krystek, P., Peters, R.J.B., Rietjens, I.M.C.M., Bouwmeester, H.

Braakhuis, H.M., Oomen, A.G., Cassee, F.R., 2016b. Grouping nanomaterials to predict their potential to induce pulmonary inflammation. Toxicology and Applied Pharmacology 299, 3-7.

Champion, J.A., Walker, A., Mitragotri, S., 2008. Role of particle size in phagocytosis of polymeric microspheres. Pharm Res 25, 1815-1821.

Chen, H., Zhang, X., Dai, S., Ma, Y., Cui, S., Achilefu, S., Gu, Y., 2013. Multifunctional gold nanostar conjugates for tumor imaging and combined photothermal and chemo-therapy. Theranostics 3, 633-649.

Chithrani, B.D., Ghazani, A.A., Chan, W.C., 2006. Determining the size and shape dependence of gold nanoparticle uptake into mammalian cells. Nano Lett 6, 662-668.

Chu, Z., Zhang, S., Zhang, B., Zhang, C., Fang, C.Y., Rehor, I., Cigler, P., Chang, H.C., Lin, G., Liu, R., Li, Q., 2014. Unambiguous observation of shape effects on cellular fate of nanoparticles. Sci Rep 4, 4495.

Dam, D.H., Lee, J.H., Sisco, P.N., Co, D.T., Zhang, M., Wasielewski, M.R., Odom, T.W., 2012. Direct observation of nanoparticle-cancer cell nucleus interactions. ACS Nano 6, 3318-3326.

de Souza Carvalho, C., Daum, N., Lehr, C.-M., 2014. Carrier interactions with the biological barriers of the lung: Advanced in vitro models and challenges for pulmonary drug delivery. Advanced Drug Delivery Reviews 75, 129-140.

Favi, P.M., Gao, M., Johana Sepulveda Arango, L., Ospina, S.P., Morales, M., Pavon, J.J., Webster, T.J., 2015. Shape and surface effects on the cytotoxicity of nanoparticles: Gold nanospheres versus gold nanostars. J Biomed Mater Res A 103, 3449-3462.

Fleischer, C.C., Payne, C.K., 2014. Nanoparticle-cell interactions: molecular structure of the protein corona and cellular outcomes. Acc Chem Res 47, 2651-2659.

Fytianos, K., Rodriguez-Lorenzo, L., Clift, M.J., Blank, F., Vanhecke, D., von Garnier, C., Petri-Fink, A., Rothen-Rutishauser, B., 2015. Uptake efficiency of surface modified gold nanoparticles does not correlate with functional changes and cytokine secretion in human dendritic cells in vitro. Nanomedicine 11, 633-644.

Herzog, F., Clift, M.J., Piccapietra, F., Behra, R., Schmid, O., Petri-Fink, A., Rothen-Rutishauser, B., 2013. Exposure of silver-nanoparticles and silver-ions to lung cells in vitro at the air-liquid interface. Part Fibre Toxicol 10, 11.

Hidalgo, A., Cruz, A., Pérez-Gil, J., 2015. Barrier or carrier? Pulmonary surfactant and drug delivery. European Journal of Pharmaceutics and Biopharmaceutics 95, 117-127.

Holder, A.L., Marr, L.C., 2013. Toxicity of silver nanoparticles at the air-liquid interface. Biomed Res Int 2013, 328934.

Kim, S., Ryu, D.Y., 2013. Silver nanoparticle-induced oxidative stress, genotoxicity and apoptosis in cultured cells and animal tissues. J Appl Toxicol 33, 78-89.

Kimlin, L., Kassis, J., Virador, V., 2013. 3D in vitro tissue models and their potential for drug screening. Expert Opin Drug Discov 8, 1455-1466.

Klein, S.G., Cambier, S., Hennen, J., Legay, S., Serchi, T., Nelissen, I., Chary, A., Moschini, E., Krein, A., Blömeke, B., Gutleb, A.C., 2017. Endothelial responses of the alveolar barrier in vitro in a dose-controlled exposure to diesel exhaust particulate matter. Part Fibre Toxicol, vol. 14, London.

Klein, S.G., Hennen, J., Serchi, T., Blömeke, B., Gutleb, A.C., 2011. Potential of coculture in vitro models to study inflammatory and sensitizing effects of particles on the lung. Toxicology in Vitro 25, 1516-1534.

Klein, S.G., Serchi, T., Hoffmann, L., Blömeke, B., Gutleb, A.C., 2013. An improved 3D tetraculture system mimicking the cellular organisation at the alveolar barrier to study the potential toxic effects of particles on the lung. Part Fibre Toxicol, vol. 10, p. 31.

Kodiha, M., Wang, Y.M., Hutter, E., Maysinger, D., Stochaj, U., 2015. Off to the organelles - killing cancer cells with targeted gold nanoparticles. Theranostics 5, 357-370.

Lenz, A.G., Karg, E., Brendel, E., Hinze-Heyn, H., Maier, K.L., Eickelberg, O., Stoeger, T., Schmid, O., 2013. Inflammatory and oxidative stress responses of an alveolar epithelial cell line to airborne zinc oxide nanoparticles at the air-liquid

interface: a comparison with conventional, submerged cell-culture conditions. Biomed Res Int 2013, 652632.

Mülhopt, S., Dilger, M., Diabaté, S., Schlager, C., Krebs, T., Zimmermann, R., Buters, J., Oeder, S., Wäscher, T., Weiss, C., Paur, H.-R., 2016. Toxicity testing of combustion aerosols at the air–liquid interface with a self-contained and easy-to-use exposure system. Journal of Aerosol Science 96, 38-55.

Müller, L., Gasser, M., Raemy, D.O., Herzog, F., Brandenberger, C., Schmid, O., Gehr, P., Rothen-Rutishauser, B., Clift, M.J.D., - Realistic exposure methods for investigating the interaction of nanoparticles with the lung at the air-liquid interface in vitro. - 30.

Nel, A., Xia, T., Madler, L., Li, N., 2006. Toxic potential of materials at the nanolevel. Science 311, 622-627.

Niikura, K., Matsunaga, T., Suzuki, T., Kobayashi, S., Yamaguchi, H., Orba, Y., Kawaguchi, A., Hasegawa, H., Kajino, K., Ninomiya, T., Ijiro, K., Sawa, H., 2013. Gold nanoparticles as a vaccine platform: influence of size and shape on immunological responses in vitro and in vivo. ACS Nano 7, 3926-3938.

Oberdörster, G., Oberdörster, E., Oberdörster, J., 2005. Nanotoxicology: An Emerging Discipline Evolving from Studies of Ultrafine Particles. Environ Health Perspect, vol. 113, pp. 823-839.

Raemy, D.O., Grass, R.N., Stark, W.J., Schumacher, C.M., Clift, M.J., Gehr, P., Rothen-Rutishauser, B., 2012. Effects of flame made zinc oxide particles in human lung cells - a comparison of aerosol and suspension exposures. Part Fibre Toxicol 9, 33.

Romero, V.H., Kereselidze, Z., Egido, W., Michaelides, E.A., Santamaria, F., Peralta, X.G., 2014. Nanoparticle assisted photothermal deformation of individual neuronal organelles and cells. Biomed Opt Express 5, 4002-4012.

Rothen-Rutishauser, B.M., Kiama, S.G., Gehr, P., 2005. A three-dimensional cellular model of the human respiratory tract to study the interaction with particles. Am J Respir Cell Mol Biol 32, 281-289.

Secondo, L.E., Liu, N.J., Lewinski, N.A., 2017. Methodological considerations when conducting in vitro, air-liquid interface exposures to engineered nanoparticle aerosols. Crit Rev Toxicol 47, 225-262.

Shrivastava, R., Kushwaha, P., Bhutia, Y.C., Flora, S., 2016. Oxidative stress following exposure to silver and gold nanoparticles in mice. Toxicol Ind Health 32, 1391-1404.

Srivastava, M., Singh, S., Self, W.T., 2012. Exposure to silver nanoparticles inhibits selenoprotein synthesis and the activity of thioredoxin reductase. Environ Health Perspect 120, 56-61.

Stoehr, L.C., Endes, C., Radauer-Preiml, I., Boyles, M.S., Casals, E., Balog, S., Pesch, M., Petri-Fink, A., Rothen-Rutishauser, B., Himly, M., Clift, M.J., Duschl, A., 2015. Assessment of a panel of interleukin-8 reporter lung epithelial cell lines

to monitor the pro-inflammatory response following zinc oxide nanoparticle exposure under different cell culture conditions. Part Fibre Toxicol 12, 29.

Talamini, L., Violatto, M.B., Cai, Q., Monopoli, M.P., Kantner, K., Krpetic, Z., Perez-Potti, A., Cookman, J., Garry, D., C, P.S., Boselli, L., Pelaz, B., Serchi, T., Cambier, S., Gutleb, A.C., Feliu, N., Yan, Y., Salmona, M., Parak, W.J., Dawson, K.A., Bigini, P., 2017. Influence of Size and Shape on the Anatomical Distribution of Endotoxin-Free Gold Nanoparticles. ACS Nano 11, 5519-5529.

Vance, M.E., Kuiken, T., Vejerano, E.P., McGinnis, S.P., Hochella, M.F., Rejeski, D., Hull, M.S., 2015. Nanotechnology in the real world: Redeveloping the nanomaterial consumer products inventory. Beilstein J Nanotechnol 6, 1769-1780.

Xie, X., Liao, J., Shao, X., Li, Q., Lin, Y., 2017. The Effect of shape on Cellular Uptake of Gold Nanoparticles in the forms of Stars, Rods, and Triangles. Sci Rep 7, 3827.

Yacobi, N.R., Fazllolahi, F., Kim, Y.H., Sipos, A., Borok, Z., Kim, K.-J., Crandall, E.D., 2011. Nanomaterial interactions with and trafficking across

Chapter 3:

Do nanoparticle physico-chemical properties and developmental exposure window influence nano ZnO embryotoxicity in *Xenopus laevis*?

Patrizia Bonfanti[1]*, Elisa Moschini[1]*, **Melissa Saibene[1]**, Renato Bacchetta[2],
Leonardo Rettighieri[3], Lorenzo Calabri[3], Anita Colombo[1], Paride Mantecca[1#]

[1]*Dept. Earth and Environmental Sciences, POLARIS Research Centre, University of Milano Bicocca, 1 Piazza della Scienza, 20126 Milan (MI) – Italy*
[2]*Department of Biosciences, University of Milan, 26 via Celoria, 20133, Milan, Italy*
[3]*Tec Star S.r.l., Viale Europa, 40, 41011 Campogalliano (MO) – Italy*

*These authors contributed equally to the work

#Corresponding author: Paride Mantecca, Dept. Earth and Environmental, Research Centre POLARIS, University of Milano Bicocca, 1 piazza della Scienza, 20126, Milan, Italy

ABSTRACT

The growing global production of zinc oxide nanoparticles (ZnONPs) suggests a realistic increase in the environmental exposure to a such nanomaterial, making the knowledge of its biological reactivity and its safe-by-design synthesis mandatory.

In this study the embriotoxicy of ZnONPs specifically synthesized for industrial purposes with different size, shape (round, rod) and surface coating (PEG, PVP) was tested using the Frog Embryo Teratogenesis Assay-*Xenopus* (FETAX) to identify potential target tissues and the most sensitive developmental stages.

The ZnONPs did not cause embryolethality but induced a high incidence of malformations, in particular misfolded gut and abdominal oedema. Smaller-round NPs resulted more effective than the bigger-rod ones and PEGylation determined a reduction in embryotoxicity.

Ingestion appeared the most relevant exposure route. Only the embryos exposed from the stomodeum opening showed anatomical and histological lesions to the intestine, mainly referable to a swelling of paracellular spaces among enterocytes.

In conclusion ZnONPs differing in shape and surface coating displayed similar toxicity in *X. laevis* embryos and shared the same tissue target. Nevertheless, we cannot exclude that the physico-chemical characteristics may influence the severity of such effects. Further research efforts are mandatory to ensure the synthesis of safer nanoZnO containing products.

1. Introduction

The explosion of the nanotech revolution implies that new and previously unknown materials are introduced into the environment, generating new ecological relationships among living and non-living systems, with unpredictable scenarios on the long term effects on human and environmental health. Thus the health and environmental safety issues of nanotechnology represents today an urgent concern to be addressed by the scientific and regulatory communities.

The industrial sectors employing nanotechnologies are exponentially increasing, determining that thousands of products are already commercialized and even more are predicted to invade the market in the next future. This of course will determine an increase in the risk for humans and environment to come in contact with new nanomaterials (NMs). At present, there is a huge knowledge gap between the use of NMs and the possible health risks. Trying to fill the gap, the newborn nanotoxicology discipline has the mission to unravel the toxicological properties of the huge number of NMs already employed and to orient the safe nanotech future development.

In the vast NM catalogue, nano metal oxides (nMeOs) represent one of the wider used category in industrial applications and they are produced in thousands of tons per year globally. Due to a such mass production they are predicted to be relevant nanocontaminants in the future. After nanosized Titanium dioxide ($nTiO_2$), nano Zinc oxide (nZnO) results to be the most abundantly produced (Bondarenko *et al.*, 2013).

Nano ZnO has recently attracted a big interest for its UV protective and antibacterial capacities, which make it suitable for a wide range of applications (Nohynek *et al.*, 2010). Its action as stabilizer agent has also promoted the use in food, cosmetics and other consumer products, such as paints. For the aims of this work, ZnONPs have been obtained from a supplier who developed different

formulations of un-coated and coated NM to be used as antibacterial and UV filter fillers for polymers and paints.

Since this diffuse and large scale applications, nZnO represents one of the prioritized NM to be considered for regulation as confirmed by the abundant literature available about its toxicological effects.

Many studies investigated the nZnO effects on human cells and laboratory mammals, pointing out the relevant cytotoxic and inflammatory potency of this NM (Pandurangam & kim, 2015). Besides, nZnO probably represent the only NM which has been incontrovertibly associated to a specific human disease (the Metal Fume Fever), a chronic inflammatory status manifested in welding fume chronically exposed workers (Gerberding 2005).

Adverse effects after nZnO exposure were reported also in aquatic organisms throughout the trophic chain (Gerberding 2005; Ates *et al.*, 2015), nevertheless it has been used as a dietary supplement in human and livestock (Rincker *et al.*, 2005). Several papers agree in attributing to nZnO a heavy acute toxic effect on different ecologically relevant groups, like algae, bacteria, crustaceans (Aruoja *et al.*, 2009; Blinova *et al.*, 2010; Heinlaan *et al.*, 2008; Santo *et al.*, 2014). In respect to Vertebrates, nZnO was seen adversely affecting zebrafish embryos and adults (Brun *et al.*, 2014; Bai *et al.*, 2010; Xiong *et al.*, 2011; Zhu *et al.*, 2009), as well as the normal development of the amphibian *Xenopus laevis* (Bacchetta *et al.*, 2012; Nations *et al.*, 11a; Nations *et al.*, 11b). In two previous papers we demonstrated that nZnO specifically targets gut development, producing histological and molecular effects in function of NP dimensions, being the smaller NP the most effective (Bacchetta *et al.*, 2012; Bacchetta *et al.*, 2014).

Since the nanotoxicity studies targeted to the reproductive and developmental aspects are rather scanty and considering that the nZnO mechanism of action during embryogenesis are not fully understood, in this work we investigated the relationships between the ZnO NP properties and the developmental alterations

produced. In particular the present work has been focused onto the comparative embryotoxic effects of differently shaped and coated ZnONPs. Smaller round *vs* bigger rod NPs and PVP and PEG surface-coated *vs* uncoated NPs were tested in order to establish which NP properties might be involved more than others in inducing the specific toxicity outputs and thus possibly listed to be considered as target in a safe-by-design study. In addition we performed further assays, by exposing embryos throughout different developmental windows to characterize which embryonic stages resulted more sensitive to nZnO exposure. The results mainly show that the different ZnONPs induce similar embryotoxic effects, targeting the same organ – the intestine – with ingestion as the primary uptake route. The surface coating with PEG seems a possible way to reduce embryotoxicity of ZnONPs during *Xenopus* development.

2. Materials and methods

2.1. Chemicals and NPs used

All analytical grade reagents, human corionic gonadotropin (HCG), 3-amino-benzoic acid ethyl ester (MS222), salts for FETAX solution, $ZnSO_4$ were purchased from Sigma-Aldrich S.r.l., Italy.

The different ZnONPs used were supplied by TecStar S.r.l. (Campogalliano, Modena, Italy); they were produced by gas phase pyrolysis methods.

The ZnONPs used are indicated as follow: sZnO (smaller round NPs), bZnO (bigger rod). These NPs are here tested both nude and surface coated with polyvinylpyrrolidone (PVP10K) or polyethylene glycol (PEG400) and indicated as PVP-sZnO, PEG-sZnO and so on.

Functionalization of nanoparticles is obtained by TecStar proprietary wet chemical procedures.

All suspensions and stock solutions were prepared in FETAX whose composition in mg/L was 625 NaCl, 96 NaHCO$_3$, 30 KCl, 15 CaCl$_2$, 60 CaSO$_4$·2H$_2$O, and 70 MgSO$_4$, at pH 7.6-8.0. Test suspensions (1, 10, 50 and 100mg/L) were sonicated for 10min in a Branson 2510 sonifier and stored in the dark at 4°C.

2.2. NP synthesis and characterization

Morphology of dry uncoated NPs were obtained by analyzing images of high resolution secondary electron mycroscopy (HR-SEM), equipped with field emission electron source (FEI STRATA DB235M, 30kV beam voltage).

Crystal phase of dry uncoated NPs was invesigated by X-ray diffraction (XRD) analysis (Panalytical XPERT PRO with Cu anode). Effective NP diameters and their size distributions were measured by transmission electron microscopy (TEM). ZnONPs (sZnO, bZnO) were suspended in distilled water, sonicated for 1 min and vortexed. Aliquots of 3µl of NP suspension (100mg/L) were immediately pipetted and deposited onto Formvar®-coated 200 mesh Copper grids, excess of water was gently blotted by filter paper. Once dried, grids were directly inserted in a Jeol-JEM1220 transmission electron microscope operating at 100kV and images taken using a dedicated Lheritier LH72WA-TEM camera.

2.3. Characterization of NP dispersions

Once obtained the final NP dispersions in FETAX solution, Dinamic Light Scatering (DLS) and ICP-OES measurements were performed to characterize the NP hydrodynamic behaviour and dissolution respectively.

For DLS and Z-potential measurement, a Nanosizer ZS (Malvern Instruments Ltd) was used; dry ZnONPs were dispersed in both ultrapure water and FETAX solution using the same methods adopted to generate test solution. Every measure is the average value of five independent measures.

To estimate the NP dissolution and the possible contribution to toxicity of Zn^{2+} dissolved in FETAX solution at embryo exposure conditions, coated and uncoated bZnO and sZnO suspensions were collected at 24 h after the beginning of embryo exposure (t24) and after 96 h (end of the toxicity tests, t96). The collected solutions were ultrafiltrated using centrifuge tubes VIVASPIN 6 with a molecular weight cut off of 10,000 Da (Sartorius Stedim Biotech GmbH, Goettingen, Germany). The Zn^{2+} concentration in ZnO NP-free ultrafiltrated solution was measured by Inductively Coupled Plasma Optical Emission Spectrometry (ICP-OES) with a Perkin-Elmer Optima 7000 DV (Perkin-Elmer, Santa Clara, CA, USA). The analyses were conducted on samples from two independent bioassays and each measurement was replicated three times.

2.4. FETAX assay

Adult *X. laevis* were purchased from Centre de Ressources Biologiques *Xénopes* (Université de Rennes 1, Rennes Cedex), maintained in aquariums with dechlorinated tap-water at a $22\pm2°C$, alternating 12h light/dark cycles and fed a semi synthetic diet (Mucedola S.r.L., Settimo Milanese, Italy) three times a week. FETAX test was run according to the standard protocol ASTM (1998). Embryos were obtained from the natural breeding of pairs of adult *X. laevis* previously injected with HCG in the dorsal lymph sac (females: 300IU; males: 150IU). Breeding tanks were filled with FETAX solution and well aerated before introducing the couples. Amplexus normally ensued within 2 to 6h and the deposition of fertilized eggs occurred from 9 to 12h after injection. After breeding, adults were removed and embryos collected and dejelled with 2,25% of L-cystein in FETAX solution (pH=8). Normally cleaved embryos at midblastula stage (stage 8), 5 h post-fertilization (hpf; Nieuwkoop & Faber 1956) were selected for testing and placed in 6.0 cm glass Petri dishes containing 10ml of control or test solution. For each female the plates were duplicated. All the

Petri were incubated in a thermostatic chamber at 23±0.5 °C until the end of the test (96 hpf) and each day the test solutions were renewed and the dead embryos removed. At this moment mortality and malformation data were generated as endpoints of the assay. For each experimental group, the number of dead larvae was recorded and survivors were anaesthetized with MS-222 at 100mg/L and evaluated for single malformations by examining each specimen under a dissecting microscope. At the end of the bioassays, surviving normal larvae were formalin fixed for growth retardation measurements. Each assay was repeated at least three times under the same experimental conditions.

2.5. Experimental design

The experimental design was set up as following. 1) To probe the embryotoxic potency of differently sized and shaped ZnONPs, a conventional FETAX assay (exposure over stages 8-46) was conducted by exposing embryos to sZnO and bZnO at increasing concentrations of 1, 10, 50 and 100 mg/L; 2) to test a possible influence of surface coating in the observed embryotoxic properties, further comparative FETAX assays (stages 8-46) were performed using PVP- and PEG-coated sZnO and bZnO at the effective concentration of 50mg/L; 3) to establish the NP uptake route and the most sensitive developmental windows further experiments were conducted by exposing embryos to sZnO and bZnO from stage 8 to stage 39 or from stage 39 to stage 46. The results were compared with the exposure during the whole embryogenetic period (stages 8-46). The developmental windows were selected according to the beginning of the FETAX assay (mid-blastula, stage 8, 5 hpf) and the opening of the stomodeum (stage 39, 2 days 8 hpf), indicating the likelihood for NP ingestion. Stage 46 (4 days 10 hpf) corresponds to the end of the primary organogenisis – end of the FETAX assay. 4). At the end of test (96 hpf), pools of stage 46 embryos coming from the different exposure conditions and exposed to effective concentration of 50mg/L

were randomly selected and immediately stored at -80°C for measurement of Superoxide Dismutase (SOD) enzymatic activity, a biomarker of oxidative stress, or processed for light and electron microscopy analyses.

2.6. Superoxide Dismutase (SOD) enzymatic activity

Total SOD activity (Cu/ Zn-, Mn-, and Fe-SOD) was quantified by the SOD Assay Kit (Cayman, Ann Arbor, MI, USA) according to the manufacturer instructions The test used a tetrazolium salt to detect superoxide radicals generated by xanthine oxidase. One unit (U) of SOD activity correspond to the quantity of enzyme yielding 50% dismutation of superoxide radical.

Pools of 20 embryos, collected from each treatment group exposed to the effective concentration of 50mg/L, were homogenized in 1 ml of 20 mM cold HEPES buffer (pH=7.2). Than the homogenates were centrifuged at 1500 g for 5 min at 4 °C. A volume of 200 µl of radical detection solution were added to 10 µl of the supernatants or SOD standard solutions in a 96 well plate. The reaction was initiated by adding xantine oxidase solution and absorbance was measured at 450 nm with a multiplate reader (Multiskan Ascent Thermo Scientific Co., Italy). Data were normalised for the protein content of each sample, determined by the BCA method using BSA as a standard, and expressed as mean specific SOD activity (U/mg proteins) ± SEM of three independent experiments.

2.7. Light and electron microscopy analyses

For light and transmission electron microscopy (TEM) analyses, embryos were randomly selected at the end of the FETAX assays and fixed in 2,5% glutaraldehyde in 0.1M sodium cacodylate buffered solution at pH 7.4. After several washes in the same buffer, larvae were post-fixed in 1% OsO_4 for 1.5 h at 4°C, dehydrated in a graded ethanol series, then transferred in 100% propylene oxide. Infiltration was subsequently performed with propylene oxide and

embedding resin (Araldite-Epon) at volumetric proportions of 2:1 for 1.5 h, 1:1 overnight, and finally 1:2 for 1.5 h. Embryos were then left in 100% pure resin for 4 h, and polymerization was performed at 60 °C for 48 h. Semithin sections of 0.5 μm were obtainedby a Reichert Ultracut E microtome, collected onto microscope slides and stained with 1% toluidine blue to be screened under the light microscope and to select the region of interest for TEM observations. Ultrathin sections of 50 nm of the intestinal loops were collected on 200 mesh uncoated copper grids and not counterstained to avoid contaminations by lead citrate and uranyle acetate that ultimately may interfere with metal NP visualization. Samples were analysed using a Jeol JEM1220 transmission electron microscope operating at an accelerating voltage of 80kV and equipped with a Lheritier LH72WA-TEM digital camera.

2.8. Data Collection and statistical analysis

The number of dead embryos versus their total number at the beginning of the test led to the mortality percentages and the number of malformed larvae versus the total number of surviving ones gave the malformed larva percentages. Data are presented as the average±SEM. The data were tested for homogeneity and normality. If these assumptions were met, oneway analysis of variance (ANOVA) was performed, and otherwise, the non-parametric Kruskal–Wallis test was applied. Significance level was set at $p<0.05$. The incidence of specific malformations were investigated with Chi-square, with the Yates's correction for continuity ($\chi2$ test), or Fisher's Exact tests (FE test). Concentrations causing 50% lethality or malformation at 96 hpf were calculated, when possible, and classified as lethal (LC50) or teratogenic (TC50), respectively. These were obtained following the elaboration of the lethality and malformation data by the Probit analysis (Finney 1971), using the US EPA Probit Analysis Program, version 1.5.

The Teratogenic Index (TI), useful in estimating the teratogenic risk associated with the tested compounds, was the LC50/TC50 ratio (Dawson & Bantle 1987).

3. Results

3.1. NP physical and chemical characteristics

The morphology and the XRD pattern of sZnO and bZnO are reported in Fig. 1. SEM and TEM pictures clearly show that sZnO sample (Fig. 1a, b) is made of round NPs while bZnO (Fig. 1c, d) is composed of bigger rod-shaped NPs.
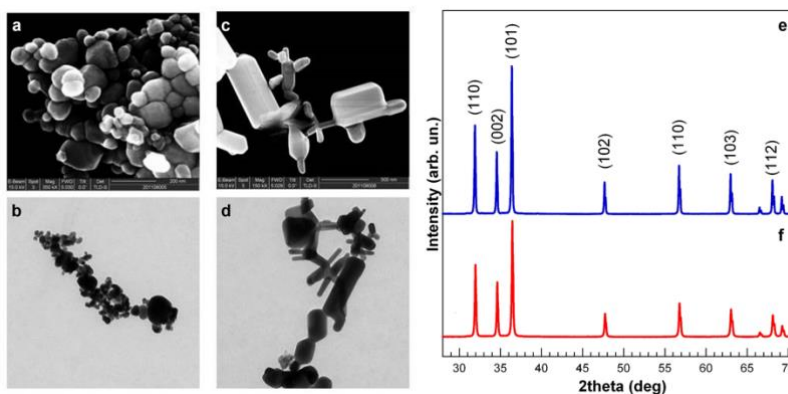
Figure 1. *Physical and chemical characterization of ZnO nanoparticles. SEM and TEM images of sZnO (a, b) and bZnO (c, d). XRD analysis of dry sZnO (e) and bZnO (f); main planes for zincite chrystal are reported*

XRD pattern of dry ZnO NPs was studied using a diffraction angle 28° - 71°: all the peaks are in 100% phase matching with the ZnO hexagonal phase of zincite chrystal and no other characteristic impurities peaks were detected (Fig. 1 e and f).

The line broadening in the peaks determine the crystallite size of ZnO and the average crystalline size of dry ZnO NPs can be estimated by well-known Scherrer's relation.

Table I reports the main results obtained from DLS analysis of hydrodynamic diameters and surface charge (z-potential) and XRD analysis of crystalline size.

Table I Results from DLS, zeta potential and XRD analysis**.**

	Hydrodinamic Diameter (nm)	Zeta Potential (mV)	Average Crystalline Size (nm)
sZnO	819	+3.7	70
bZnO	579	−12.8	98
PVP-sZnO	355	+15.3	-
PEG-sZnO	237	+19.6	-
PVP-bZnO	454	−10.5	-
PEG-bZnO	685	+3.8	-

Using of mechanical and ultrasonication techniques were not enough to obtain homogeneous suspensions of particles in FETAX medium. All the nZnO show the tendency to aggregate as testified by the values of the hydrodynamic diameter determined by DLS.

Nevertheless, coated ZnO NPs seemed to be separated from each other by dispersion techniques in a more efficient way; this effect may be caused by steric repulsion induced by the presence of the polymeric coating on particle surface.

Zeta potential measurements show that sZnO has positive charge and the functionalization of these particles with PEG and PVP slightly increase Z-potential values.

Nude and PVP-coated bZnO show a negative charge while PEGbZnO a positive one.

In our experimental conditions the concentration of Zn^{2+} measured after 24h and 96h by ICP-OES was lower than 0.3 mg/L and and independent of the NP incubation time. for both nude and coated NPs (Figure S1).
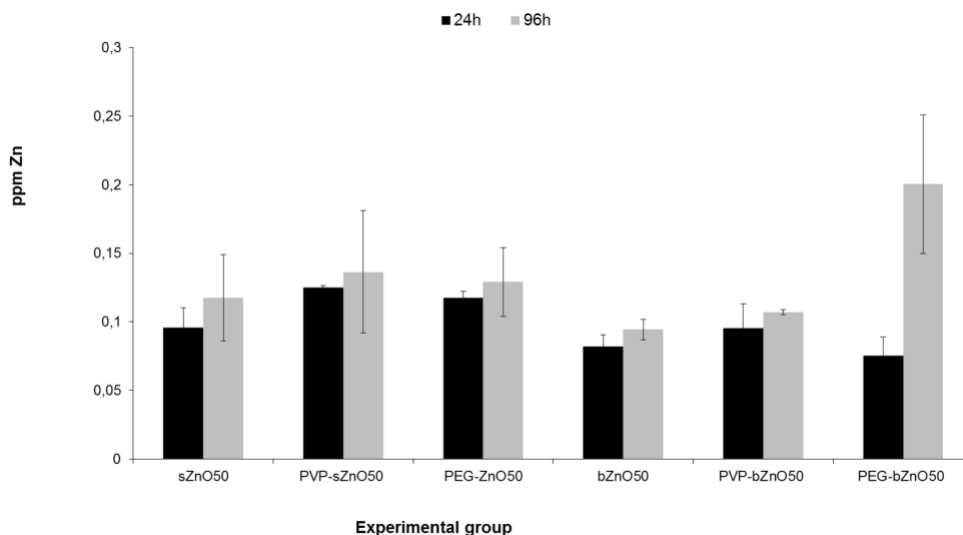
Figure S1. Levels of dissolved ions from sZnO and bZnO after 24 h and 96 h from the beginning of the FETAX assay measured by ICP-OES.

These results confirm that ZnO NPs are very poorly soluble in FETAX medium.

3.2. Comparative embryotoxicity of differently sized and shaped ZnONPs

The physicochemical properties, such as size and shape, along with the effective concentration of ZnONPs, were evaluated by the comparative toxicity of sZnO and bZnO on *Xenopus laevis* embryos (Fig. 2).

At the end of the 96 hpf period of exposure, both NPs were not embryolethal over the concentration range of 1-100 mg/L. On the other hand we observed a concentration dependent increase in malformation rates in the range of 1-50 mg/L, that are statistically different from the control starting from the concentration of 10 mg/L for both sZnO and bZnO.

The embryotoxicity of sZnO appears to be higher than that of bZnO especially in embryos exposed to 50 mg/L, even if the malformation percentage mean values of the two types of ZnONPs were not statistically different. Nevertheless, the 96 h TC50 values calculated by probit method in the range 1-50 mg/L, were of 17.9
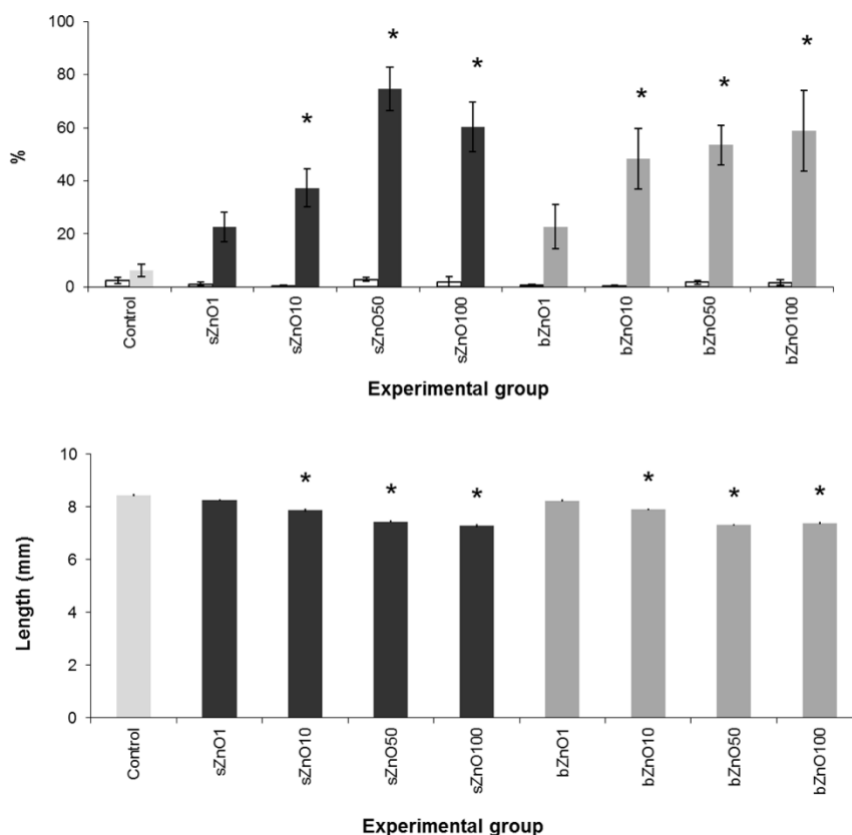
Figure 2. Comparative FETAX results after exposure of embryos to 1-100 mg/L of sZnO and bZnO. a) mortality (empty columns) and malformation (filled columns) rates; b) growth retardation. Bars= SEM; *statistically different from control ($p<0.05$, ANOVA +Fisher LSD Method)

mg/L for sZnO and 59.47 mg/L for bZnO, suggesting that sZnO has an higher embryotoxic potential than bZnO. However, it is not possible to calculate the TI because of the low mortality recorded that did not allow to estimate the LC50. This suggests that the TI values would be many times greater than 3 and so sZnO and bZnO should be considered "highly teratogenic" compounds according to Dawson and Bantle (1987).

Exposure to 50 mg/L of ZnONPs, more than 70% of embryos for sZnO and more than 50% for bZnO were abnormal; irregular gut coiling and abdominal or cardiac oedema were the most frequent abnormality observed (Fig. 3).
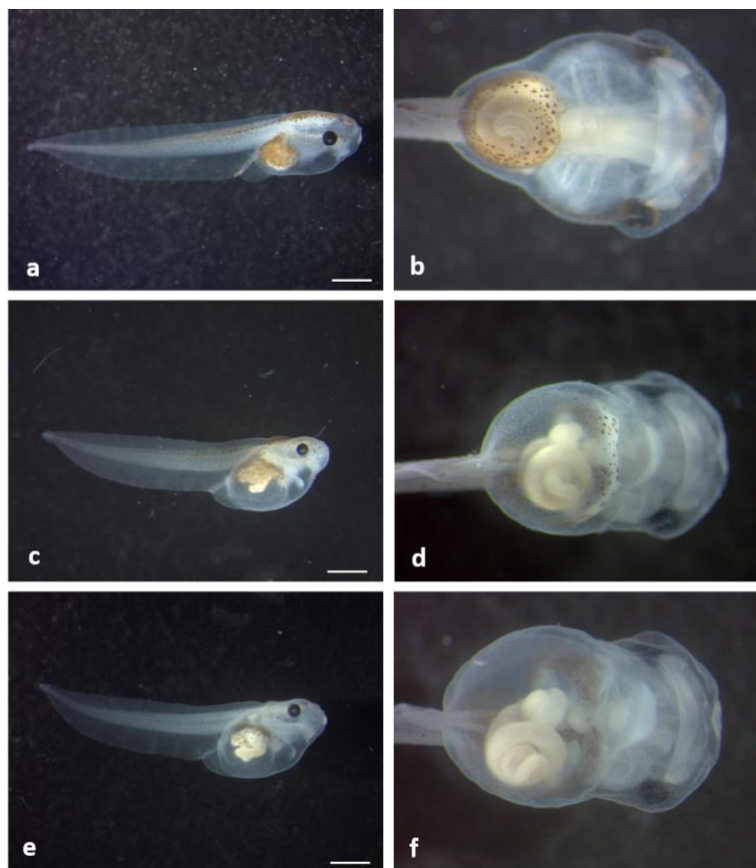
Figure 3*. Xenopus laevis larvae at the end of the FETAX test. (a) lateral and (b) ventral view of a control; (c) lateral and (d) ventral view of an embryo exposed to 50 mg /L sZnO; (e) lateral and (f) ventral view of an embryo exposed to 50 mg/L bZnO. The treated larvae show abnormal gut coiling, abdominal and cardiac oedemas and a slight dorsal tail flexure. (b,d,f) original magnification 4x. Bars= 1mm.*

It is noteworthy that the sZnO affected more heavily the gut coiling in comparison with bZnO as demonstrated by the Chi square test of the specific malformations (Tab 2).

Table II Malformation patterns in embryos exposed to sZnO and bZnO

	Control	sZnO (mg/L)				bZnO (mg/L)			
		1	10	50	100	1	10	50	100
Living larvae	247	247	249	258	173	243	249	257	169
Malformation									
Severe n (%)	3 (1,2)	5 (2,0)	8 (3,2)	4 (1,6)	7 (4,0)	1 (0,4)	3 (1,2)	9 (3,5)	2 (1,2)
Gut n (%)	4 (1,6)	35 (14,2)[b]	66 (26,5)[b]	116 (45,0)[bc]	79 (45,7)[bc]	29 (11,9)[b]	71 (28,5)[b]	70 (27,2)[b]	48 (28,4)[b]
Edema n (%) cardiac	0	0	2 (0,8)	31 (12,0)[b]	4 (2,3)[a]	2 (0,8)	32 (12,9)[b]	12 (4,7)[b]	0
abdominal	8 (3,2)	15 (6,1)	34 (13,7)[b]	90 (34,9)[b]	39 (22,5)[b]	19 (7,8)[a]	70 (28,1)[b]	57 (22,2)[b]	47 (27,8)[b]
Dorsal flexure n (%)	0	0	2 (0,8)	13 (5,0)[b]	1 (0,6)	0	0	8 (3,1)[b]	16 (9,5)[b]

(Percentages based on number of malformations/number of the living).
[a] Chi square test;p<0.05 versus control.
[b] Chi square test; p <0.001 versus control.
[c] Chi square test; p <0.001 sZnO versus the corresponding concentration of bZnO.

As reported for the malformation rate a significant growth retardation was observed starting from 10 mg/L for both the ZnO NPs and a concentration dependent response was also detected up to 100 mg/L (Fig. 2b).

In conclusion, considering comparative embryotoxicity results, the sZnO and the bZnO have resulted in a significant malformation incidence and growth inhibition, in which the size and the shape of the NPs play a role.

3.3. Influence of polymer surface coating on ZnO NP embryotoxicity

Based on previous embryotoxicity experiments 50 mg/L of ZnO NPs was selected as effective concentration in order to assess the influence of surface coating on embryotoxicity of the considered nanoparticles. We performed a specific FETAX assay comparing nude and polymer-coated (PVP and PEG) sZnO and bZnO and the results were showed in Fig. 4.
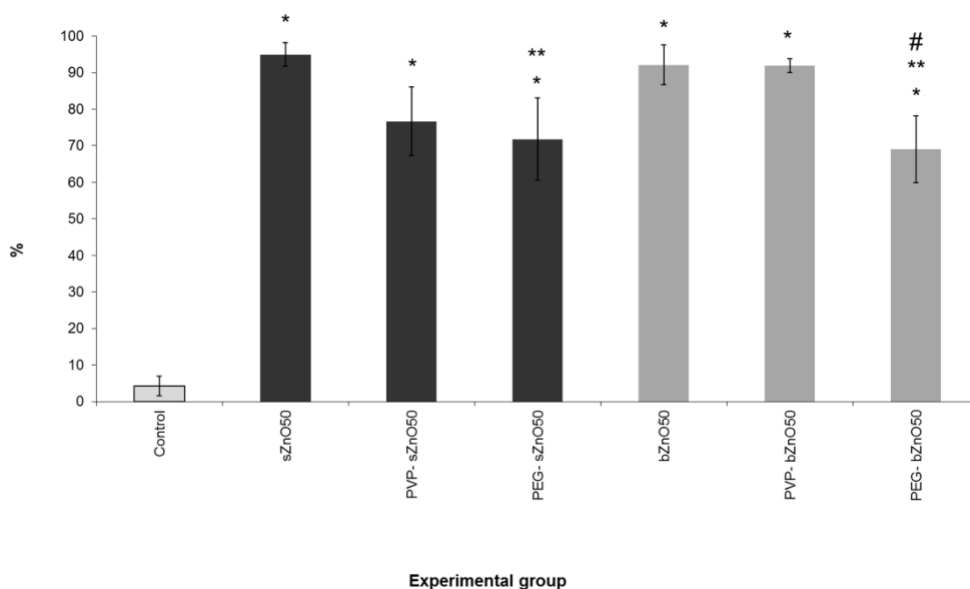
Figure 4. *Comparative FETAX malformation percentages after exposure of embryos to nude and polymer-coated sZnO and bZnO at 50 mg/L. Bars= SEM; *statistically different from control at p<0.001, **statistically different from the corresponding nude nanoparticles at p<0.05, # statistically different from the corresponding PVP coated bZnO at p< 0.05, ANOVA +Fisher LSD Method.*

No embryo lethality was observed (data not shown), while it was confirmed that high and similar incidence of malformations was induced by both sZnO and bZnO. From the comparison of the coated with the nude ZnONPs, it emerged a significant reduction in malformation rate in embryos treated with PEG coated sZnO respect to the nude ones and in those treated with PEG coated bZnO compared with the corresponding nude and PVP-coated nanoparticles. Similarly to what observed in embryos treated with nude NPs, coated ZnO NPs affected once again mainly gut coiling, abdominal and cardiac cavities causing oedema. While being lower in percentage in the embryos treated with polymer coated nanoparticles, this kind of gross malformations were still high and statistically significant compared to the control.

These findings suggest that PEG is able to significantly reduce the damages induced by the ZnONPs, even if the embryotoxic effect remains high.

3.4. Ingestion-dependent toxicity of ZnONPs

Since the exposure during whole embryogenesis (stages 8-46) highlighted that gut was the main target of the ZnONP embryotoxicity, two specific developmental windows were chosen to evaluate if the ingestion of ZnONPs could be responsible for the detected malformations. A first group of embryos was exposed to ZnONPs before the stomodeum opening (from stage 8 to 39); in this period the embryo surface is the only route of exposure. A second group of embryos was exposed to ZnONPs after stomodeum opening (from stage 39 to stage 46); during these stages embryos begin to ingest water and suspended materials.

Fig 5 summarize the results obtained by these different exposure conditions.
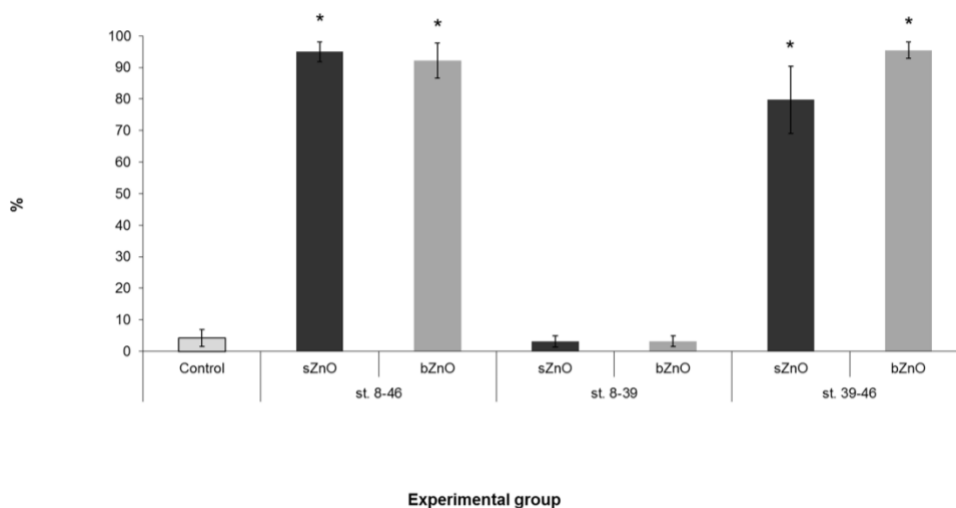
Figure 5. *Percentages of malformed embryos after exposure to sZnO and bZnO at 50 mg/L in different developmental windows. St.8-46, exposure during the whole embryogenesis as in FETAX protocol; St. 8-39, exposure from blastula to the stomodeum opening (56 hpf); St. 39-46, exposure from stomodeum opening to the end of the primary organogenesis. * Statistically different from control at p<0.001, ANOVA +Fisher LSD Method.*

We observed that both sZnO and bZnO at 50mg/L induced malformation rates comparable to those of conventional FETAX only when the exposure began after stomodeum opening. On the contrary, malformation rates comparable to the control were recorded in embryo groups exposed during the first developmental windows. These data suggest that the ingestion represents the main route of uptake for both ZnONPs.

3.5. Oxidative stress responses

Oxidative stress induced by 50 mg/L of nude and polymer-coated sZnO and bZnO in stage 46 whole embryos of all experimental groups was investigated by measuring SOD activity, that provides the first defense against ROS toxicity. As shown in Fig. 6 we observed a slight but not significant decrease in SOD activity if compared to the control in all the experimental groups. This result suggests that the production of ROS potentially induced by ZnO NPs exposure, if any, is not able to elicit a clear alteration in SOD activity, at least if it is measured in pools of whole embryos and not in single embryos or in target organ.
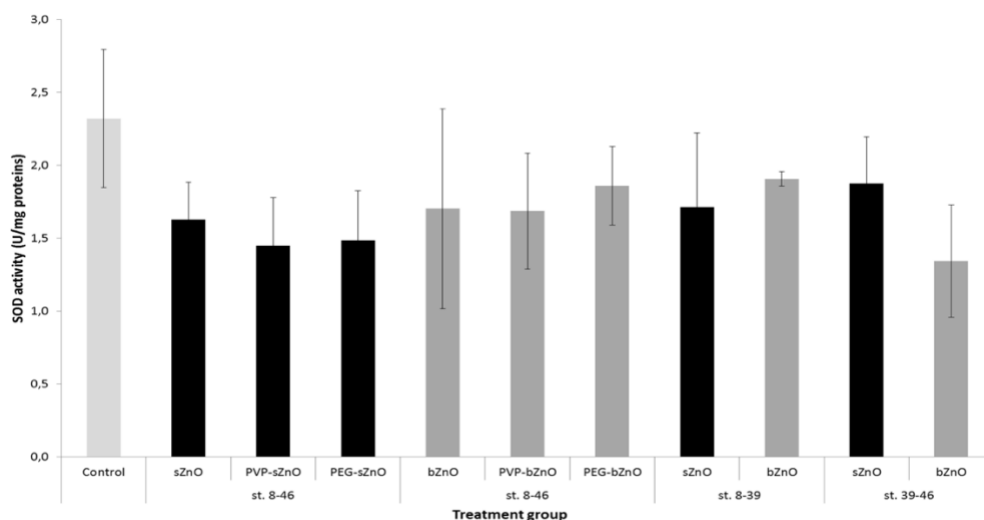
Figure 6. *SOD enzymatic activity in embryos exposed to nude and polymer-coated sZnO and bZnO 50 mg/L during different developmental stages.*

3.5. Histological and ultrastructural effects of ZnONPs on small intestine

Since abnormal gut coiling was the main feature of ZnONP treated embryos, preliminary histological and ultrastructural analyses of small intestine were performed (Fig. 7).

Despite the severity of the gut anatomical abnormality induced by ZnONPs, no obvious signs of histological damages were noted in bZnO treated embryos (Fig. 7b), while very mild tissue lesions were observed in embryos exposed to sZnO (Fig. 7c, d and g, h). These alterations were mainly consistent in a swelling of paracellular spaces in intestinal mucosa and detachment of some enterocytes from the basal lamina. On the contrary, the brush border of enterocytes was not affected.

Figure 7. Light (a-d) and electron microscopy (e-h) imaging of the X. laevis small intestine. Transversal sections at level of an intestinal loop of a control (a), bZnO (b) and sZnO (c, d) exposed embryos. Magnification of sZnO intestinal loop (d) shows the swelling of paracellular spaces between cells (white arrow) and detachment in some regions of epithelial cells from basal lamina (*). These damages are more evident in the detail of junctional complex between two enterocytes (g, black arrow) and of basal portion (h, *) of sZnO exposed embryos in comparison with control (e, black arrow and f, *).
▶=brush border; gl=gut lumen. Next page.
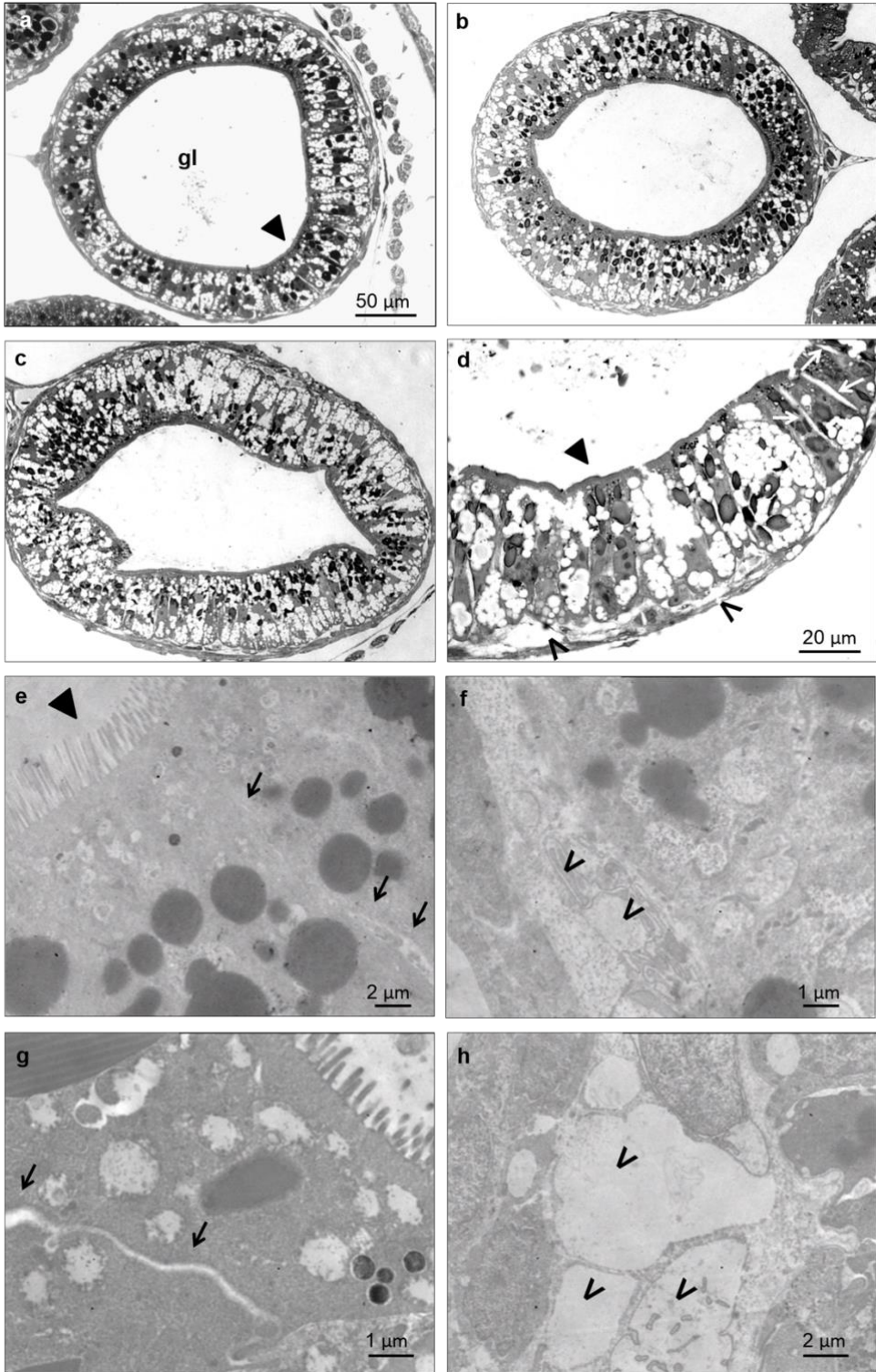
4. Discussion

Thousands of papers fill the literature of the last 15 years with the toxic effects of many different nanomaterials on *in vitro* and *in vivo* systems. Nevertheless, many aspects in nanotoxicology are still critical and need substantial improvements to make this discipline mature. According to the authors, an in deep mechanistic knowledge of the NP toxicity and an increase in the efforts devoted to the study of reproductive and developmental toxicity of new NMs should be considered mandatory in the actual second life of nanotoxicology.

This work is our contribute to increase the knowledge about these aspects and is focused on the developmental effects and the mode of action of the massively produced and widely used nano Zinc oxide. A panel of six ZnONPs, differing in size, shape and surface coating, was used to understand if and how these NMs affect *Xenopus laevis* embryos, by considering the most sensible developmental stages and the main NP target organs.

The following discussion is organized in 3 different paragraphs accordingly to the three different aspects evaluated.

4.1. Comparative toxicity of differently sized and shaped ZnONPs

Basing on our results, sZnO and bZnO induced comparable effects on *X. laevis* embryos. No mortality was observed after exposure to both NPs, while the percentage of malformed larvae and the growth retardation significantly increased starting from the concentration of 10 mg/L (Fig. 2). Anyway sZnO resulted to be more effective at 50 mg/L, where the highest malformation score was observed, while it decreased at 100 mg/L. This result suggests a reduced biovailability of sZnO, likely dependent on the stronger NP agglomeration at the highest concentration, as also proposed by Bai *et al.* (2010) for nZnO of 30 nm in water suspension. For this reason, the calculation of TC50 in the range of 1-

100 mg/L tested was possible only for bZnO and it resulted to be 48.9 mg/L. Instead, TC50 re-calculation in the range of 1-50 mg/L resulted to be of 17.9 mg/L for sZnO and 59.47 mg/L for bZnO. Taken together these results reinforce the evidence that smaller and round-shaped ZnONPs are more embryotoxic than bigger rod-shaped ones. Very similar effects were reported in an our previous study, where the embryotoxiciy of two differently sized commercial nZnOs similar in shape was compared (Bacchetta *et al.*, 2014). In addition, since both NPs did not induce mortality in *Xenopus* embryos, according to Dawson and Bantle (1987) the estimated teratogenic index (TI) should be higher than 3 for both nZnOs, allowing to consider these NPs as potential teratogens.

In our previous papers (Bacchetta *et al.*, 2012; Bacchetta *et al.*, 2014) we already suggested the potential teratogenic action of nZnO; the news from this work is that the teratogenic effect is almost independent from the NP size and shape, although the NP physic-chemical characteristic may contribute to aggravate such effect.

Several papers report the toxicity of different metal oxide nanoparticles on zebrafish embryos and many of them investigated the toxicity of nZnO (Brun *et al.*, 2014; Bai *et al.*, 2010; Zhu *et al.*, 2008; Xia *et al.*, 2011; Zhao *et al.*, 2013; Chen *et al.*, 2014). By comparing our results with those available on zebrafish, we can argue that the sensitivity to nZnO of the amphibian and fish developing embryos should be considered quite similar. Bai and collaborators (2010) observed that ZnONPs killed zebrafish embryos at 50 and 100 mg/L, while at lower concentrations they reduced body length, induced malformations and retarded embryo hatching. Also Zhu and collaborators (Zhu *et al.*, 2009) evidenced that nZnO affects hatching rate of zebrafish and reported an 84-h EC50 value of 23.06 mg/L.

Many researchers agree in indicating that embryotoxic effects are dependent on the MeONP properties rather than on the dissolved ions (Bai *et al.*, 2010; Zhu *et*

al., 2008; Zhu *et al.*, 2009). According to these authors, the metal cations dissolved from the NPs only partially contributed to the nZnO toxicity. On the contrary, other authors have reported that the nZnO toxicity in both in vitro and in vivo systems are strongly dependent from the NP dissolution (Brun *et al.*, 2014) Although the question is still debated, the solubility of nZnO can be highly dependent on the suspension medium (e.g. media added with serum albumin or ions in comparison with pure water), the initial particle size and pH (Reed *et al.*, 2012).

As already observed (Bacchetta *et al.*, 2012; Bacchetta *et al.*, 2014) the ZnONP dissolution in FETAX medium, a saline solution with a pH around 8.0, is very poor and also in this study the maximum Zn^{2+} concentration measured in NP suspension ultrafiltrates were lower than 0.5 ppm (Supplement 1). No embryotoxic effects were observed in *Xenopus* embryos exposed to zinc ions from $ZnSO_4$ at concentrations similar to those measured by ICP-OES according to Bacchetta *et al.* (2012) and Mantecca *et al.* (2015).

Basing on these findings we can affirm that in our experimental conditions size and shape didn't significantly affect NP dissolution in FETAX medium making the contribution of Zn ions to toxicity on *Xenopus* embryos very low. On the contrary, although the effects elicited by the sZnO and bZnO NPs could be considered qualitatively similar, the smaller round NPs resulted more effective. Probably it could be a consequence of the higher surface reactivity and the easier cell uptake. It is in fact well proven that round shaped NPs in the size range of 10-30 nm are preferentially taken up by cells through endocytosis (Soenen *et al.*, 2011; Albanese *et al.*, 2012).

Looking at the results of the oxidative stress biomarker SOD (Fig. 6), it is evident that nZnO exposure induced an enzymatic activity depletion, although not statistically different from the control. Again, the sZnO seemed to be more effective than bZnO. Many literature data support the oxidative changes in cells

and developing embryos as main responses to nZnO (Zhao *et al.*, 2013; Xiong *et al.*, 2011) and we also recently demonstrated that *Xenopus* embryo exposure to nZnOs results in antioxidant genes up-regulation (Bacchetta *et al.*, 2014), although the correspondent increment in the enzymatic activity is not always evident. As previously discussed, this may be attributable to the limitation of having to perform the analysis on pools of whole embryos and not on single target organ due to the small dimension of the embryos. Moreover, the developing *Xenopus* are provided of good antioxidant defenses, including enzymes such as SOD and the GSH-related system (Rizzo *et al.*, 2007), able to buffer the ROS production in cells during embryonic development.

4.2. Effects of polymer-surface coating

Polymer-surface coating is a technique widely used in industry to obtain final commercial products (e.g. paintings, additives) with better performances. In fact, this modification basically can improve the dispersion of poorly soluble NPs by modifying the surface properties of particles. Several papers underline the key role of the surface properties of ZnONPs in controlling cytotoxicity, demonstrating the reduction of toxicity in *in vitro* and *in vivo* systems after exposure to coated NPs (Xia *et al.*, 2011; Luo *et al.*, 2014). The specific surface area and/or surface reactivity of ZnONPs govern NP-biological interactions by regulating cellular nanoparticle uptake or altering both the intracellular or extracellular Zn dissolution.

Although the observed malformation rates after exposure to coated NPs were significantly higher compared to the control group, our results highlighted that surface modification of particles with PVP and PEG is able to decrease embryotoxicity of ZnONPs. In particular PEGylation appears to be more effective in reducing the toxicity of the bZnO. This is in agreement with Luo and collaborators study (Luo *et al.*, 2014) in which it has been evidenced that the

PEGylation of ZnONPs decreases their cytotoxicity in comparison with other surface modifications by reducing the cellular uptake.

4.3. Route of exposure, nZnO's target organs and sensitive developmental window

In our previous studies (Bacchetta *et al.*, 2012; Bacchetta *et al.*, 2014), we have already demonstrated that ZnONPs are highly embryotoxic and that gut is the main affected organ. In particular, the smallest ZnONPs tested were more effective in inducing more severe histopathological effects at the gut mucosa level, with the epithelium severely eroded (Bacchetta *et al.*, 2014). In the present work the intestine resulted to be again the target organ and the abnormal gut coiling was the principal malformation recorded. Nevertheless, embryo histopathological screening and gut ultrastructural analysis revealed only a slight alteration of intestinal mucosa, ascribable to detachment between adjacent cells and from basal lamina as previously described.

The choice to perform the exposure of embryos to ZnONPs in two developmental windows (before and after stomodeum opening) allows us to demonstrate that *Xenopus laevis* embryos become susceptible to nZnO with the acquisition of grazing behavior following the stomodeum opening. By this route an increasing amount of suspended and aggregated NP sedimented on the bottom of Petri dish reach gut lumen. Conversely, if the exposure is limited to the developmental period in which the embryo is enveloped by fertilization membrane, the ZnONPs are not anymore able to induce embryotoxicity. This results suggest that the fertilization membrane could represent a barrier toward ZnONPs or, if not, the skin of the embryos is not the preferential route for NP internalization. On the contrary zebrafish embryos are highly sensitive to ZnONPs during early developmental stages because the interaction of NPs with chorion affects the hatching (Bai *et al.*, 2010; Zhu *et al.*, 2008).

5. Conclusions

ZnONPs differing in size, shape and polymeric surface coating produced similar toxicity in *X. laevis* embryos, targeted the same organ and shared similar mode of action. Besides we cannot rule out how the specific physical and chemical characteristics may influence the severity of such effects. From one side our results evidence the potential adverse effects on environmental health, from the other side they suggest the possibility to modify nZnO properties during the synthesis in order to modulate the toxic effects and produce safer NMs.

Contribution

The candidate participated in the FETAX tests, performed the histological analyses and collaborated in the manuscript preparation.

References

Albanese, A.; Tang, P. S.; Chan, W. C., The effect of nanoparticle size, shape, and surface chemistry on biological systems. *Annu Rev Biomed Eng* **2012,** *14*, 1-16.

American Society for Testing and Materials (ASTM). **1998**. Standard guide for conducting the Frog Embryo Teratogenesis Assay-*Xenopus* (FETAX) E-1439–E1498.

Aruoja, V.; Dubourguier, H. C.; Kasemets, K.; Kahru, A., Toxicity of nanoparticles of CuO, ZnO and TiO2 to microalgae Pseudokirchneriella subcapitata. *Sci Total Environ* **2009,** *407* (4), 1461-8.

Ates, M.; Arslan, Z.; Demir, V.; Daniels, J.; Farah, I. O., Accumulation and toxicity of CuO and ZnO nanoparticles through waterborne and dietary exposure of goldfish (Carassius auratus). *Environ Toxicol* **2015,** *30* (1), 119-28.

Bacchetta, R.; Moschini, E.; Santo, N.; Fascio, U.; Del Giacco, L.; Freddi, S.; Camatini, M.; Mantecca, P., Evidence and uptake routes for Zinc oxide nanoparticles through the gastrointestinal barrier in *Xenopus laevis*. *Nanotoxicology* **2014,** *8* (7), 728-44.

Bacchetta, R.; Santo, N.; Fascio, U.; Moschini, E.; Freddi, S.; Chirico, G.; Camatini, M.; Mantecca, P., Nano-sized CuO, TiO$_2$ and ZnO affect *Xenopus laevis* development. *Nanotoxicology* **2012,** *6* (4), 381-98.

Bai, J.; Zhong, X.; Jiang, S.; Huang, Y.; Duan, X., Graphene nanomesh. *Nat Nanotechnol* **2010,** *5* (3), 190-4.

Blinova, I.; Ivask, A.; Heinlaan, M.; Mortimer, M.; Kahru, A., Ecotoxicity of nanoparticles of CuO and ZnO in natural water. *Environ Pollut* **2010,** *158* (1), 41-7.

Bondarenko, O.; Juganson, K.; Ivask, A.; Kasemets, K.; Mortimer, M.; Kahru, A., Toxicity of Ag, CuO and ZnO nanoparticles to selected environmentally relevant test organisms and mammalian cells in vitro: a critical review. *Arch Toxicol* **2013,** *87* (7), 1181-200.

Brun, N. R.; Lenz, M.; Wehrli, B.; Fent, K., Comparative effects of zinc oxide nanoparticles and dissolved zinc on zebrafish embryos and eleuthero-embryos: importance of zinc ions. *Sci Total Environ* **2014,** *476-477*, 657-66.

Chen, T.-H.; Lin, C.-C.; Meng, P.-J., Zinc oxide nanoparticles alter hatching and larval locomotor activity in zebrafish (Danio rerio). *Journal of Hazardous Materials* **2014,** *277* (0), 134-140.

Dawson, D. A.; Bantle, J. A., Development of a reconstituted water medium and preliminary validation of the frog embryo teratogenesis assay--*Xenopus* (FETAX). *J Appl Toxicol* **1987,** *7* (4), 237-44.

Finney D.J., Probit analysis. 3rd ed. *Cambridge: Cambridge University Press* **1971**

Gerberding JL. Toxicological profile for zinc. Atlanta: U.S. Department of Health and Human Services, Agency for Toxic Substances and Disease Registry; **2005**. pp. 11–118.

Heinlaan, M.; Dubourguier, H. C.; Arbeille, B.; Prensier, G.; Kahru, A., Electron microscopy of daphnia magna midgut epithelium upon acute exposure to CuO nanoparticles: Toxic effect of Cu-ions confirmed? *Toxicology Letters* **2010,** *196, Supplement* (0), S286.

Heinlaan, M.; Ivask, A.; Blinova, I.; Dubourguier, H. C.; Kahru, A., Toxicity of nanosized and bulk ZnO, CuO and TiO2 to bacteria Vibrio fischeri and crustaceans Daphnia magna and Thamnocephalus platyurus. *Chemosphere* **2008,** *71* (7), 1308-16.

Heinlaan, M.; Kahru, A.; Kasemets, K.; Arbeille, B.; Prensier, G.; Dubourguier, H. C., Changes in the Daphnia magna midgut upon ingestion of copper oxide nanoparticles: a transmission electron microscopy study. *Water Res* **2011,** *45* (1), 179-90.

Klein, M. J.; Guillaumée, M.; Wenger, B.; Andrea Dunbar, L.; Brugger, J.; Heinzelmann, H.; Pugin, R., Inexpensive and fast wafer-scale fabrication of nanohole arrays in thin gold films for plasmonics. *Nanotechnology* **2010,** *21* (20), 205301.

Luo, M.; Shen, C.; Feltis, B. N.; Martin, L. L.; Hughes, A. E.; Wright, P. F.; Turney, T. W., Reducing ZnO nanoparticle cytotoxicity by surface modification. *Nanoscale* **2014,** *6* (11), 5791-8.

Mantecca, P.; Moschini, E.; Bonfanti, P.; Fascio, U.; Perelshtein, I.; Lipovsky, A.; Chirico, G.; Bacchetta, R.; Del Giacco, L.; Colombo, A.; Gedanken, A., Toxicity Evaluation of a New Zn-Doped CuO Nanocomposite With Highly Effective Antibacterial Properties. *Toxicol Sci* **2015**. DOI 10.1093/toxsci/kfv067

Moschini, E.; Gualtieri, M.; Colombo, M.; Fascio, U.; Camatini, M.; Mantecca, P., The modality of cell-particle interactions drives the toxicity of nanosized CuO and TiO_2 in human alveolar epithelial cells. *Toxicol Lett* **2013,** *222* (2), 102-16.

Mouchet, F.; Landois, P.; Sarremejean, E.; Bernard, G.; Puech, P.; Pinelli, E.; Flahaut, E.; Gauthier, L., Characterisation and in vivo ecotoxicity evaluation of double-wall carbon nanotubes in larvae of the amphibian *Xenopus laevis*. *Aquat Toxicol* **2008,** *87* (2), 127-37.

Nations, S.; Long, M.; Wages, M.; Canas, J.; Maul, J. D.; Theodorakis, C.; Cobb, G. P., Effects of ZnO nanomaterials on *Xenopus laevis* growth and development. *Ecotoxicol Environ Saf* **2011b,** *74* (2), 203-10.

Nations, S.; Wages, M.; Cañas, J. E.; Maul, J.; Theodorakis, C.; Cobb, G. P., Acute effects of Fe_2O_3, TiO_2, ZnO and CuO nanomaterials on *Xenopus laevis*. *Chemosphere* **2011a,** *83* (8), 1053-61.

Nieuwkoop P.D.; Faber J., Normal table of *Xenopus laevis* (Daudin). *Amsterdam: North Holland Publishing Co.* **1956**

Nohynek, G. J.; Antignac, E.; Re, T.; Toutain, H., Safety assessment of personal care products/cosmetics and their ingredients. *Toxicol Appl Pharmacol* **2010,** *243* (2), 239-59.

Pandurangan, M.; Kim, D., In vitro toxicity of zinc oxide nanoparticles: a review. *Journal of Nanoparticle Research C7 - 158* **2015,** *17* (3), 1-8.

Reed, R. B.; Ladner, D. A.; Higgins, C. P.; Westerhoff, P.; Ranville, J. F., Solubility of nano-zinc oxide in environmentally and biologically important matrices. *Environ Toxicol Chem* **2012,** *31* (1), 93-9.

Rincker, M. J.; Hill, G. M.; Link, J. E.; Meyer, A. M.; Rowntree, J. E., Effects of dietary zinc and iron supplementation on mineral excretion, body composition, and mineral status of nursery pigs. *J Anim Sci* **2005,** *83* (12), 2762-74.

Rizzo, A.; Li, Y.; Kudera, S.; Della Sala, F.; Zanella, M.; Parak, W. J.; Cingolani, R.; Manna, L.; Gigli, G., Blue light emitting diodes based on fluorescent CdSe∕ZnS nanocrystals. *Applied Physics Letters* **2007,** *90* (5), 051106.

Santo, N.; Fascio, U.; Torres, F.; Guazzoni, N.; Tremolada, P.; Bettinetti, R.; Mantecca, P.; Bacchetta, R., Toxic effects and ultrastructural damages to Daphnia magna of two differently sized ZnO nanoparticles: does size matter? *Water Res* **2014,** *53*, 339-50.

Skjolding, L. M.; Winther-Nielsen, M.; Baun, A., Trophic transfer of differently functionalized zinc oxide nanoparticles from crustaceans (Daphnia magna) to zebrafish (Danio rerio). *Aquat Toxicol* **2014,** *157*, 101-8.

Soenen, S. J. H.; Himmelreich, U.; Nuytten, N.; De Cuyper, M., Cytotoxic effects of iron oxide nanoparticles and implications for safety in cell labelling. *Biomaterials* **2011,** *32* (1), 195-205.

Xia, T.; Zhao, Y.; Sager, T.; George, S.; Pokhrel, S.; Li, N.; Schoenfeld, D.; Meng, H.; Lin, S.; Wang, X.; Wang, M.; Ji, Z.; Zink, J. I.; Madler, L.; Castranova, V.; Nel, A. E., Decreased dissolution of ZnO by iron doping yields nanoparticles with reduced toxicity in the rodent lung and zebrafish embryos. *ACS Nano* **2011,** *5* (2), 1223-35.

Xiong, D.; Fang, T.; Yu, L.; Sima, X.; Zhu, W., Effects of nano-scale TiO2, ZnO and their bulk counterparts on zebrafish: acute toxicity, oxidative stress and oxidative damage. *Sci Total Environ* **2011,** *409* (8), 1444-52.

Xiong, D.; Fang, T.; Yu, L.; Sima, X.; Zhu, W., Effects of nano-scale TiO2, ZnO and their bulk counterparts on zebrafish: acute toxicity, oxidative stress and oxidative damage. *Sci Total Environ* **2011,** *409* (8), 1444-52.

Zhao, X.; Wang, S.; Wu, Y.; You, H.; Lv, L., Acute ZnO nanoparticles exposure induces developmental toxicity, oxidative stress and DNA damage in embryo-larval zebrafish. *Aquat Toxicol* **2013,** *136-137*, 49-59.

Zhu, X.; Wang, J.; Zhang, X.; Chang, Y.; Chen, Y., The impact of ZnO nanoparticle aggregates on the embryonic development of zebrafish (Danio rerio). *Nanotechnology* **2009,** *20* (19), 195103.

Zhu, X.; Zhu, L.; Duan, Z.; Qi, R.; Li, Y.; Lang, Y., Comparative toxicity of several metal oxide nanoparticle aqueous suspensions to Zebrafish (Danio rerio) early developmental stage. *J Environ Sci Health A Tox Hazard Subst Environ Eng* **2008,** *43* (3), 278-84.

Chapter 4:

Teratogenic hazard of BPEI-coated Silver nanoparticles to *Xenopus laevis*

Anita Colombo[1], **Melissa Saibene[1]**, Elisa Moschini[1,2], Patrizia Bonfanti[1],
Maddalena Collini[3], Kaja Kasemets[1,4], Paride Mantecca[1*]

[1]*Department of Earth and Environmental Sciences, Research Centre POLARIS, University of Milano-Bicocca, 1, Piazza della Scienza 20126 Milan, Italy*
[2]*Environmental Research and Innovation (ERIN) Department, Luxembourg Institute of Science and Technology (LIST), 5 avenue des Hauts-Forneaux, L-4362 Esch-sur-Alzette, Luxembourg*
[3]*Department of Physic, University of Milano-Bicocca, 2, piazza della Scienza 20126 Milan, Italy*
[4]*Laboratory of Environmental Toxicology, National Institute of Chemical Physics and Biophysics, Akadeemia tee 23, 12618 Tallinn, Estonia*

[*]Corresponding author: Paride Mantecca, Dept. Earth and Environmental, Research Centre POLARIS, University of Milano Bicocca, 1 piazza della Scienza, 20126, Milan, Italy

ABSTRACT

Silver nanoparticles (AgNPs) are among the most exploited antimicrobial agents and are used in many consumer products. Size and surface reactivity are critical physico-chemical properties responsible for NPs toxicity and surface coatings, often used to functionalize or stabilize AgNPs, can influence their toxic profile and biocompatibility. In the current study the developmental toxicity of 1) negatively charged citrate-coated AgNPs (Cit-AgNPs), 2) positively charged branched polyethylenimine-coated AgNPs (BPEI-AgNPs), and 3) Ag^+ (from 0.0625 to 0.75 mg Ag/L) was investigated by the standard Frog Embryo Teratogenesis Assay – *Xenopus* (FETAX). In order to identify the most sensitive developmental phase, embryos were also exposed to the AgNPs during different embryonic stages. Morphological and bio-physical studies were performed to characterize tissue lesions and NP uptake.

The results suggest that Ag^+ was strongly embryo-lethal. Contrary to Cit-AgNPs, the positively charged BPEI-AgNPs exert a concentration-dependent effect on lethality and malformations of embryos. The BPEI-AgNPs showed the highest teratogenic index (TI=1.6), pointing out the role of functional coating in determining the developmental hazard.

The highest susceptibility to BPEI-AgNPs was during the early embryogenesis, when embryos are still enclosed in the fertilization envelope, and the post-stomodeum opening stages, when NPs ingestion occurs. In BPEI-AgNPs treated larvae, the histological examination revealed irregular intestinal diverticula coupled with edematous connective tissue. Small NPs aggregates are mapped throughout the intestinal mucosa by two-photon excitation microscopy. We conclude that a teratogenic risk may be associated to BPEI-AgNPs exposure, but the modality of NP-tissue interactions and the teratogenic mechanism need further investigations to be better defined.

Keywords: silver nanoparticles; surface coating; Xenopus laevis; developmental toxicity

1. Introduction

According to the most recent nanotechnology consumer product inventories, silver represents the most frequently used nanomaterial. Out of the 1814 consumer products listed, 435 contain silver nanoparticles (AgNPs), accounting for the 24% of the already marketed nanomaterials (NMs) (Vance *et al.*, 2015). The reasons why AgNPs are so widely used reside in their high efficacy as antimicrobial and in their catalytic and conductivity activity. The antimicrobial properties, in particular, make these NPs widely applied in healthcare, biomedicine, textile industry and food sector (e.g. in food packaging). Since these widespread applications, AgNPs are predicted to be released into the aquatic environment from the use of consumer products, as evidenced in several papers (Benn and Westerhoff, 2008, Geranio *et al.*, 2009, Kaegi *et al.*, 2010). According to the studies on the predicted environmental concentration (PEC), AgNPs are pointed out as the most hazardous NM, posing serious concerns toward the environmental health and thus deserves careful future evaluations (Gottschalk *et al.*, 2013). In addition to the large presence in already marketed products, the threat to environmental health mainly derives from the high toxicity AgNPs displays toward non-target organisms, as abundantly reported in literature. AgNPs in fact are highly toxic not only to bacteria, but also to yeasts, algae, crustaceans and mammalian cells, within a range of concentrations comparable to the ones having bactericidal effects (Bondarenko *et al.*, 2013a). These authors also evidenced that the toxicity was crucially dependent on both Ag^+ dissolved from particles and NP's size.

The size- and dissolution-dependent toxicity is today a relatively well established paradigm to explain the effects of metal- and metal oxide-based NMs and the literature is full of papers reporting on it (Scown *et al.*, 2010, Lee *et al.*, 2012, Misra *et al.*, 2012, Kasemets *et al.*, 2013, Ma *et al.*, 2013, Ivask *et al.*, 2014a, Bonfanti *et al.*, 2015, He *et al.*, 2015). Focusing on AgNPs, extracellular and intracellular dissolution was retained to be the leading mechanism driving toward cell toxicity, since comparable toxicity was seen in cells and organisms exposed to Ag^+ and AgNPs (Lubick, 2008, Kim *et al.*, 2011, Kim and Ryu, 2013 , Singh and Ramarao, 2012, Yang *et al.*, 2012, Zhao and Wang, 2012, van Aerle *et al.*, 2013, Hadrup and Lam, 2014, Volker *et al.*, 2015).

Xiu *et al.* (2012) even demonstrated that the toxicity of various AgNPs – with different sizes and coated with PVP or PEG – strictly follows the concentration-dependent pattern of Ag^+ in exposed *E. coli*. They suggested that the environmental impact of AgNPs could be mitigated mainly through the modulation of Ag^+ release. It can be achieved by reducing particle oxidation, limiting oxygen availability, but also playing with NP size and surface coating. In a recent work, Le Ouay and Stellacci, (2015) underlined the key role of particle oxidation and the consequent Ag^+ release as main factors driving the action mechanism of AgNPs antibacterial activity. In addition these authors stressed also the importance of the NP surface physical and chemical properties, since they are strictly connected to the potential Ag^+ release. These considerations pointed out how the tuning of AgNPs surface properties may modulate the biological responses, opening up the possibility to engineer AgNPs by a safe-by-design approach.

Although a huge amount of toxicity studies about AgNPs is currently available, the reproductive and developmental effects of NMs are until now an underexplored field, worthy of additional research efforts. Embryogenesis can be considered as one of the most sensitive life stage, since even small perturbations

occurring during e.g. body axes formation, neurulation and organogenesis may strongly affect the entire life of an individual. Since environmental pollutants and/or pharmaceuticals, which do not show acute and chronic toxicity on adults, may influence the embryo development, a developmental toxicity screening is mandatory. This approach is of particular relevance for the emerging contaminants and new drugs, today mainly represented by nanomaterials (NMs), among which nano silver (nAg) should be considered a priority since its large use and possible risks for human and environment health. Little is known on the nAg influence during the embryo development. To this respect most of the available data come from studies using zebrafish (Asharani *et al.*, 2008, Bar-Ilan *et al.*, 2009, Powers *et al.*, 2011, Massarsky *et al.*, 2013), while, to the best of our knowledge, no reports still exist on amphibian development.

In zebrafish AgNPs have been proved to be embryotoxic at concentrations of 1-50 mg/L depending on the NPs characteristics. The main malformations observed were abnormal body axes, twisted notochord, small head jaw and snout malformations, slow blood flow and hemorrhages, pericardial edema and cardiac arrhythmia, and stunted growth (Asharani *et al.*, 2008, Bar-Ilan *et al.*, 2009, Massarsky *et al.*, 2013). These effects were seen to be dependent on size - smaller the NP higher the effect (Bar-Ilan *et al.*, 2009, Browning *et al.*, 2013) - while the main mode of action remains to be established, even if gene expression data in exposed zebrafish embryos provide support for the hypothesis that the toxicity caused by AgNPs is principally associated with dissolved silver ions (van Aerle *et al.*, 2013).

Despite this well-established knowledge, few efforts have been yet devoted to study the role of surface coating in modulating the AgNPs developmental toxicity. Hence, this work aims to understand if and how differently surface coated AgNPs, varying also in surface charge, affect *Xenopus laevis* development.

The amphibian *X. laevis* is historically used as a model in embryogenesis studies. After the Frog Embryo Teratogenesis Assay – *Xenopus* (FETAX) standardization (ASTM, 1998), it is also widely used to screen the teratogenic potential of environmental contaminants and pharmaceuticals (Fort and Paul, 2002, Bonfanti *et al.*, 2004, Chae *et al.*, 2015, Williams *et al.*, 2015). Recently FETAX has been applied even to study the embryotoxic effects and the mode of action of NMs, metal oxides in particular (Nations *et al.*, 2011, Bacchetta *et al.*, 2012). Moreover, the model flexibility allowed to investigate the most sensitive developmental windows (Bonfanti *et al.*, 2015) and the modality of NP-tissue interactions contributing to the embryotoxic effects (Bacchetta *et al.*, 2014).

Since no data are yet available on Ag-induced developmental effects on amphibians – a key sensitive group to environmental perturbations (Kiesecker *et al.*, 2001, Collins, 2010) – and up to now only few literature data report on the influence of different AgNPs surface functional coatings on embryotoxicity, the present work aims to fill these gaps.

To do it two commercially available differently coated AgNPs, namely the negatively charged citrate-coated and the positively charged branched polyethylenimine-coated (Cit-AgNPs and BPEI-AgNPs, respectively), and $AgNO_3$ as ionic control have been comparatively tested using FETAX assay. The endpoints – i.e. mortality, malformations and growth retardation – have been measured after 96h exposure and the most sensitive developmental windows have been identified by exposing embryos at different stages. The 96h LC50, EC50 and teratogenic index (TI) have been retrieved. The histopathological effects have been investigated through routine protocols, while NPs have been tracked by non-linear (two-photon excitation, TPE) microscopy.

2. Materials and Methods

2.1. Chemicals and NPs used

BPEI-AgNPs and Cit-AgNPs were purchased from nanoComposix (Prague, Czech Republic; www.nanocomposix.com). AgNPs were from the BioPure line, guaranteed sterile and endotoxin-free. As reported in the product datasheet the functionalization of the NPs was obtained by wet chemical procedures and the primary size of BPEI-AgNPs and Cit-AgNPs was ~10±2 nm. AgNPs suspensions were kept at +4°C in the dark.

Particles are supplied as aqueous solution at the concentration of 1 g Ag/L. Working concentrations of both AgNPs (0.125, 0.25, 0.5 and 0.75 mg/L) were obtained by diluting the stock solutions in FETAX medium, whose composition was (mg/L): 625 NaCl, 96 $NaHCO_3$, 30 KCl, 15 $CaCl_2$, 60 $CaSO_4 \cdot 2H_2O$ and 70 $MgSO_4$, pH 7.6–8.0. The suspensions were then vortexed for 30 sec in order to obtain homogeneous dispersion of particles.

All analytical-grade reagents, human chorionic gonadotropin (HCG), 3-amino-benzoic acid ethyl ester (MS222), salts for FETAX solution, Silver Nitrate ($AgNO_3$) were purchased from Sigma-Aldrich S.r.l. (Milan, Italy).

2.2. AgNPs characterization

The primary size and shape of AgNPs were studied by a Jeol-JEM 1220 transmission electron microscope (TEM) operating at 80 kV. Drop (~5 μl) of AgNPs (100 mg Ag/L in deionized (DI) water) was pipetted onto the 300 mesh Formvar®-coated copper grid (Electron Microscopy Sciences, EMS) and the excess of water was gently blotted. The samples were air dried before the TEM examination.

Hydrodynamic diameter (D_h) and ζ-potential of AgNPs was studied in FETAX medium and in DI water at 50 mg Ag/L using Zetasizer Nano ZS90 (Malvern

Instruments, UK). The D_h was measured in a clear 2 mL cuvette and the ζ-potential in 1 mL folded capillary cell (DTS1061, Malvern Instruments, UK) after 0 h and 24 h incubation at room temperature (RT). Samples were vortexed prior to each measurement.

UV-visible light (UV-vis) absorption spectra of BPEI-AgNPs (20 mg Ag/L) and Cit-AgNPs (12.5 mg Ag/L) in FETAX medium and in DI water was measured on a transparent 96-well polystyrene microplate (Falcon), 200 µl per well, in the range of 300-700 nm (measurement step 2 nm) using the microplate spectrophotometer (Tecan Infinite M200 PRO, Switzerland) after incubation for 0 h and 24 h at RT. Samples were vortexed prior to the measurement.

Sedimentation of AgNPs in FETAX medium and DI water was studied in a clear 2 mL polypropylene cuvette at 2 mg Ag/L after 0 and 24 h incubation at RT spectrophotometrically at 420 nm.

Solubility of the studied AgNPs in FETAX medium was studied in the abiotic conditions (i.e., without embryos). BPEI-AgNPs and Cit-AgNPs (0.5 mg Ag/L) were incubated in FETAX solution for 24 h at the same conditions used for the exposure experiments. Then, samples were ultra-filtrated using ultra-filtration tubes with a molecular weight cut-off of 10 kDa (Vivaspin®6, 10000 MWCO PES, Sartorius, Germany) at 4000 g for 30 min at 37°C (Heraeus Biofuge, UK) to remove the non-soluble fraction of AgNPs. Filtrates were acidified by 65% HNO_3 (final HNO_3 concentration 2%) and was measured by ICP-OES (Perkin-Elmer Optima 7000 DV, Santa Clara, CA, USA).

2.3. FETAX Assay

Adult *X. laevis* were housed and embryos generated according to the routine procedures adopted in our lab and already described (Bonfanti *et al.*, 2015). Before the embryo selection and the beginning of the test, the jelly coat was removed by swirling the embryos for 1−3 min in a 2.25% L-cysteine solution (pH 8.1).

Embryotoxicity tests were conducted according to the standard guide for the FETAX (ASTM, 1998). Normally-cleaved embryos at the midblastula stage (Stage 8), 5 h post-fertilization (hpf) (Nieuwkoop and Faber, 1956), were selected for testing and groups of 25 embryos from each female were randomly placed in covered 6.0 cm glass Petri dishes containing 10 mL of control or test solution. Two duplicates for each female were used. All of the Petri dishes were incubated in a thermostatic chamber at $23 \pm 0.5°C$ until the end of the test (96 hpf).

Exposure solutions were changed daily, and dead embryos were counted and removed. At the end of the assay surviving larvae of each experimental group were anaesthetized with MS-222 at 100 mg/L and screened for single morphological abnormalities by examining each larva under a dissecting microscope (Zeiss, Germany).

Mortality and malformation percentages were used to calculate the LC50 (concentration causing 50% lethality) and EC50 (concentration inducing teratogenesis in 50% of surviving embryos) for each experimental group. Surviving normal larvae were formalin fixed to estimate the growth retardation by measuring head−tail length with the digitizing software AxioVision. Each assay was repeated at least three times under the same experimental conditions.

2.4. Experimental Design

The experimental design was set up as follow:

(1) The embryotoxicity was assessed using the conventional FETAX protocol. *Xenopus* embryos were exposed over stages 8-46 to freshly prepared AgNPs suspensions (0.125, 0.25, 0.5 and 0.75 mg Ag/L) and AgNO$_3$ solutions (0.0625, 0.125, 0.25 and 0.5 mg Ag/L). The concentration range was selected in order to obtain a good concentration response curve, in terms of mortality and malformations, and therefore calculate LC50 and EC50. Control (not exposed) embryos were incubated in standard FETAX medium.

(2) In order to identify the most sensitive developmental windows the embryos were exposed to AgNPs and Ag^+ at 0.5 mg Ag/L from Stage 8 (mid-blastula, 5 hpf;) to Stage 28 (32 hpf, before hatching); from Stage 28 (32 hpf, after hatching) to Stage 39 (2 days and 8 hpf; opening of the stomodeum, preceding the acquisition of grazing behavior); from Stage 39 to Stage 46 (4 days and 10 hpf; end of the primary organogenesis). (3) At the end of the tests (96 hpf), pools of Stage 46 larvae were randomly selected and processed for light and two-photon excitation microscopy.

2.5. Histological analysis

For light microscopy analyses, larvae were randomly selected at the end of the FETAX assays and fixed in 10% formaldehyde and processed for embedding in paraffin. The samples were transversely cut from eye to proctodeum into serial sections 6 μm thick, then mounted on glass slides and stained with haematoxylin and eosin (H&E). The sections were finally examined by a Zeiss Axioplan light microscope, equipped with an Axiocam MRc5 digital camera. Ten specimens for each experimental group were histologically screened.

2.6. Two photon excitation microscopy

Formalin fixed larvae were bleached in a 3% H_2O_2/0.5% KOH medium for 2 h to avoid possible interference due to the larva pigmentation. After bleaching, specimens were routinely embedded in paraffin and 6 μm thick sections at the abdominal level, where most of the major organs are visible, were obtained. The sections, mounted on glass slides, were then dewaxed, hydrated and finally observed under an optical microscope (BX51, Olympus) equipped for two photon microscopy imaging.

The infrared laser source (Mai Tai HP+DeepSee, Spectra Physics, USA), with pulses of 120 fs full width at half maximum and 80 MHz repetition frequency, is

coupled through the FV300 (Olympus, Japan) scanning head. All the measurements were acquired through a 25X, 1.05 NA, 2 mm WD, Olympus objective (XL Plan N, Olympus, Japan). The fluorescence signal promoted at λ=800 nm is steered to a non-descanned unit and split into two channels: the green channel (BP filter at 535/50 nm) and a red channel (BP filter at 600/40 nm) by a dichroic beam splitter. Additional details on the setup and its optical characterization can be found in (Caccia *et al.*, 2008). Z- series of images (1024 x 1024 pixels, one slice/0.5 µm), have been acquired with a Kalman filter in order to increase the signal to noise ratio, and shown as a full projection. The field of view was: 190 µm x 190 µm for the BPEI-AgNPs and the control samples and 161 µm x 161 µm for the Cit-AgNPs samples.

2.7. Data Collection and Statistical Analysis

The number of dead embryos *versus* their total number at the beginning of the test led to the mortality percentages, and the number of malformed larvae *versus* the total number of surviving ones gave the malformed larva percentages. Data are expressed as the average ± SEM. The data were tested for homogeneity and normality.

When these assumptions were met, one-way analysis of variance (ANOVA) was performed; otherwise the non-parametric Kruskal–Wallis test was applied. The significance level was set at $p < 0.05$. The incidence of specific malformations was investigated by chi-square method, using Yates's correction for continuity ($\chi 2$ test) or Fisher's exact tests (FE test). When possible concentrations causing 50% lethality or malformation at 96 hpf were calculated and classified as lethal (LC50) or teratogenic (EC50), respectively. These values were obtained following the elaboration of the lethality and malformation percentages by the Probit analysis (Finney, 1971), using the U.S. EPA Probit Analysis Program, Version 1.5. The Teratogenic Index (TI), useful in estimating the teratogenic risk

associated with the tested compounds, is represented by the LC50/EC50 ratio (Dawson and Bantle, 1987).

3. Results

3.1. AgNPs characterization

According to the producer information the BPEI-AgNPs and Cit-AgNPs are round-shaped and sized ~10±0.2 nm. TEM micrographs confirm the NPs size and shape declared for both AgNPs, although the size variability seemed to be larger (Fig. 1).
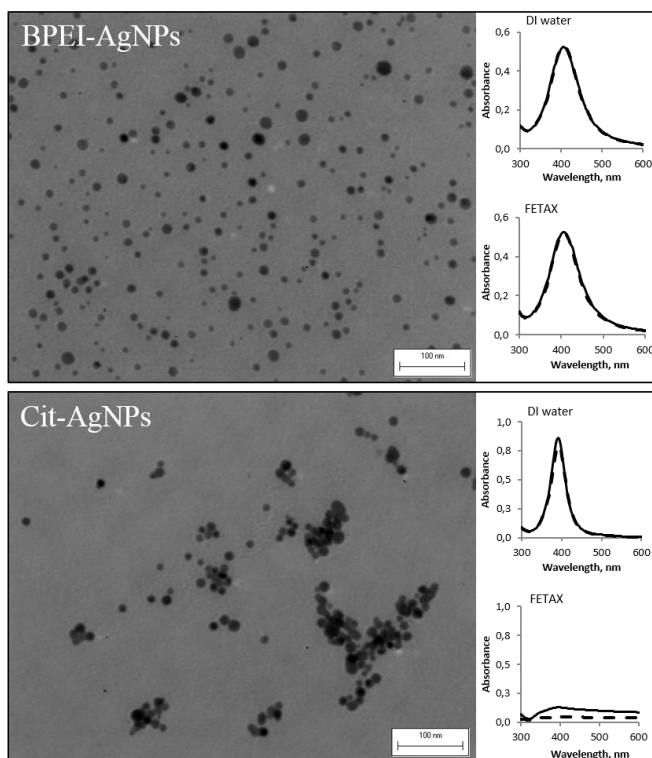
Figure 1. *TEM micrographs (left panel) and UV-vis absorption spectra (right panel) of BPEI-AgNPs and Cit-AgNPs; UV-vis absorption spectra of BPEI-AgNPs (20.0 mg Ag/L) and Cit-AgNPs (12.5 mg Ag/L) was performed in FETAX medium and in DI water after 0 h (solid line) and 24 h (dashed line) incubation at room temperature.*
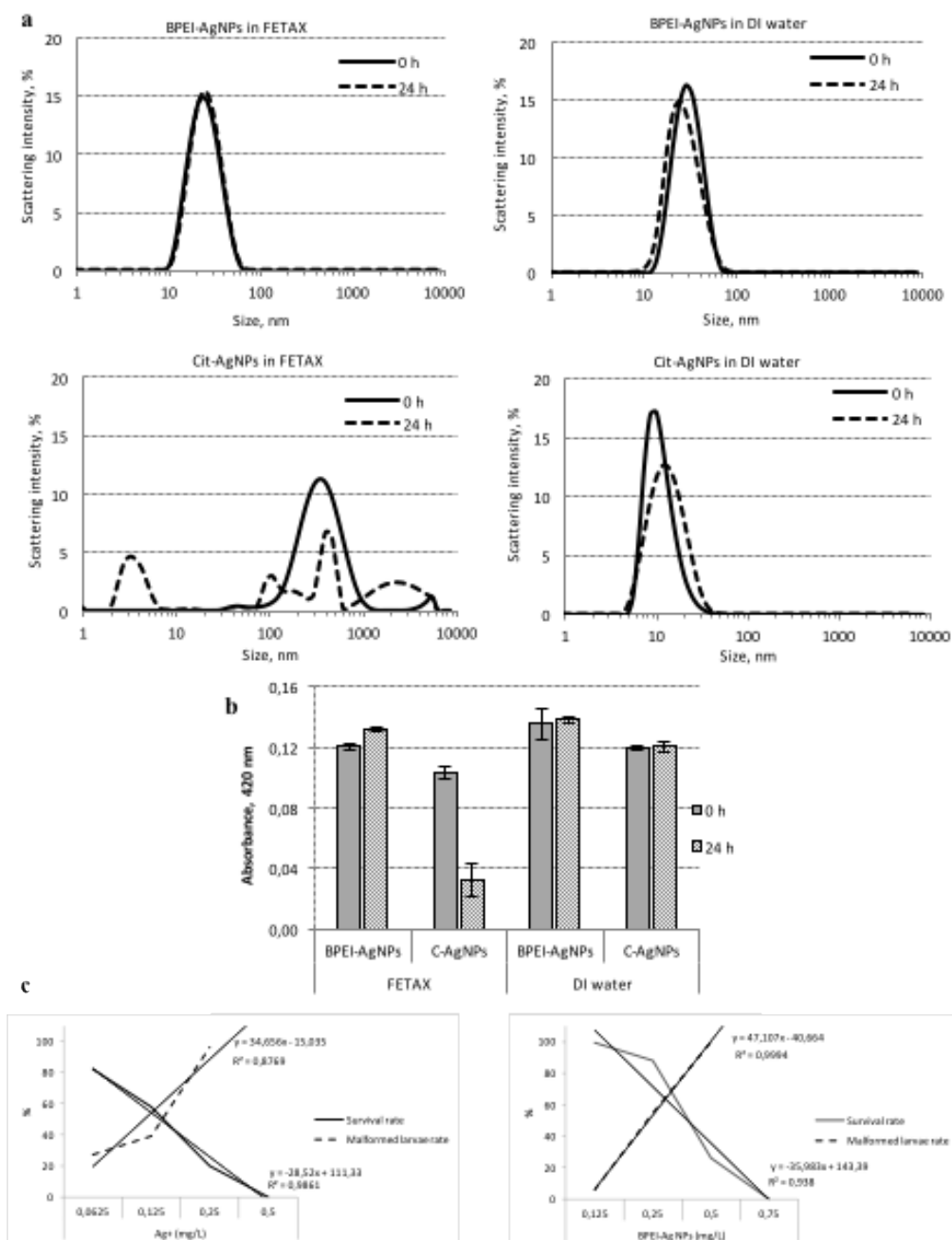
Figure S1. a) Hydrodynamic size distribution BPEI-AgNPs and Cit-AgNPs in FETAX and in deionized (DI) water (50 mg Ag/L) after 0 h and 24 h incubation at room temperature; b) Sedimentation of BPEI-AgNPs and Cit-AgNPs in FETAX and in DI water (2 mg Ag/L) after 0 h and 24 h incubation at room temperature; c) Dose-dependent effect of BPEI-AgNPs and Ag⁺ in 96 hpf larvae. As the concentration of NPs or ions increases, the malformation rate also rises while the survival rate decreases in a linear manner.

The average hydrodynamic diameter (D_h) of BPEI-AgNPs in FETAX medium was 22.8 ± 3.0 nm and 20.7 ± 0.1 nm, at 0 h and at 24 h, respectively (Table 1). BPEI-AgNPs in FETAX medium were well dispersed (pdi ~ 0.2), stable (no increase in D_h during 24 h incubation) and showed narrow one-peak size distribution (Fig.S1, a and b). Differently from BPEI-AgNPs, Cit-AgNPs agglomerated in FETAX medium and settled during 24 h incubation (Fig. S1c). Cit-AgNPs D_h was 365 ± 78 nm and 1088 ± 25 nm, at 0h and at 24 h, respectively, and the size-distribution showed the presence of differently-sized particles' populations (Fig. S1). Furthermore, the colour of Cit-AgNPs FETAX suspension turned from brownish-yellow to black within few minutes after the preparation (data not shown).

Table I. Hydrodynamic size (Dh) and ζ-potential of branched-polyethylenimine-(BPEI-AgNPs) and citrate-coated AgNPs (Cit-AgNPs) in FETAX medium and and deionized water (DI) (50 mg Ag/L) after 0 and 24 h incubation at room temperature.

AgNPs	Primary size[a] nm	Medium	Hydrodynamic size, nm[b] (pdi)		z-potential, mV	
			0 h	24 h	0 h	24 h
BPEI-AgNPs	10.2±2.0	FETAX	22.8±3.0 (0.20)	20.7±0.1 (0.22)	+9.50±1.8	+13.3± 3.5
		DI	26.4±4.7 (0.23)	24.6±0.1 (0.26)	+33.4±0.5	+36.6± 38
Cit-AgNPs	10.3±2.0	FETAX	365±78 (0.29)	1088±25 (0.77)	-34.2±1.6	-13.9± 2.6
		DI	14.6±0.6 (0.18)	14.9±0.3 (0.22)	-30.9± 0.9	-33.0±1.3

[a] producer (nanoComposix) TEM data ; [b] pdi –polydispersity index

UV-vis absorption analysis also confirmed the stability of BPEI-AgNPs (plasmon peak at 406 nm) and instability of Cit-AgNPs in FETAX medium (Fig. 1). Indeed, already after the preparation (0 h) of Cit-AgNPs suspension in FETAX medium the UV-vis absorption peak at the range of 400-500 nm was almost missing (Fig. 1). The ζ-potential of BPEI-AgNPs and Cit-AgNPs in FETAX medium was positive (+9- +13 mV) or negative (-33 mV), respectively (Table 1). Interestingly the ζ-potential of Cit-AgNPs in FETAX was quite high, but still Cit-AgNPs agglomerated and settled visibly.

BPEI-AgNPs and Cit-AgNPs were characterized also in DI water to assess the effect of medium (e.g., presence of Ag-bounding ligands) on the physico-chemical properties of the studied AgNPs. Results showed that BPEI-AgNPs had the comparable average D_h, UV-vis absorption spectra and settling properties in both test medium (Fig. 1, S1, Table 1) while Cit-AgNPs had different properties. In DI water Cit-AgNPs 24-h D_h was ~15 nm (in FETAX 1088 nm) (Table 1) and UV-vis analyses showed the presence of the characteristic spectra for AgNPs even after 24 h incubation (Fig. 1).

In FETAX medium, 24-h solubility of BPEI-AgNPs and Cit-AgNPs tested at 0.5 mg Ag/L by ICP was 2.6±1.7% and 3.6±0.3 %, respectively. The small solubility of BPEI-AgNPs was also confirmed by the UV-vis analysis (Fig. 1). As the Cit-AgNPs agglomerated and settled during the 24 h incubation, the UV-vis based solubility determination was not applicable.

3.2. *Comparative embryotoxicity of differently coated silver nanoparticles and silver ions*

Fig. 2a shows the concentration-response curves for mortality and malformations after exposure to BPEI-AgNPs, Cit-AgNPs and Ag^+. In each experiment, control group showed ≤4% mortality and malformation percentages within the range of 0.07-8% with an average of 1.7%, well below the 10% retained acceptable for the FETAX assay. The average length for control larvae was 9.1±0.6 mm (Fig. 2b).

The negatively charged Cit-AgNPs did not exert an appreciable embryotoxicity and teratogenicity, even at the highest tested concentration (0.75 mg/L), since mortality and malformation rates were not statistically different from control. On the contrary, positively charged BPEI-AgNPs and Ag^+ induced a linear concentration-dependent effect on lethality and malformations (Fig. 2a, S3).

Compared with Ag^+, BPEI-AgNPs were three times less lethal to embryos as evidenced by the 96 hpf LC50 values (Table 2).
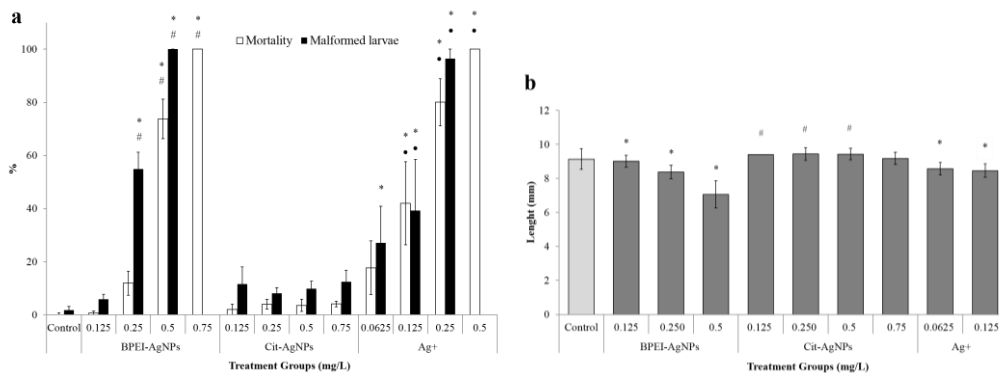
Figure 2. *FETAX results a) Comparative embryotoxicity of AgNPs and Ag^+ expressed as mortality and malformation rates; all values are given as mean±standard error; * statistically different from control; # statistically different from the corresponding concentration of Cit-AgNPs; • statistically different from the corresponding concentration of BPEI-AgNPs (p<0.05, ANOVA + Fisher LSD Method). b) Growth inhibition observed in stage 46 X. laevis larvae after 96 h of exposure to AgNPs and Ag^+. Data are expressed as mean length ± SEM; * statistically significant decrease versus control; # statistically significant increase versus control (p<0.05, ANOVA + Dunn's test).*

Table II. Median lethal concentration (96 hpf LC50), median teratogenic concentration (96 hpf TC50) (determined by US EPA Probit Analysis Program, version 1.5, with 95% confidence

	96 hpf		
Treatment	**LC50 (mg/L)**	**TC50 (mg/L)**	**TI**
BPEI-AgNPs	0.385 (0.296-0.469)	0.240 (0.226-0.253)	1.6
Cit-AgNPs	136820.25 (n.d.)	3768661.5 (n.d.)	0.036
Ag^+	0.137 (0.067-0.206)	0.128 (n.d)	1.07

n.d. denotes not determined

The 100% of mortality was reached after exposure to the highest concentration of BPEI-AgNPs tested (0.75 mg/L), and to 0.5 mg/L of Ag^+; however, considering the daily screening requested by FETAX protocol, the peak of mortality for these concentrations was recorded at 48 hpf for both BPEI-AgNPs and Ag^+ (data not shown).

Instead, malformation rate increased drastically at the concentration 0.25 mg Ag/L for both BPEI-AgNPs and Ag$^+$. The median 96 hpf EC50 was 0.24 mg Ag/L for BPEI-AgNPs and 0.128 mg/L for Ag$^+$ (Table 2). Based on these values the calculated teratogenic index (TI) was 1.60 for BPEI-AgNPs and 1.07 for Ag$^+$. Because the BPEI-AgNPs TI value is greater than 1.5, we can attribute to this compound a moderate teratogenic potential, according to American Society for Testing and Materials guide (1998).

This result is also deducible from the larger separation of concentration ranges that produce mortality and malformation in BPEI-AgNPs than in Ag$^+$ (compare the slopes of the straight lines related to malformation and survival percentages at the concentrations tested in Fig S3).

As last FETAX endpoint we measured the head-tail length of not malformed embryos; significant growth inhibition was observed after exposure to both BPEI-AgNPs and Ag$^+$ compared to the unexposed control group (Fig. 2b), starting from the lowest concentrations tested. It means that the MCIG (Minimum Concentration to Inhibit Growth) may be even lower for both BPEI-AgNPs and Ag$^+$.

Multiple malformations were registered in BPEI-AgNPs and Ag$^+$ exposed embryos that appeared in a concentration dependent manner (Table 3).

Table III. Malformation pattern in stage 46 larvae caused by 96 h exposure to coated AgNPs and Ag$^+$.

	Control	BPEI-AgNPs (mg/L)			Cit-AgNPs (mg/L)				Ag$^+$ (mg/L)		
		0.125	0.25	0.5	0.125	0.25	0.5	0.75	0.0625	0.125	0.25
Living larvae	340	140	212	76	138	231	284	233	96	104	48
Monster	4 (1.2)	2 (1.4)	3 (1.4)	5 (6.6)[a]	3 (2.2)	4 (1.7)	2 (0.7)	1 (0.4)	2 (2.1)	2 (1.0)	6 (6.25)[a]
Gut miscoiling	7 (2.1)	4 (2.9)	112 (52.8)[a]	70 (92.1)[a]	3 (2.2)	9 (3.9)	26 (9.2)[a]	24 (10.3)[a]	7 (7.3)[b]	15 (14.4)[a]	34 (70.8)[a]
Edema Cardiac			7 (3.3)[a]	20 (26.3)[a]		1 (0.4)	2 (0.7)		5 (5.2)[a]	1 (1.0)	2 (4.2)[a]
Abdominal	1 (0.3)	1 (0.7)	27 (12.7)[a]	15 (19.7)[a]	6 (4.3)[a]	6 (2.6)[b]	2 (0.7)	7 (3)[a]	1 (1.0)	2 (1.9)	7 (14.6)[a]
Tail flexure	1 (0.3)		2 (0.9)	18 (23.7)[a]	3 (2.1)[b]	3 (1.3)	10 (3.5)[a]	3 (1.7)	6 (6.3)[a]	2 (1.9)	10 (20.8)[a]
Craniofacial defects			9 (4.2)[a]	4 (5.3)[a]		1 (0.4)	1 (0.4)	2 (0.9)	26 (27.1)[a]	5 (4.8)[a]	19 (39.6)[a]
Hemorrhage	1 (0.3)	1 (0.7)	7 (3.3)[a]	11 (14.5)[a]	1 (0.7)	1 (0.4)		3 (1.7)	1 (1.0)	3 (2.9)	2 (4.2)[a]

(Percentages based on number of malformations/number of those living)
[a] chi square test: *p<0.001 versus control*
[b] chi square test: *p<0.05 versus control*

The most common induced phenotypes ranged from uncorrected gut coiling to cardiac and abdominal oedemas and from tail flexure to craniofacial defects. The

severity of these abnormalities was higher in Ag^+ than in BPEI-AgNPs exposed embryos (Fig. 3).
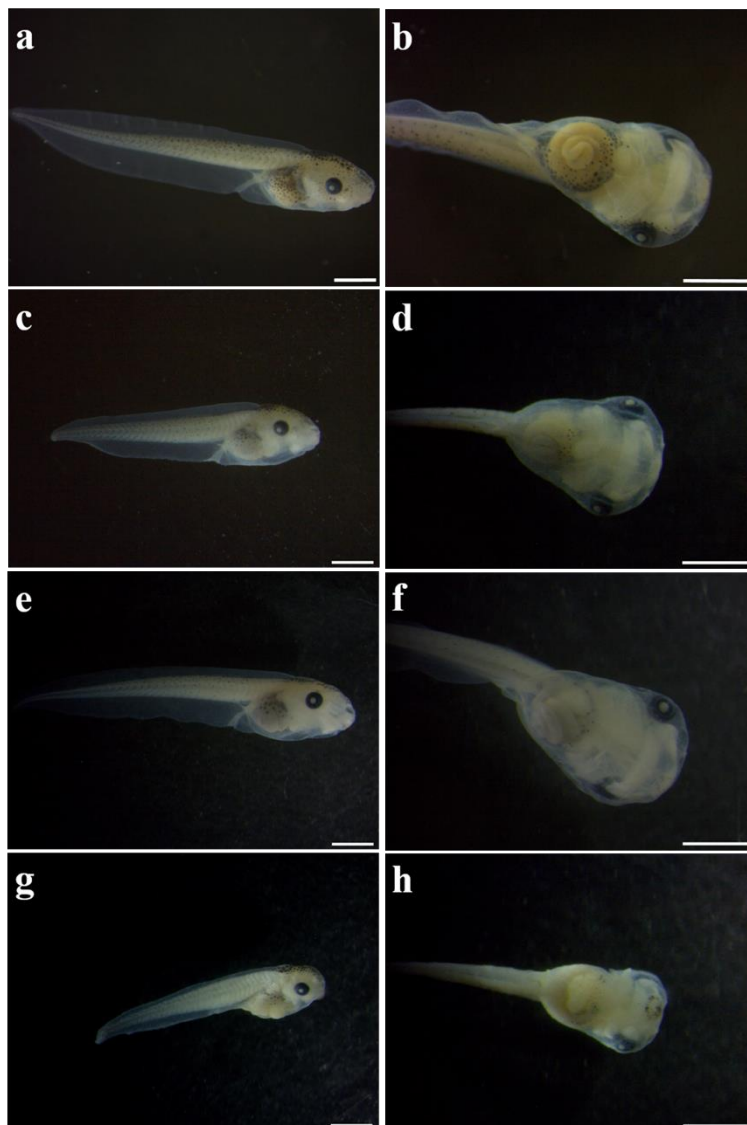
Figure 3. *Lateral (a, c, e, g) and ventral (b, d, f, h) view of X. laevis larvae at 96 hpf. Control larva (a, b), larva exposed to 0.5 mg Ag/L BPEI-AgNPs (c, d), 0.5 mg Ag/L Cit-AgNPs (e, f), 0.25 mg/L Ag^+ (g, h). Scale bar =1mm.*

Sporadic and slight increase in the percentages of the same malformations has been observed also in Cit-AgNPs exposed embryos (Table 3). In addition BPEI-

AgNPs were able to modify the fertilization envelope, which appeared yellowish and sticky, reducing and sometimes preventing the embryo hatching (Fig. 4).
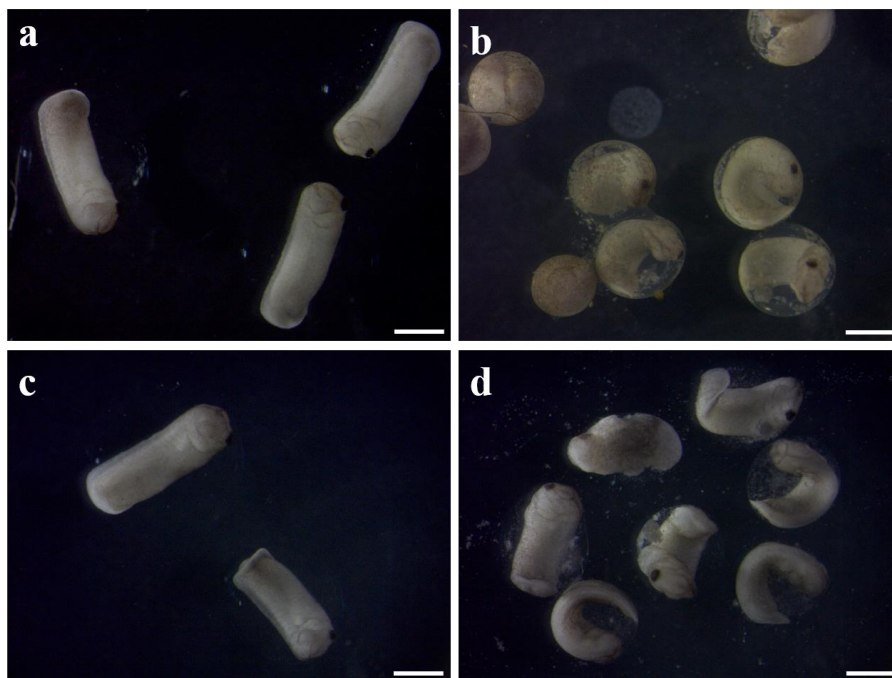
Figure 4. Steromicroscopy images of Stage 28 X. laevis embryos. Control group (a), BPEI-AgNPs (b), Cit-AgNPs (c) and Ag$^+$ (d) exposed groups. Scale bar=1mm.

3.3. Developmental window dependent-toxicity of coated silver NPs and silver ions

Xenopus early development is marked by events such as the hatching or the stomodeum opening which can be more critical regarding the potential NP-embryo interactions. For this reason, we decided to expose the embryos during three subsequent developmental windows to better investigate their sensitivity in function of the developmental stage.

During the first window (from stage 8 to stage 28) embryos were surrounded by the fertilization envelope which acts as a protective barrier. The daily screening of all the experimental groups allowed to detect significant alterations of the

fertilization envelope only in BPEI-AgNPs exposed embryos (see Fig. 4). The second selected window (from stage 28 to stage 39) is characterized by a passive embryo-NP interaction only through the thin epithelium that lines the external surface of the embryo. During the third window (from stage 39 to stage 46), the stomodeum opens and the embryo acquires a grazing behavior, facilitating active NPs intake.

A significant decrease of mortality has been evidenced in larvae exposed to BPEI-AgNPs in all the selected developmental windows in comparison to exposure over the whole embryogenesis period (Stages 8-46) (Fig. 5).
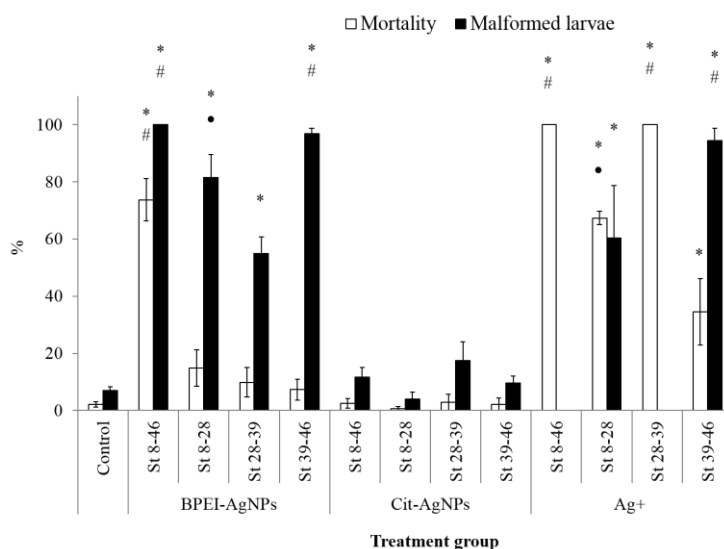
Figure 5. Embryotoxic responses expressed as mortality and malformation rates after exposure to BPEI-AgNPs, Cit-AgNPs and Ag$^+$ (0.5 mg/L) during the three different developmental windows compared to the conventional FETAX exposure. Stages 8-46, conventional FETAX exposure; Stages 8-28, exposure from mid-blastula to hatching; Stages 28-39, exposure from hatching to the stomodeum opening; Stages 39-46, exposure from stomodeum opening to the end of the primary organogenesis. Significant difference from control (*), among equivalent exposure conditions during different developmental windows (#), and from the third window (•) (p<0.05, ANOVA + Fisher LSD Method).

In contrast, the teratogenic effect remained high, even if the significant malformation rates related to the first and the third developmental windows

confirm the pre-hatching and stomodeum post-opening as the most critical periods for the exposure to BPEI-AgNPs (Fig. 5).

The embryos have displayed an elevated susceptibility to silver ions after the hatching when the embryolethality rate was not different from that observed during the of whole embryogenesis exposure. Ag^+-induced embryotoxicity during the third window resulted statistically lower than in conventional FETAX but the malformation percentage raised to a value close to 100%.

3.4. Histopathological analysis and NP tracking

To characterize the observed gross malformations induced by BPEI-AgNPs, Cit-AgNPs (0.5 mg/L) and Ag^+ (0.25 mg/L), serial transverse 6μm sections of larvae at stage 46, stained with H&E, were prepared. The observation of transversal histological sections at level of diencephalon, rhombencephalon, spinal cord and intestine revealed changes in morphology and localization of primitive organs in treated larvae compared with controls (Fig. 6).

In particular, the larvae exposed to BPEI-AgNPs and Ag^+ show craniofacial abnormalities, slight cardiac and abdominal swelling with abnormal arrangement of the intestinal loops, while the morphology and distribution of the internal organs show only mild abnormalities in larvae exposed to Cit-AgNPs.

Since abnormal gut coiling was the main feature of treated larvae, we focused our attention on small and large intestine using a higher magnification (Fig. 7).
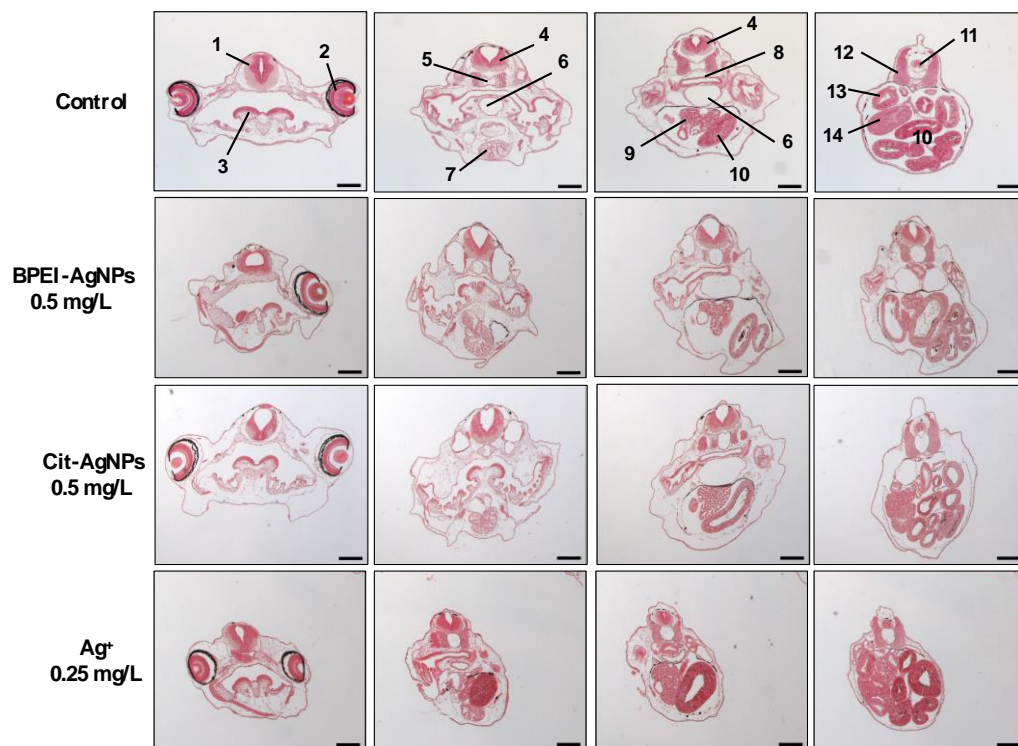
Figure 6. *Histological transversal sections of stage 46 X. laevis larvae at level of diencephalon (column 1), rhombencephalon (column 2), spinal cord (column 3) and intestine (column 4). Note the altered morphology and localization of primitive organs in the treated larvae compared to control. 1=diencephalon; 2=eye; 3=velar plate; 4=rhombencephalon; 5=notochord; 6=trachea; 7=heart; 8=esophagus; 9=liver; 10=intestine; 11=spinal cord; 12=somite; 13=duodenum; 14=oesophagus-stomach transition. Scale bar= 50μm.*

Silver ions appear to delay the normal morphogenesis of gut epithelium affecting the physiological time table of endoderm cell elongation, polarity and orientation process as the endoderm cells are still relatively yolk filled (Fig. 7d). BPEI-AgNPs perturb gut coiling as evidenced by the abnormal arrangement of the intestinal loops, loosely disposed in density and, sometimes, fused together (Fig. 7b). Nevertheless, the morphogenesis of the intestinal epithelium is not hampered even if the epithelium is less thick than control and in some regions appears to be detached from the basal membrane. Lastly, Cit-AgNPs do not interfere with the

digestive epithelial morphogenesis and the physiological resorption of yolk platelets (Fig. 7c).
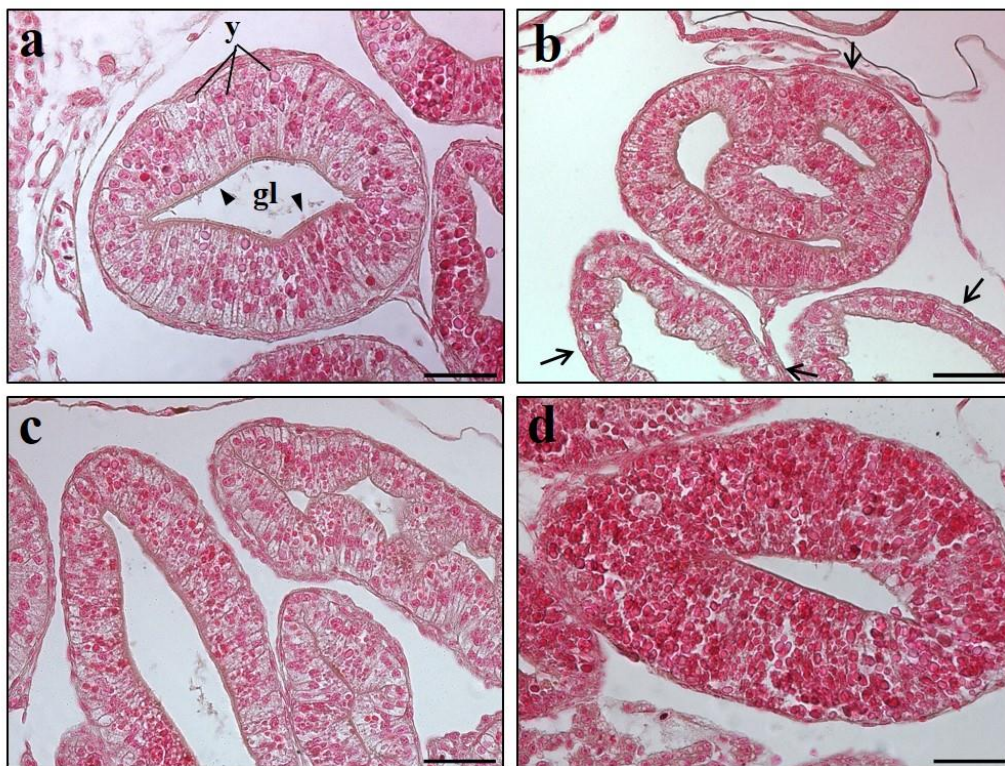
Figure 7. *Histological cross sections of intestinal loops in stage 46 X. laevis larvae exposed to AgNPs and Ag⁺. Control (a), 0.5 mg Ag/L BPEI- (b), 0.5 mg Ag/L Cit- (c) AgNPs and 0.25 mg/L Ag⁺ (d) exposed larvae. gl= gut lumen; arrowhead= brush border; y= yolk platelet; arrow= detach from basal membrane. Scale bar= 50μm.*

Using the two-photon excitation microscopy technique, both BPEI- and Cit-AgNPs were mapped in the gut lumen (Fig. 8). Moreover, as it can be observed in the red channel (Fig. 8 middle column) where AgNPs fluorescence is visible, Cit-AgNPs were mainly restricted along the enterocyte brush border, whereas BPEI-AgNPs were localized and scattered inside the enterocytes.
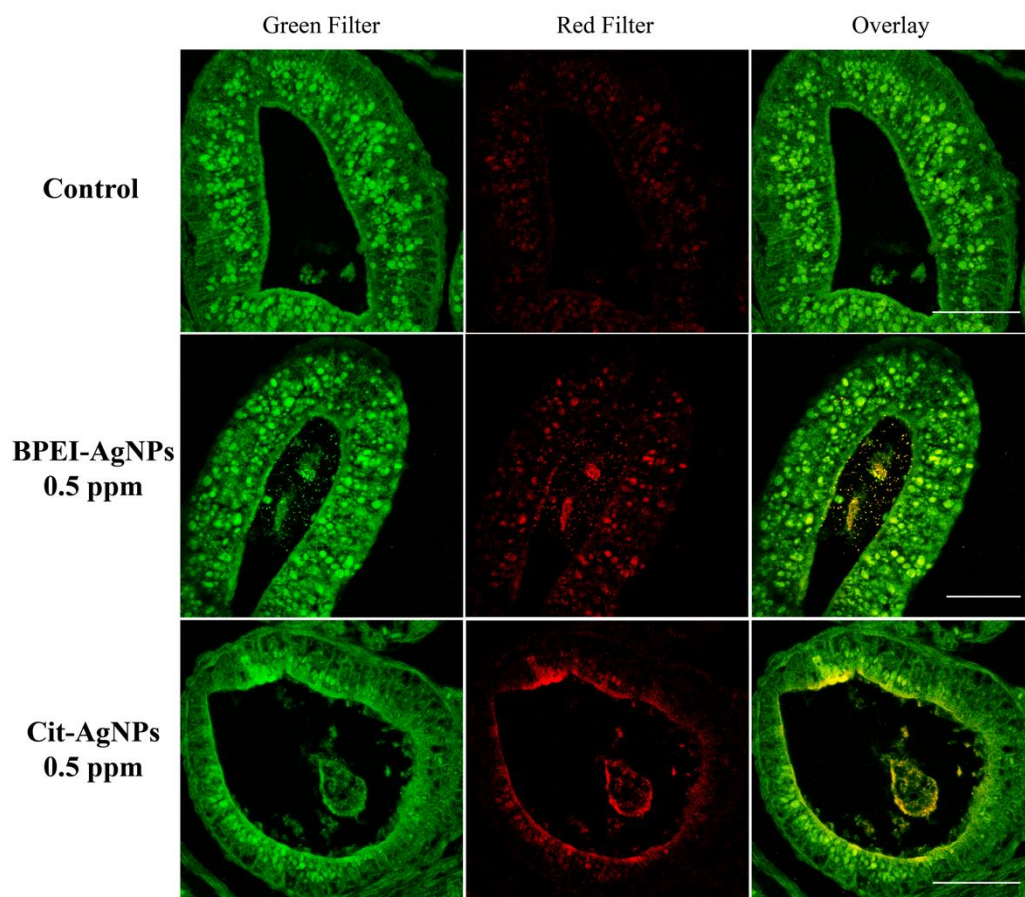
Figure 8. *Two-photon excitation confocal microscopy images taken from small intestine diverticula of stage 46 X. laevis larvae. a) control; b) 0.5 mg Ag/L BPEI-AgNPs treated larva; c) 0.5 mg Ag/L Cit-AgNPs treated larva. NP signal is clearly visible in the red channel (middle column) where the Xenopus intestinal tissue autofluorescence is negligible. In the green channel (left column), both autofluorescence and the nanoparticles emissions are visible. The right column is a superposition of the images obtained in the two channels, where in yellow is shown the colocalization of the two si*

4. Discussion

The main results shown above demonstrate that although Ag^+ induced the lowest LC50 and EC50 in *X. laevis* larvae, specific effects can be attributed to the Ag nanoformulations. In particular, it has been proven that the BPEI-coated AgNPs,

with positive surface charge, can be considered teratogenic given the high larval malformations score and the relatively high TI, while no obvious adverse effects were observed after embryo exposure to Cit-AgNPs. The sections below are aimed to discuss the reasons of this specific developmental toxicity. The NPs behavior in the medium and the modality of bio-interaction with embryo stages and tissues will be mainly considered.

4.1. AgNPs versus soluble Ag embryotoxicity: comparative analysis and role of the NPs behavior in FETAX medium

Ag^+ were highly embryolethal to *Xenopus* having - 96-h LC50 of 0.137 mg/L, the surviving larvae at the end of the FETAX test also resulted seriously malformed, with EC50 of 0.128 mg/L. Due to these evidences, the calculated TI of 1.07 suggested Ag^+ as a non-teratogen element, according to (Bantle *et al.*, 1999). To the best of our knowledge, our report is the first on Ag^+ embryotoxicity to amphibians and clearly points out that even very low Ag^+ concentrations in FETAX medium are able to kill embryos, suggesting it as a potential environmental hazard even when is not nanosized.

It is widely accepted that the AgNPs toxic effects to living organisms and cells mainly derive from the solubilized Ag ions (Navarro *et al.*, 2008, van Aerle *et al.*, 2013). Particle solubilization may occur both in extra- and intra-cellular environment, but many evidences suggest that the ions dissolved intracellularly after NPs cell uptake may constitute the main mechanism associate to the AgNPs toxicity. Known under the name of "Trojan horse", this mechanism has been described in many cells exposed to many different NPs, metals and metal oxides in particular (Sabella *et al.*, 2014), and today - together with the oxidative stress one - is considered the best paradigm to explain the enhanced toxicity of the nanosized materials. Thanks to the use of metal-specific recombinant luminescent bacteria, further has been demonstrated that the toxicity of AgNPs

to bacteria is significantly correlated not only to the level of extracellularly dissolved ions, but more specifically to the amount of bioavailable Ag^+ (Bondarenko *et al.*, 2013b).

DLS and UV-Vis analyses of studied AgNPs showed that BPEI-AgNPs were stable in the FETAX medium, but Cit-AgNPs agglomerated and settled already during the first minutes after the suspension preparation (Table 1, Fig.1, Fig. S2). Different stabilizing agents (e.g., citrate) and polymer coatings are used to increase the AgNPs dispersibility and colloidal stability due to the charge and steric repulsion forces (Tolaymat *et al.*, 2010, Fabrega *et al.*, 2011). It has been shown that citrate stabilized AgNPs were more unstable than polymer-coated particles in the chloride-containing medium while the citrate is weakly bound to the surface of the particles (Tejamaya *et al.*, 2012) resulting in the formation of insoluble silver-chlorocomplexes and precipitation (Levard *et al.*, 2013, Groh *et al.*, 2015). In our work the solubility of surface functionalized AgNPs in FETAX medium has been estimated by ICP-OES and comparatively by UV-vis absorption spectroscopy that has already been used with success in several published papers on AgNPs (Zook *et al.*, 2011, Ivask *et al.*, 2014b). It can be noted that the solubility of the studied AgNPs was low (2–4%) and is in line with the data obtained in many other papers where the AgNPs toxicity has been studied on different model organisms and cell cultures, and thus involving the use of many different test media (Ivask *et al.*, 2014c, Kaosaar *et al.*, 2016).

Considering these evidences on comparable AgNPs solubility and the extremely different results coming from the embryotoxicity screening, we can conclude that the main biological responses determined by the exposure to the Cit- and BPEI-AgNPs did not depend upon the extracellularly dissolved Ag^+, but were mainly the consequence of the specific physico-chemical behavior imparted to the NPs by the surface functional molecules. This result is in agreement with data

obtained in zebrafish embryos where none of the phenotypic defects observed in AgNPs treatment were noted in the Ag$^+$ treated embryos (Asharani *et al.*, 2008). It is worthy of attention that, contrary to Ag$^+$, no effects were evident in *Xenopus* embryos exposed to Cit-AgNPs, even at the highest test concentrations, neither in term of mortality nor in term of malformations. This result is in line with those obtained in zebrafish embryos by (Osborne *et al.*, 2013) who found that coating AgNPs with citrate significantly decreased toxicity. On the other hand, at the same concentrations at which Cit-AgNPs are completely ineffective, the BPEI-coated ones are extremely embryotoxic (96h LC50 0.385 mg/L), especially inducing high malformation scores (96h EC50 0.240 mg/L). Variable acute toxicity levels of AgNPs with LC50 ranging from 0.0346 to 250 mg/L were reported in different fish species (Cho *et al.*, 2013), in dependence on different sizes, coating agents , developmental stages and exposure duration. In zebrafish embryos, uncoated AgNPs with a size comparable to our BPEI-AgNPs showed a lower embryotoxicity with a 120-h LC50 value of 13.5 mg/L(Bar-Ilan *et al.*, 2009). In another study on zebrafish embryos, BSA and starch coated AgNPs with a size of 5-20 nm, display a LC50 value of 25.5- mg/L.

Even if the LC50 and EC50 values are higher than environmental concentrations of 0.09–2.63 ng/L (Gottschalk *et al.*, 2009), it is expected that the increase in production of AgNPs will cause the increase of the predicted environmental concentrations in the future, with a consequent risk for aquatic environment.

These results obtained in zebrafish, together with our Cit-AgNPs data, support the hypothesis that the coating agent plays a crucial role in delivering different degree of NPs toxicity. Although in different papers the phenotypic effects induced by AgNPs on fish development were investigated, to the best of our knowledge no EC50 data have been identified. The present is the first work reporting that a NM, i.e. the BPEI-coated AgNPs, may be considered a

teratogenic hazard, having a TI=1.6. It is thus difficult to compare the teratogenicity of the here studied AgNPs in *Xenopus laevis* with other models.

4.2. AgNPs ingestion and bio-interactions at the intestinal barrier level

The most appreciable abnormalities have been recorded at the abdominal level of the embryos where severe oedemas coupled with irregular gut coiling were characteristic of the BPEI-AgNPs treated embryos. This evidence is in agreement with both the light and two-photon excitation microscopy observations, showing most of the histopathological lesions and the NPs luminescence signal at the same level (see Figs. 6, 8). It is also consistent with the results obtained from exposing embryos to BPEI-AgNPs from stage 39 to stage 46, after the stomodeum opening, since when embryos freely swallow materials from the water column. The exposure during this developmental window, allowed to obtain percentages of malformed embryos up to almost 100%, similar to the exposure along the all embryogenetic events considered throughout the FETAX test (stage 8-46) (see Fig. 5). This clearly supports the hypothesis that ingestion is the main exposure route to AgNPs, and translocation through the intestinal barrier the main uptake mechanism. Previous works already demonstrated that aquatic organisms, like *Daphnia magna* and zebrafish, are mainly exposed to NMs mainly through ingestion (Santo *et al.*, 2014, Osborne *et al.*, 2015, Xiao *et al.*, 2015) and also our recent studies on *X. laevis* exposed to metal oxide NPs evidenced for the first time that even during embryogenesis, the intestine was the mostly affected organ (Bacchetta *et al.*, 2012, Bacchetta *et al.*, 2014, Bonfanti *et al.*, 2015). After exposure of adult zebrafish to 20 nm and 110 nm Cit-AgNPs, (Osborne *et al.*, 2015) observed that gills and intestine were the main affected organs, where histopathological lesions occurred in concomitance with the highest Ag accumulation in the tissues. Of course during *Xenopus* development no external gills are present and most of the gas exchange occurs through the skin for most

of the primary organogenesis. Our microscopic observations, in addition, did not reveal NPs at the skin level, corroborating the speculation that AgNPs – both positively and negatively charged – are mainly taken up by developing embryos through the intestinal epithelium. Our TPE results support the idea that the positively charged BPEI-coated AgNPs are more prone to interact with the cell membranes and to be internalized at least by the epithelial cells lining the gut. This particular NP behavior can be conferred by either the positive surface charge, that permits the electrostatic interactions with the negatively charged surface of the outer cell membranes (Jain *et al.*, 2010) or the presence of the BPEI, that may carry NPs through the cell compartments. Indeed, one reason why BPEI-coated AgNPs can exert their specific teratogenic action in *Xenopus* embryos may reside in the specific ability of PEI – a cationic dispersant - to deliver materials to cells by avoiding the acidic lysosomal pathway. The PEI transfection capacity is indeed dependent on the specific ability to lead to the osmotic swelling and rupture of the endosomes, with the consequent release of the vector into the cytoplasm (Akinc *et al.*, 2005). The same mechanism can be shared by the BPEI-coated AgNPs, that can be released inside the enterocytes after having being ingested and internalized by endocytosis, making the NP surface free for oxidative dissolution and the consequent Ag^+-mediated oxidative damage to proteins, lipids and nucleic acids (Le Ouay and Stellacci, 2015). In the nematode *C. elegans* exposed to Cit-AgNPs and $AgNO_3$, it has been recently demonstrated that the AgNPs *in vivo* toxicity – but not that of $AgNO_3$ - is crucially driven by the particle uptake by early endosomes, since endocytosis-deficient mutants and worms exposed to chloropromazine –a clathrin-mediate endocytosis inhibitor – were less sensitive than wild-type and chloropromazine untreated ones respectively (Maurer *et al.*, 2016). Organ-specific and size-dependent AgNPs toxicity has been moreover shown in zebrafish, where the smaller NPs were more prone to be retained at the basolateral level of the

intestinal epithelial cells and are able to disrupt Na^+/K^+ ATPase pump (Osborne *et al.*, 2015). Taken together the aforementioned data sustain the idea that the 10 nm BPEI-AgNPs may specifically hit *Xenopus* developing intestine, penetrating enterocytes through endocytosis and inducing cell toxicity after endosomal disruption. Of course this hypothesis on the biological mode of action of the BPEI-AgNPs requires further experimental evidences.

4.3. AgNPs effects on early embryogenesis: relevance of NPs surface properties and implications for reprotox safety assessment

A second possible mechanism of BPEI-AgNPs tissue interaction and teratogenicity should be taken into consideration. After exposure to BPEI-AgNPs during embryo stages 8-28, *Xenopus* larvae finally displayed significantly high malformation percentages (see Fig. 5). This indicates that during segmentation, gastrulation and early organogenesis – including neurulation -, when embryos are still surrounded by the fertilization envelope, NPs significantly interact and affect embryo structures. From our evidences it is clear that BPEI-AgNPs are effectively adsorbed by the fertilization envelope (Fig. 4b), although no clear evidence of particle penetration inside the embryo tissues have been achieved from this study. No NPs in fact has been mapped inside central nervous system and or somites. On the contrary, as shown in Fig. 4b, the NPs adsorption onto the fertilization coating turned it brownish and sticky, with the consequence of a delayed embryo hatching. Although no appreciable malformations can be detected soon after hatching in BPEI-AgNPs exposed embryos this contact might have had influenced the molecular or physiological events during the early developmental stages, since significant malformations appeared during the later stages. Of course this aspect is worthy of further investigations, but is coherent with the findings of (Ong *et al.*, 2014), who reported that NPs are able to affect zebrafish hatching by interacting with the ZHE1 hatching enzyme. In this latter

paper, where the effective NPs concentrations were in the range 10-100 nm, it was also underlined that the effects were mediated by the NPs themselves rather than the corresponding dissolved metal ions, further supporting our findings that the teratogenic hazard posed by the positively-charged BPEI-AgNPs derived from the peculiar nano-bio-interaction. Moreover, in our study the BPEI-AgNPs were effective already at concentrations well below 0.5 mg Ag/L. Together these observations point out that surface coating and charge of AgNPs, even at very low concentrations, may contribute to modulate the effects on the very sensitive early embryogenetic phases.

The earlier developmental stages have been already suggested to be the much more sensitive ones by (Browning *et al.*, 2013), who demonstrated that the phenotypes obtained after zebrafish treatment with AgNPs strictly depend on NP size and embryonic developmental stages of exposure. They concluded by suggesting that AgNPs can potentially enable target-specific studies and therapy for embryo development, but considering our results surface coating should be necessarily included in this NP properties' list.

The developmental toxicity is one of the priority aspects to be addressed to guarantee NM safety. In mammals of course the placenta represents an extremely important biological barrier able to prevent or modulate the access and effects of xenobiotics to the fetus. Pietroiusti *et al.*, (2013) reviewed the effects of different NMs on the placental barrier, indicating that some NPs may both cross and damage placental and fetal tissues, suggesting also to pay attention to the different mammalian developmental periods, since e.g. in the first 10 days of pregnancy in rodents, corresponding to the first trimester in the humans, the primitive placenta is leakier and thus more prone to allow NP crossing. Nevertheless, by using inert fluorescent polystyrene particles of different sizes, it has been demonstrated that up to 500 nm NPs were taken up by the mouse placenta and can even cross it. Moreover the smaller ones (20 nm and 40 nm) can

induce throphoblast cell apoptosis (Huang *et al.*, 2015). Anyway the issue of NM translocation and cytotoxic effects on placental barrier and fetus is far to be well understood. In a recent paper, (Austin *et al.*, 2016) evidenced that 10 nm citrate-coated AgNPs intravenously injected in pregnant mice preferentially ended up in maternal liver, spleen and visceral yolk sac, and although potential effects on embryo growth were arguable, the NP uptake by fetus was negligible. These studies, in parallel with our findings on the potential teratogenic hazard of the positively-charged BPEI-coated AgNPs highlight the need to further explore the role of particle size and coating in determining the fate and toxicity of AgNPs during development, to address both the safety and the potential biomedical applications of Ag-based engineered NMs.

5. Conclusions

This is the first report on AgNPs effects on amphibian development. The focus was on very small (10 nm) particles either positively charged – BPEI-coated – or negatively charged – citrate-coated -. Due to the coating molecule, the Cit-AgNPs resulted innocuous to embryos, likely as a consequence of both particle agglomeration and less capability to cross the epithelial barriers. The positively charged BPEI-coated AgNPs induced severe effects on embryo development posing teratogenic hazard, with NPs interacting with and disrupting embryo tissues, intestine in particular. Additional adverse developmental toxicity outcomes may also derive from the bio-interaction with the early embryo stages. These are likely the consequences of the peculiar physico-chemical properties conferred by the BPEI surface coating. The effects of the BPEI-AgNPs are worthy of further investigations to better understand the cellular and molecular mechanisms behind their action.

Contribution

The candidate participated in the FETAX tests, performed the histological analyses and collaborated in the manuscript preparation.

References

Akinc, A., Thomas, M., Klibanov, A.M. & Langer, R., 2005. Exploring polyethylenimine-mediated DNA transfection and the proton sponge hypothesis. *J Gene Med,* 7**,** 657-63.

American Society for Testing and Materials (ASTM). 1998. Standard guide for conducting the Frog Embryo Teratogenesis Assay-*Xenopus* (FETAX) E-1439– E1498.

Asharani, P.V., Lian Wu, Y., Gong, Z. & Valiyaveettil, S., 2008. Toxicity of silver nanoparticles in zebrafish models. *Nanotechnology,* 19**,** 255102.

Austin, C.A., Hinkley, G.K., Mishra, A.R., Zhang, Q., Umbreit, T.H., Betz, M.W., B, E.W., Casey, B.J., Francke-Carroll, S., Hussain, S.M., Roberts, S.M., Brown, K.M. & Goering, P.L., 2016. Distribution and accumulation of 10 nm silver nanoparticles in maternal tissues and visceral yolk sac of pregnant mice, and a potential effect on embryo growth. *Nanotoxicology,* 10**,** 654-61.

Bacchetta, R., Moschini, E., Santo, N., Fascio, U., Del Giacco, L., Freddi, S., Camatini, M. & Mantecca, P., 2014. Evidence and uptake routes for Zinc oxide nanoparticles through the gastrointestinal barrier in *Xenopus laevis*. *Nanotoxicology,* 8**,** 728-44.

Bacchetta, R., Santo, N., Fascio, U., Moschini, E., Freddi, S., Chirico, G., Camatini, M. & Mantecca, P., 2012. Nano-sized CuO, TiO(2) and ZnO affect *Xenopus laevis* development. *Nanotoxicology,* 6**,** 381-98.

Bantle, J.A., Finch, R.A., Fort, D.J., Stover, E.L., Hull, M., Kumsher-King, M. & Gaudet-Hull, A.M., 1999. Phase III interlaboratory study of FETAX. Part 3. FETAX validation using 12 compounds with and without an exogenous metabolic activation system. *J Appl Toxicol,* 19**,** 447-72.

Bar-Ilan, O., Albrecht, R.M., Fako, V.E. & Furgeson, D.Y., 2009. Toxicity assessments of multisized gold and silver nanoparticles in zebrafish embryos. *Small,* 5**,** 1897-910.

Benn, T.M. & Westerhoff, P., 2008. Nanoparticle silver released into water from commercially available sock fabrics. *Environ Sci Technol,* 42**,** 4133-9.

Bondarenko, O., Juganson, K., Ivask, A., Kasemets, K., Mortimer, M. & Kahru, A., 2013a. Toxicity of Ag, CuO and ZnO nanoparticles to selected environmentally relevant test organisms and mammalian cells in vitro: a critical review. *Arch Toxicol,* 87**,** 1181-200.

Bondarenko, O., Ivask, A., Kakinen, A., Kurvet, I. & Kahru, A., 2013b. Particle-cell contact enhances antibacterial activity of silver nanoparticles. *PLoS One,* 8**,** e64060.

Bonfanti, P., Colombo, A., Orsi, F., Nizzetto, I., Andrioletti, M., Bacchetta, R., Mantecca, P., Fascio, U., Vailati, G. & Vismara, C., 2004. Comparative teratogenicity of Chlorpyrifos and Malathion on *Xenopus laevis* development. *Aquatic Toxicology,* 70**,** 189-200.

Bonfanti, P., Moschini, E., Saibene, M., Bacchetta, R., Rettighieri, L., Calabri, L., Colombo, A. & Mantecca, P., 2015. Do Nanoparticle Physico-Chemical Properties and Developmental Exposure Window Influence Nano ZnO Embryotoxicity in *Xenopus laevis*? *Int J Environ Res Public Health,* 12**,** 8828-48.

Browning, L.M., Lee, K.J., Nallathamby, P.D. & Xu, X.H., 2013. Silver nanoparticles incite size- and dose-dependent developmental phenotypes and nanotoxicity in zebrafish embryos. *Chem Res Toxicol,* 26**,** 1503-13.

Caccia, M., Sironi, L., Collini, M., Chirico, G., Zanoni, I. & Granucci, F., 2008. Image filtering for two-photon deep imaging of lymphonodes. *Eur Biophys J,* 37**,** 979-87.

Chae, J.P., Park, M.S., Hwang, Y.S., Min, B.H., Kim, S.H., Lee, H.S. & Park, M.J., 2015. Evaluation of developmental toxicity and teratogenicity of diclofenac using *Xenopus* embryos. *Chemosphere,* 120**,** 52-8.

Cho, J.G., Kim, K.T., Ryu, T.K., Lee, J., Kim, J.E., Kim, J., Lee, B.C., Jo, E.H., Yoon, J., Eom, I., Choi, K. & Kim, P., 2013. Stepwise Embryonic Toxicity of Silver Nanoparticles on *Oryzias latipes*. *Biomed Res Int,* 2013.

Collins, J.P., 2010. Amphibian decline and extinction: what we know and what we need to learn. *Dis Aquat Organ,* 92**,** 93-9.

Dawson, D.A. & Bantle, J.A., 1987. Development of a reconstituted water medium and preliminary validation of the frog embryo teratogenesis assay-*Xenopus* (FETAX). *J Appl Toxicol,* 7**,** 237-44.

Fabrega, J., Luoma, S.N., Tyler, C.R., Galloway, T.S. & Lead, J.R., 2011. Silver nanoparticles: behaviour and effects in the aquatic environment. *Environ Int,* 37**,** 517-31.

Finney, D.J., 1971. Statisical logic in the monitoring of reactions to therapeutic drugs. *Methods Inf Med,* 10**,** 237-45.

Fort, D.J. & Paul, R.R., 2002. Enhancing the predictive validity of Frog Embryo Teratogenesis Assay-*Xenopus* (FETAX). *J Appl Toxicol,* 22**,** 185-91.

Geranio, L., Heuberger, M. & Nowack, B., 2009. The behavior of silver nanotextiles during washing. *Environ Sci Technol,* 43**,** 8113-8.

Gottschalk, F., Kost, E. & Nowack, B., 2013. Engineered nanomaterials in water and soils: a risk quantification based on probabilistic exposure and effect modeling. *Environ Toxicol Chem,* 32**,** 1278-87.

Groh, K.J., Dalkvist, T., Piccapietra, F., Behra, R., Suter, M.J. & Schirmer, K., 2015. Critical influence of chloride ions on silver ion-mediated acute toxicity of silver nanoparticles to zebrafish embryos. *Nanotoxicology,* 9**,** 81-91.

Hadrup, N. & Lam, H.R., 2014. Oral toxicity of silver ions, silver nanoparticles and colloidal silver-a review. *Regul Toxicol Pharmacol,* 68**,** 1-7.

He, X., Aker, W.G., Fu, P.P. & Hwang, H.-M., 2015. Toxicity of engineered metal oxide nanomaterials mediated by nano-bio-eco-interactions: a review and perspective. *Environmental Science: Nano,* 2**,** 564-582.

Huang, J.P., Hsieh, P.C., Chen, C.Y., Wang, T.Y., Chen, P.C., Liu, C.C., Chen, C.C. & Chen, C.P., 2015. Nanoparticles can cross mouse placenta and induce trophoblast apoptosis. *Placenta,* 36**,** 1433-41.

Ivask, A., Juganson, K., Bondarenko, O., Mortimer, M., Aruoja, V., Kasemets, K., Blinova, I., Heinlaan, M., Slaveykova, V. & Kahru, A., 2014a. Mechanisms of toxic action of Ag, ZnO and CuO nanoparticles to selected ecotoxicological test organisms and mammalian cells in vitro: a comparative review. *Nanotoxicology,* 8 Suppl 1**,** 57-71.

Ivask, A., Kurvet, I., Kasemets, K., Blinova, I., Aruoja, V., Suppi, S., Vija, H., Käkinen, A., Titma, T., Heinlaan, M., Visnapuu, M., Koller, D., Kisand, V. & Kahru, A., 2014b. Size-Dependent Toxicity of Silver Nanoparticles to Bacteria, Yeast, Algae, Crustaceans and Mammalian Cells *In Vitro*. *In* A. Quigg (ed.) *PLoS One.* San Francisco, USA.

Ivask, A., Elbadawy, A., Kaweeteerawat, C., Boren, D., Fischer, H., Ji, Z., Chang, C.H., Liu, R., Tolaymat, T., Telesca, D., Zink, J.I., Cohen, Y., Holden, P.A. & Godwin, H.A., 2014c. Toxicity mechanisms in *Escherichia coli* vary for silver nanoparticles and differ from ionic silver. *ACS Nano,* 8**,** 374-86.

Jain, K., Kesharwani, P., Gupta, U. & Jain, N.K., 2010. Dendrimer toxicity: Let's meet the challenge. *International Journal of Pharmaceutics,* 394**,** 122-142.

Kaegi, R., Sinnet, B., Zuleeg, S., Hagendorfer, H., Mueller, E., Vonbank, R., Boller, M. & Burkhardt, M., 2010. Release of silver nanoparticles from outdoor facades. *Environmental Pollution,* 158**,** 2900-2905.

Kaosaar, S., Kahru, A., Mantecca, P. & Kasemets, K., 2016. Profiling of the toxicity mechanisms of coated and uncoated silver nanoparticles to yeast *Saccharomyces cerevisiae* BY4741 using a set of its 9 single-gene deletion mutants defective in oxidative stress response, cell wall or membrane integrity and endocytosis. *Toxicol In Vitro,* 35**,** 149-62.

Kasemets, K., Suppi, S., Kunnis-Beres, K. & Kahru, A., 2013. Toxicity of CuO nanoparticles to yeast *Saccharomyces cerevisiae* BY4741 wild-type and its nine isogenic single-gene deletion mutants. *Chem Res Toxicol,* 26**,** 356-67.

Kiesecker, J.M., Blaustein, A.R. & Belden, L.K., 2001. Complex causes of amphibian population declines. *Nature,* 410**,** 681-4.

Kim, J., Kim, S. & Lee, S., 2011. Differentiation of the toxicities of silver nanoparticles and silver ions to the Japanese medaka (*Oryzias latipes*) and the cladoceran *Daphnia magna*. *Nanotoxicology,* 5**,** 208-14.

Kim, S. & Ryu, D.Y., 2013. Silver nanoparticle-induced oxidative stress, genotoxicity and apoptosis in cultured cells and animal tissues. *J Appl Toxicol,* 33**,** 78-89.

Le Ouay, B. & Stellacci, F., 2015. Antibacterial activity of silver nanoparticles: A surface science insight. *Nano Today,* 10**,** 339-354.

Lee, K.J., Browning, L.M., Nallathamby, P.D., Desai, T., Cherukui, P.K. & Xu, X.H.N., 2012. In Vivo Quantitative Study of Sized-Dependent Transport and

Toxicity of Single Silver Nanoparticles Using Zebrafish Embryos. *Chem Res Toxicol,* 25**,** 1029-46.

Levard, C., Mitra, S., Yang, T., Jew, A.D., Badireddy, A.R., Lowry, G.V. & Brown, G.E., Jr., 2013. Effect of chloride on the dissolution rate of silver nanoparticles and toxicity to E. coli. *Environ Sci Technol,* 47**,** 5738-45.

Lubick, N., 2008. Nanosilver toxicity: ions, nanoparticles--or both? *Environ Sci Technol,* 42**,** 8617.

Ma, H., Williams, P.L. & Diamond, S.A., 2013. Ecotoxicity of manufactured ZnO nanoparticles--a review. *Environ Pollut,* 172**,** 76-85.

Massarsky, A., Dupuis, L., Taylor, J., Eisa-Beygi, S., Strek, L., Trudeau, V.L. & Moon, T.W., 2013. Assessment of nanosilver toxicity during zebrafish (*Danio rerio*) development. *Chemosphere,* 92**,** 59-66.

Maurer, L.L., Yang, X., Schindler, A.J., Taggart, R.K., Jiang, C., Hsu-Kim, H., Sherwood, D.R. & Meyer, J.N., 2016. Intracellular trafficking pathways in silver nanoparticle uptake and toxicity in *Caenorhabditis elegans*. *Nanotoxicology,* 10**,** 831-5.

Misra, S.K., Dybowska, A., Berhanu, D., Luoma, S.N. & Valsami-Jones, E., 2012. The complexity of nanoparticle dissolution and its importance in nanotoxicological studies. *Science of The Total Environment,* 438**,** 225-232.

Nations, S., Wages, M., Cañas, J.E., Maul, J., Theodorakis, C. & Cobb, G.P., 2011. Acute effects of Fe2O3, TiO2, ZnO and CuO nanomaterials on *Xenopus laevis*. *Chemosphere,* 83**,** 1053-1061.

Navarro, E., Piccapietra, F., Wagner, B., Marconi, F., Kaegi, R., Odzak, N., Sigg, L. & Behra, R., 2008. Toxicity of silver nanoparticles to *Chlamydomonas reinhardtii*. *Environ Sci Technol,* 42**,** 8959-64.

Nieuwkoop P.D., & Faber J., 1956. *Normal table of Xenopus laevis (Daudin) Amsterdam*: *North Holland Publishing Co.*

Ong, K.J., Zhao, X., Thistle, M.E., Maccormack, T.J., Clark, R.J., Ma, G., Martinez-Rubi, Y., Simard, B., Loo, J.S., Veinot, J.G. & Goss, G.G., 2014. Mechanistic insights into the effect of nanoparticles on zebrafish hatch. *Nanotoxicology,* 8**,** 295-304.

Osborne, O.J., Johnston, B.D., Moger, J., Balousha, M., Lead, J.R., Kudoh, T. & Tyler, C.R., 2013. Effects of particle size and coating on nanoscale Ag and TiO(2) exposure in zebrafish (*Danio rerio*) embryos. *Nanotoxicology,* 7**,** 1315-24.

Osborne, O.J., Lin, S., Chang, C.H., Ji, Z., Yu, X., Wang, X., Xia, T. & Nel, A.E., 2015. Organ-Specific and Size-Dependent Ag Nanoparticle Toxicity in Gills and Intestines of Adult Zebrafish. *ACS Nano,* 9**,** 9573-84.

Pietroiusti, A., Campagnolo, L. & Fadeel, B., 2013. Interactions of engineered nanoparticles with organs protected by internal biological barriers. *Small,* 9**,** 1557-72.

Powers, C.M., Levin, E.D., Seidler, F.J. & Slotkin, T.A., 2011. Silver exposure in developing zebrafish produces persistent synaptic and behavioral changes. *Neurotoxicology and Teratology,* 33**,** 329-332.

Sabella, S., Carney, R.P., Brunetti, V., Malvindi, M.A., Al-Juffali, N., Vecchio, G., Janes, S.M., Bakr, O.M., Cingolani, R., Stellacci, F. & Pompa, P.P., 2014. A general mechanism for intracellular toxicity of metal-containing nanoparticles. *Nanoscale.* 7052-61.

Santo, N., Fascio, U., Torres, F., Guazzoni, N., Tremolada, P., Bettinetti, R., Mantecca, P. & Bacchetta, R., 2014. Toxic effects and ultrastructural damages to *Daphnia magna* of two differently sized ZnO nanoparticles: does size matter? *Water Res,* 53**,** 339-50.

Scown, T.M., Santos, E.M., Johnston, B.D., Gaiser, B., Baalousha, M., Mitov, S., Lead, J.R., Stone, V., Fernandes, T.F., Jepson, M., Van Aerle, R. & Tyler, C.R., 2010. Effects of aqueous exposure to silver nanoparticles of different sizes in rainbow trout. *Toxicol Sci,* 115**,** 521-34.

Singh, R.P. & Ramarao, P., 2012. Cellular uptake, intracellular trafficking and cytotoxicity of silver nanoparticles. *Toxicol Lett,* 213**,** 249-59.

Tejamaya, M., Romer, I., Merrifield, R.C. & Lead, J.R., 2012. Stability of citrate, PVP, and PEG coated silver nanoparticles in ecotoxicology media. *Environ Sci Technol,* 46**,** 7011-7.

Tolaymat, T.M., El Badawy, A.M., Genaidy, A., Scheckel, K.G., Luxton, T.P. & Suidan, M., 2010. An evidence-based environmental perspective of manufactured silver nanoparticle in syntheses and applications: a systematic review and critical appraisal of peer-reviewed scientific papers. *Sci Total Environ,* 408**,** 999-1006.

Van Aerle, R., Lange, A., Moorhouse, A., Paszkiewicz, K., Ball, K., Johnston, B.D., De-Bastos, E., Booth, T., Tyler, C.R. & Santos, E.M., 2013. Molecular mechanisms of toxicity of silver nanoparticles in zebrafish embryos. *Environ Sci Technol,* 47**,** 8005-14.

Vance, M.E., Kuiken, T., Vejerano, E.P., Mcginnis, S.P., Hochella, M.F., Rejeski, D. & Hull, M.S., 2015. Nanotechnology in the real world: Redeveloping the nanomaterial consumer products inventory. *Beilstein J Nanotechnol,* 6**,** 1769-80.

Volker, C., Kampken, I., Boedicker, C., Oehlmann, J. & Oetken, M., 2015. Toxicity of silver nanoparticles and ionic silver: Comparison of adverse effects and potential toxicity mechanisms in the freshwater clam *Sphaerium corneum*. *Nanotoxicology,* 9**,** 677-85.

Williams, J.R., Rayburn, J.R., Cline, G.R., Sauterer, R. & Friedman, M., 2015. Effect of allyl isothiocyanate on developmental toxicity in exposed *Xenopus laevis* embryos. *Toxicology Reports,* 2**,** 222-227.

Xiao, Y., Vijver, M.G., Chen, G. & Peijnenburg, W.J., 2015. Toxicity and accumulation of Cu and ZnO nanoparticles in *Daphnia magna*. *Environ Sci Technol,* 49**,** 4657-64.

Xiu, Z.M., Zhang, Q.B., Puppala, H.L., Colvin, V.L. & Alvarez, P.J., 2012. Negligible particle-specific antibacterial activity of silver nanoparticles. *Nano Lett,* 12**,** 4271-5.

Yang, X., Gondikas, A.P., Marinakos, S.M., Auffan, M., Liu, J., Hsu-Kim, H. & Meyer, J.N., 2012. Mechanism of silver nanoparticle toxicity is dependent on dissolved silver and surface coating in *Caenorhabditis elegans*. *Environ Sci Technol,* 46**,** 1119-27.

Zhao, C.M. & Wang, W.X., 2012. Importance of surface coatings and soluble silver in silver nanoparticles toxicity to *Daphnia magna*. *Nanotoxicology,* 6**,** 361-70.

Zook, J.M., Long, S.E., Cleveland, D., Geronimo, C.L. & Maccuspie, R.I., 2011. Measuring silver nanoparticle dissolution in complex biological and environmental matrices using UV-visible absorbance. *Anal Bioanal Chem,* 401**,** 1993-2002.

Discussion

Different *in vitro* models for a complete NP safe assessment

Thousands of papers fill the literature of the last 15 years with the toxic effects of many different nanomaterials on *in vitro* and *in vivo* systems. Nevertheless, many aspects in nanotoxicology are still critical and need substantial improvements to make this discipline mature.

An in deep mechanistic knowledge of the NP toxicity and an increase in the efforts devoted to the study of reproductive and developmental toxicity of new NMs should be considered mandatory in the actual second life of nanotoxicology. Different models for a complete assessment has been proposed in this thesis, models with an even more high complexity. On a simple alveolar monoculture (A549 line, Chapter 1) were describe the cytotoxic effects of three different shaped nZnO. A novel 3D tetraculture alveolar model was chosen to describe the effects of three different shaped PEGylated AuNPs (Chapter 2). Then the embryotoxic effects of nZnO and AgNPs were considered on *Xenopus laevis* (Chapter 3 and 4, respectively).

The main goal of this manuscript was indeed to propose three *in vitro* models, with different complexity and features to better understand the behavior of NPs showing several physico-chemical properties often not shared among them. Interestingly, despite these numerous differences some common aspects will be pointed out, as the important role of NP shape, independently from the NP used and the model chosen.

A549 monoculture as a simple first step to assess NP toxicity

The main route of human exposure to NPs is represented by inhalation. The alveolar sacs represent the last and thinner barrier between air and organism, where interaction between cells and NPs can occur.

Monoculture systems are the most suitable models used to study the effects of inhaled chemical and particles. Obviously, the use of a single cell line is a simplification of a complex system as the lung is, but a monoculture system is an easy, fast and anyway valid model for screening the effects of certain chemicals and particles. In this work, the A549 Human Alveolar Adenocarcinoma Cell Line was chosen because it is an established model of Type II alveolar epithelium widely used to perform lung toxicity experiments (Foster *et al.*, 1998). As reported by Foster *et al.*, (1998), A549 cells have many important biological properties of Type II alveolar cells, as membrane bound inclusions that resemble lamellar bodies, distinct polarization and extensive cytoplasmic extensions, even if the formation of tight junctions is not definitively confirmed. On one side, Elbert *et al.*, (1999) suggested that A549 cells did not express zonula occludens-1 protein, the marker of tight junctions; on the other side Rothen-Rutishauser *et al.*, (2008) have shown that A549 cells are able to create a barrier and generate Trans Epithelial Electrical Resistance (TEER), which is a good requisite for the development of an intact epithelium characterized also by the presence of thigh junctions (Agu and Ugwoke, 2011; Geys *et al.*, 2006).

1. The effects of differently shaped nZnO on A549 cell line

The monoculture of A549 cells was selected to assess the effects of three different shaped nZnOs (Chapter 1). NZnO represents one of the prioritized NMs to be considered for regulation because of its wide range of applications as stabilizer and antibacterial and UV protective agent (Nohynek *et al.*, 2010).

Many studies investigated nZnO effects on human cells and laboratory mammals, pointing out their relevant cytotoxic and inflammatory potency (Pandurangan and Kim, 2015). In other papers, the toxicity of nZnO is discussed in different vertebrate and invertebrate models (Ates *et al.*, 2015; Bonfanti *et al.*, 2015; Brun

et al., 2014; Mantecca *et al.*, 2015; Santo *et al.*, 2014; Skjolding *et al.*, 2014). Nevertheless, safety, toxicity and in particular the interactions of this nMeO with biological systems are not yet fully understood (Pandurangan and Kim, 2015). These bio-interactions are critical in many fields of NM application, such as phototherapy (El-Sayed *et al.*, 2006; West and Halas, 2003), imaging (Weissleder, 2006) and drugs/gene delivery (Panyam and Labhasetwar, 2003; Whitehead *et al.*, 2009), which require NPs to cross the cell membrane to reach their cytosolic or nuclear target. It follows that the study of the interactions of NPs with cells needs to be expanded also in view of the possible toxic effects arising from these interactions.

In several papers (Chithrani and Chan, 2007; Chithrani *et al.*, 2006; Jiang *et al.*, 2008; Osaki *et al.*, 2004; Rejman *et al.*, 2004; Wang *et al.*, 2010), researchers pointed out the dependent correlation between particle size with an increase in NP internalization increasing the particle size (approximatively until 50 nm that represents an optimum).

In HeLa cells, it has been shown that small rods with a length of 40 nm can be readily absorbed by cells compared to rods with one dimension greater than 50 nm, suggesting that a large contact area between NP and cell membrane leads to a reduction in terms of availability of binding sites necessary for receptor mediated endocytosis (Chithrani *et al.*, 2006).

In this study, three different forms of nZnO, comparable in size (< 100 nm) but different in shape (round, rod-like and cubic) were selected with the aim to verify if the shape can influence the modality of interaction with the cells. The results obtained indicate that the shape is a NP feature that drives significantly their bio-interactions with the A549 cell line.

Here we evaluated different parameters, such as intracellular ROS production, lysosomal activity and NP dissolution, after screening cell viability at increasing concentrations of NPs ($0 - 30\,\mu\mathrm{g/mL}$). All the NPs were quite cytotoxic for A549

cells after 24 hours of exposure; in particular S-nZnO induced a significant decrease in cell viability starting from the concentration of 20 µg/mL, while for R-nZnO and C-nZnO the effect started to be significant at 25 µg/mL.

This work highlight once again how small differences in few phisico-chemical properties could attribute to particles with the same chemical composition, significantly different behaviours at the bio-interface.

2. Intracellular ROS production is independent from shape

Intracellular ROS production is known to be a typical cell response to NP treatment (Nel *et al.*, 2006). After 24 h of exposure to nZnOs, all the three compounds induced a significant and comparable increase in intracellular ROS production unlike Zn^{++} ions.

It is interesting to note that ZnO NPs with different shapes induce a similar response in terms of production of ROS into intracellular environmental without inducing high level of cell mortality. Generation of ROS was previously demonstrated to occur in A549 cells exposed to ZnO NPs (Hsiao and Huang, 2011). In the same paper, it has been shown that the coating of nZnO with TiO_2 moderated its toxicity by curtailing the release of zinc ions and decreasing the contact area of the ZnO cores. This suggest that ROS generation by ZnO NPs is mainly due to intracellular Zn^{++} ions release that is independent by the NP shape.

3. Shape drives the NP internalization

One of the mechanisms of ZnO nanoparticles toxicity is based on the dissolution of NPs in the lysosomes that lead to the increase of intra-lysosomal Zn^{++} levels and consequent lysosomal destabilization (Pandurangan and Kim, 2015).

In our study, S-nZnO and R-nZnO seem to dissolve in the intracellular environment releasing Zn^{++}, which partially co-localized with lysosomes as

shown in the images obtained by fluorescence microscopy. In both cases, the number and the size of lysosomes appeared also increased.

We could hypothesize that the spherical and rod-like nZnOs interact with cells entering by the classical endocytic pathway, engulfing lysosomes (which they increase in size and number) and finally releasing Zn^{++} due to the acidic pH in the lysosomal vesicles. Interestingly, the green fluorescence resulted in spot shaped signals, sometimes not completely co-localized with the red fluorescence of healthy lysosomes. This could indicate that the dissolution occurred earlier in those lysosomes affecting their membrane thus compromising the ability of the Lysotracker to stain damaged organelles.

The above mentioned hypothesis could explain also why the cubical nZnO results less toxic than the other ones. Apparently this nanomaterial does not dissolve into the lysosomal environment as testified by both confocal and flow cytometry analysis since the fluorescence measured in C-ZnO was almost comparable to that from control cells. Probably C-nZnO enters cells following some mechanisms different from endocytosis thus escaping the classical intralysosomal dissolution. This pointed out once again the key role played by the intracellular release of metal ions in inducing nZnO cytotoxicity and how the shape could be an important aspect influencing the modality of internalization and the subsequent toxic effects.

3D *in vitro* models: the best choice to predict NP effects at the tissue level

Inhalation studies were generally performed *in vivo*, which has the advantage of allowing the direct investigation at organ and organism levels functions (Secondo *et al.*, 2017).

However, the discussion regarding the use of laboratory animals well discussed and summarized in the 3R strategy (Replacement, Reduction and Refinement)

proposed by Russel and Burch (1959), place the development and proposal of alternative methods a real challenge to deal with nowadays.

The use of 3D *in vitro* models represents a valid and efficient alternative to predict the acute toxicity of inhaled substances (de Souza Carvalho *et al.*, 2014; Müller *et al.*). Recently, Secondo *et al.* (2017) compared studies *in vivo* and *in vitro* exposure to several NPs (silver, zinc oxide, titanium dioxide and multi-walled carbon nanotubes) observing that the responses in term of cytotoxicity and inflammation were similar.

It is in general well accepted that the introduction and the development of new *in vitro* realistic models could boost the reduction of animals used in toxicological studies, overcoming some ethical issues and decreasing the experimental costs.

In the last years, numerous 3D *in vitro* lung models have been proposed for inhalation toxicology studies. These models, more or less complex, mimic the tissue organization trying to approach the response of the human lung tissue (Blank *et al.*, 2006; Braakhuis *et al.*, 2016; Kim and Ryu, 2013; Klein *et al.*, 2013; Rothen-Rutishauser *et al.*, 2005).

However, it is necessary that the *in vitro* models that are to replace the experimental animals provide a certain level of realism and accuracy for the prediction of *in vivo* effects. The organ complexity is difficult to recreate *in vitro*, nevertheless co-culture 3D models represent a good compromise to predict NP inhalation effects.

Since it is well known that different cell types communicate continuously with each other, testing NPs toxicity on monoculture does not seem the best choice, if the aim is to predict NPs toxicity at tissue level. For example, the presence of epithelial cells, e.g. A549 cells, or cells belonging to the immune system such as macrophages bring different response if taken as mono- or co-culture. Indeed, in a previous work, Klein *et al.* (2013) showed different responses of a mono-, bi- and tetra-culture after the same exposure conditions.

In this study, for the first time, the complex 3D *in vitro* alveolar model proposed by Klein *et al.* (2013) is used to assess the toxic potential on the human respiratory system of three different shaped AuNPs. The model is composed by four different cell lines: endothelial cells (EA.hy296), epithelial cells (A549), mast cells (HMC-1) and macrophage-like cells (differentiated THP-1 cells); cells were grown at the ALI on Transwell inserts and exposed to nebulized AuNP suspensions using the VitroCell® Cloud System

1. Air-Liquid-Interface (ALI) exposure

To better understand the effects of NPs it is important to select the most suitable cell lines and exposure condition for the *in vitro* models. For instance, since NPs are able to reach the deepest lung part (alveoli), it is a good choice to focus the development of alternative *in vitro* models for inhalation nanotoxicology on *in vitro* Air-Liquid-Interface (ALI) alveolar models, making use of alveoli-specific cell lines.

In vitro models could be composed by one or more cell lines, in submerged condition or at the ALI. Obviously, a 3D *in vitro* model that includes more than one relevant cell lines and exposes at the ALI provides more realistic conditions for the realistic characterization of the effects of inhaled particles (de Souza Carvalho *et al.*, 2014).

The ALI condition seems more sensitive and realistic than the submerged condition, even with comparable doses of exposure. One major difference between the submerged condition and the ALI condition is that, in "real life", inhaled particles would not encounter any liquid before they deposit on the alveolar membrane, which is covered with lung surfactant. On the contrary, in submerged conditions NPs will be dispersed in cell culture medium (CCM) prior

of encountering the cells (Herzog *et al.*, 2013; Holder and Marr, 2013; Lenz *et al.*, 2013; Stoehr *et al.*, 2015).

The presence of CCM will change the NPs properties, e.g. dimension (formation of agglomerates) and will favour the formation of the protein corona modifying the surface of NPs and leading to a modulation of the NP toxicity (Holder *et al.*, 2008). In other terms, the ALI condition mimics better the inhalation scenario and holds the promise of providing more reliable results (Mülhopt *et al.*, 2016).

The alveolar surface is characterized by the presence of surfactant, a thin layer of surface-active lipid-protein material that protects the cells. Its main function is to reduce the surface tension at the air-liqiuid-interface preventing the lung collapse and favouring the gas exchange. It is approximatively composed by lipids (90%) and protein (10%) (Hidalgo *et al.*, 2015). The large presence of macromolecules in the surfactant could modify the agglomeration state of the NPs. For this reason, in this study NPs was characterized, in terms of dimension and agglomerate formation, after 1 hour of incubation with a lung surfactant (poractant alfa, CUROSURF®, which was kindly provided by Chiesi Pharmaceutic).

VitroCell® Cloud System allowed to expose cells cultured at the air/liquid interface directly to nebulized NP suspensions (known concentration – homogeneous deposition). This system has been specifically designed for dose-controlled and spatially uniform deposition of aerosols from liquids and suspensions. In this way is possible the screening of inhaled drugs and to perform toxicity tests of inhaled substances including nanoparticle suspensions.

2. An innovative 3D tetra-culture alveolar model

The first version of the system used in this study was proposed by (Alfaro-Moreno *et al.*, 2008). In that model a co-culture of A549, THP-1 and HCM-1 was seeded on the bottom of the well, while the endothelial cells were seeded at the

apical side of transwell insert membrane. With this organization, not only the insert membrane, but also a layer of CCM separated the triculture from the endothelial layer. In the modified version (Klein *et al.*, 2011) the same tri-culture is seeded onto the porous membrane on the apical side of the insert and the endothelial cells are placed on the basolateral side of the same insert membrane. This new arrangement allowed to better mimic the *in vivo* anatomy of the alveolar region.

Even so, the model presents the ratio of A549, THP-1 and HMC-1 cells not so close to the physiological situation. The seeding ratios are most likely not resembling the *in vivo* condition because there might be an overrepresentation of macrophage-like cells (Thorax, 1992) and mast cells (Heard, 1989), compared to endothelial and epithelial cells. The rationale for this seeding ratios is mainly based on methodological arguments. The protocols necessary to study the tetraculture response after exposure require a higher number of cells than the physiological condition. The same happens when applying -omic techniques, such as transcriptomics, that require higher quantities of cells. In order to reduce the technical complexity of such experiments, the authors decided to increase the number of immune cells present in the system (Klein *et al.*, 2013).

The advanced tetraculture *in vitro* alveolar model proposed by Klein *et al.*, (2011) was used in this work to assess for the first time the effects induced by nebulized AuNPs of different shapes on human lungs.

3. The AuNP shape influence the effects on the tetraculture model

Among the most used NPs, there are the AuNPs which find applications in cosmetic products and in the health field (Vance *et al.*, 2015). Indeed, due to their biocompatibility, AuNPs are the most NPs used in nanomedicine as potential

nanocarrier for active principles (drug delivery), as nanosensor-sensing, and in photothermal therapy or tracking (Fytianos *et al.*, 2015).

The AuNPs used in this study have been prepared endotoxin-free, suitable for biological application, ensuring solubility in water and stability in biologically relevant media. The set of Pegylated AuNPs with comparable size (around 60 nm) included Gold Nano Spheres (GNPs), Gold Nano Rods (GNRs) and Gold Nano Stars (GNSs). AuNPs were produced within the framework of the FP7 project FutureNanoNeeds, coordinated by Prof. Kenneth Dawson (UCD – Dublin, Ireland).

After 24 hour of exposure viability, cytotoxicity (levels of Lactate Dehydrogenase, LDH), release of Interleukin-8 (IL-8), NP presence and uptake were evaluated.

The viability of the model was evaluated incubating cells (both apical and basolateral side) with a solution of Resazurin in CCM; active and viable cells are able to internalize and metabolize this blue dye, which becomes fluorescent. By measuring the fluorescence of the metabolized compound, it is possible to obtain information regarding the cell metabolism, considered as an index of cell viability. Endothelial cells were not affected in term of cell activity and no significant differences could be observed after 24 hours of treatment (Chapter 2 – Figure 4b). Instead, in the apical side after exposure to 1.7 $\mu g/cm^2$ of GNPs a significant decrease of viable cells was detectable compared to the control group (Chapter 2 – Figure 4a).

The reduced viability indicates that one or maybe more cell lines is affected by the treatment with GNPs. Unfortunately, it is not possible to figure out which cell line is mainly involved in this process. Maybe, the activation of macrophage-like cells, involved in the NPs phagocytosis, and the degranulation of the mast cells in response to an inflammatory state (Chapter 2 – Figure 6) contribute to create a stressful environment for A549 cells. However, in this case one could expect a

higher inflammatory status at the 1.7 µg/cm^2 dose and, in parallel, stronger decrease of cell viability at 0.34 µg/cm^2. The decrease in term of viability probably is not observed at the highest dose (1.7 µg/cm^2) because in this case prevail the cytotoxic aspect of all AuNPs (Chapter 2 – Figure 5). Another possible explanation of absence of decrease of cell viability could be due to a false positive result, due to interferences from the AuNPs, which are fluorescent at similar wavelengths of the resazurin.

Our results demonstrate that AuNPs (GNPs, GNRs and GNSs) exposure, after 24 hours, has the potential to cause cytotoxicity and inflammation.

Cytotoxicity was evaluated in term of release in the CCM of LDH, which is subsequent to damages to the cell membranes. In order to evaluate the cytotoxicity of AuNPs, basolateral medium recovered after 24 hours of treatment was used to measure the release of LDH (Chapter 2 – Figure 5).

The Lactate Dehydrogenase is an oxidoreductase enzyme involved in the cellular respiration that catalyses the transformation of the pyruvate into L-Lactate, involving the reduction of NADH to NAD$^+$. This enzyme is ubiquitary and it is quite stable, principally for these reasons LDH is often use as a marker of cytotoxicity. The release in the media of this enzyme is an index of compromised cell membrane.

In our experiments, it is possible to observe a significant increase in the level of LDH after the exposure to the highest dose (1.7 µg/cm^2) of all AuNPs. In the case of GNSs there was a relevant statistical increase also after the exposure to the lower dose (0.34 µg/cm^2) compared to the control group.

The high levels of LDH are index of cell death. Unfortunately, it is not possible to distinguish which cell lines are involved in this process and the cytotoxicity can only be considered as a "tissue response".

It is well established that inflammation is the main response after exposure to NPs (Nel *et al.*, 2006; Shrivastava *et al.*, 2016). IL-8 was chosen to evaluate the

inflammatory response of the model. IL-8 is a chemoattractant cytokine produced by a variety of tissue and blood cells. Unlike many other cytokines it has a distinct target specificity for the neutrophil, with only weak effects on other blood cells (Bickel 1993). Many different cells have the ability to produce IL-8 when appropriately stimulated. The expression of IL-8 mRNA and the release of the biologically active cytokine was observed in endothelial cells, fibroblasts from different tissues, keratinocytes, synovial cells, chondrocytes, several types of epithelial cells as well as some tumour cells. Interestingly, even neutrophils can synthesize IL-8, and may thus intensify their own recruitment to sites of inflammation (Baggiolini and Clark-Lewis, 1992).

The inflammatory response maybe is due to the epithelial cells that are suffering after the exposure to AuNPs. The released IL-8 can activate macrophage-like cells, which, in turn, can release additional IL-8 as a response to the inflammatory state. *In vivo,* this mechanism has the physiological function to beckon *in situ* other macrophages and immune cells cells to better react to the treat.

GNRs do not cause decrease in term of viability (both sides of the insert), no release of IL-8 and no cytotoxicity, if not only at the highest dose. Rod-like NP seem not able to cause cell membrane damages. In this case, the dose seems to play a key role in cell response after 24 hours of exposure.

GNSs probably cause serious damages at the cell membrane level with their numerous tips, peculiarity of their star-like shape. Tips can cause physical damages, disrupting the cell membrane during the interaction cell-NPs. Indeed, no differences between the doses of exposure were observed.

Concerning the GNPs, they caused a decreasing of viability and an increasing of cytotoxicity after exposure to the highest dose, while the release of IL-8 was significant only after exposure to 0.34 $\mu g/cm^2$. We can hypothesize that the effects are dose-dependent, the lowest dose bring only an inflammation response

that culminate into a decrease of viability and simultaneously a high LDH release increasing.

AuNP uptake, which is the amount of gold internalized by cells, was evaluated by the ICP-MS technique. This technique allowed detecting the amount of the studied element in the samples, in our case Au.

Chu *et al.*, (2014) assessed various particles, including large (150 nm) Gold Nano Star (AuNST) and Gold Nano Sphere (AuNSP) in their work. The authors demonstrated that, because of their sharp surface structures, nanostars could readily disrupt the endosomal membranes of human liver carcinoma cells and reside in the cytoplasm for an extended period, irrespective of their surface compositions, charges, materials, and sizes. Alternatively, following endocytosis, nanospheres would reside in the endosomes of the cells under stable conditions, where they would adapt with endosome maturation or be easily excreted by exocytosis.

In one other paper (Favi *et al.*, 2015), the authors hypothesized that the potential mechanism of cell death by the synthesized AuNSTs is that the nanoparticles enter the cells via endocytosis (Chu *et al.*, 2014), concentrate in the nuclei (Romero *et al.*, 2014) and in the cytoplasm (Chen *et al.*, 2013; Dam *et al.*, 2012), and induce dose-dependent cell death via mechanical damage (Kodiha *et al.*, 2015). Additional AuNST optimization for future research consideration is to synthesize AuNSTs with controlled size distribution, branch length and number of branched tips, and analysed the effect of these modified AuNST on cells and on native tissue. Controlling the size distribution, branch length, and the number of branched tips of these AuNSTs has the potential to enable further tuning of the optical properties for the AuNSTs for potential medical detection and treatment. The level of cellular uptake does not simply depend on surface area or charge, but also on the shape, which is another important factor in determining the level of uptake (Niikura *et al.*, 2013). Comparing rod-like and spherical AuNPs, the

first ones were the most efficiently uptaken. This results are in agreement with our data in which comparing only the uptake of GNPs and GNRs, the amount of gold in cells expose to GNRs is higher, compared to the exposure to the spherical counterpart.

Xie *et al.*, (2017) evaluated the intracellular concentrations of gold by the inductively coupled plasma atomic emission spectrometer (ICP-AES). Shape and time-dependent cellular uptake was observed. The cellular uptake of PEGylated-Gold Nano Triangles (P-GNTs) was the greatest, followed by PEGylated-Gold NanoRods (P-GNRs) and PEGylated-Gold Nano Stars (P-GNSs). Their results suggested that nanoparticle shape played an important role in cellular uptake even if they observed a higher uptake for GNRs than GNSs.

In our experiments, first the apical and the basolateral side of the inserts were considered separately (Chapter 2 – Figure 7 a and b), then we considered also the compartment together (Chapter 2 – Figure 7 c). In the apical side, nevertheless represent the side of exposure no significant amount of gold was found in cells after 24 hours of exposure to GNPs and GNRs, as compared to the untreated controls; instead, GNSs were present in the apical tri-culture following a clear dose dependent increasing.

In the basolateral side, we observed a statistically significant amount of gold per cell only after exposure to 1,7 µg/cm^2 GNRs and specially GNSs, with no differences between the doses used.

Our study highlighted that Au GNSs are uptaken in a dose-dependent way by epithelial cells. GNPs and GNRs are uptaken at a much lower rate, and, even if Au is above the limit of detection, the observed results are statistically different from the untreated control. This confirms that the is also a shape-dependent effects, with GNSs being uptaken, while Au particles and Au rods are not. Similar observations can be done for translocation from the apical to basolateral compartment. Also in this case a shape-dependent effect observable, with GNSs

being translocated much more than particles and rods. However, in this case the dose-dependent relationship could not be confirmed. These results are really interesting because they clarify that there is a distinct translocation of GNSs trough the model and the insert membrane. A further confirmation of the presence intercellular exchange and communication among the different cell lines; once again the model resulted a valid condition to better understand the bio-interaction occurring between NPs and cells.

Looking back also to the LDH release results, we can hypotheses that GNS cytotoxicity is not strictly related to the NPs uptake as we could not observe a dose-dependent increase in cytotoxicity.

Obviously, the presence of four different cell lines hinders the possibility to determine which cell line is the main target in the cytotoxicity or uptake processes.

Nevertheless, despite the contradictory results, previous studies and our own investigations show that the shape of AuNPs is one of the most important aspect involved in NP uptake considering different cell lines and experimental conditions.

In addition, in this work we exposed our model also to AgNPs and AgNO$_3$ (supplementary material – Figure S4, S5 and S6), as expected the model modulated its response in the different conditions. We can clearly affirm that the model is a suitable and valid approach in the screening of nebulized NP suspension.

Xenopus laevis:
a valid *in vitro* model for aquatic and developmental NM toxicity

Xenopus laevis represents a classical model for characterizing the effects of chemicals and recently of NPs on the development of this Amphibian with a correlation to humans around 80% (Fort and Paul, 2002).

The effects of a panel of six ZnO NPs, differing in size, shape and surface coating, was used to understand if and how these NMs affect *Xenopus laevis* embryos, by considering the most sensible developmental stages and the main NP target organs.

In addition, this model was chosen also to describe the effects of two differently coated AgNPs: the positively charged BPEI-AgNPs and the negatively charged Cit-AgNPs.

The published papers (Chapter 3 and 4) are the first reporting that NMs, e.g. the BPEI-coated AgNPs, s-nZnO and b-nZO, may be considered a teratogenic hazards, having a Teratogenic Index > 1.6. Moreover, the main result of these studies was that the specific effects can be attribute to the NPs themselves and not on the ions that might be eventually released by NP dissolution. Both, ZnO and Ag NPs, affected the embryos at the abdominal level, conveying the gut as the target organ for these NMs.

The developmental toxicity is one of the priority issues to be addressed to guarantee NM safety. In Mammals of course the placenta represents an extremely important biological barrier able to prevent or modulate the access of xenobiotics to the fetus. Pietroiusti *et al.*, (2013) reviewed the effects of different NMs on the placental barrier, indicating that some NPs may both cross and damage placental and fetal tissues, suggesting also to pay attention to the different mammalian developmental periods, since e.g. in the first 10 days of pregnancy in rodents, corresponding to the first trimester in the humans, the primitive placenta is leakier and thus more prone to allow NP crossing.

Anyway the issue of NM translocation and cytotoxic effects on placental barrier and fetus is far to be well understood.

The sections below are aimed to discuss the bio-interactions between embryos and NPs. Although we have used different NPs, some aspects are shared, reason why *Xenopus laevis* could be proposed as a valid model for NP toxicological

screening.

1. Size and Shape affect NP embryotoxicity

The effects in term of size and shape on the developing embryos were discussed in the Chapter 3. Basing on our results, sZnO and bZnO, despite the different size, caused comparable effects on the embryos in term of mortality. While, concerning the malformation rate, the small form resulted more effective at 50 mg/L showing the highest malformation score. Interestingly there is a decrease of the percentage of malformed embryos after exposure to sZnO at 100 mg/L. This data could be due to a reduced bioavaibility of sZnO, consequent to an important agglomeration of these NPs (Bai *et al.*, 2010); for this reason it was no possible to calculate the TC_{50} in the range of $1 - 100$ mg/L. Instead, the TC_{50} in the range of $1 - 50$ mg/L was calculated for both NPs resulting to be 17.9 mg/L for sZnO and 59.47 mg/L for bZnO. In the light of this calculation is clear that the small and round nZnO is more embryotoxic than the bigger rod-like counterpart.

Additionally, according to Dawson and Bantle (1987) the Teratogenic Index (TI) was estimated: for both NPs it resulted higher than 3, threshold to consider these NMs as potential teratogens.

The results are in line with a previous work (Bacchetta *et al.*, 2014) in which two differently sized commercial nZnOs similar in shape was compared.

In previous papers (Bacchetta *et al.*, 2014; Bacchetta *et al.*, 2012) the authors already suggested the potential teratogenic action of nZnO; the news from these works is that the teratogenic effect is almost independent from the NP size and shape, although the NP physico-chemical characteristic may contribute to aggravate and modulate such effect.

The toxicity of several metal oxide NPs was investigated also on Zebrafish embryos (Albanese *et al.*, 2012; Bai *et al.*, 2010; Brun *et al.*, 2014; Rizzo *et al.*, 2007; Soenen *et al.*, 2011; Zhao *et al.*, 2013). Taken into account those results, it is possible to affirm that developing Amphibian and fish show similar sensitivity to nZnO.

About the results on the oxidative stress biomarker, the SOD activity (Figure 6 – Chapter 3), there are some evidences that the exposure to nZnO induced enzymatic activity depletion, nonetheless, no significantly differences from the control group were observed. Also in this case the smaller form resulted to be more effective than the b-nZnO. In the literature, some studies support the hypothesis that the oxidative changes in cells and developing embryos is the main responses to nZnO (Xiong *et al.*, 2011; Zhao *et al.*, 2013). Moreover, it was also recently demonstrated that *Xenopus* embryo exposure to nZnOs results in antioxidant genes up-regulation (Bacchetta *et al.*, 2014), although the correspondent increment in the enzymatic activity is not always evident. The lack of clear evidence in SOD activity modulation could be attributable to a limitation of having to perform the analysis on pools of whole embryos and not on a single embryo or even better on a specific target organ. Moreover, the developing *Xenopus* are provided of good antioxidant defenses, including enzymes such as SOD and the GSH-related system (Rizzo *et al.*, 2007), able to buffer the ROS production in cells during embryonic development.

The higher surface activity and the easier cell uptake may are the reasonable explanation for the higher toxicity of small and round nZnO. Indeed, as already mentioned above, it is quite well established that round shaped NPs in the size range of 10-30 nm are preferentially taken up by cells through endocytosis (Albanese *et al.*, 2012; Soenen *et al.*, 2011).

Taken together these data, although the effects elicited by the sZnO and bZnO NPs could be considered qualitatively similar, the smaller round NPs resulted more effective.

2. The key role of Coating Agents in NP toxicity

The coating technique allows, especially in the industrial field to obtain NMs with even better performances in commercial products as paintings or additives. Indeed, the surface modifications can improve the NP dispersion. Surface modifications can have an important role in modulating the toxicity of NPs. For instance, several papers underline the key role of the surface properties of nZnO in controlling cytotoxicity, demonstrating the reduction of toxicity in *in vitro* and *in vivo* systems after exposure to coated NPs (Luo *et al.*, 2014; Xia *et al.*, 2011) In this study, the recorded malformation rates after exposure to coated nZnO (PVP and PEG) were significantly higher than the control group, however our results highlighted that surface modification of particles is able to decrease embryotoxicity of ZnONPs. The PEGylation, in particular, seems to be more effective in reducing the toxicity of both s-nZnO and bnZnO when compared with the nude ones. This observation is in agreement with the study of Luo and collaborators (2014) in which it has been evidenced that the coating of ZnONPs with PEG decreases their cytotoxicity in comparison with other surface modifications by reducing the cellular uptake.

Coating agents play a key role also in AgNPs toxicity (Chapter 4). Differently charged surface coatings such as stabilizing agents (e.g., citrate) and polymers are used to increase the AgNPs dispersion and colloidal stability because they confer steric repulsion forces (Fabrega *et al.*, 2011; Tolaymat *et al.*, 2010); here, BPEI and Citrate have been taken as example. Interestingly, it has been shown that citrate coated AgNPs were more unstable than polymer-coated particles in

the chloride-containing medium used in FETAX experiments, while the citrate is weakly bound to the surface of the particles (Tejamaya *et al.*, 2012) producing insoluble silver-chlorocomplexes and precipitation (Groh *et al.*, 2015; Levard *et al.*, 2013).

As it was found in Zebrafish (Osborne *et al.*, 2013), we found in *Xenopus* that coating AgNPs with citrate significantly decreased toxicity.

Instead, at the same concentrations at which Cit-AgNPs are completely ineffective, the BPEI-coated AgNPs are extremely embryotoxic (96h LC_{50} = 0.385 mg/L), inducing high malformation scores (96h EC_{50} = 0.240 mg/L).

In zebrafish embryos, uncoated AgNPs with a size comparable to our BPEI-AgNPs showed a lower embryotoxicity with a 120-h LC_{50} value of 13.5 mg/L (Bar-Ilan *et al.*, 2009). In another study on zebrafish embryos, BSA and starch coated AgNPs with a size of 5-20 nm, display a LC_{50} value of 25.5- mg/L.

The LC_{50} and EC_{50} calculated from our data are definitively higher than the environmental concentration of 0.09 – 2.63 ng/L reported by Gottschalk *et al.*, (2013). Nevertheless, it is not uncertain that the continuous increasing production of this kind of metal NM could cause an increase of the predicted environmental concentration with risks for aquatic organisms. One reason why BPEI-coated AgNPs can exert their specific teratogenic action in *Xenopus* embryos may reside in the specific ability of PEI (a cationic dispersant) to deliver materials to cells by avoiding the acidic lysosomal pathway. Akinc *et al.*, (2005) suggested that the PEI transfection capacity is indeed dependent on the specific ability to lead to the osmotic swelling and rupture of the endosomes, with the consequent release of the vector into the cytoplasm. The same mechanism may be shared by the BPEI-coated AgNPs; the polymer can be released inside the enterocytes after NP ingestion by the embryos and internalization by endocytosis, making the surface free for oxidative dissolution and consequent Ag^+-mediated oxidative damage to proteins, lipids and nucleic acids (Le Ouay and Stellacci, 2015). It has been

recently demonstrated in the nematode *C. elegans* exposed to Cit-AgNPs and AgNO$_3$, that only the AgNPs *in vivo* toxicity is crucially driven by the particle uptake by early endosomes, since endocytosis-deficient mutants and worms exposed to chloropromazine, in order to inhibit the clathrin-mediate endocytosis, were less sensitive than wild-type and chloropromazine untreated ones respectively (Maurer *et al.*, 2016).

BPEI-AgNPs have the capability to interact with embryo tissues exerting teratogenicity. A possible explanation of bio-interaction will be proposed in the following section.

Embryos exposed to BPEI-AgNPs during the first developmental stages (8 − 28, before the stomodeum opening) at the end of the FETAX test displayed statistically significant malformation percentages (Figure 5 − Chapter 4). This observation means that the embryos during segmentation and early organogenesis, neurulation included, are affected by the bio-interaction with NPs.

BPEI-AgNPs are able to be adsorbed by the fertilization membrane surrounding the embryos during this first developmental window (Figure 4 b − Chapter 4), nonetheless, there are not clear evidences of a particle penetration into the embryo tissues. Indeed, no NPs were found at the level of the central nervous system or the somites. Going back to the bio-interaction between NPs and fertilization membrane, it was showed how these interactions bring the membrane to become brownish and sticky. That modification prevented the normal embryo hatching, delaying or even preventing this developmental step.

Since malformations were not detected soon after the hatching in embryos exposed to BPEI-AgNPs, we hypothesized that these bio-interaction may influence molecular or physiological process during the first developmental stages and only during the later stages of the development was possible to detect the malformations.

Clearly, this aspect needs further experimental investigations, but is coherent with the findings of Ong *et al.*, (2014), who reported that NPs are able to affect zebrafish hatching by interacting with the ZHE1 hatching enzyme. In this latter paper, it was also underlined that the effects were mediated by the NPs themselves rather than the corresponding dissolved metal ions, further supporting our findings that the teratogenic hazard posed by the positively-charged BPEI-AgNPs derived from the peculiar nano-bio-interaction and they are not related to the dissolved ions. Moreover, in our study the BPEI-AgNPs were effective already at concentrations well below 0.5 mg Ag/L. Together these observations point out that surface coating and charge of AgNPs, even at very low concentrations, may contribute to modulate the effects on the very sensitive early embryogenetic phases.

It has been suggested that the earlier developmental stages are more sensitive than the other ones (Browning *et al.*, 2013). These authors demonstrated how the Zebrafish phenotypes obtained after exposure to AgNPs are dependent on NP size and embryonic developmental stages of exposure. Concluding their work, they suggest that AgNPs can potentially enable target-specific studies and therapy for embryo development, but in the light of our results surface coating should be necessarily included in this NP properties' list.

Our findings on the potential teratogenic hazard of the positively-charged BPEI-coated AgNPs highlight the need to further explore the role of particle size and coating in determining the fate and toxicity of AgNPs during development, to address both the safety and the potential biomedical applications of Ag-based engineered NMs.

Overall, the data reported for coated nZnOs and AgNPs in *Xenopus* embryos support the hypothesis that the coating agent plays a crucial role in delivering different degree of NPs toxicity.

3. Particles or ions, which/what is the guilty in nanotoxicology?

About the embryotoxic effects, many researchers argued that they are mainly dependent on the NPs properties than on the dissolved ions (Bai *et al.*, 2010; Zhao *et al.*, 2013; Zhu *et al.*, 2009), but some other argue the contrary suggesting an embryotoxic effect based on the cations dissolution from NPs (Brun *et al.*, 2014). Although the question is still debated, the solubility of nZnO can be highly dependent on the suspension medium (e.g. media added with serum albumin or ions in comparison with pure water), the initial particle size and pH (Luo *et al.*, 2014).

In our experimental condition (Chapter 3), using the FETAX medium, a saline solution with the pH around 8, the dissolution of nZnO is very low, indeed the maximum Zn^{2+} concentration measured in NP suspension ultrafiltrates were lower than 0.5 ppm (Figure S1). Nevertheless, no effects were observed on embryos after exposure to $ZnSO_4$ (concentrations similar to those measured by ICP-OES according to (Bacchetta *et al.*, 2012)and (Mantecca *et al.*, 2015)).

Basing on these findings, we can affirm that in our experimental conditions size and shape didn't significantly affect NP dissolution in FETAX medium making the contribution of Zn ions to toxicity on *Xenopus* embryos very low.

On the contrary, the Ag ions resulted to be highly embryolethal to *Xenopus laevis* with a 96 h LC50 0f 0.137 mg/L; additionally, the survived larvae at the end of the test were seriously malformed and the EC50 resulted to be of 0.128 mg/L (Chapter 4). The calculated TI of 1.07 suggested Ag^+ as a non-teratogen element (Bantle *et al.*, 1999). The embryolethality of Ag ions in *Xenopus* was never highlighted in previous literature. This result, indeed, suggests it as a potential environmental hazard even when it is not nanosized.

It is widely accepted that the AgNPs toxic effects on living organisms and cells mainly derive from the release of Ag ions from NPs (Navarro *et al.*, 2008; van

Aerle *et al.*, 2013). Particle dissolution may occur both in extra- and intra-cellular environment, but many evidences suggest that the ions dissolved especially intracellularly after NP cell uptake and this process may constitute the main mechanism associated to the AgNPs toxicity.

This mechanism, called the "Trojan horse mechanism", has been described in some works in which cells were exposed to different NPs, both metal and metal oxide NMs (Sabella *et al.*, 2014), and nowadays is considered the best paradigm to explain the enhanced toxicity of the nanosized materials, taken with the oxidative stress mechanism. For instance, Bondarenko and colleagues (2013) demonstrated, using metal-specific recombinant luminescence bacteria, that the toxicity of AgNPs to bacteria is significantly correlated not only to the level of extracellularly dissolved ions, but more specifically to the amount of bioavailable Ag^+.

In our study, DLS and UV-Vis analyses showed that BPEI-AgNPs were stable in the FETAX medium, but Cit-AgNPs agglomerated and settled down already during the first minutes after the suspension preparation (Table 1, Figure 1, Figure S2 – Chapter 4).

To assess the AgNP solubility, ICP-OES technique was used and compared to UV-vis absorption spectroscopy (Ivask *et al.*, 2014b; Zook *et al.*, 2011). Our NPs resulted little soluble (2-4%), results in line with previous published papers involving different models and test media (Ivask *et al.*, 2014a; Ivask *et al.*, 2014b; Kaosaar *et al.*, 2016).

Considering these evidences on comparable AgNPs solubility and the extremely different results coming from the embryotoxicity screening, we can affirm that the obtained biological responses were determined by the exposure to the AgNPs and did not depend on the extracellular dissolution of Ag^+. In particular they were mainly the consequence of the specific physico-chemical properties given to NPs by the surface functional coating agents. This is in agreement with data obtained

in zebrafish embryos where none of the phenotypic defects observed after exposure to AgNPs were noted in the Ag^+ treated embryos (Asharani *et al.*, 2008).

Interestingly, no effects were pointing out in *Xenopus* embryos treated with Cit-AgNPs, compared to Ag^+ treatment, even at the highest test concentrations, neither in term of mortality nor in term of malformations.

4. NP ingestion affect the developing embryo intestine

Concerning the route of exposure to NPs in *Xenopus laevis* embryos, this study demonstrated that metal oxide (nZnO – Chapter 3) and metal (AgNPs – Chapter 4) NPs are embryotoxic affecting mainly the gut. The same result was obtained in previous papers on *Xenopus* embryos exposed to NPs (Bacchetta *et al.*, 2012; Bacchetta *et al.*, 2014).

In our study, the smaller form of nZnO were more effective than the bigger one and the coated forms (PVP and PEG) resulted to be safer. The intestine was the target organ and the principal malformation resulted to be an abnormal gut coiling. Nevertheless, histopathological screening and gut ultrastructural analysis revealed only a slight alteration of the intestinal mucosa, ascribable to detachment between adjacent cells and from basal lamina.

The choice to perform the exposure of embryos to NPs in two developmental windows (before and after stomodeum opening) allows us to demonstrate once again that *Xenopus laevis* embryos become susceptible to NPs with the acquisition of grazing behavior following the stomodeum opening.

This is due to an increasing amount of NPs settled on the bottom of the Petri dish taken by embryos able to graze. NPs are in this way able to reach the gut lumen and accumulate.

Limiting the exposure before the opening of the stomodeum the embryos are protected by the fertilization membrane and the nZnO is not effective. These data suggest that the fertilization envelope of the early embryonic stages represents a barrier against the adverse environment in which embryos grow and the skin is not the preferential route of NP internalization.

On the contrary, some authors showed that zebrafish embryos are highly sensitive to ZnONPs during early developmental stages because the interaction of NPs with chorion affects the hatching (Bai *et al.*, 2010; Zhao *et al.*, 2013).

After exposure to AgNPs the most frequent malformation was again at the abdominal level, where embryos showed severe oedemas and abnormal gut coiling, especially when treated with BPEI-AgNPs. These observations were performed both with light and two-photon excitation microscope. Most of the histopathological damages were observed at the same level of the NP luminescence signal (Figure 6 and 8 – Chapter 4).

Similar results were obtained from exposing embryos to BPEI-AgNPs from stage 39 to stage 46, after the stomodeum opening, since embryos start to freely swallow materials from the water column and from the bottom of the Petri dish, once they acquire the grazing behavior.

The exposure during this second developmental window, caused percentages of malformed embryos up to almost 100%, similar to the exposure along the all embryogenetic events considered throughout the entire FETAX test (stage 8 – 46; Figure 5 – Chapter 4).

The observation obtained with the exposure to nZnO and AgNPs after the stomodeum opening suggest again that the ingestion is the main exposure route to NPs, and translocation through the intestinal barrier the main uptake mechanism.

Previous works already demonstrated that aquatic organisms, such as *Daphnia magna* and zebrafish, are mainly exposed to NMs mainly through ingestion

(Osborne *et al.*, 2015; Santo *et al.*, 2014; Xiao *et al.*, 2015).

As a whole, the results of experiments on *Xenopus* embryos exposed to different types of NPs reported in this study (Chapter 3 and 4), along with the previous published papers on *Xenopus* (Bacchetta *et al.*, 2014; Bacchetta *et al.*, 2012; Bonfanti *et al.*, 2015), evidenced for the first time that even during embryogenesis, the intestine was the mainly affected organ.

Concerning the AgNP exposure some authors (Osborne *et al.*, 2015) pointed out that not only the gut, but also the gills were a target organ in adult Zebrafish exposed to Cit-AgNPs; the histopathological lesions occurred in concomitance with the highest Ag accumulation in the tissues. Of course during *Xenopus* development no external gills are present and most of the gas exchange occurs through the skin for most of the primary organogenesis.

Our morphological observations, even so revealed the absence of NPs at the skin level, both Cit-AgNPs and BPEI-AgNPs, reinforcing furthermore the hypothesis about the ingestion of NPs by grazing embryos.

In addition, the results of Two Photon Excitation microscopy support the idea that the positively charged BPEI-coated AgNPs are more incline in the bio-interactions with the cell membranes and to be internalized at least by the epithelial cells lining the gut. This behavior could be conferred by the positive surficial charge, that allows the electrostatic interactions with the negatively charged surface of the outer cell membranes (Jain *et al.*, 2010) or maybe the presence of BPEI itself, carrying NPs through the cell compartments.

Concluding this section, our data support the assumption that the BPEI-AgNPs damaged specifically the *Xenopus* gut in developing entering the enterocytes through endocytosis and inducing cell toxicity after endosomal disruption. Of course this hypothesis on the biological mode of action of the BPEI-AgNPs requires further experimental evidences.

References

Agu, R.U., Ugwoke, M.I., 2011. In vitro and in vivo testing methods for respiratory drug delivery. Expert Opin Drug Deliv 8, 57-69.

Akinc, A., Thomas, M., Klibanov, A.M., Langer, R., 2005. Exploring polyethylenimine-mediated DNA transfection and the proton sponge hypothesis. J Gene Med 7, 657-663.

Albanese, A., Tang, P.S., Chan, W.C., 2012. The effect of nanoparticle size, shape, and surface chemistry on biological systems. Annu Rev Biomed Eng 14, 1-16.

Alfaro-Moreno, E., Nawrot, T.S., Vanaudenaerde, B.M., Hoylaerts, M.F., Vanoirbeek, J.A., Nemery, B., Hoet, P.H., 2008. Co-cultures of multiple cell types mimic pulmonary cell communication in response to urban PM10. Eur Respir J 32, 1184-1194.

Allen, T.M., Austin, G.A., Chonn, A., Lin, L., Lee, K.C., 1991. Uptake of liposomes by cultured mouse bone marrow macrophages: influence of liposome composition and size. Biochim Biophys Acta 1061, 56-64.

Asharani, P.V., Lian Wu, Y., Gong, Z., Valiyaveettil, S., 2008. Toxicity of silver nanoparticles in zebrafish models. Nanotechnology 19, 255102.

Ates, M., Arslan, Z., Demir, V., Daniels, J., Farah, I.O., 2015. Accumulation and toxicity of CuO and ZnO nanoparticles through waterborne and dietary exposure of goldfish (Carassius auratus). Environ Toxicol 30, 119-128.

Bacchetta, R., Moschini, E., Santo, N., Fascio, U., Del Giacco, L., Freddi, S., Camatini, M., Mantecca, P., 2014. Evidence and uptake routes for Zinc oxide nanoparticles through the gastrointestinal barrier in *Xenopus* laevis. Nanotoxicology 8, 728-744.

Bacchetta, R., Santo, N., Fascio, U., Moschini, E., Freddi, S., Chirico, G., Camatini, M., Mantecca, P., 2012. Nano-sized CuO, TiO(2) and ZnO affect Xenopus laevis development. Nanotoxicology 6, 381-398.

Baggiolini, M., Clark-Lewis, I., 1992. Interleukin-8, a chemotactic and inflammatory cytokine. FEBS Letters 307, 97-101.

Bai, J., Zhong, X., Jiang, S., Huang, Y., Duan, X., 2010. Graphene nanomesh. Nat Nanotechnol 5, 190-194.

Bantle, J.A., Finch, R.A., Fort, D.J., Stover, E.L., Hull, M., Kumsher-King, M., Gaudet-Hull, A.M., 1999. Phase III interlaboratory study of FETAX. Part 3. FETAX validation using 12 compounds with and without an exogenous metabolic activation system. J Appl Toxicol 19, 447-472.

Bar-Ilan, O., Albrecht, R.M., Fako, V.E., Furgeson, D.Y., 2009. Toxicity assessments of multisized gold and silver nanoparticles in zebrafish embryos. Small 5, 1897-1910.

Blank, F., Rothen-Rutishauser, B.M., Schurch, S., Gehr, P., 2006. An optimized in vitro model of the respiratory tract wall to study particle cell interactions. J Aerosol Med 19, 392-405.

Bonfanti, P., Moschini, E., Saibene, M., Bacchetta, R., Rettighieri, L., Calabri, L., Colombo, A., Mantecca, P., 2015. Do Nanoparticle Physico-Chemical Properties and Developmental Exposure Window Influence Nano ZnO Embryotoxicity in Xenopus laevis? Int J Environ Res Public Health 12, 8828-8848.

Braakhuis, H.M., Giannakou, C., Peijnenburg, W.J., Vermeulen, J., van Loveren, H., Park, M.V., 2016. Simple in vitro models can predict pulmonary toxicity of silver nanoparticles. Nanotoxicology 10, 770-779.

Browning, L.M., Lee, K.J., Nallathamby, P.D., Xu, X.H., 2013. Silver nanoparticles incite size- and dose-dependent developmental phenotypes and nanotoxicity in zebrafish embryos. Chem Res Toxicol 26, 1503-1513.

Brun, N.R., Lenz, M., Wehrli, B., Fent, K., 2014. Comparative effects of zinc oxide nanoparticles and dissolved zinc on zebrafish embryos and eleuthero-embryos: importance of zinc ions. Sci Total Environ 476-477, 657-666.

Chen, H., Zhang, X., Dai, S., Ma, Y., Cui, S., Achilefu, S., Gu, Y., 2013. Multifunctional gold nanostar conjugates for tumor imaging and combined photothermal and chemo-therapy. Theranostics 3, 633-649.

Chithrani, B.D., Chan, W.C., 2007. Elucidating the mechanism of cellular uptake and removal of protein-coated gold nanoparticles of different sizes and shapes. Nano Lett 7, 1542-1550.

Chithrani, B.D., Ghazani, A.A., Chan, W.C., 2006. Determining the size and shape dependence of gold nanoparticle uptake into mammalian cells. Nano Lett 6, 662-668.

Chu, Z., Zhang, S., Zhang, B., Zhang, C., Fang, C.Y., Rehor, I., Cigler, P., Chang, H.C., Lin, G., Liu, R., Li, Q., 2014. Unambiguous observation of shape effects on cellular fate of nanoparticles. Sci Rep 4, 4495.

Dam, D.H., Lee, J.H., Sisco, P.N., Co, D.T., Zhang, M., Wasielewski, M.R., Odom, T.W., 2012. Direct observation of nanoparticle-cancer cell nucleus interactions. ACS Nano 6, 3318-3326.

Dawson, D.A., Bantle, J.A., 1987. Development of a reconstituted water medium and preliminary validation of the frog embryo teratogenesis assay--Xenopus (FETAX). J Appl Toxicol 7, 237-244.

de Souza Carvalho, C., Daum, N., Lehr, C.-M., 2014. Carrier interactions with the biological barriers of the lung: Advanced in vitro models and challenges for pulmonary drug delivery. Advanced Drug Delivery Reviews 75, 129-140.

El-Sayed, I.H., Huang, X., El-Sayed, M.A., 2006. Selective laser photo-thermal therapy of epithelial carcinoma using anti-EGFR antibody conjugated gold nanoparticles. Cancer Letters 239, 129-135.

Elbert, K.J., Schafer, U.F., Schafers, H.J., Kim, K.J., Lee, V.H., Lehr, C.M., 1999. Monolayers of human alveolar epithelial cells in primary culture for pulmonary absorption and transport studies. Pharm Res 16, 601-608.

Fabrega, J., Luoma, S.N., Tyler, C.R., Galloway, T.S., Lead, J.R., 2011. Silver nanoparticles: behaviour and effects in the aquatic environment. Environ Int 37, 517-531.

Favi, P.M., Gao, M., Johana Sepulveda Arango, L., Ospina, S.P., Morales, M., Pavon, J.J., Webster, T.J., 2015. Shape and surface effects on the cytotoxicity of nanoparticles: Gold nanospheres versus gold nanostars. J Biomed Mater Res A 103, 3449-3462.

Fort, D.J., Paul, R.R., 2002. Enhancing the predictive validity of Frog Embryo Teratogenesis Assay--Xenopus (FETAX). J Appl Toxicol 22, 185-191.

Foster, K.A., Oster, C.G., Mayer, M.M., Avery, M.L., Audus, K.L., 1998. Characterization of the A549 cell line as a type II pulmonary epithelial cell model for drug metabolism. Exp Cell Res 243, 359-366.

Fytianos, K., Rodriguez-Lorenzo, L., Clift, M.J., Blank, F., Vanhecke, D., von Garnier, C., Petri-Fink, A., Rothen-Rutishauser, B., 2015. Uptake efficiency of surface modified

gold nanoparticles does not correlate with functional changes and cytokine secretion in human dendritic cells in vitro. Nanomedicine 11, 633-644.

Geys, J., Coenegrachts, L., Vercammen, J., Engelborghs, Y., Nemmar, A., Nemery, B., Hoet, P.H., 2006. In vitro study of the pulmonary translocation of nanoparticles: a preliminary study. Toxicol Lett 160, 218-226.

Gottschalk, F., Kost, E., Nowack, B., 2013. Engineered nanomaterials in water and soils: a risk quantification based on probabilistic exposure and effect modeling. Environ Toxicol Chem 32, 1278-1287.

Groh, K.J., Dalkvist, T., Piccapietra, F., Behra, R., Suter, M.J., Schirmer, K., 2015. Critical influence of chloride ions on silver ion-mediated acute toxicity of silver nanoparticles to zebrafish embryos. Nanotoxicology 9, 81-91.

Hanaor, D., Michelazzi, M., Leonelli, C., Sorrell, C.C., 2012. The effects of carboxylic acids on the aqueous dispersion and electrophoretic deposition of ZrO2. Journal of the European Ceramic Society 32, 235-244.

Harush-Frenkel, O., Debotton, N., Benita, S., Altschuler, Y., 2007. Targeting of nanoparticles to the clathrin-mediated endocytic pathway. Biochem Biophys Res Commun 353, 26-32.

He, C., Hu, Y., Yin, L., Tang, C., Yin, C., 2010. Effects of particle size and surface charge on cellular uptake and biodistribution of polymeric nanoparticles. Biomaterials 31, 3657-3666.

Heath, T.D., Lopez, N.G., Papahadjopoulos, D., 1985. The effects of liposome size and surface charge on liposome-mediated delivery of methotrexate-gamma-aspartate to cells in vitro. Biochim Biophys Acta 820, 74-84.

Herzog, F., Clift, M.J., Piccapietra, F., Behra, R., Schmid, O., Petri-Fink, A., Rothen-Rutishauser, B., 2013. Exposure of silver-nanoparticles and silver-ions to lung cells in vitro at the air-liquid interface. Part Fibre Toxicol 10, 11.

Hidalgo, A., Cruz, A., Pérez-Gil, J., 2015. Barrier or carrier? Pulmonary surfactant and drug delivery. European Journal of Pharmaceutics and Biopharmaceutics 95, 117-127.

Holder, A.L., Marr, L.C., 2013. Toxicity of silver nanoparticles at the air-liquid interface. Biomed Res Int 2013, 328934.

Hsiao, I.L., Huang, Y.J., 2011. Titanium oxide shell coatings decrease the cytotoxicity of ZnO nanoparticles. Chem Res Toxicol 24, 303-313.

Ivask, A., Elbadawy, A., Kaweeteerawat, C., Boren, D., Fischer, H., Ji, Z., Chang, C.H., Liu, R., Tolaymat, T., Telesca, D., Zink, J.I., Cohen, Y., Holden, P.A., Godwin, H.A., 2014a. Toxicity mechanisms in Escherichia coli vary for silver nanoparticles and differ from ionic silver. ACS Nano 8, 374-386.

Ivask, A., Kurvet, I., Kasemets, K., Blinova, I., Aruoja, V., Suppi, S., Vija, H., Käkinen, A., Titma, T., Heinlaan, M., Visnapuu, M., Koller, D., Kisand, V., Kahru, A., 2014b. Size-Dependent Toxicity of Silver Nanoparticles to Bacteria, Yeast, Algae, Crustaceans and Mammalian Cells In Vitro. In: Quigg, A. (Ed.) PLoS One, vol. 9, San Francisco, USA.

Jain, K., Kesharwani, P., Gupta, U., Jain, N.K., 2010. Dendrimer toxicity: Let's meet the challenge. International Journal of Pharmaceutics 394, 122-142.

Jiang, W., Kim, B.Y., Rutka, J.T., Chan, W.C., 2008. Nanoparticle-mediated cellular response is size-dependent. Nat Nanotechnol, vol. 3, England, pp. 145-150.

Kaosaar, S., Kahru, A., Mantecca, P., Kasemets, K., 2016. Profiling of the toxicity mechanisms of coated and uncoated silver nanoparticles to yeast Saccharomyces cerevisiae BY4741 using a set of its 9 single-gene deletion mutants defective in oxidative stress response, cell wall or membrane integrity and endocytosis. Toxicol In Vitro 35, 149-162.

Kettler, K., Veltman, K., van de Meent, D., van Wezel, A., Hendriks, A.J., 2014. Cellular uptake of nanoparticles as determined by particle properties, experimental conditions, and cell type. Environ Toxicol Chem 33, 481-492.

Kim, S., Ryu, D.Y., 2013. Silver nanoparticle-induced oxidative stress, genotoxicity and apoptosis in cultured cells and animal tissues. J Appl Toxicol 33, 78-89.

Klein, S.G., Hennen, J., Serchi, T., Blömeke, B., Gutleb, A.C., 2011. Potential of coculture in vitro models to study inflammatory and sensitizing effects of particles on the lung. Toxicology in Vitro 25, 1516-1534.

Klein, S.G., Serchi, T., Hoffmann, L., Blömeke, B., Gutleb, A.C., 2013. An improved 3D tetraculture system mimicking the cellular organisation at the alveolar barrier to study the potential toxic effects of particles on the lung. Part Fibre Toxicol, vol. 10, p. 31.

Kodiha, M., Wang, Y.M., Hutter, E., Maysinger, D., Stochaj, U., 2015. Off to the organelles - killing cancer cells with targeted gold nanoparticles. Theranostics 5, 357-370.

Le Ouay, B., Stellacci, F., 2015. Antibacterial activity of silver nanoparticles: A surface science insight. Nano Today 10, 339-354.

Lenz, A.G., Karg, E., Brendel, E., Hinze-Heyn, H., Maier, K.L., Eickelberg, O., Stoeger, T., Schmid, O., 2013. Inflammatory and oxidative stress responses of an alveolar epithelial cell line to airborne zinc oxide nanoparticles at the air-liquid interface: a comparison with conventional, submerged cell-culture conditions. Biomed Res Int 2013, 652632.

Levard, C., Mitra, S., Yang, T., Jew, A.D., Badireddy, A.R., Lowry, G.V., Brown, G.E., Jr., 2013. Effect of chloride on the dissolution rate of silver nanoparticles and toxicity to E. coli. Environ Sci Technol 47, 5738-5745.

Luo, M., Shen, C., Feltis, B.N., Martin, L.L., Hughes, A.E., Wright, P.F., Turney, T.W., 2014. Reducing ZnO nanoparticle cytotoxicity by surface modification. Nanoscale 6, 5791-5798.

Mantecca, P., Moschini, E., Bonfanti, P., Fascio, U., Perelshtein, I., Lipovsky, A., Chirico, G., Bacchetta, R., Del Giacco, L., Colombo, A., Gedanken, A., 2015. Toxicity Evaluation of a New Zn-Doped CuO Nanocomposite With Highly Effective Antibacterial Properties. Toxicol Sci.

Maurer, L.L., Yang, X., Schindler, A.J., Taggart, R.K., Jiang, C., Hsu-Kim, H., Sherwood, D.R., Meyer, J.N., 2016. Intracellular trafficking pathways in silver nanoparticle uptake and toxicity in Caenorhabditis elegans. Nanotoxicology 10, 831-835.

Mülhopt, S., Dilger, M., Diabaté, S., Schlager, C., Krebs, T., Zimmermann, R., Buters, J., Oeder, S., Wäscher, T., Weiss, C., Paur, H.-R., 2016. Toxicity testing of combustion aerosols at the air–liquid interface with a self-contained and easy-to-use exposure system. Journal of Aerosol Science 96, 38-55.

Müller, L., Gasser, M., Raemy, D.O., Herzog, F., Brandenberger, C., Schmid, O., Gehr, P., Rothen-Rutishauser, B., Clift, M.J.D., - Realistic exposure methods for investigating the interaction of nanoparticles with the lung at the air-liquid interface in vitro. - 30.

Navarro, E., Piccapietra, F., Wagner, B., Marconi, F., Kaegi, R., Odzak, N., Sigg, L., Behra, R., 2008. Toxicity of silver nanoparticles to Chlamydomonas reinhardtii. Environ Sci Technol 42, 8959-8964.

Nel, A., Xia, T., Madler, L., Li, N., 2006. Toxic potential of materials at the nanolevel. Science 311, 622-627.

Niikura, K., Matsunaga, T., Suzuki, T., Kobayashi, S., Yamaguchi, H., Orba, Y., Kawaguchi, A., Hasegawa, H., Kajino, K., Ninomiya, T., Ijiro, K., Sawa, H., 2013. Gold nanoparticles as a vaccine platform: influence of size and shape on immunological responses in vitro and in vivo. ACS Nano 7, 3926-3938.

Nohynek, G.J., Antignac, E., Re, T., Toutain, H., 2010. Safety assessment of personal care products/cosmetics and their ingredients. Toxicol Appl Pharmacol 243, 239-259.

Ong, K.J., Zhao, X., Thistle, M.E., Maccormack, T.J., Clark, R.J., Ma, G., Martinez-Rubi, Y., Simard, B., Loo, J.S., Veinot, J.G., Goss, G.G., 2014. Mechanistic insights into the effect of nanoparticles on zebrafish hatch. Nanotoxicology 8, 295-304.

Osaki, F., Kanamori, T., Sando, S., Sera, T., Aoyama, Y., 2004. A quantum dot conjugated sugar ball and its cellular uptake. On the size effects of endocytosis in the subviral region. J Am Chem Soc 126, 6520-6521.

Osborne, O.J., Johnston, B.D., Moger, J., Balousha, M., Lead, J.R., Kudoh, T., Tyler, C.R., 2013. Effects of particle size and coating on nanoscale Ag and TiO(2) exposure in zebrafish (Danio rerio) embryos. Nanotoxicology 7, 1315-1324.

Osborne, O.J., Lin, S., Chang, C.H., Ji, Z., Yu, X., Wang, X., Xia, T., Nel, A.E., 2015. Organ-Specific and Size-Dependent Ag Nanoparticle Toxicity in Gills and Intestines of Adult Zebrafish. ACS Nano 9, 9573-9584.

Pandurangan, M., Kim, D., 2015. In vitro toxicity of zinc oxide nanoparticles: a review. Journal of Nanoparticle Research C7 - 158 17, 1-8.

Panyam, J., Labhasetwar, V., 2003. Biodegradable nanoparticles for drug and gene delivery to cells and tissue. Advanced Drug Delivery Reviews 55, 329-347.

Patil, S., Sandberg, A., Heckert, E., Self, W., Seal, S., 2007. Protein adsorption and cellular uptake of cerium oxide nanoparticles as a function of zeta potential. Biomaterials 28, 4600-4607.

Pietroiusti, A., Campagnolo, L., Fadeel, B., 2013. Interactions of engineered nanoparticles with organs protected by internal biological barriers. Small 9, 1557-1572.

Raz, A., Bucana, C., Fogler, W.E., Poste, G., Fidler, I.J., 1981. Biochemical, morphological, and ultrastructural studies on the uptake of liposomes by murine macrophages. Cancer Res 41, 487-494.

Rejman, J., Oberle, V., Zuhorn, I.S., Hoekstra, D., 2004. Size-dependent internalization of particles via the pathways of clathrin- and caveolae-mediated endocytosis. Biochem J 377, 159-169.

Rizzo, A., Li, Y., Kudera, S., Della Sala, F., Zanella, M., Parak, W.J., Cingolani, R., Manna, L., Gigli, G., 2007. Blue light emitting diodes based on fluorescent CdSe/ZnS nanocrystals. Applied Physics Letters 90, 051106.

Romero, V.H., Kereselidze, Z., Egido, W., Michaelides, E.A., Santamaria, F., Peralta, X.G., 2014. Nanoparticle assisted photothermal deformation of individual neuronal organelles and cells. Biomed Opt Express 5, 4002-4012.

Rothen-Rutishauser, B., Blank, F., Muhlfeld, C., Gehr, P., 2008. In vitro models of the human epithelial airway barrier to study the toxic potential of particulate matter. Expert Opin Drug Metab Toxicol 4, 1075-1089.

Rothen-Rutishauser, B.M., Kiama, S.G., Gehr, P., 2005. A three-dimensional cellular model of the human respiratory tract to study the interaction with particles. Am J Respir Cell Mol Biol 32, 281-289.

Sabella, S., Carney, R.P., Brunetti, V., Malvindi, M.A., Al-Juffali, N., Vecchio, G., Janes, S.M., Bakr, O.M., Cingolani, R., Stellacci, F., Pompa, P.P., 2014. A general mechanism for intracellular toxicity of metal-containing nanoparticles. Nanoscale, vol. 6, pp. 7052-7061.

Santo, N., Fascio, U., Torres, F., Guazzoni, N., Tremolada, P., Bettinetti, R., Mantecca, P., Bacchetta, R., 2014. Toxic effects and ultrastructural damages to Daphnia magna of two differently sized ZnO nanoparticles: does size matter? Water Res 53, 339-350.

Secondo, L.E., Liu, N.J., Lewinski, N.A., 2017. Methodological considerations when conducting in vitro, air-liquid interface exposures to engineered nanoparticle aerosols. Crit Rev Toxicol 47, 225-262.

Shrivastava, R., Kushwaha, P., Bhutia, Y.C., Flora, S., 2016. Oxidative stress following exposure to silver and gold nanoparticles in mice. Toxicol Ind Health 32, 1391-1404.

Skjolding, L.M., Winther-Nielsen, M., Baun, A., 2014. Trophic transfer of differently functionalized zinc oxide nanoparticles from crustaceans (Daphnia magna) to zebrafish (Danio rerio). Aquat Toxicol 157, 101-108.

Soenen, S.J.H., Himmelreich, U., Nuytten, N., De Cuyper, M., 2011. Cytotoxic effects of iron oxide nanoparticles and implications for safety in cell labelling. Biomaterials 32, 195-205.

Stoehr, L.C., Endes, C., Radauer-Preiml, I., Boyles, M.S., Casals, E., Balog, S., Pesch, M., Petri-Fink, A., Rothen-Rutishauser, B., Himly, M., Clift, M.J., Duschl, A., 2015. Assessment of a panel of interleukin-8 reporter lung epithelial cell lines to monitor the pro-inflammatory response following zinc oxide nanoparticle exposure under different cell culture conditions. Part Fibre Toxicol 12, 29.

Tejamaya, M., Romer, I., Merrifield, R.C., Lead, J.R., 2012. Stability of citrate, PVP, and PEG coated silver nanoparticles in ecotoxicology media. Environ Sci Technol 46, 7011-7017.

Tolaymat, T.M., El Badawy, A.M., Genaidy, A., Scheckel, K.G., Luxton, T.P., Suidan, M., 2010. An evidence-based environmental perspective of manufactured silver nanoparticle in syntheses and applications: a systematic review and critical appraisal of peer-reviewed scientific papers. Sci Total Environ 408, 999-1006.

van Aerle, R., Lange, A., Moorhouse, A., Paszkiewicz, K., Ball, K., Johnston, B.D., de-Bastos, E., Booth, T., Tyler, C.R., Santos, E.M., 2013. Molecular mechanisms of toxicity of silver nanoparticles in zebrafish embryos. Environ Sci Technol 47, 8005-8014.

Vance, M.E., Kuiken, T., Vejerano, E.P., McGinnis, S.P., Hochella, M.F., Rejeski, D., Hull, M.S., 2015. Nanotechnology in the real world: Redeveloping the nanomaterial consumer products inventory. Beilstein J Nanotechnol 6, 1769-1780.

Wang, S.H., Lee, C.W., Chiou, A., Wei, P.K., 2010. Size-dependent endocytosis of gold nanoparticles studied by three-dimensional mapping of plasmonic scattering images. J Nanobiotechnology, vol. 8, p. 33.

Weissleder, R., 2006. Molecular imaging in cancer. Science 312, 1168-1171.

West, J.L., Halas, N.J., 2003. Engineered nanomaterials for biophotonics applications: improving sensing, imaging, and therapeutics. Annu Rev Biomed Eng 5, 285-292.

Whitehead, K.A., Langer, R., Anderson, D.G., 2009. Knocking down barriers: advances in siRNA delivery. Nat Rev Drug Discov 8, 129-138.

Xia, T., Zhao, Y., Sager, T., George, S., Pokhrel, S., Li, N., Schoenfeld, D., Meng, H., Lin, S., Wang, X., Wang, M., Ji, Z., Zink, J.I., Madler, L., Castranova, V., Nel, A.E., 2011. Decreased dissolution of ZnO by iron doping yields nanoparticles with reduced toxicity in the rodent lung and zebrafish embryos. ACS Nano 5, 1223-1235.

Xiao, Y., Vijver, M.G., Chen, G., Peijnenburg, W.J., 2015. Toxicity and accumulation of Cu and ZnO nanoparticles in Daphnia magna. Environ Sci Technol 49, 4657-4664.

Xie, X., Liao, J., Shao, X., Li, Q., Lin, Y., 2017. The Effect of shape on Cellular Uptake of Gold Nanoparticles in the forms of Stars, Rods, and Triangles. Sci Rep 7, 3827.

Xiong, D., Fang, T., Yu, L., Sima, X., Zhu, W., 2011. Effects of nano-scale TiO2, ZnO and their bulk counterparts on zebrafish: acute toxicity, oxidative stress and oxidative damage. Sci Total Environ 409, 1444-1452.

Zhao, C.M., Wang, W.X., 2012. Size-dependent uptake of silver nanoparticles in Daphnia magna. Environ Sci Technol 46, 11345-11351.

Zhao, X., Wang, S., Wu, Y., You, H., Lv, L., 2013. Acute ZnO nanoparticles exposure induces developmental toxicity, oxidative stress and DNA damage in embryo-larval zebrafish. Aquatic Toxicology 136–137, 49-59.

Zhu, Z.J., Rotello, V.M., Vachet, R.W., 2009. Engineered nanoparticle surfaces for improved mass spectrometric analyses. Analyst 134, 2183-2188.

Zook, J.M., Long, S.E., Cleveland, D., Geronimo, C.L., MacCuspie, R.I., 2011. Measuring silver nanoparticle dissolution in complex biological and environmental matrices using UV-visible absorbance. Anal Bioanal Chem 401, 1993-2002.

Conclusion

The thesis proposed three different *in vitro* models to perform nanotoxicological studies. The models present different levels of complexity, from a simple lung monoculture (A549), to a tetra-culture alveolar model and then a whole developing organism at (*Xenopus laevis*).

Despite the differences between the models and the NPs used, we can find some common results that suggest critical aspects in the NP interactions with biological systems.

The main finding of the studies presented in this thesis is that, beside chemical composition of NPs, the different physico-chemical properties can finally affect the bio-interactions and the toxicity of NPs, suggesting, in a SbD approach, the selection of particular physico-chemical properties as the first way to obtain safer nanomaterials.

In all the presented studies, the shape is taken into account to describe the effects of NPs, metal-oxides (nZnO) and metal-based (AuNPs and AgNPs).

In Chapter 1 (paper in preparation), it was evidenced that the nZnO of cubical form induced low levels of oxidative stress on A549, did not affect the lysosomal activity and t was not characterised by a strong intracellular dissolution compared to the round and rod-like forms, thus resulting less cytotoxic for the lung monoculture.

In Chapter 2 (paper in preparation) it was presented the novel and innovative 3D *in vitro* tetra-culture, used for the first time, of to study the effects of NPs, in particular of three differently shaped AuNPs (GNPs, GNRs and GNSs). In addition, to test the model capability to modulate its response to different exposures, we assessed also the exposure to AgNPs. Our results clearly show that the model is perfectly suitable for this kind of studies and how the shape influence the bio-interaction between NPs and the tetra-culture, particularly, the star-like AuNPs seems to be the more effective, while the rod-like AuNPs were found to be the safest.

Then the Chapters 3 (Bonfanti et al., 2015) and 4 (Colombo et al., 2017) discussed the effects of NPs on the development of *Xenopus laevis*. In this case, not only the shape, but also the coating agents were taken into account.

ZnONPs differing in size, shape and polymeric surface coating, used in Chapter 3, produced similar toxicity in *X. laevis* embryos, targeted the same organ and shared similar mode of action. Besides, we cannot rule out how the specific physical and chemical characteristics may influence the severity of such effects. Considering only the shape, anyway, we can affirm that the round-small nZnO resulted more embryotoxic than the big-rod-like counterparts.

From one side our results evidence the potential adverse effects on environmental health, from the other side they suggest the possibility to modify nZnO properties during the synthesis in order to modulate the toxic effects and produce safer NMs.

In Chapter 4, the focus was on very small (10 nm) particles, BPEI-coated or citrate-coated AgNPs. Due to the coating molecule, the negative Cit-AgNPs resulted innocuous to embryos, likely as a consequence of both particle agglomeration and less capability to cross the cell membrane barrier. The positively charged BPEI-coated AgNPs induced, instead, severe effects on embryo development posing teratogenic hazard, with NPs interacting with and disrupting embryo tissues, intestine in particular. Additional adverse developmental toxicity outcomes may also derive from the bio-interaction with the early embryo stages. These are likely the consequences of the peculiar physico-chemical properties conferred by the BPEI surface coating.

Concluding, no matter which is the model taken into account, in all the cases of study proposed, the NP shape represents one of the crucial aspects driving the bio-interaction, both with metal oxide- and metal-based NPs.

Taken together the results show that the use of several and so different *in vitro* models represents clearly a useful tool to investigate the interactions between NPs and biological systems. The models proposed, each one with its own peculiar

features, advantages and disadvantages, are perfectly suitable for nanotoxicological studies and allow to describe the NM behaviour at cellular, tissue and organ level. This wide range of observations could increase our knowledge specially in the light to improve nanotechnologies in term of SbD approach.

Attachments

Article

Do Nanoparticle Physico-Chemical Properties and Developmental Exposure Window Influence Nano ZnO Embryotoxicity in *Xenopus laevis*?

Patrizia Bonfanti [1],[†]**, Elisa Moschini** [1],[†]**, Melissa Saibene** [1]**, Renato Bacchetta** [2]**,
Leonardo Rettighieri** [3]**, Lorenzo Calabri** [3]**, Anita Colombo** [1] **and Paride Mantecca** [1],[*]

[1] Department Earth and Environmental Sciences, POLARIS Research Centre, University of Milano
   Bicocca, 1 Piazza della Scienza, 20126 Milan, Italy;
   E-Mails: patrizia.bonfanti@unimib.it (P.B.); elisa.moschini@unimib.it (E.M.);
   m.saibene2@campus.unimib.it (M.S.); anita.colombo@unimib.it (A.C.)
[2] Department of Biosciences, University of Milan, 26 via Celoria, 20133 Milan, Italy;
   E-Mail: renato.bacchetta@unimi.it
[3] Tec Star S.r.l., Viale Europa, 40, 41011 Campogalliano, Italy;
   E-Mails: rettighieri@tec-star.it (L.R.); calabri@tec-star.it (L.C.)

[†] These authors contributed equally to this work.

[*] Author to whom correspondence should be addressed; E-Mail: paride.mantecca@unimib.it.

Academic Editor: Mónica Amorim

Abstract: The growing global production of zinc oxide nanoparticles (ZnONPs) suggests a realistic increase in the environmental exposure to such a nanomaterial, making the knowledge of its biological reactivity and its safe-by-design synthesis mandatory. In this study, the embryotoxicity of ZnONPs (1–100 mg/L) specifically synthesized for industrial purposes with different sizes, shapes (round, rod) and surface coatings (PEG, PVP) was tested using the frog embryo teratogenesis assay-*Xenopus* (FETAX) to identify potential target tissues and the most sensitive developmental stages. The ZnONPs did not cause embryolethality, but induced a high incidence of malformations, in particular misfolded gut and abdominal edema. Smaller, round NPs were more effective than the bigger, rod ones, and PEGylation determined a reduction in embryotoxicity. Ingestion appeared to be the most relevant exposure route. Only the embryos exposed from the stomodeum opening showed anatomical and histological lesions to the intestine, mainly referable to a swelling

of paracellular spaces among enterocytes. In conclusion, ZnONPs differing in shape and surface coating displayed similar toxicity in *X. laevis* embryos and shared the same target organ. Nevertheless, we cannot exclude that the physico-chemical characteristics may influence the severity of such effects. Further research efforts are mandatory to ensure the synthesis of safer nano-ZnO-containing products.

1. Introduction

The explosion of the nanotech revolution implies that new and previously-unknown materials are introduced into the environment, generating new ecological relationships among living and non-living systems, with unpredictable scenarios for the long-term effects on human and environmental health.

Trying to fill the gap between the use of nanomaterials (NMs) and the possible health risks, the newborn nanotoxicology discipline has the mission to unravel the toxicological properties of the huge number of NMs already employed and to orient safe nanotech future development.

In the vast NM catalogue, nano-metal oxides (nMeOs) represent one of the more widely-used categories in industrial applications, and they are globally produced in thousands of tons per year.

After nanosized titanium dioxide (nTiO$_2$), nano-zinc oxide (nZnO) was the most abundantly produced [1]. Its action as a stabilizer agent has promoted the use in food, cosmetics and other consumer products, such as paints, and recently, it has attracted great interest for its UV-protective and antibacterial capacities, which make it suitable for a wide range of applications [2].

Accordingly, nZnO represents one of the prioritized NM to be considered for regulation as confirmed by the abundant literature available about its toxicological effects.

Many studies investigated nZnO effects on human cells and laboratory mammals, pointing out the relevant cytotoxic and inflammatory potency of this NM [3]. Besides, nZnO probably represents the only NM that has been uncontrovertibly associated with a specific human disease, metal fume fever a chronic inflammatory status manifested in workers chronically-exposed to welding fume [4].

Adverse effects after nZnO exposure were reported also in aquatic organisms throughout the trophic chain [5,6]; nevertheless, it has been used as a dietary supplement in human and livestock [7]. Several papers agree about attributing to nZnO a heavy acute toxic effect on different ecologically-relevant groups, like algae, bacteria and crustaceans [8–11]. With respect to vertebrates, nZnO was seen to be adversely affecting zebrafish embryos and adults [12–15], as well as the normal development of the amphibian *Xenopus laevis* [16–18]. In two previous papers, we demonstrated that nZnO specifically targets gut development, producing histological and molecular effects as a function of NP dimension, the smaller NPs being the most effective [16,19].

Since the nanotoxicity studies targeting the reproductive and developmental aspects are rather scanty and considering that the nZnO mechanism of action during embryogenesis is not fully understood, in this work, we investigated the relationships between the ZnONP properties and the developmental alterations produced.

In particular, we focused attention on the comparative embryotoxic effects of differently-shaped and -coated ZnONPs obtained from a supplier, who developed different formulations of nano-ZnO to be used as antibacterial and UV filter fillers for polymers and paints.

Smaller, round *vs*. bigger, rod NPs and PVP and PEG surface-coated *vs*. uncoated NPs were tested in order to establish which NP properties might be involved more than others in inducing the specific toxicity outputs and, thus, possibly listed to be considered as targets in a safe-by-design study. In addition, we performed further assays by exposing embryos throughout different developmental windows to characterize which embryonic stages are more sensitive to nZnO exposure. Our findings mainly show that the different ZnONPs induce similar embryotoxic effects, targeting the same organ, the intestine, with ingestion as the primary uptake route. The surface coating with PEG seems a possible way to reduce the embryotoxicity of ZnONPs during *Xenopus* development.

2. Materials and Methods

2.1. Chemicals and NPs Used

All analytical-grade reagents, human chorionic gonadotropin (HCG), 3-amino-benzoic acid ethyl ester (MS222), salts for FETAX solution and $ZnSO_4$ were purchased from Sigma-Aldrich S.r.l., Italy.

The different ZnONPs used were supplied by TecStar S.r.l. (Campogalliano, Modena, Italy); they were produced by gas phase pyrolysis methods.

The ZnONPs used are indicated as follow: sZnO (smaller, round NPs), bZnO (bigger, rod). These NPs tested here are both nude and surface-coated with polyvinylpyrrolidone (PVP10K) or polyethylene glycol (PEG400) and indicated as PVP-sZnO, PEG-sZnO, and so on.

The functionalization of nanoparticles is obtained by TecStar proprietary wet chemical procedures.

All suspensions and stock solutions were prepared in FETAX, whose composition in mg/L was 625 NaCl, 96 $NaHCO_3$, 30 KCl, 15 $CaCl_2$, 60 $CaSO_4 \cdot 2H_2O$ and 70 $MgSO_4$, at pH 7.6–8.0. Test suspensions (1, 10, 50 and 100 mg/L) were sonicated for 10 min in a Branson 2510 sonifier and stored in the dark at 4 °C.

2.2. NP Characterization

The size and morphology of uncoated NPs were investigated by high-resolution scanning electron microscopy (HR-SEM) equipped with a field emission electron source (FEI STRATA DB235M, 30-kV beam voltage). ZnONPs (sZnO, bZnO) were also characterized by transmission electron microscopy (TEM). For this purpose, they were suspended in distilled water, sonicated for 1 min and vortexed. Aliquots of 3 µL of NP suspension (100 mg/L) were immediately pipetted and deposited onto Formvar®-coated 200 mesh copper grids; the excess of water was gently blotted by filter paper. Once dried, grids were directly inserted into a Jeol-JEM1220 transmission electron microscope operating at 100 kV, and images were taken using a dedicated Lheritier LH72WA-TEM camera.

The crystalline size and phase of uncoated NPs were investigated by X-ray diffraction (XRD) analysis (Panalytical XPERT PRO with Cu anode).

2.3. Characterization of NP Suspensions

Dynamic light scattering (DLS) and inductively coupled plasma optical emission spectrometry (ICP-OES) measurements were performed to characterize the NP hydrodynamic behavior and dissolution, respectively, in FETAX medium.

For DLS and Z-potential measurement, a Nanosizer ZS (Malvern Instruments Ltd) was used. Suspensions of coated and uncoated sZnO and bZnO were prepared in FETAX solution and immediately analyzed; the reported values represent the mean of five independent measures.

To estimate the NP dissolution and the possible contribution to the toxicity of Zn^{2+} dissolved in FETAX medium during the exposure, the suspensions of coated and uncoated bZnO and sZnO were collected after 24 h and 96 h from the beginning of the test.

Then, they were ultrafiltrated using centrifuge tubes VIVASPIN 6 with a molecular weight cut-off of 10,000 Da (Sartorius Stedim Biotech GmbH, Goettingen, Germany). The Zn^{2+} concentration in ZnONP-free ultrafiltrated solutions was measured by ICP-OES with a Perkin-Elmer Optima 7000 DV (Perkin-Elmer, Santa Clara, CA, USA). The analyses were conducted on samples from two independent bioassays, and each measurement was replicated three times.

2.4. FETAX Assay

Adult *X. laevis* were purchased from Centre de Ressources Biologiques *Xénopes* (Université de Rennes 1, Rennes Cedex), maintained in aquariums with dechlorinated tap water at a 22 ± 2 °C, alternating 12-h light/dark cycles and fed a semi-synthetic diet (Mucedola S.r.L., Settimo Milanese, Italy) three times a week.

The FETAX test was run according to the standard protocol ASTM [20]. Embryos were obtained from the natural breeding of pairs of adult *X. laevis* previously injected with HCG in the dorsal lymph sac (females: 300 IU; males: 150 IU). Breeding tanks were filled with FETAX solution and well aerated before introducing the couples. Amplexus normally ensued within 2–6 h, and the deposition of fertilized eggs occurred from 9–12 h after injection. After breeding, adults were removed and embryos collected and degelled with 2.25% of L-cysteine in FETAX solution (pH 8.0). Normally-cleaved embryos at the midblastula stage (Stage 8), 5 h post-fertilization (hpf) [21], were selected for testing and placed in 6.0-cm glass Petri dishes containing 10 mL of control or test solution. For each female, the plates were duplicated. All of the Petri dishes were incubated in a thermostatic chamber at 23 ± 0.5 °C until the end of the test (96 hpf), and each day, the test solutions were renewed and the dead embryos removed. At this moment, mortality and malformation data were generated as endpoints of the assay. For each experimental group, the number of dead larvae was recorded, and survivors were anaesthetized with MS-222 at 100 mg/L and evaluated for single malformations by examining each specimen under a dissecting microscope. At the end of the bioassays, surviving normal larvae were formalin fixed for growth retardation measurements. Each assay was repeated at least three times under the same experimental conditions.

2.5. Experimental Design

The experimental design was set up as follows: (1) to probe the embryotoxic potency of differently-sized and -shaped ZnONPs, a conventional FETAX assay (exposure over Stages 8–46) was conducted by exposing embryos to sZnO and bZnO at increasing concentrations of 1, 10, 50 and 100 mg/L; (2) to test a possible influence of surface coating in the observed embryotoxic properties, further comparative FETAX assays (Stages 8–46) were performed using PVP- and PEG-coated sZnO and bZnO at the effective concentration of 50 mg/L; (3) to establish the NP uptake route and the most sensitive developmental windows, further experiments were conducted by exposing embryos to sZnO and bZnO from Stage 8 (mid-blastula, 5 hpf; beginning of FETAX assay) to Stage 39 (2 days 8 hpf; opening of the stomodeum), corresponding to the likelihood for NP ingestion, and from Stage 39–Stage 46 (4 days 10 hpf; end of the primary organogenesis that is the end of the FETAX assay); the results obtained from these different exposure conditions were compared to the results from the exposure during the whole embryogenetic period (Stages 8–46); (4) at the end of the test (96 hpf), pools of Stage 46 embryos of each exposure condition and exposed to an effective concentration of 50 mg/L were randomly selected and immediately stored at −80 °C for measurement of superoxide dismutase (SOD) enzymatic activity, a biomarker of oxidative stress, or processed for light and electron microscopy analyses.

2.6. Superoxide Dismutase Enzymatic Activity

Total SOD activity (Cu/Zn-, Mn- and Fe-SOD) was quantified by the SOD Assay Kit (Cayman, Ann Arbor, MI, USA) according to the manufacturer's instructions. The test uses a tetrazolium salt to detect superoxide radicals generated by xanthine oxidase. One unit (U) of SOD activity corresponds to the quantity of enzyme yielding 50% dismutation of superoxide radical.

Pools of 20 embryos, collected from each treatment group exposed to the effective concentration of 50 mg/L, were homogenized in 1 mL of 20 mM cold HEPES buffer (pH 7.2). Then, the homogenates were centrifuged at 1500× *g* for 5 min at 4 °C. A volume of 200 μL of radical detection solution was added to 10 μL of the supernatants or SOD standard solutions in a 96-well plate. The reaction was initiated by adding xanthine oxidase solution, and absorbance was measured at 450 nm with a multiplate reader (Multiskan Ascent Thermo Scientific Co., Italy). Data were normalized for the protein content of each sample, determined by the BCA method using BSA as a standard, and expressed as mean specific SOD activity (U/mg proteins) ± SEM of three independent experiments.

2.7. Light and Electron Microscopy Analyses

For light and TEM analyses, embryos were randomly selected at the end of the FETAX assays and fixed in 2.5% glutaraldehyde in 0.1 M sodium cacodylate buffered solution at pH 7.4. After several washes in the same buffer, larvae were post-fixed in 1% OsO_4 for 1.5 h at 4 °C, dehydrated in a graded ethanol series, then transferred in 100% propylene oxide. Infiltration was subsequently performed with propylene oxide and embedding resin (Araldite-Epon) at volumetric proportions of 2:1 for 1.5 h, 1:1 overnight and, finally, 1:2 for 1.5 h. Embryos were then left in 100% pure resin for 4 h, and polymerization was performed at 60 °C for 48 h. Semi-thin sections of 0.5 μm were obtained by a

Reichert Ultracut E microtome, collected onto microscope slides and stained with 1% toluidine blue to be screened under the light microscope and to select the region of interest for TEM observations. Ultra-thin sections of 50 nm of the intestinal loops were collected on 200-mesh uncoated copper grids and not counterstained to avoid contaminations by lead citrate and uranyl acetate that ultimately may interfere with metal NP visualization. Samples were analyzed using a Jeol JEM1220 transmission electron microscope operating at an accelerating voltage of 80 kV and equipped with a Lheritier LH72WA-TEM digital camera.

2.8. Data Collection and Statistical Analysis

The number of dead embryos *versus* their total number at the beginning of the test led to the mortality percentages, and the number of malformed larvae *versus* the total number of surviving ones gave the malformed larva percentages. Data are presented as the average ± SEM. The data were tested for homogeneity and normality. When these assumptions were met, one-way analysis of variance (ANOVA) was performed, and otherwise, the non-parametric Kruskal–Wallis test was applied. The significance level was set at $p < 0.05$. The incidence of specific malformations was investigated with chi-square, with Yates's correction for continuity ($\chi 2$ test) or Fisher's exact tests (FE test). Concentrations causing 50% lethality or malformation at 96 hpf were calculated, when possible, and classified as lethal (LC_{50}) or teratogenic (TC_{50}), respectively. These were obtained following the elaboration of the lethality and malformation data by the probit analysis [22], using the U.S. EPA Probit Analysis Program, Version 1.5. The Teratogenic Index (TI), useful in estimating the teratogenic risk associated with the tested compounds, is represented by the LC_{50}/TC_{50} ratio [23].

3. Results

3.1. NP Physical and Chemical Characteristics

SEM and TEM pictures clearly show that the sZnO sample (Figure 1a,b) is made of round NPs, while bZnO (Figure 1c,d) is composed of bigger, rod-shaped NPs. The mean sizes for sZnO and bZnO (maximum dimension) were 63 ± 29 nm and 334 ± 208 nm, respectively.
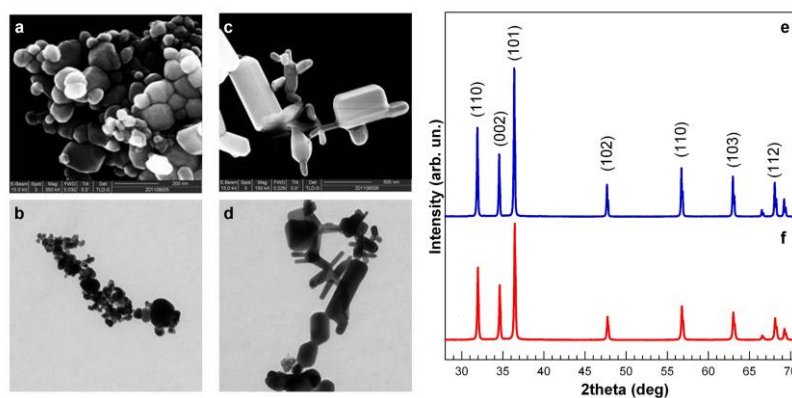

Figure 1. Physical and chemical characterization of ZnO nanoparticles. SEM and TEM images of sZnO (smaller, round) (**a**,**b**) and bZnO (bigger, rod) (**c**,**d**). XRD analysis of dry sZnO (**e**) and bZnO (**f**); the main planes for zincite crystal are reported.

The XRD pattern of dry ZnO NPs was studied using a diffraction angle 28°–71°. All of the peaks have 100% phase matching with the ZnO hexagonal phase of zincite crystal, and no other characteristic impurity peaks were detected (Figure 1e,f).

The line broadening in the peaks determines the crystallite size of ZnO, and the average crystalline size of dry ZnO NPs can be estimated by the well-known Scherrer relation.

Table S1 reports the main results obtained from DLS analysis of hydrodynamic diameters and surface charge (Z-potential) and XRD analysis of crystalline size.

The use of mechanical and ultrasonication techniques was not enough to obtain homogeneous suspensions of particles in FETAX medium. All of the ZnONPs show the tendency to aggregate, as testified by the values of the hydrodynamic diameter determined by DLS.

Nevertheless, coated ZnONPs seemed to be separated from each other by dispersion techniques in a more efficient way; this effect may be caused by steric repulsion induced by the presence of the polymeric coating on the particle surface.

Zeta potential measurements show that sZnO has a positive charge, and the functionalization of these particles with PEG and PVP slightly increases the Z-potential values. Nude and PVP-coated bZnO show a negative charge, while PEG-bZnO a positive one. Anyway values of the Z-potential in the range of −30 mV and +30 mV generally indicate unstable suspensions.

In our experimental conditions, the concentration of Zn^{2+} measured after 24 h and 96 h by ICP-OES was lower than 0.3 mg/L and independent of the NP incubation time for both nude and coated NPs (see Figure S1).

These results confirm that ZnO NPs are very poorly soluble in FETAX medium.

3.2. Comparative Embryotoxicity of Differently-Sized and -Shaped ZnONPs

The physicochemical properties, such as size and shape, along with the effective concentration of ZnONPs were evaluated by the comparative toxicity of sZnO and bZnO on *Xenopus laevis* embryos (Figure 2).

At the end of the test, mortality values were lower than 3% and not significantly different from the control for both NPs (data not shown). On the other hand we observed a concentration-dependent increase in malformation rates in the range of 1–50 mg/L that is statistically different from the control starting from a concentration of 10 mg/L for both sZnO and bZnO.

The embryotoxicity of sZnO appears to be higher than that of bZnO, especially in embryos exposed to 50 mg/L, even if the malformation percentage mean values of the two types of ZnONPs were not statistically different. Nevertheless, the 96 h TC_{50} values calculated by the probit method in the range 1–50 mg/L were 17.9 mg/L for sZnO and 59.47 mg/L for bZnO, suggesting that sZnO has a higher embryotoxic potential than bZnO. However, it is not possible to calculate the TI, because of the low mortality recorded, which did not allow estimating the LC_{50}.

After exposure to 50 mg/L of ZnONPs, more than 70% of the embryos for sZnO and more than 50% for bZnO were abnormal; irregular gut coiling and abdominal or cardiac edema were the most frequent abnormalities observed (Figure 3).
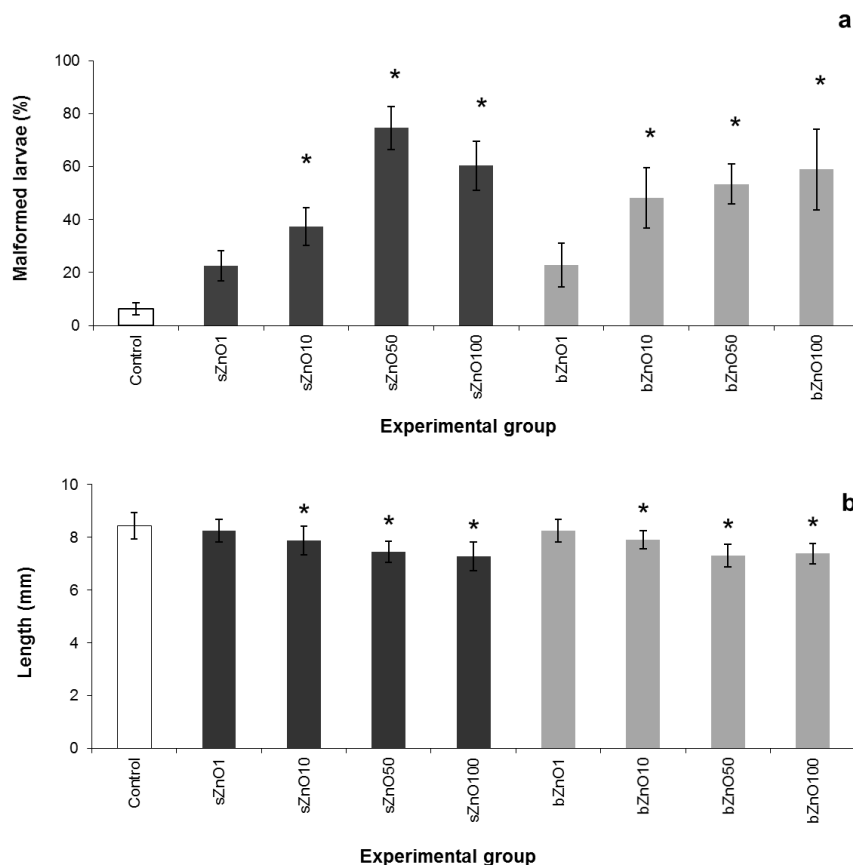
Figure 2. Comparative FETAX results after exposure of embryos to 1–100 mg/L of sZnO and bZnO. (**a**) Malformation rates; (**b**) growth retardation. Dark grey = sZnO-exposed larvae; light grey = bZnO-exposed larvae; bars = SEM; * statistically different from the control ($p < 0.05$, ANOVA + Fisher LSD method).

It is noteworthy that the sZnO affected the gut coiling more heavily in comparison to bZnO, as demonstrated by the chi-square test of the specific malformations (Table 1).

As reported for the malformation rate, a significant growth retardation was observed starting from 10 mg/L for both ZnO NPs, and a concentration-dependent response was also detected up to 100 mg/L (Figure 2b).

In conclusion, considering the comparative embryotoxicity results, sZnO and the bZnO have resulted in a significant malformation incidence and growth inhibition, in which the size and the shape of the NPs play a role.
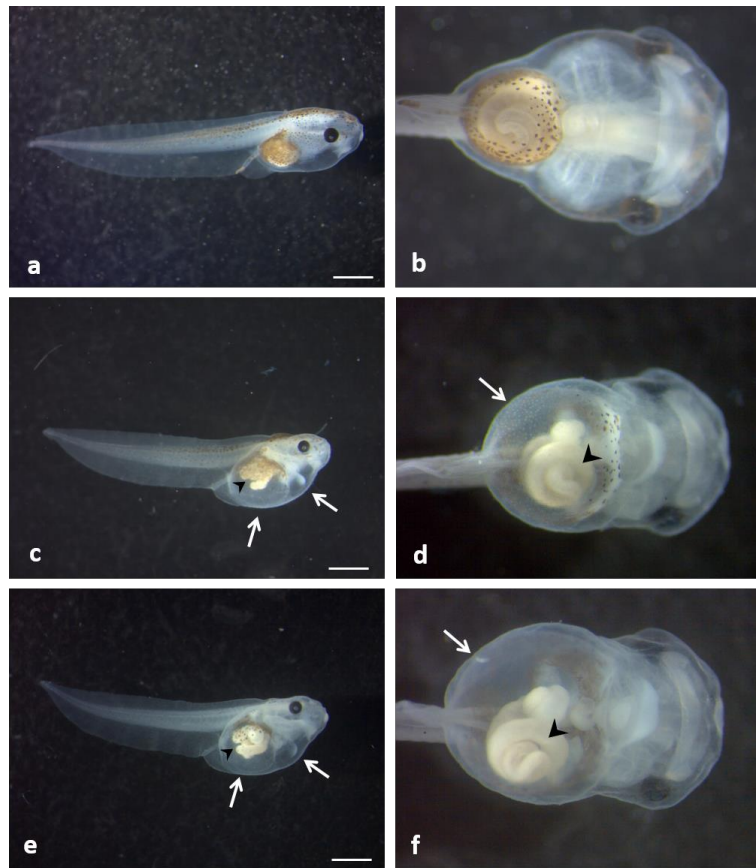
Figure 3. *Xenopus laevis* larvae at the end of the FETAX test. (**a**) Lateral and (**b**) ventral view of a control; (**c**) lateral and (**d**) ventral view of an embryo exposed to 50 mg /L sZnO; (**e**) lateral and (**f**) ventral view of an embryo exposed to 50 mg/L bZnO. The treated larvae show abnormal gut coiling (arrow head), abdominal and cardiac edemas (empty arrow) and a slight dorsal tail flexure. (b,d,f) Original magnification: 4×. Bars = 1 mm.

3.3. Influence of Polymer Surface Coating on ZnONP Embryotoxicity

Based on previous embryotoxicity experiments, 50 mg/L of ZnONPs was selected as the effective concentration in order to assess the influence of surface coating on the embryotoxicity of the considered nanoparticles. We performed a specific FETAX assay comparing nude and polymer-coated (PVP and PEG) sZnO and bZnO, and the results are shown in Figure 4.

Table 1. Malformation patterns in embryos exposed to sZnO and bZnO.

	sZno (mg/L)					bZnO (mg/L)			
	Control	**1**	**10**	**50**	**100**	**1**	**10**	**50**	**100**
Living Larvae	247	247	249	258	173	243	249	257	169
Malformation									
Severe n (%)	3 (1.2)	5 (2.0)	8 (3.2)	4 (1.6)	7 (4.0)	1 (0.4)	3 (1.2)	9 (3.5)	2 (1.2)
Gut n (%)	4 (1.6)	35 (14.2) [b]	66 (26.5) [b]	116 (45.0) [b,c]	79 (45.7) [b,c]	29 (11.9) [b]	71 (28.5) [b]	70 (27.2) [b]	48 (28.4) [b]
Edema n(%) Cardiac	0	0	2 (0.8)	31 (12.0) [b]	4 (2.3) [a]	2 (0.8)	32 (12.9) [b]	12 (4.7) [b]	0
Abdominal	8 (3.2)	15 (6.1)	34 (13.7) [b]	90 (34.9) [b]	39 (22.5) [b]	19 (7.8) [a]	70 (28.1) [b]	57 (22.2) [b]	47 (27.8) [b]
Dorsal Flexure n (%)	0	0	2 (0.8)	13 (5.0) [b]	1 (0.6)	0	0	8 (3.1) [b]	16 (9.5) [b]

Percentages based on the number of malformations/the number of those living. [a] Chi-square test; $p < 0.05$ *versus* control. [b] Chi-square test; $p < 0.001$ *versus* control. [c] Chi-square test; $p < 0.001$ sZnO *versus* the corresponding concentration of bZnO.
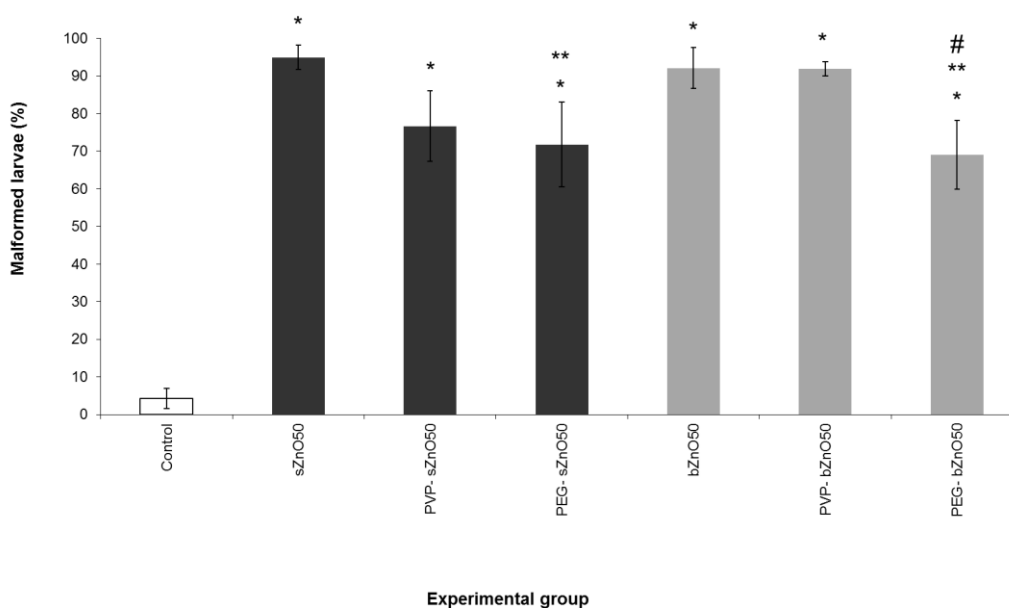
Figure 4. Comparative FETAX malformation percentages after exposure of embryos to nude and polymer-coated sZnO and bZnO at 50 mg/L. Dark grey = sZnO-exposed larvae; light grey = bZnO-exposed larvae. Bars = SEM; * statistically different from the control at $p < 0.001$; ** statistically different from the corresponding nude nanoparticles at $p < 0.05$; # statistically different from the corresponding PVP-coated bZnO at $p < 0.05$, ANOVA + Fisher LSD method.

No embryolethality was observed (data not shown), while it was confirmed that a high and similar incidence of malformations was induced by both sZnO and bZnO. From the comparison of the coated to the nude ZnONPs, a significant reduction in malformation rate emerged in embryos treated with PEG-coated sZnO with respect to the nude ones and in those treated with PEG-coated bZnO compared to the corresponding nude and PVP-coated nanoparticles. Similarly to what was observed in embryos treated with nude NPs, coated ZnONPs once again affected mainly the gut coiling, abdominal and cardiac cavities, causing edema. While being lower in percentage in the embryos treated with polymer-coated nanoparticles, these kinds of gross malformations were still high and statistically significant compared to the control.

These findings suggest that PEG is able to significantly reduce the damage induced by the ZnONPs, even if the embryotoxic effect remains high.

3.4. Ingestion-Dependent Toxicity of ZnONPs

Since the exposure during whole embryogenesis (Stages 8–46) highlighted that gut was the main target of the ZnONP embryotoxicity, two specific developmental windows were chosen to evaluate if the ingestion of ZnONPs could be responsible for the detected malformations. The first group of embryos was exposed to ZnONPs before the stomodeum opening (from Stage 8–39); in this period, the embryo surface is the only route of exposure. A second group of embryos was exposed to ZnONPs after stomodeum opening (from Stage 39–Stage 46); during these stages, embryos begin to ingest water and suspended materials.

Figure 5 summarize the results obtained by these different exposure conditions.
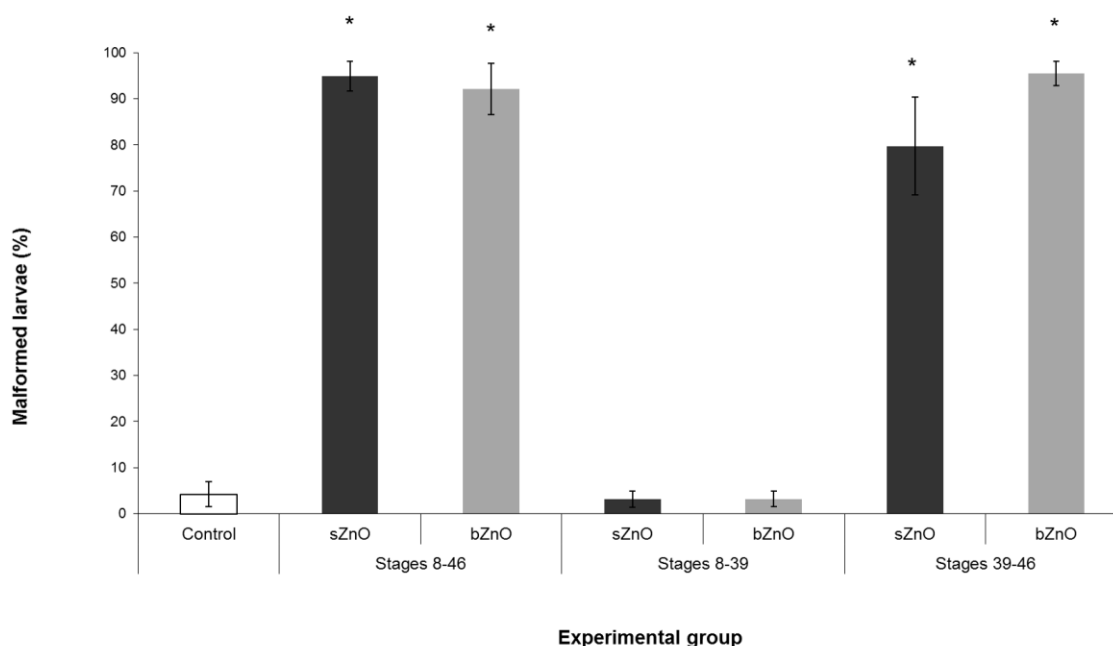

Figure 5. Percentages of malformed embryos after exposure to sZnO and bZnO at 50 mg/L in different developmental windows. Dark grey = sZnO-exposed larvae; light grey = bZnO-exposed larvae. Stages 8–46, exposure during the whole embryogenesis as in the FETAX protocol; Stages 8–39, exposure from blastula to the stomodeum opening (two days 8 hpf); Stages 39–46, exposure from stomodeum opening to the end of the primary organogenesis. * Statistically different from control at $p < 0.001$, ANOVA + Fisher LSD method.

We observed that both sZnO and bZnO at 50 mg/L induced malformation rates comparable to those of conventional FETAX only when the exposure began after stomodeum opening. On the contrary, malformation rates comparable to the control were recorded in embryo groups exposed during the first developmental window. These data suggest that ingestion represents the main route of uptake for both ZnONPs.

3.5. Oxidative Stress Responses

Oxidative stress induced by 50 mg/L of nude and polymer-coated sZnO and bZnO at Stage 46 whole embryos of all experimental groups was investigated by measuring SOD activity, which provides the first defense against ROS toxicity. As shown in Figure 6, we observed a slight, but not significant, decrease in SOD activity if compared to the control in all of the experimental groups. This result suggests that the production of ROS potentially induced by ZnONPs exposure, if any, is not able to elicit a clear alteration in SOD activity, at least if it is measured in pools of whole embryos and not in single embryos or in target organ.
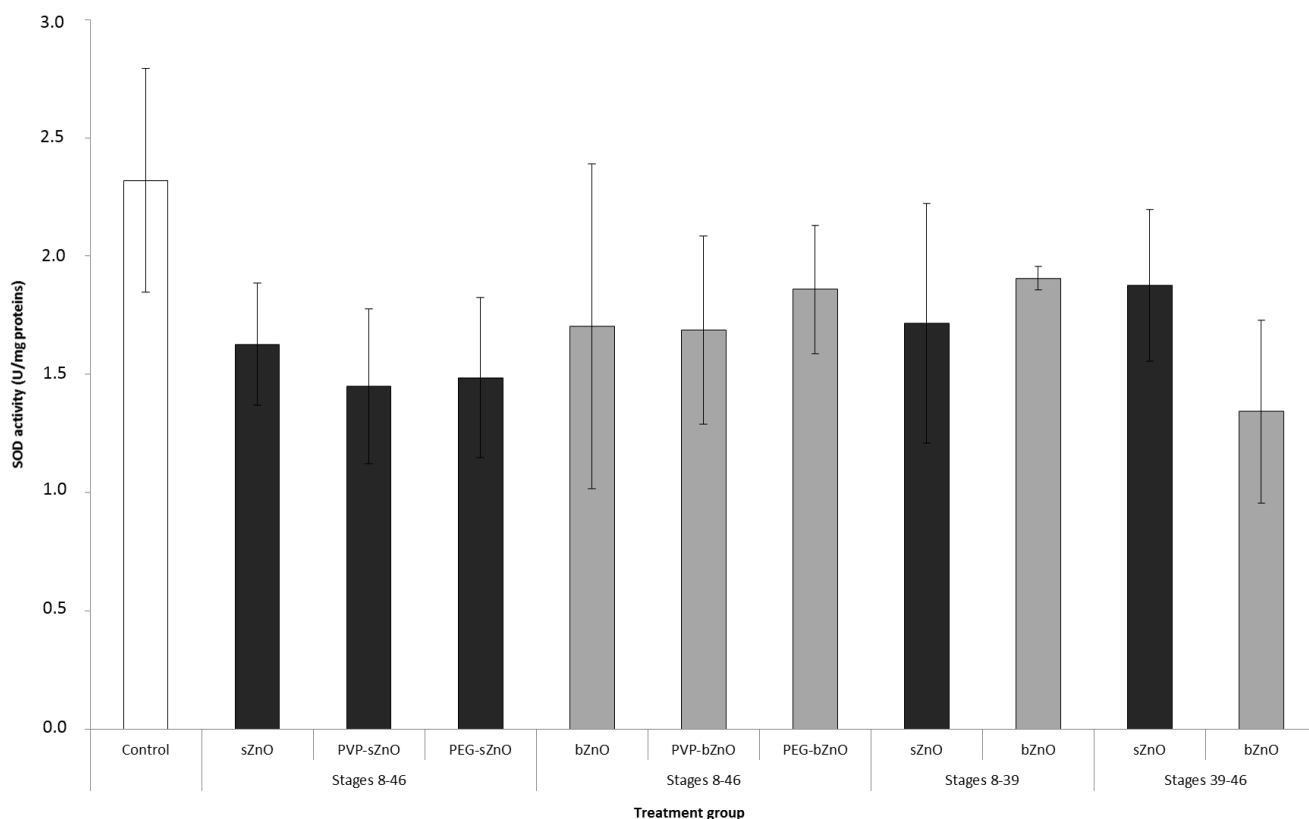
Figure 6. SOD enzymatic activity in embryos exposed to nude and polymer-coated sZnO and bZnO 50 mg/L during different developmental stages. Dark grey = sZnO-exposed larvae; light grey = bZnO-exposed larvae.

3.5. Histological and Ultrastructural Effects of ZnONPs on Small Intestine

Since abnormal gut coiling was the main feature of ZnONP-treated embryos, preliminary histological and ultrastructural analyses of small intestine were performed (Figure 7).

Despite the severity of the gut anatomical abnormality induced by ZnONPs, no obvious signs of histological damages were noted in bZnO-treated embryos (Figure 7b), while very mild tissue lesions were observed in embryos exposed to sZnO (Figure 7c,d,g,h). These alterations mainly consisted of a swelling of paracellular spaces in intestinal mucosa and detachment of some enterocytes from the basal lamina. On the contrary, the brush border of enterocytes was not affected.

4. Discussion

Thousands of papers fill the literature of the last 15 years with the toxic effects of many different nanomaterials on *in vitro* and *in vivo* systems. Nevertheless, many aspects in nanotoxicology are still critical and need substantial improvements to make this discipline mature. According to the authors, an in depth mechanistic knowledge of the NP toxicity and an increase in the efforts devoted to the study of the reproductive and developmental toxicity of new NMs should be considered mandatory in the actual second life of nanotoxicology.
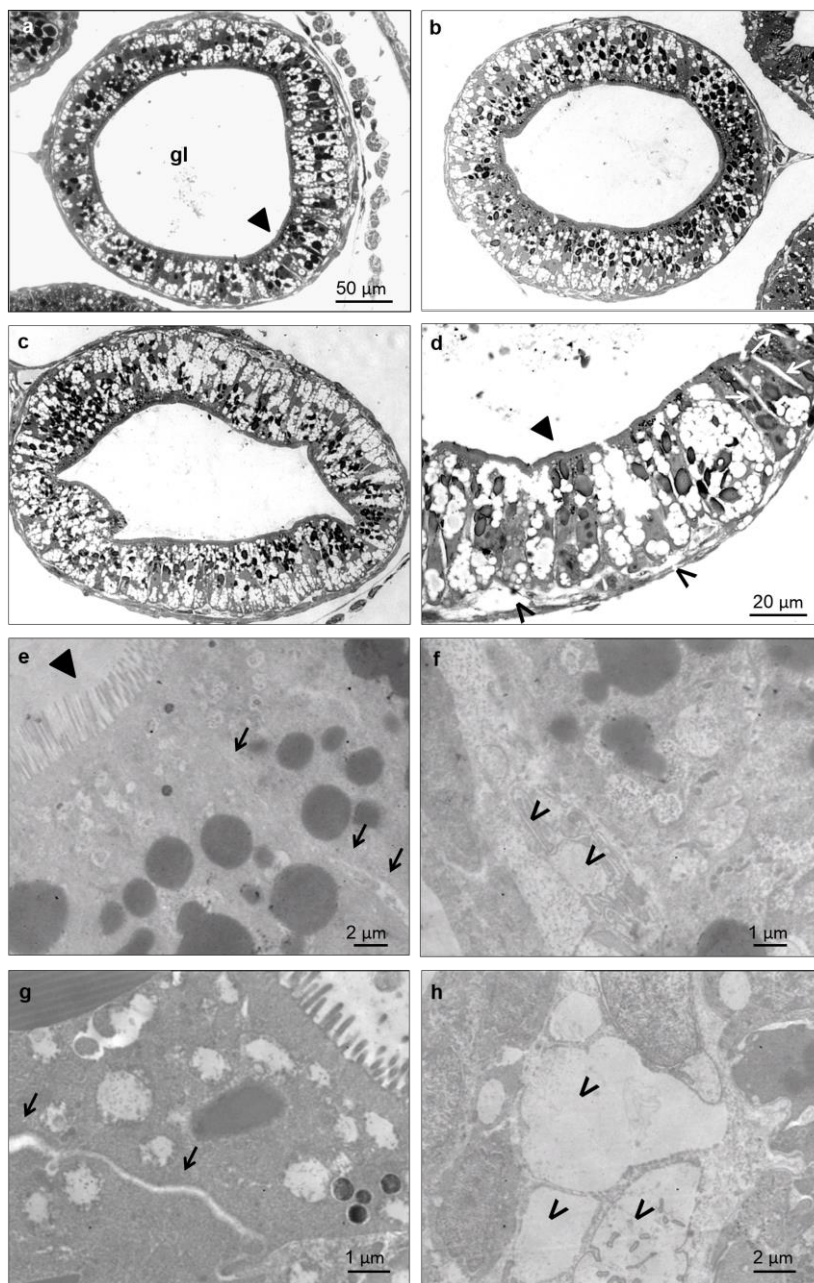
Figure 7. Light (**a–d**) and electron microscopy (**e–h**) imaging of the *X. laevis* small intestine. Transversal sections at the level of an intestinal loop of a control (a), bZnO (b) and sZnO (c,d) exposed embryos. Magnification of the sZnO intestinal loop (d) shows the swelling of paracellular spaces between cells (empty arrow) and detachment in some regions of epithelial cells from basal lamina (*). These damages are more evident in the detail of the junctional complex between two enterocytes (g) (black arrow) and of the basal portion (h) (*) of sZnO-exposed embryos in comparison to the control (e) (black arrow) and (f) (*). ► = brush border; gl = gut lumen.

This work is our contribution to increasing the knowledge of these aspects, and it is focused on the developmental effects and the mode of action of the massively-produced and widely-used nano-zinc oxide. A panel of six ZnONPs, differing in size and shape (big and rod or small and round) and in

surface coating (PEG, PVP), was used to understand if and how these NMs affect *Xenopus laevis* embryos by considering the most sensible developmental stages and the main NP target organs.

The following discussion is organized into three paragraphs according to the three different aspects evaluated.

4.1. Comparative Toxicity of Differently-Sized and -Shaped ZnONPs

Based on our results, sZnO and bZnO induced comparable effects on *X. laevis* embryos. No mortality was observed after exposure to both NPs, while the percentage of malformed larvae and the growth retardation significantly increased starting from the concentration of 10 mg/L (Figure 2). Anyway, sZnO was more effective at 50 mg/L, where the highest malformation score was observed, while it decreased at 100 mg/L. This result suggests a reduced bioavailability of sZnO, likely dependent on the stronger NP agglomeration at the highest concentration, as also proposed by Bai *et al.* [13] for nZnO of 30 nm in water suspension. For this reason, the calculation of TC_{50} in the tested range of 1–100 mg/L was possible only for bZnO, and it was 48.9 mg/L. Instead, TC_{50} re-calculation in the range of 1–50 mg/L was 17.9 mg/L for sZnO and 59.47 mg/L for bZnO. Taken together, these results reinforce the evidence that smaller and round-shaped ZnONPs are more embryotoxic than bigger, rod-shaped ones. Similar findings were obtained exposing *Daphnia magna* to commercial forms of ZnONPs, as reported in Santo *et al.* [11]. In this paper, the acute toxicity of small-sized particles was higher than the bigger ones. Very similar effects were also reported in our previous study on *Xenopus laevis*, where the embryotoxicity of two differently-sized commercial nZnOs similar in shape was compared [19].

Although it was not possible to calculate the teratogenic index, based on our results, the estimated TI should be many times greater than three, and then, sZnO and bZnO should be considered "highly teratogenic" compounds according to Dawson and Bantle [23].

In our previous papers [16,19], we already suggested the potential teratogenic action of nZnO; the news from this work is that the teratogenic effect is almost independent of the NP size and shape, although the NP physico-chemical characteristics may contribute to aggravating such an effect.

Several papers report the toxicity of different metal oxide nanoparticles on zebrafish embryos, and many of them investigated the toxicity of nZnO [12,13,24–27]. By comparing our results to those available on zebrafish, we can argue that the sensitivity to nZnO of the amphibian and fish developing embryos should be considered quite similar. Bai and collaborators [13] observed that ZnONPs killed zebrafish embryos at 50 and 100 mg/L, while at lower concentrations, they reduced body length, induced malformations and retarded embryo hatching. Furthermore, Zhu and collaborators [15] evidenced that nZnO affects the hatching rate of zebrafish and reported an 84-h EC_{50} value of 23.06 mg/L.

Many researchers agree that embryotoxic effects are dependent on the MeONP properties rather than on the dissolved ions [13,15,24]. According to these authors, the metal cations dissolved from the NPs only partially contributed to the nZnO toxicity. On the contrary, other authors have reported that the nZnO toxicity in both *in vitro* and *in vivo* systems are strongly dependent on NP dissolution [12]. Although the question is still debated, the solubility of nZnO can be highly dependent on the suspension medium (e.g., media added with serum albumin or ions in comparison to pure water), the initial particle size and pH [28].

As already observed [16,19], the ZnONP dissolution in FETAX medium, a saline solution with a pH around 8.0, is very poor, and also in this study, the maximum Zn^{2+} concentration measured in NP suspension ultrafiltrates was lower than 0.5 ppm (Figure S1). No embryotoxic effects were observed in *Xenopus* embryos exposed to zinc ions from $ZnSO_4$ at concentrations similar to those measured by ICP-OES according to Bacchetta *et al*. [16] and Mantecca *et al*. [29].

Based on these findings, we can affirm that in our experimental conditions, size and shape did not significantly affect NP dissolution in FETAX medium, making the contribution of Zn ions to toxicity on *Xenopus* embryos very low.

On the contrary, although the effects elicited by the sZnO and bZnO NPs could be considered qualitatively similar, the smaller, round NPs were more effective.

The embryotoxicity induced by 50 mg/L sZnO was slightly higher than that induced by bZnO, and sZnO affected more heavily the gut coiling in comparison to bZnO, as reported in the Results Section. No influence of size nor shape was detected on growth retardation.

These finding could be attributed to the higher surface reactivity and the easier cell uptake of sZnO. It is in fact well proven that round-shaped NPs in the size range of 10–30 nm are preferentially taken up by cells through endocytosis [30,31].

Looking at the results of the oxidative stress biomarker SOD (Figure 6), it is evident that nZnO exposure induced an enzymatic activity depletion, although not statistically different from the control. Again, the sZnO seemed to be more effective than bZnO. Many literature data support the oxidative changes in cells and developing embryos as the main responses to nZnO [14,26], and we also recently demonstrated that *Xenopus* embryo exposure to nZnOs results in antioxidant genes' upregulation [19], although the correspondent increment in the enzymatic activity is not always evident. As previously discussed, this may be attributable to the limitation of having to perform the analysis on pools of whole embryos and not on a single target organ due to the small dimensions of the embryos. Moreover, the developing *Xenopus* have good antioxidant defenses, including enzymes, such as SOD and the GSH-related system [32], able to buffer the ROS production in cells during embryonic development.

4.2. Effects of Polymer Surface Coating

Polymer surface coating is a technique widely used in industry to obtain final commercial products (e.g., paintings, additives) with better performances. In fact, this modification basically can improve the dispersion of poorly-soluble NPs by modifying the surface properties of particles. Several papers underline the key role of the surface properties of ZnONPs in controlling cytotoxicity, demonstrating the reduction of toxicity in *in vitro* and *in vivo* systems after exposure to coated NPs [25,33]. The specific surface area and/or surface reactivity of ZnONPs govern NP-biological interactions by regulating cellular nanoparticle uptake or altering both the intracellular or extracellular Zn dissolution.

In our work, although the observed malformation rates after exposure to coated NPs were significantly higher compared to the control group, the results highlighted that surface modification of particles with PVP and PEG is able to decrease the embryotoxicity of ZnONPs. In particular, PEGylation appears to be more effective at reducing the toxicity of both NPs.

Sometimes, the surface coating can improve the dispersion of poorly-soluble NPs by modifying particle aggregation and settling.

Comparing DLS results of PEG-bZnO and bZnO, we could assume that, in our experimental conditions, these particles have a quite similar hydrodynamic behavior (analogous hydrodynamic diameter, -30 mV $<$ Z-potential $<$ $+30$ mV); therefore, we can also hypothesize that the modality of larvae-NP interaction, and the amount of ingested NPs are quite comparable; nevertheless, the rate of malformed larvae is lower in the PEG-bZnO- than in the bZnO-exposed larvae.

For the small, round-shaped ZnONPs, we can affirm that the hydrodynamic diameter of the PEG-sZnO is significantly lower than that of the sZnO. Different scenarios could be thus hypothesized. If the PEG-NPs are more stable in suspension, they are more bioavailable for larvae by swallowing from the water column, while non-PEGylated NPs are more prone to settle down, being bioavailable by larvae grazing from the bottom. In this first scenario, the decreasing in embryotoxicity after exposure to the PEG-sZnO can be explained only by a reduced toxicity of the PEGylated NPs. In a second scenario, where grazing can be considered as a major feeding behavior determining NP uptake, the reduced embryotoxicity after exposure to PEG-sZnO could be the consequence of the reduced bioavailability of the PEG-sZnO, which is more stable in suspension with respect to the uncoated ones.

In both scenarios, PEGylation appears to be effective at reducing the embryotoxicity of sZnONPs. This is in agreement with Luo and collaborators study [33], who evidenced that the PEGylation of ZnONPs decreases their cytotoxicity in comparison to other surface modifications by reducing the cellular uptake.

4.3. Route of Exposure, nZnOs Target Organs and the Sensitive Developmental Window

In our previous studies [16,19], we have already demonstrated that ZnONPs are highly embryotoxic and that gut is the main affected organ. In particular, the smallest ZnONPs tested were more effective at inducing more severe histopathological effects at the gut mucosa level, with the epithelium severely eroded [19]. In the present work, the intestine was again the target organ, and the abnormal gut coiling was the principal malformation recorded. Nevertheless, embryo histopathological screening and gut ultrastructural analysis revealed only a slight alteration of intestinal mucosa, ascribable to detachment between adjacent cells and from basal lamina, as previously described, mainly after exposure to sZnO.

The choice of performing the exposure of embryos to ZnONPs in two developmental windows (before and after stomodeum opening) allows us to demonstrate that *Xenopus laevis* embryos become more susceptible to nZnO also with the acquisition of grazing behavior following the stomodeum opening. By this route, an increasing amount of suspended and aggregated NP sedimented on the bottom of the Petri dish reach the gut lumen. Conversely, if the exposure is limited to the developmental period in which the embryo is enveloped by the fertilization membrane, the ZnONPs are no longer able to induce embryotoxicity. These results suggest that the fertilization membrane could represent a barrier toward ZnONPs or, if not, the skin of the embryos is not the preferential route for NP internalization. On the contrary, zebrafish embryos are highly sensitive to ZnONPs during early developmental stages due to the high solubility of zinc in zebrafish culture medium and because of the NP interaction with chorion, affecting hatching [13,24].

5. Conclusions

ZnONPs differing in size, shape and polymeric surface coating produced significant and qualitatively similar toxicity in *X. laevis* embryos.

Nevertheless, this work points out that the ingestion is the main exposure route, and the gut is the most sensitive organ in developing *Xenopus* embryos exposed to nZnO. Specific physical and chemical characteristics affect the mode of action of these NPs and influence the severity of the effects. Smaller, round ZnONPs were more effective than bigger, rod-shaped ZnONPs, while PEGylation seemed to be effective at reducing the toxicity of the sZnONPs.

From one side, our results evidence the potential adverse effects of nZnO on environmental health; from the other side, they suggest the possibility of playing with NP properties during the synthesis in order to modulate the toxic effects and to produce safer NMs.

Supplementary

Table S1. Characterization by DLS of ZnONPs in FETAX medium and XRD analysis.

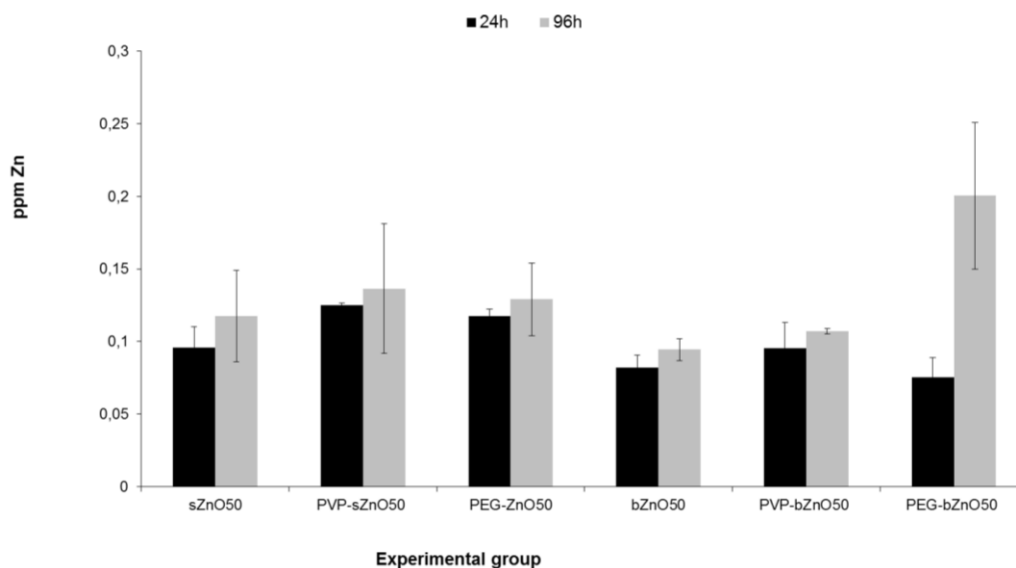|	Hydrodinamic Diameter (nm)	Zeta Potential (mV)	Average Crystalline Size (nm)
sZnO	819	+3.7	70
bZno	579	−12.8	98
PVP-sZnO	355	+15.3	-
PEG-sZnO	237	+19.6	-
PVP-bZnO	454	−10.5	-
PEG-bZnO	685	+3.8	-

Figure S1. Levels of dissolved ions from sZnO and bZnO after 24 h and 96 h from the beginning of the FETAX assay measured by ICP-OES.

Acknowledgements

Author Contributions

Patrizia Bonfanti, Elisa Moschini and Anita Colombo performed the FETAX tests and elaborated the results; Melissa Saibene and Renato Bacchetta performed the histological analyses, while Anita Colombo and Paride Mantecca were mainly involved in the TEM analyses. Leonardo Rettighieri and Lorenzo Calabri performed the NP characterization. Patrizia Bonfanti, Elisa Moschini and Anita Colombo coordinated the preparation of the manuscript. Paride Mantecca is responsible for the project design, supervised the work and revised the final version of the paper.

Conflicts of Interest

The authors report no conflicts of interest. The authors alone are responsible for the content and writing of the paper.

References

1. Bondarenko, O.; Juganson, K.; Ivask, A.; Kasemets, K.; Mortimer, M.; Kahru, A. Toxicity of Ag, CuO and ZnO nanoparticles to selected environmentally relevant test organisms and mammalian cells *in vitro*: A critical review. *Arch. Toxicol.* **2013**, *87*, 1181–1200.
2. Nohynek, G.J.; Antignac, E.; Re, T.; Toutain, H. Safety assessment of personal care products/cosmetics and their ingredients. *Toxicol. Appl. Pharmacol.* **2010**, *243*, 239–259.
3. Pandurangan, M.; Kim, D. *In vitro* toxicity of zinc oxide nanoparticles: A review. *J. Nanopart. Res.* **2015**, *17*, 1–8.
4. Gerberding, J.L. *Toxicological Profile for Zinc*; Department of Health and Human Services, Agency for Toxic Substances and Disease Registry: Atlanta, GA, USA, 2005; pp. 11–118.
5. Skjolding, L.M.; Winther-Nielsen, M.; Baun, A. Trophic transfer of differently functionalized zinc oxide nanoparticles from crustaceans (*Daphnia magna*) to zebrafish (*Danio rerio*). *Aquat. Toxicol.* **2014**, *157*, 101–108.
6. Ates, M.; Arslan, Z.; Demir, V.; Daniels, J.; Farah, I.O. Accumulation and toxicity of CuO and ZnO nanoparticles through waterborne and dietary exposure of goldfish (*Carassius auratus*). *Environ. Toxicol.* **2015**, *30*, 119–128.
7. Rincker, M.J.; Hill, G.M.; Link, J.E.; Meyer, A.M.; Rowntree, J.E. Effects of dietary zinc and iron supplementation on mineral excretion, body composition, and mineral status of nursery pigs. *J. Anim. Sci.* **2005**, *83*, 2762–2774.

8. Aruoja, V.; Dubourguier, H.C.; Kasemets, K.; Kahru, A. Toxicity of nanoparticles of CuO, ZnO and TiO₂ to microalgae *Pseudokirchneriella subcapitata*. *Sci. Total Environ.* **2009**, *407*, 1461–1468.

9. Blinova, I.; Ivask, A.; Heinlaan, M.; Mortimer, M.; Kahru, A. Ecotoxicity of nanoparticles of CuO and ZnO in natural water. *Environ. Pollut.* **2010**, *158*, 41–47.

10. Heinlaan, M.; Ivask, A.; Blinova, I.; Dubourguier, H.C.; Kahru, A. Toxicity of nanosized and bulk ZnO, CuO and TiO₂ to bacteria Vibrio fischeri and crustaceans *Daphnia magna* and *Thamnocephalus platyurus*. *Chemosphere* **2008**, *71*, 1308–1316.

11. Santo, N.; Fascio, U.; Torres, F.; Guazzoni, N.; Tremolada, P.; Bettinetti, R.; Mantecca, P.; Bacchetta, R. Toxic effects and ultrastructural damages to *Daphnia magna* of two differently sized ZnO nanoparticles: Does size matter? *Water Res.* **2014**, *53*, 339–350.

12. Brun, N.R.; Lenz, M.; Wehrli, B.; Fent, K. Comparative effects of zinc oxide nanoparticles and dissolved zinc on zebrafish embryos and eleuthero-embryos: Importance of zinc ions. *Sci. Total Environ.* **2014**, *476–477*, 657–666.

13. Bai, W.; Zhang, Z.; Tian, W., He, X.; Ma, Y.; Zhao, Y.; Chai, Z. Toxicity of zinc oxide nanoparticles to zebrafish embryo: A physicochemical study of toxicity mechanism. *J. Nanopart. Res.* **2010**, *12*, 1645–1654.

14. Xiong, D.; Fang, T.; Yu, L.; Sima, X.; Zhu, W. Effects of nano-scale TiO₂, ZnO and their bulk counterparts on zebrafish: Acute toxicity, oxidative stress and oxidative damage. *Sci. Total Environ.* **2011**, *409*, 1444–1452.

15. Zhu, X.; Wang, J.; Zhang, X.; Chang, Y.; Chen, Y. The impact of ZnO nanoparticle aggregates on the embryonic development of zebrafish (*Danio rerio*). *Nanotechnology* **2009**, *20*, doi:10.1088/0957-4484/20/19/195103.

16. Bacchetta, R.; Santo, N.; Fascio, U.; Moschini, E.; Freddi, S.; Chirico, G.; Camatini, M.; Mantecca, P. Nano-sized CuO, TiO₂ and ZnO affect *Xenopus laevis* development. *Nanotoxicology* **2012**, *6*, 381–398.

17. Nations, S.; Wages, M.; Cañas, J.E.; Maul, J.; Theodorakis, C.; Cobb, G.P. Acute effects of Fe₂O₃, TiO₂, ZnO and CuO nanomaterials on *Xenopus laevis*. *Chemosphere* **2011**, *83*, 1053–1061.

18. Nations, S.; Long, M.; Wages, M.; Canas, J.; Maul, J.D.; Theodorakis, C.; Cobb, G.P. Effects of ZnO nanomaterials on *Xenopus laevis* growth and development. *Ecotoxicol. Environ. Saf.* **2011**, *74*, 203–210.

19. Bacchetta, R.; Moschini, E.; Santo, N.; Fascio, U.; Del Giacco, L.; Freddi, S.; Camatini, M.; Mantecca, P. Evidence and uptake routes for Zinc oxide nanoparticles through the gastrointestinal barrier in *Xenopus laevis*. *Nanotoxicology* **2014**, *8*, 728–744.

20. American Society for Testing and Materials. *Standard Guide for Conducting the Frog Embryo Teratogenesis Assay-Xenopus (FETAX)*; ASTM: Pennsylvania, PA, USA, 1998.

21. Nieuwkoop P.D.; Faber J. Normal Table of *Xenopus Laevis* (Daudin); North Holland Publishing Co.: Amsterdam, Netherlands, 1956.

22. Finney, D.J. *Probit Analysis*, 3rd ed.; Cambridge University Press: Cambridge, UK, 1971.

23. Dawson, D.A.; Bantle, J.A. Development of a reconstituted water medium and preliminary validation of the frog embryo teratogenesis assay—*Xenopus* (FETAX). *J. Appl. Toxicol.* **1987**, *7*, 237–244.

24. Zhu, X.; Zhu, L.; Duan, Z.; Qi, R.; Li, Y.; Lang, Y. Comparative toxicity of several metal oxide nanoparticle aqueous suspensions to Zebrafish (Danio rerio) early developmental stage. *J. Environ. Sci. Health Tox. Hazard. Subst. Environ. Eng.* **2008**, *43*, 278–284.

25. Xia, T.; Zhao, Y.; Sager, T.; George, S.; Pokhrel, S.; Li, N.; Schoenfeld, D.; Meng, H.; Lin, S.; Wang, X.; Wang, M.; Ji, Z.; Zink, J.I.; Madler, L.; Castranova, V.; Nel, A.E. Decreased dissolution of ZnO by iron doping yields nanoparticles with reduced toxicity in the rodent lung and zebrafish embryos. *ACS Nano* **2011**, *5*, 1223–1235.

26. Zhao, X.; Wang, S.; Wu, Y.; You, H.; Lv, L. Acute ZnO nanoparticles exposure induces developmental toxicity, oxidative stress and DNA damage in embryo-larval zebrafish. *Aquat. Toxicol.* **2013**, *136–137*, 49–59.

27. Chen, T.-H.; Lin, C.-C.; Meng, P.-J. Zinc oxide nanoparticles alter hatching and larval locomotor activity in zebrafish (*Danio rerio*). *J. Hazard. Mater.* **2014**, *277*, 134–140.

28. Reed, R.B.; Ladner, D.A.; Higgins, C.P.; Westerhoff, P.; Ranville, J.F. Solubility of nano-zinc oxide in environmentally and biologically important matrices. *Environ. Toxicol. Chem.* **2012**, *31*, 93–99.

29. Mantecca, P.; Moschini, E.; Bonfanti, P.; Fascio, U.; Perelshtein, I.; Lipovsky, A.; Chirico, G.; Bacchetta, R.; Del Giacco, L.; Colombo, A.; Gedanken, A. Toxicity evaluation of a new Zn-doped Cuo nanocomposite with highly effective antibacterial properties. *Toxicol. Sci.* **2015**, doi:10.1093/toxsci/kfv067.

30. Soenen, S.J.H.; Himmelreich, U.; Nuytten, N.; De Cuyper, M. Cytotoxic effects of iron oxide nanoparticles and implications for safety in cell labelling. *Biomaterials* **2011**, *32*, 195–205.

31. Albanese, A.; Tang, P.S.; Chan, W.C. The effect of nanoparticle size, shape, and surface chemistry on biological systems. *Annu. Rev. Biomed. Eng.* **2012**, *14*, 1–16.

32. Rizzo, A.; Li, Y.; Kudera, S.; Della Sala, F.; Zanella, M.; Parak, W.J.; Cingolani, R.; Manna, L.; Gigli, G. Blue light emitting diodes based on fluorescent CdSe/ZnS nanocrystals. *Appl. Phys. Lett.* **2007**, *90*, doi:10.1063/1.2426899.

33. Luo, M.; Shen, C.; Feltis, B.N.; Martin, L.L.; Hughes, A.E.; Wright, P.F.; Turney, T.W. Reducing ZnO nanoparticle cytotoxicity by surface modification. *Nanoscale* **2014**, *6*, 5791–5798.
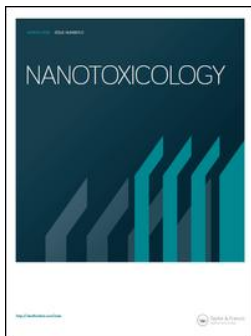
Teratogenic hazard of BPEI-coated silver nanoparticles to Xenopus laevis

Anita Colombo, Melissa Saibene, Elisa Moschini, Patrizia Bonfanti, Maddalena Collini, Kaja Kasemets & Paride Mantecca

Taylor & Francis
Taylor & Francis Group

Check for updates

ORIGINAL ARTICLE

Teratogenic hazard of BPEI-coated silver nanoparticles to *Xenopus laevis*

Anita Colombo[a], Melissa Saibene[a], Elisa Moschini[a,b], Patrizia Bonfanti[a], Maddalena Collini[c], Kaja Kasemets[a,d] and Paride Mantecca[a]

[a]Department of Earth and Environmental Sciences, Research Centre POLARIS, University of Milano-Bicocca, Milan, Italy; [b]Environmental Research and Innovation (ERIN) Department, Luxembourg, Institute of Science and Technology (LIST), Esch-sur-Alzette, Luxembourg; [c]Department of Physic, University of Milano-Bicocca, Milan, Italy; [d]Laboratory of Environmental Toxicology, National Institute of Chemical Physics and Biophysics, Tallinn, Estonia

ABSTRACT

Silver nanoparticles (AgNPs) are among the most exploited antimicrobial agents and are used in many consumer products. Size and surface reactivity are critical physico-chemical properties responsible for NPs toxicity, and surface coatings, often used to functionalize or stabilize AgNPs, can influence their toxic profile and biocompatibility. In the current study the developmental toxicity of (1) negatively charged citrate-coated AgNPs (Cit-AgNPs), (2) positively charged branched polyethylenimine-coated AgNPs (BPEI-AgNPs), and (3) Ag$^+$ (from 0.0625 to 0.75 mg Ag/L) was investigated by the standard Frog Embryo Teratogenesis Assay – *Xenopus* (FETAX). In order to identify the most sensitive developmental phase, embryos were also exposed during different embryonic stages. Morphological and bio-physical studies were performed to characterize tissue lesions and NP uptake. The results suggest that Ag$^+$ was strongly embryo-lethal. Contrary to Cit-AgNPs, the positively charged BPEI-AgNPs exert a concentration-dependent effect on lethality and malformations of embryos. The BPEI-AgNPs showed the highest teratogenic index (TI = 1.6), pointing out the role of functional coating in determining the developmental hazard. The highest susceptibility to BPEI-AgNPs was during early embryogenesis, when embryos are still enclosed in the fertilization envelope, and the post-stomodeum opening stages, when NPs ingestion occurs. In BPEI-AgNPs treated larvae, the histological examination revealed irregular intestinal diverticula coupled with edematous connective tissue. Small NPs aggregates are mapped throughout the intestinal mucosa and secondary target organs by two-photon excitation microscopy. We conclude that a teratogenic risk may be associated with BPEI-AgNPs exposure, but the modality of NP-tissue interactions and the teratogenic mechanism need further investigations to be better defined.

Introduction

According to the most recent nanotechnology consumer product inventories, silver represents the most frequently used nanomaterial. Out of the 1814 consumer products listed, 435 contain silver nanoparticles (AgNPs), accounting for 24% of the already marketed nanomaterials (NMs) (Vance et al., 2015). The reasons why AgNPs are so widely used reside in their high efficacy as antimicrobial agents and in their catalytic and conductivity activity. The antimicrobial properties, in particular, make these NPs widely applied in healthcare, biomedicine, the textile industry, and the food sector (e.g. in food packaging). With these widespread applications, AgNPs are predicted to be released into the aquatic environment from the use of consumer products, as evidenced in several papers (Benn & Westerhoff, 2008; Geranio et al., 2009; Kaegi et al., 2010). According to the studies on the predicted environmental concentration (PEC), AgNPs are pointed out as the most hazardous NM, posing serious concerns toward environmental health and thus deserving careful future evaluation (Gottschalk et al., 2013). In addition to the large presence in already marketed products, the threat to environmental health mainly derives from the high toxicity that AgNPs display toward non-target organisms, as abundantly reported in the literature. AgNPs, in fact, are highly

toxic not only to bacteria, but also to yeasts, algae, crustaceans and mammalian cells, within a range of concentrations comparable to the ones having bactericidal effects (Bondarenko et al., 2013). These authors also provided evidence that the toxicity was crucially dependent on both Ag$^+$ dissolved from particles and NP's size.

Size- and dissolution-dependent toxicity is today a relatively well-established paradigm to explain the effects of metal- and metal oxide-based NMs, and the literature is full of papers reporting on it (Bonfanti et al., 2015; He et al., 2015; Ivask et al., 2014b; Kasemets et al., 2013; Lee et al., 2012; Ma et al., 2013; Misra et al., 2012; Scown et al., 2010). Focusing on AgNPs, extracellular and intracellular dissolution was determined to be the leading mechanism driving cell toxicity, since comparable toxicity was seen in cells and organisms exposed to Ag$^+$ (Hadrup & Lam, 2014; Kim & Ryu, 2013; Kim et al., 2011; Lubick, 2008; Singh & Ramarao, 2012; van Aerle et al., 2013; Volker et al., 2015; Yang et al., 2012; Zhao & Wang, 2012).

Xiu et al. (2012) demonstrated that in Escherichia *coli* the toxicity of various AgNPs – with different sizes and coated with PVP or PEG – strictly follows the concentration-dependent pattern of Ag$^+$. They suggested that the environmental impact of AgNPs

could be mitigated mainly through the modulation of Ag^+ release. Modulation of Ag^+ release can be achieved by reducing particle oxidation, limiting oxygen availability, and also by varying NP size and surface coating. In a recent work, Le Ouay and Stellacci (2015) underlined the key role of particle oxidation and the consequent Ag^+ release as main factors driving the AgNPs antibacterial activity. In addition, these authors stressed the importance of the NP surface physical and chemical properties, since they are strictly connected to the potential Ag^+ release. These considerations pointed out how the tuning of AgNPs surface properties may modulate the biological responses, opening up the possibility to engineer AgNPs by a safe-by-design approach.

Although a huge number of toxicity studies on AgNPs are currently available, the reproductive and developmental effects are worthy of additional research efforts. Embryogenesis can be considered as one of the most sensitive life stages, since even small perturbations occurring during, e.g., body axes formation, neurulation and organogenesis, may strongly affect the entire life of an individual. Most of the available data on AgNP embryotoxicity come from studies using zebrafish (Asharani et al., 2008; Bar-Ilan et al., 2009; Massarsky et al., 2013; Powers et al., 2011), while, to the best of our knowledge, no reports exist on amphibians.

In zebrafish, AgNPs have been proved to be embryotoxic at concentrations of 1-50 mg/L. The effects were seen to be dependent on size – the smaller the NP, the greater the effect (Bar-Ilan et al., 2009; Browning et al., 2013) – while the main mode of action remains to be established. Gene expression data in exposed zebrafish embryos support the hypothesis that the toxicity caused by AgNPs mainly depends on dissolved silver ions (van Aerle et al., 2013).

By using the standard Frog Embryo Teratogenesis Assay – *Xenopus,* FETAX (ASTM, 1998), this work aims to understand if and how differently surface coated AgNPs, varying also in surface charge, may induce developmental toxicity.

FETAX is widely used to screen the teratogenic potential of environmental contaminants and pharmaceuticals (Bonfanti et al., 2004; Chae et al., 2015; Fort & Paul, 2002; Williams et al., 2015) and has been recently applied to NMs, metal oxides, in particular (Bacchetta et al., 2012; Nations et al., 2011). Moreover, the model flexibility allows investigation of the most sensitive developmental windows (Bonfanti et al., 2015) and the modality of NP-tissue interactions contributing to the embryotoxic effects (Bacchetta et al., 2014).

Two commercially available differently coated AgNPs, namely, the negatively charged citrate-coated and the positively charged branched polyethylenimine-coated (Cit-AgNPs and BPEI-AgNPs, respectively), and $AgNO_3$ as ionic control have been comparatively tested. The endpoints – i.e., mortality, malformations and growth retardation – have been measured after 96 h exposure and the most sensitive developmental windows have been identified by exposing embryos at different stages. The 96 h LC50, EC50 and teratogenic index (TI) have been measured. The histopathological effects have been investigated by light microscopy, while NPs have been tracked by non-linear (two-photon excitation, TPE) microscopy.

This approach allowed us to identify the developmental hazard (including the TI) specifically caused by the positively charged BPEI-coated AgNPs and to link it with the bio-interactions at the embryonic tissue level.

Materials and methods

Chemicals and NPs used

BPEI-AgNPs and Cit-AgNPs were purchased from nanoComposix (Prague, Czech Republic; www.nanocomposix.com). AgNPs were

from the BioPure line, guaranteed sterile and endotoxin-free. As reported in the product datasheet, the functionalization of the NPs was obtained by wet chemical procedures, and the primary size of BPEI-AgNPs and Cit-AgNPs was $\sim$10 ± 2 nm. AgNPs suspensions were kept at +4 °C in the dark.

Particles are supplied as an aqueous solution at a concentration of 1 g Ag/L. Working concentrations of both AgNPs (0.125, 0.25, 0.5 and 0.75 mg/L) were obtained by diluting the stock solutions in FETAX medium, whose composition was (mg/L): 625 NaCl, 96 $NaHCO_3$, 30 KCl, 15 $CaCl_2$, 60 $CaSO_4 \cdot 2H_2O$ and 70 $MgSO_4$, pH 7.6–8.0. The suspensions were then vortexed for 30 s in order to obtain homogeneous dispersion of particles.

All analytical-grade reagents, human chorionic gonadotropin (HCG), 3-amino-benzoic acid ethyl ester (MS222), salts for FETAX solution, silver nitrate ($AgNO_3$), sodium citrate and polyethylenimine (branched) were purchased from Sigma-Aldrich (Milan, Italy).

AgNPs characterization

The primary size and shape of AgNPs were studied using a Jeol-JEM 1220 transmission electron microscope (TEM) operating at 80 kV. One drop ($\sim$5 μl) of AgNPs (100 mg Ag/L in deionized (DI) water) was pipetted onto the 300-mesh Formvar®-coated copper grid (Electron Microscopy Sciences, EMS) and the excess water was gently blotted. The samples were air dried before the TEM examination.

Hydrodynamic diameter (D_h) and ζ-potential of AgNPs was studied in FETAX medium and in DI water at 50 mg Ag/L using a Zetasizer Nano ZS90 (Malvern Instruments, UK). The D_h was measured in a clear 2 mL cuvette and the ζ-potential in a 1 mL folded capillary cell (DTS1061, Malvern Instruments, UK) after 0 h and 24 h incubation at room temperature (RT). Samples were vortexed prior to each measurement.

UV-visible light (UV-Vis) absorption spectra of BPEI-AgNPs (20 mg Ag/L) and Cit-AgNPs (12.5 mg Ag/L) in FETAX medium and in DI water were measured on a transparent 96-well polystyrene microplate (Falcon), 200 μl per well, in the range of 300–700 nm (measurement step, 2 nm) using a microplate spectrophotometer (Tecan Infinite M200 PRO, Switzerland) after incubation for 0 h and 24 h at RT. Samples were vortexed prior to the measurement.

Sedimentation of AgNPs in FETAX medium and DI water was studied in a clear 2 mL polypropylene cuvette at 2 mg Ag/L after 0 and 24 h incubation at RT spectrophotometrically at 420 nm.

Solubility of the AgNPs in FETAX medium was studied under abiotic conditions (i.e., without embryos). BPEI-AgNPs and Cit-AgNPs (0.5 mg Ag/L) were incubated in FETAX solution for 24 h at the same conditions used for the exposure experiments. Then, samples were ultra-filtrated using ultra-filtration tubes with a molecular weight cutoff of 10 kDa (Vivaspin®6, 10000 MWCO PES, Sartorius, Germany) at 4000 g for 30 min at 37 °C (Heraeus Biofuge, UK) to remove the non-soluble fraction of AgNPs. Filtrates were acidified with 65% HNO_3 (final HNO_3 concentration 2%) and Ag content was measured by ICP-OES (Perkin-Elmer Optima 7000 DV, Santa Clara, CA).

FETAX assay

Adult *Xenopus laevis* were housed and embryos generated according to the routine procedures adopted in our lab and already described (Bonfanti et al., 2015). Before the embryo selection and the beginning of the test, the jelly coat was removed by swirling the embryos for 1 − 3 min in a 2.25% L-cysteine solution (pH 8.1).

Embryotoxicity tests were conducted according to the standard guide for the FETAX (ASTM, 1998). Normally-cleaved embryos at

the midblastula stage (Stage 8) (Nieuwkoop & Faber, 1956), 5 h post-fertilization (hpf), were selected for testing and groups of 25 embryos from each female were randomly placed in covered 6.0 cm glass Petri dishes containing 10 mL of control or test solution. Two duplicates for each female were used. All of the Petri dishes were incubated in a thermostatic chamber at $23 \pm 0.5\,°C$ until the end of the test (96 hpf).

Exposure solutions were changed daily, and dead embryos were counted and removed. At the end of the assay surviving larvae of each experimental group were anesthetized with MS-222 at 100 mg/L and screened for single morphological abnormalities by examining each larva under a dissecting microscope (Zeiss, Germany).

Mortality and malformation percentages were used to calculate the LC50 (concentration causing 50% lethality) and EC50 (concentration inducing teratogenesis in 50% of surviving embryos) for each experimental group. Surviving normal larvae were formalin fixed to estimate the growth retardation by measuring head − tail length with the digitizing software AxioVision (Zeiss, Germany). Each assay was repeated at least three times under the same experimental conditions.

Experimental design

The experimental design was set up as follows:
1. Embryotoxicity was assessed using the conventional FETAX protocol. *Xenopus* embryos were exposed over stages 8–46 to freshly prepared AgNPs suspensions (0.125, 0.25, 0.5 and 0.75 mg Ag/L) and $AgNO_3$ solutions (0.0625, 0.125, 0.25 and 0.5 mg Ag/L). The concentration range was selected in order to obtain a good concentration response curve, in terms of mortality and malformations, and therefore, allow calculation of the LC50 and EC50 of the most active compounds. Control (not exposed) embryos were incubated in standard FETAX medium.
2. In order to identify the most sensitive developmental windows, the embryos were exposed to AgNPs and Ag^+ at 0.5 mg Ag/L from Stage 8 (mid-blastula, 5 hpf) to Stage 28 (32 hpf, before hatching); from Stage 28 (32 hpf, after hatching) to Stage 39 (2 days and 8 hpf; opening of the stomodeum, preceding the acquisition of grazing behavior); from Stage 39 to Stage 46 (4 days and 10 hpf; end of the primary organogenesis).
3. At the end of the tests (96 hpf), pools of Stage 46 larvae were randomly selected and processed for light and two-photon excitation microscopy.

To address the possible contribution to embryotoxicity of the coating agents, the tests were also performed by exposing embryos to BPEI and Citrate dissolved in FETAX solution (see Supplementary information).

Histological analysis

For light microscopy analyses, larvae were randomly selected at the end of the FETAX assays and fixed in 10% formaldehyde and processed for embedding in paraffin. The samples were transversely cut from eye to proctodeum into serial sections 6 μm thick, then mounted on glass slides and stained with hematoxylin and eosin (H&E). The sections were examined using a Zeiss Axioplan light microscope equipped with an Axiocam MRc5 digital camera. Ten specimens for each experimental group were histologically screened.

Two photon excitation microscopy

Formalin fixed larvae were bleached in a 3% H_2O_2/0.5% KOH medium for 2 h to avoid possible interference due to the larva pigmentation. After bleaching, specimens were routinely embedded in paraffin and 6 μm thick sections at the abdominal level, where most of the major organs are visible, were obtained. The sections, mounted on glass slides, were then dewaxed, hydrated and finally observed under an optical microscope (BX51, Olympus) equipped for two-photon microscopy imaging.

The infrared laser source (Mai Tai HP + DeepSee, Spectra Physics, USA), with pulses of 120 fs full width at half maximum and 80 MHz repetition frequency, was coupled through the FV300 (Olympus, Japan) scanning head. All of the measurements were acquired through a 25X, 1.05 NA, 2 mm WD, Olympus objective (XL Plan N, Olympus, Japan). The fluorescence signal promoted at $\lambda = 800$ nm is steered to a non-descanned unit and split into two channels: the green channel (BP filter at 535/50 nm) and a red channel (BP filter at 600/40 nm) by a dichroic beam splitter. Additional details on the setup and its optical characterization can be found elsewhere (Caccia et al., 2008). Z- series of images (1024 × 1024 pixels, one slice/0.5 μm), have been acquired with a Kalman filter in order to increase the signal to noise ratio, and shown as a full projection. The field of view was: 190 μm × 190 μm for the BPEI-AgNPs and the control samples and 161 μm × 161 μm for the Cit-AgNPs samples.

Data collection and statistical analysis

The number of dead embryos *versus* their total number at the beginning of the test led to the mortality percentages, and the number of malformed larvae *versus* the total number of surviving ones gave the malformed larva percentages. Data are expressed as the average ± SEM. The data were tested for homogeneity and normality.

When these assumptions were met, one-way analysis of variance (ANOVA) was performed; otherwise the non-parametric Kruskal–Wallis test was applied. The significance level was set at $p < .05$. The incidence of specific malformations was investigated by chi-square method, using Yates's correction for continuity (χ^2 test) or Fisher's exact tests (FE test). When possible concentrations causing 50% lethality or malformation at 96 hpf were calculated and classified as lethal (LC50) or teratogenic (EC50), respectively. These values were obtained following the elaboration of the lethality and malformation percentages by the Probit analysis (Finney, 1971), using the U.S. EPA Probit Analysis Program, Version 1.5. The Teratogenic Index (TI), useful in estimating the teratogenic risk associated with the tested compounds, is represented by the LC50/EC50 ratio (Dawson & Bantle, 1987).

Results

AgNPs characterization

According to information supplied by the manufacturer, the BPEI-AgNPs and Cit-AgNPs were round-shaped and sized ∼10 ± 0.2 nm. TEM micrographs confirmed the NPs size and shape declared for both AgNPs, although the size variability seemed to be larger (Figure 1).

The average hydrodynamic diameter (D_h) of BPEI-AgNPs in FETAX medium was 22.8 ± 3.0 nm and 20.7 ± 0.1 nm, at 0 h and at 24 h, respectively (Table 1). BPEI-AgNPs in FETAX medium were well dispersed (pdi ∼0.2), stable (no increase in D_h during 24 h incubation) and showed a narrow one-peak size
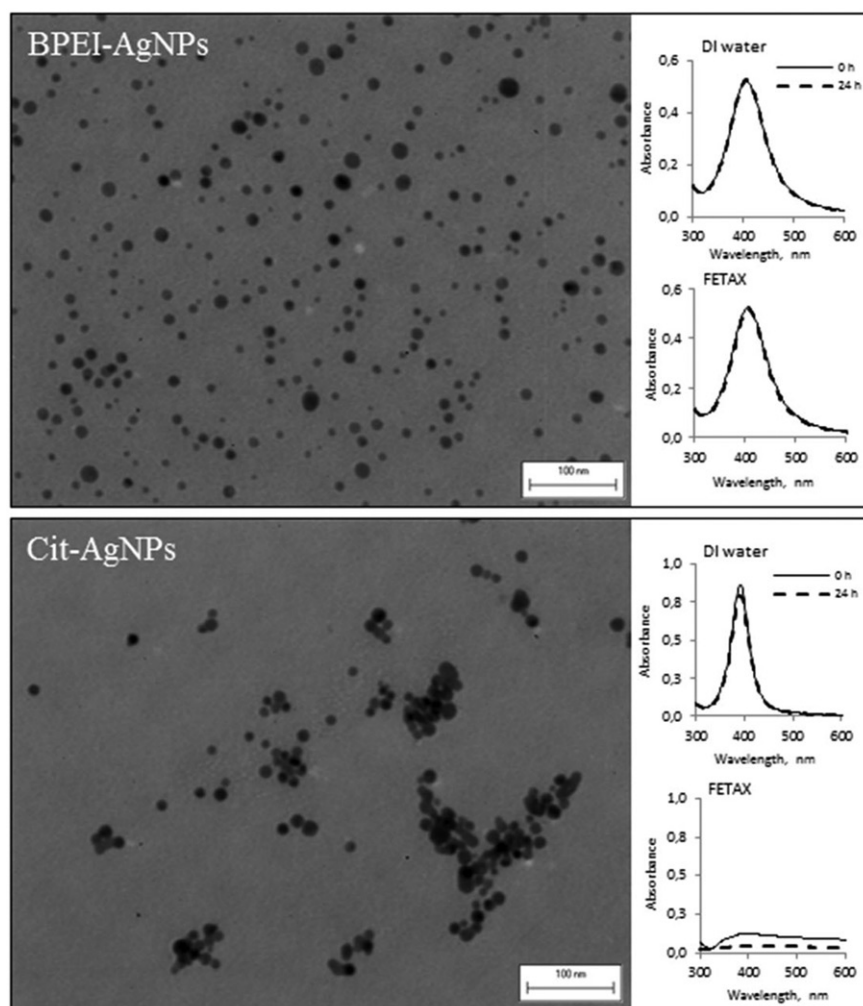
Figure 1. TEM micrographs (left panel) and UV-Vis absorption spectra (right panel) of BPEI-AgNPs and Cit-AgNPs; UV-Vis absorption spectra of BPEI-AgNPs (20 mg Ag/L) and Cit-AgNPs (12.5 mg Ag/L) was performed in FETAX medium and in DI water after 0 h (solid line) and 24 h (dashed line) incubation at room temperature.

Table 1. Hydrodynamic size (D_h) and ζ-potential of branched-polyethylenimine – (BPEI-AgNPs) and citrate-coated AgNPs (Cit-AgNPs) in FETAX medium and deionized water (DI) (50 mg Ag/L) after 0 and 24 h incubation at room temperature.

AgNPs	Primary size[a], nm	Medium	Hydrodynamic size, nm (pdi)[b]		ζ-Potential, mV	
			0 h	24 h	0 h	24 h
BPEI-AgNPs	10.2 ± 2.0	FETAX	22.8 ± 3.0 (0.20)	20.7 ± 0.1 (0.22)	$+9.50 \pm 1.8$	$+13.3 \pm 3.5$
		DI	26.4 ± 4.7 (0.23)	24.6 ± 0.1 (0.26)	$+33.4 \pm 0.5$	$+36.6 \pm 3.8$
Cit-AgNPs	10.3 ± 2.0	FETAX	365 ± 78 (0.29)	1088 ± 25 (0.77)	-34.2 ± 1.6	-13.9 ± 2.6
		DI	14.6 ± 0.6 (0.18)	14.9 ± 0.3 (0.22)	-30.9 ± 0.9	-33.0 ± 1.3

[a]Producer (nanoComposix) TEM data; [b]pdi: polydispersity index.

distribution (Figure S1). Differently from BPEI-AgNPs, Cit-AgNPs agglomerated in FETAX medium and settled during 24 h incubation (Figure S2). Cit-AgNPs D_h was 365 ± 78 nm and 1088 ± 25 nm, at 0 h and at 24 h, respectively, and the size-distribution showed the presence of differently sized particles' populations (Figure S1). Furthermore, the color of Cit-AgNPs FETAX suspension turned from brownish-yellow to black within a few minutes after the preparation (data not shown).

UV-Vis absorption analysis also confirmed the stability of BPEI-AgNPs (plasmon peak at 406 nm) and instability of Cit-AgNPs in FETAX medium (Figure 1). Indeed, already after the preparation (0 h) of Cit-AgNPs suspension in FETAX medium the UV-Vis absorption peak at the range of 400-500 nm was almost missing (Figure 1). The ζ-potential of BPEI-AgNPs and Cit-AgNPs in FETAX medium was positive ($+9 \pm 13$ mV) or negative (-33 mV),

respectively (Table 1). Interestingly the ζ-potential of Cit-AgNPs in FETAX was quite high, but still Cit-AgNPs agglomerated and settled visibly.

BPEI-AgNPs and Cit-AgNPs were characterized also in DI water to assess the effect of medium (e.g., presence of Ag-bounding ligands) on the physico-chemical properties of the studied AgNPs. Results showed that BPEI-AgNPs had comparable average D_h, UV-Vis absorption spectra and settling properties in both test media (Figures 1 and S1, Table 1) while Cit-AgNPs had different properties. In DI water Cit-AgNPs 24 h D_h was $\sim$15 nm (in FETAX, 1088 nm) (Table 1) and UV-Vis analyses showed the presence of the characteristic spectra for AgNPs even after 24 h incubation (Figure 1).

In FETAX medium, 24 h solubility of BPEI-AgNPs and Cit-AgNPs tested at 0.5 mg Ag/L by ICP was $2.6 \pm 1.7\%$ and $3.6 \pm 0.3\%$,
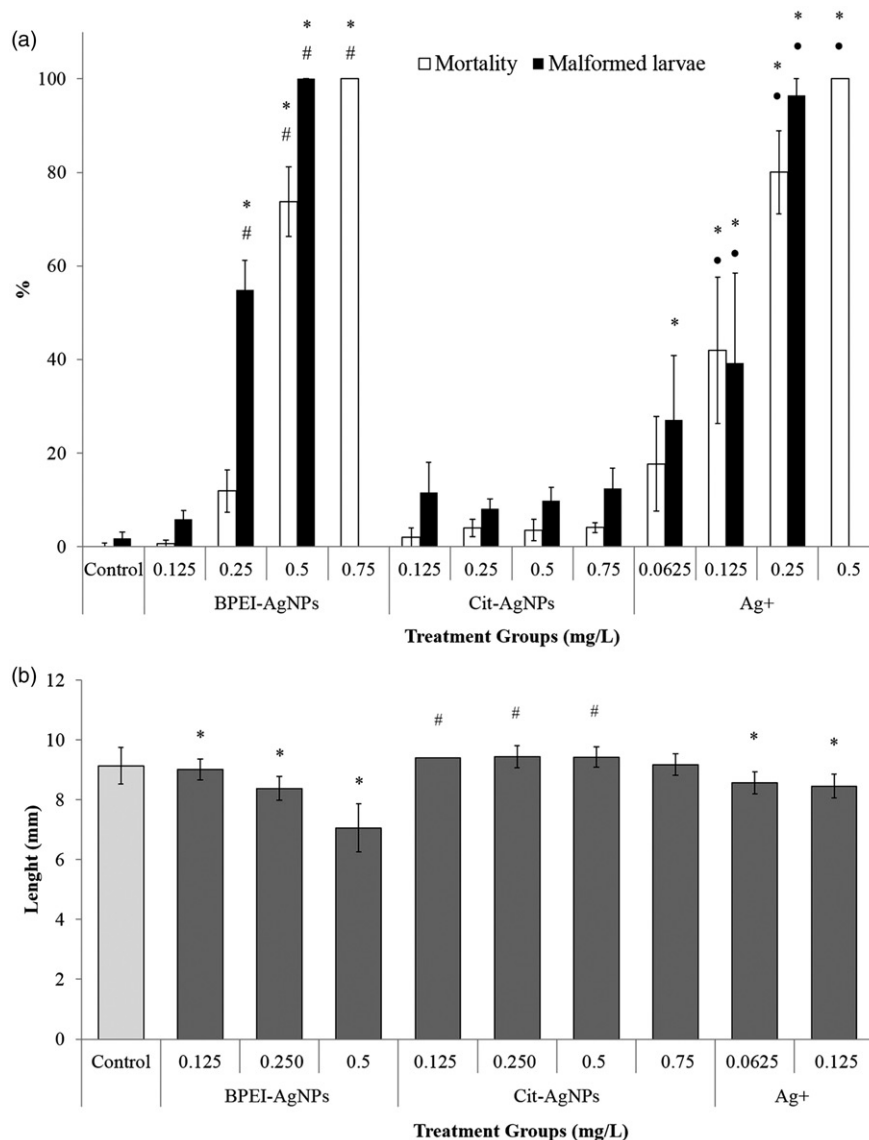
Figure 2. FETAX results. (a) Comparative embryotoxicity of AgNPs and Ag$^+$ expressed as mortality and malformation rates; all values are given as mean ± standard error; *statistically different from control; #statistically different from the corresponding concentration of Cit-AgNPs; ● statistically different from the corresponding concentration of BPEI-AgNPs ($p < .05$, ANOVA + Fisher LSD Method). (b) Growth inhibition observed in stage 46 *X. laevis* larvae after 96 h of exposure to AgNPs and Ag$^+$. Data are expressed as mean length ± SEM; *statistically significant decrease versus control; #statistically significant increase versus control ($p < .05$, ANOVA + Dunn's test).

respectively. The small solubility of BPEI-AgNPs was also confirmed by the UV-Vis analysis (Figure 1). As the Cit-AgNPs agglomerated and settled during the 24 h incubation, the UV-Vis-based solubility determination was not applicable.

Comparative embryotoxicity of differently coated silver nanoparticles and silver ions

Figures 2(a) and S3 show the concentration-response curves for mortality and malformations after exposure to BPEI-AgNPs, Cit-AgNPs and Ag$^+$. The embryotoxic effects induced by an excess of the coating agents (BPEI and Citrate) are reported in Figure S4. In each experiment, the control group showed ≤4% mortality and malformation percentages within the range of 0.07–8% with an average of 1.7%, well below the 10% retained acceptable for the FETAX assay. The average length for control larvae was 9.1 ± 0.6 mm (Figure 2(b)).

The negatively charged Cit-AgNPs did not exert an appreciable embryotoxicity and teratogenicity, even at the highest tested

concentration (0.75 mg/L), since mortality and malformation rates were not statistically different from control. On the contrary, positively charged BPEI-AgNPs and Ag$^+$ induced a linear concentration-dependent effect on lethality and malformations (Figures 2(a) and S3). Compared with Ag$^+$, BPEI-AgNPs were three times less lethal to embryos as evidenced by the 96 hpf LC50 values (Table 2).

One hundred percent mortality was reached after exposure to the highest concentration of BPEI-AgNPs tested (0.75 mg/L), and to 0.5 mg/L of Ag$^+$; however, considering the daily screening requested by the FETAX protocol, the peak of mortality for these concentrations was recorded at 48 hpf for both BPEI-AgNPs and Ag$^+$ (data not shown).

In contrast, malformation rate increased drastically at the concentration 0.25 mg Ag/L for both BPEI-AgNPs and Ag$^+$. The median 96 hpf EC50 was 0.24 mg Ag/L for BPEI-AgNPs and 0.128 mg/L for Ag$^+$ (Table 2). Based on these values the calculated teratogenic index (TI) was 1.60 for BPEI-AgNPs and 1.07 for Ag$^+$. Because the BPEI-AgNPs TI value is greater than 1.5, we can

attribute to this compound a moderate teratogenic potential, according to American Society for Testing and Materials guide (1998).

This result is also deducible from the larger separation of concentration ranges that produce mortality and malformation in BPEI-AgNPs than in Ag$^+$ (compare the slopes of the straight lines related to malformation and survival percentages at the concentrations tested in Figure S3). While the soluble Citrate was ineffective on *Xenopus* development, BPEI was able to induce significant malformation percentages (Figure S3(a, b)). The effects of the BPEI (Figure S3(a)) accounted for about 50% of the embryotoxic effects registered after BPEI-AgNPs exposure, pointing out the synergy between the NPs and the coating agent in determining the developmental hazard.

The last FETAX endpoint we measured was the head-tail length of not malformed embryos; significant growth inhibition was observed after exposure to both BPEI-AgNPs and Ag$^+$ compared to the unexposed control group (Figure 2(b)), starting from the lowest concentrations tested. This means that the MCIG (Minimum Concentration to Inhibit Growth) may be even lower for both BPEI-AgNPs and Ag$^+$.

Multiple malformations were registered in BPEI-AgNPs and Ag$^+$ exposed embryos that appeared in a concentration dependent manner (Table 3).

The most common induced phenotypes ranged from uncorrected gut coiling to cardiac and abdominal edemas and from tail flexure to craniofacial defects. The severity of these abnormalities was higher in Ag$^+$ than in BPEI-AgNPs exposed embryos (Figure 3).

Sporadic and slight increases in the percentages of the same malformations was observed also in Cit-AgNPs exposed embryos (Table 3). In addition, BPEI-AgNPs were able to modify the fertilization envelope, which appeared yellowish and sticky, reducing and sometimes preventing the embryo hatching (Figure 4).

Developmental window dependent- toxicity of coated silver NPs and silver ions

Xenopus early development is marked by events such as the hatching or the stomodeum opening, which can be more critical regarding the potential NP-embryo interactions. For this reason, we decided to expose the embryos during three subsequent developmental windows to better investigate their sensitivity as a function of the developmental stage.

During the first window (from stage 8 to stage 28) embryos were surrounded by the fertilization envelope, which acts as a protective barrier. The daily screening of all the experimental groups allowed detection of significant alterations in the fertilization envelope only in BPEI-AgNPs exposed embryos (Figure 4). The second selected window (from stage 28 to stage 39) is characterized by a passive embryo-NP interaction only through the thin epithelium that lines the external surface of the embryo. During the third window (from stage 39 to stage 46), the stomodeum opens and the embryo acquires a grazing behavior, facilitating active NPs intake.

A significant decrease in mortality was evident in larvae exposed to BPEI-AgNPs in all the selected developmental windows in comparison to exposure over the whole embryogenesis period (Stages 8–46) (Figure 5).

In contrast, the teratogenic effect remained high, even if the significant malformation rates related to the first and the third developmental windows confirm the pre-hatching and stomodeum post-opening as the most critical periods for the exposure to BPEI-AgNPs (Figure 5).

The embryos have displayed an elevated susceptibility to silver ions after hatching when the embryolethality rate was not different from that observed during the whole embryogenesis exposure. Ag$^+$-induced embryotoxicity during the third window was statistically lower than in conventional FETAX, but the malformation percentage rose to a value close to 100%.

Histopathological analysis and NP tracking

To characterize the observed gross malformations induced by BPEI-AgNPs, Cit-AgNPs (0.5 mg/L) and Ag$^+$ (0.25 mg/L), serial transverse 6 μm sections of larvae at stage 46, stained with H&E, were prepared. The observation of transversal histological sections at the level of diencephalon, rhombencephalon, spinal cord and intestine revealed changes in morphology and localization of primitive organs in treated larvae compared with controls (Figure 6).

In particular, the larvae exposed to BPEI-AgNPs and Ag$^+$ show craniofacial abnormalities, slight cardiac and abdominal swelling

Table 2. Median lethal concentration (96 hpf LC50), median teratogenic concentration (96 hpf EC50) (determined by US EPA Probit Analysis Program, version 1.5, with 95% confidence interval in parenthesis) and teratogenic index (TI = 96 hpf LC50/96 hpf EC50) after exposure to BPEI-AgNPs, Cit-AgNPs and Ag$^+$.

Treatment	96 hpf		
	LC50 (mg/L)	EC50 (mg/L)	TI
BPEI-AgNPs	0.385 (0.296–0.469)	0.240 (0.226–0.253)	1.60
Cit-AgNPs	≫0.75 (n.d.)	≫0.75 (n.d.)	(n.d.)
Ag$^+$	0.137 (0.067–0.206)	0.128 (n.d)	1.07

n.d.: not determined.

Table 3. Malformation pattern in stage 46 larvae caused by 96 h exposure to coated AgNPs and Ag$^+$.

	Control	BPEI-AgNPs (mg/L)			Cit-AgNPs (mg/L)				Ag$^+$ (mg/L)		
		0.125	0.25	0.5	0.125	0.25	0.5	0.75	0.0625	0.125	0.25
Living larvae	340	140	212	76	138	231	284	233	96	104	48
Monster	4 (1.2)	2 (1.4)	3 (1.4)	5 (6.6)[a]	3 (2.2)	4 (1.7)	2 (0.7)	1 (0.4)	2 (2.1)	2 (1.0)	6 (6.25)[a]
Gut miscoiling	7 (2.1)	4 (2.9)	112 (52.8)[a]	70 (92.1)[a]	3 (2.2)	9 (3.9)	26 (9.2)[a]	24 (10.3)[a]	7 (7.3)[b]	15 (14.4)[a]	34 (70.8)[a]
Edema											
Cardiac			7 (3.3)[a]	20 (26.3)[a]		1 (0.4)	2 (0.7)		5 (5.2)[a]	1 (1.0)	2 (4.2)[a]
Abdominal	1 (0.3)	1 (0.7)	27 (12.7)[a]	15 (19.7)[a]	6 (4.3)[a]	6 (2.6)[b]	2 (0.7)	7 (3)[a]	1 (1.0)	2 (1.9)	7 (14.6)[a]
Tail flexure	1 (0.3)		2 (0.9)	18 (23.7)[a]	3 (2.1)[b]	3 (1.3)	10 (3.5)[a]	3 (1.7)	6 (6.3)[a]	2 (1.9)	10 (20.8)[a]
Craniofacial defects			9 (4.2)[a]	4 (5.3)[a]		1 (0.4)	1 (0.4)	2 (0.9)	26 (27.1)[a]	5 (4.8)[a]	19 (39.6)[a]
Hemorrhage	1 (0.3)	1 (0.7)	7 (3.3)[a]	11 (14.5)[a]	1 (0.7)	1 (0.4)		3 (1.7)	1 (1.0)	3 (2.9)	2 (4.2)[a]

(Percentages based on number of malformations/number of those living).
[a]Chi square test: $p < .001$ versus control.
[b]Chi square test: $p < .05$ versus control.

with abnormal arrangement of the intestinal loops, while the morphology and distribution of the internal organs show only mild abnormalities in larvae exposed to Cit-AgNPs.

Since abnormal gut coiling was the main feature of treated larvae, we focused our attention on small and large intestine using a higher magnification (Figure 7).

Silver ions appeared to delay the normal morphogenesis of gut epithelium affecting the physiological time table of endoderm cell elongation, polarity and orientation process as the endoderm cells are still relatively yolk filled (Figure 7(d)). BPEI-AgNPs perturb gut coiling as evident by the abnormal arrangement of the intestinal loops, loosely disposed in density and, sometimes, fused together (Figure 7(b)). Nevertheless, the morphogenesis of the intestinal epithelium was not hampered even if the epithelium was less thick than control and in some regions appeared to be detached from the basal membrane. Lastly, Cit-AgNPs did not interfere with

the digestive epithelial morphogenesis and the physiological resorption of yolk platelets (Figure 7(c)).

Using the two-photon excitation microscopy technique, both BPEI- and Cit-AgNPs were mapped in the gut lumen (Figure 8). It can be observed in the red channel (Figure 8 middle column) where AgNPs fluorescence is mainly visible, that Cit-AgNPs were restricted along the enterocyte brush border, whereas BPEI-AgNPs were localized inside the enterocytes. Additionally, after screening of the possible secondary target organs, few scattered BPEI-AgNPs – but not Cit-AgNPs – were identified in coelomic cavity and pronephric and liver tissues (Figure 9).

Discussion

The main results shown above demonstrate that although Ag^+ induced the lowest LC50 and EC50 in *X. laevis* larvae, specific
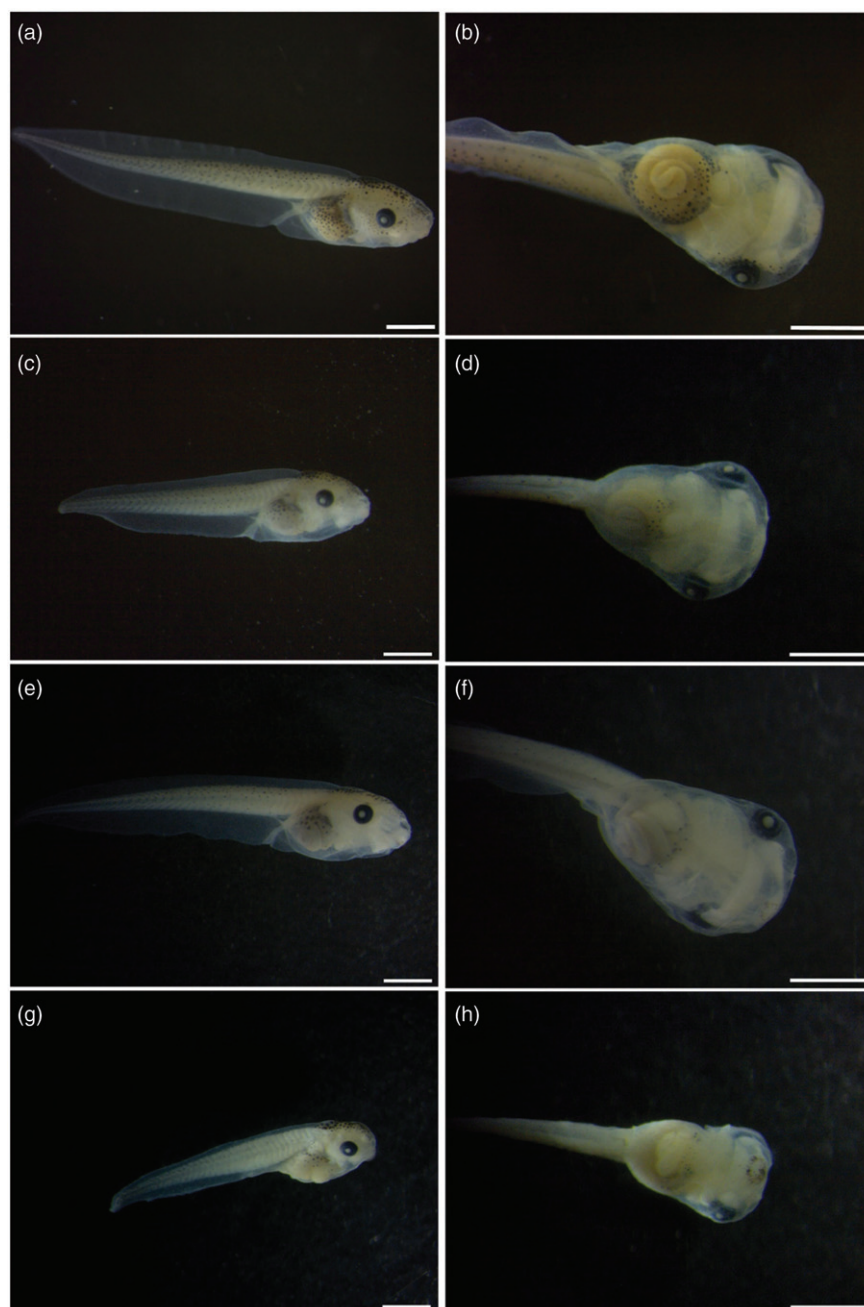

Figure 3. Lateral (a, c, e, g) and ventral (b, d, f, h) view of *X. laevis* larvae at 96 hpf. Control larva (a, b), larva exposed to 0.5 mg Ag/L BPEI-AgNPs (c, d), 0.5 mg Ag/L Cit-AgNPs (e, f), 0.25 mg/L Ag^+ (g, h). Scale bar =1 mm.
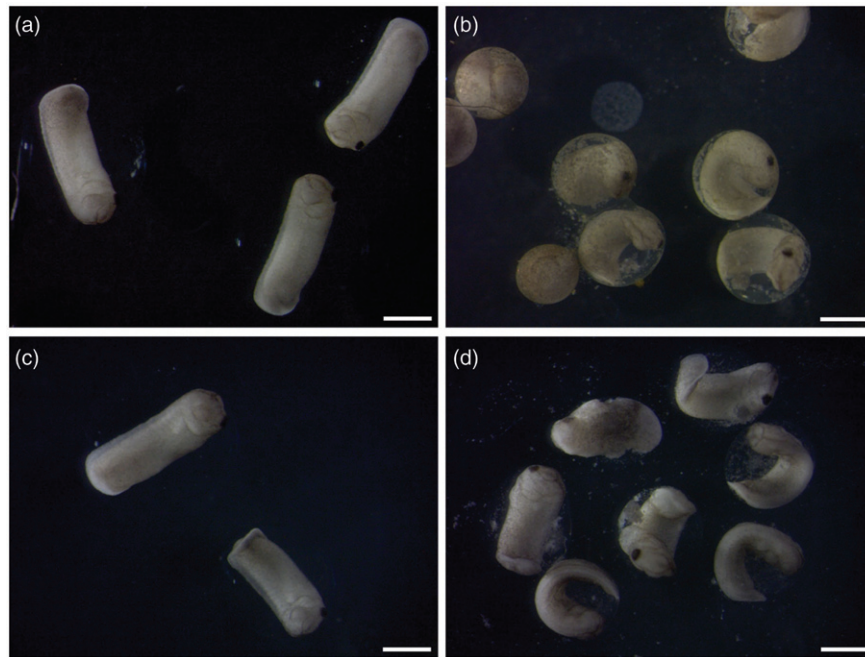
Figure 4. Steromicroscopy images of Stage 28 *X. laevis* embryos. Control group (a), BPEI-AgNPs (b), Cit-AgNPs (c) and Ag$^+$ (d) exposed groups. Scale bar $=1$ mm.
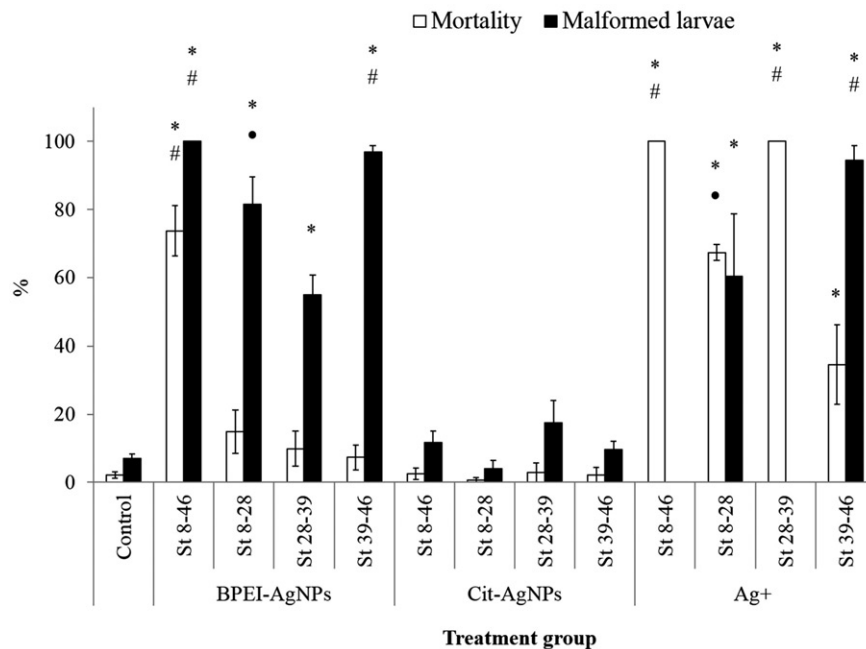

Figure 5. Embryotoxic responses expressed as mortality and malformation rates after exposure to BPEI-AgNPs, Cit-AgNPs and Ag$^+$ (0.5 mg/L) during the three different developmental windows compared to the conventional FETAX exposure. Stages 8–46, conventional FETAX exposure; Stages 8–28, exposure from mid-blastula to hatching; Stages 28–39, exposure from hatching to the stomodeum opening; Stages 39–46, exposure from stomodeum opening to the end of the primary organogenesis. Significant difference from control (*), among equivalent exposure conditions during different developmental windows (#), and from the third window (●) ($p < .05$, ANOVA + Fisher LSD Method).

effects can be attributed to the Ag nanoformulations. In particular, it has been proven that the BPEI-coated AgNPs, with positive surface charge, can be considered teratogenic given the high larval malformations score and the relatively high TI, while no obvious adverse effects were observed after embryo exposure to Cit-AgNPs at the concentrations tested. The sections below are aimed to discuss the reasons for this specific developmental toxicity. The NPs behavior in the medium and the modality of bio-interaction with embryo stages and tissues will be mainly considered.

AgNPs versus soluble Ag embryotoxicity: comparative analysis and role of the NPs behavior in FETAX medium

Ag$^+$ were highly embryotoxic to *Xenopus*, having a 96 h LC50 of 0.137 mg/L and an EC50 of 0.128 mg/L. The calculated TI of 1.07 suggested Ag$^+$ as non-teratogenic, according to Bantle et al. (1999). To the best of our knowledge, our report is the first on Ag$^+$ embryotoxicity to amphibians and clearly points out that even very low Ag$^+$ concentrations are able to kill embryos,
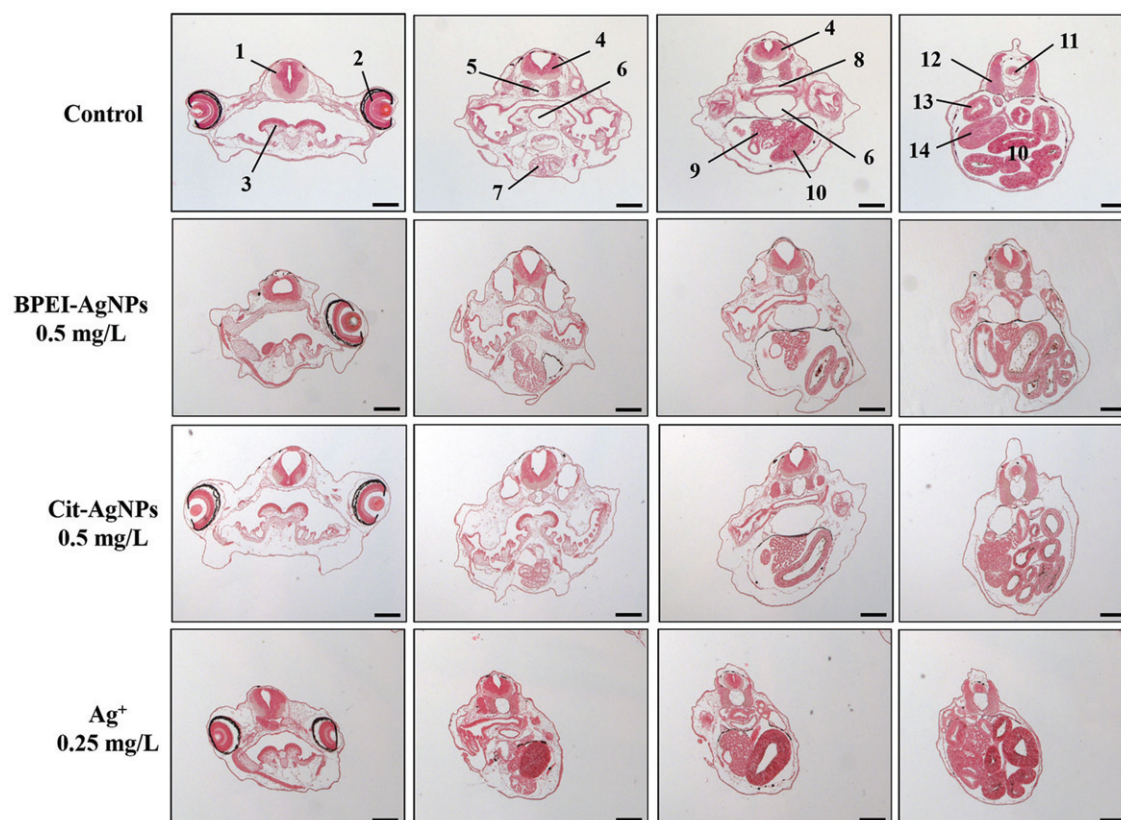
Figure 6. Histological transversal sections of stage 46 *X. laevis* larvae at level of diencephalon (column 1), rhombencephalon (column 2), spinal cord (column 3) and intestine (column 4). Note the altered morphology and localization of primitive organs in the treated larvae compared to control. 1 = diencephalon; 2 = eye; 3 = velar plate; 4 = rhombencephalon; 5 = notochord; 6 = trachea; 7 = heart; 8 = esophagus; 9 = liver; 10 = intestine; 11 = spinal cord; 12 = somite; 13 = duodenum; 14 = oesophagus-stomach transition. Scale bar = 50 μm.
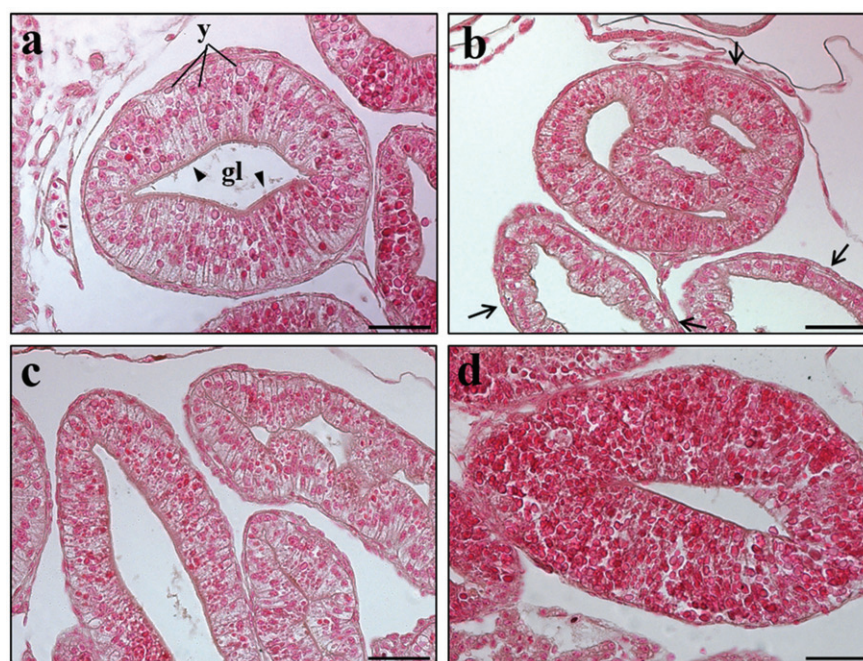

Figure 7. Histological cross sections of intestinal loops in stage 46 *X. laevis* larvae exposed to AgNPs and Ag^+. Control (a), 0.5 mg Ag/L BPEI- (b), 0.5 mg Ag/L Cit- (c) AgNPs and 0.25 mg/L Ag^+ (d) exposed larvae. gl = gut lumen; arrowhead = brush border; y = yolk platelet; arrow = detach from basal membrane. Scale bar = 50 μm.

suggesting it as a potential environmental hazard even when it is not nanosized.

It is widely accepted that the AgNPs toxic effects to living organisms and cells mainly derive from the solubilized Ag ions (Navarro et al., 2008; van Aerle et al., 2013). Particle solubilization

may occur both in extra- and intra-cellular environment, but many lines of evidence suggest that the ions dissolved intracellularly after NPs cell uptake may constitute the main mechanism associated with the AgNPs toxicity. Known under the name of "Trojan horse", this mechanism has been described in many cells exposed
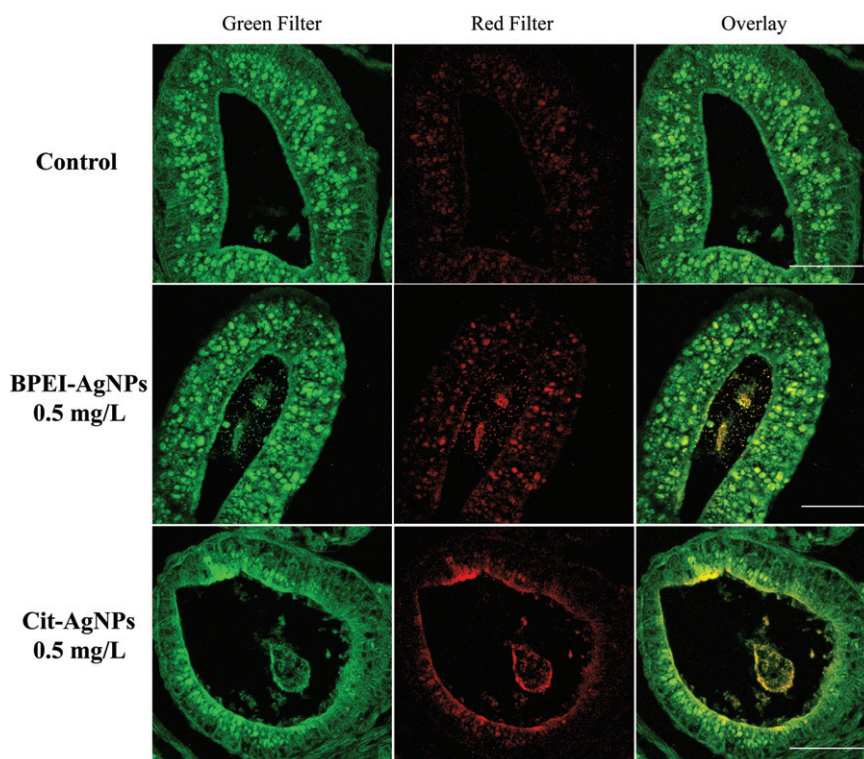
	Green Filter	Red Filter	Overlay

Figure 8. Two-photon excitation confocal microscopy images taken from small intestine diverticula of stage 46 *X. laevis* larvae. (a) Control; (b) 0.5 mg Ag/L BPEI-AgNPs treated larva; (c) 0.5 mg Ag/L Cit-AgNPs treated larva. NP signal is clearly visible in the red channel (middle column) where the *Xenopus* intestinal tissue autofluorescence is negligible. In the green channel (left column), both autofluorescence and the nanoparticles emissions are visible. The right column is a superposition of the images obtained in the two channels, where the colocalization of the two signals is well evident in the gut lumen and along the brush border. Scale bar = 50 μm.

to many different NPs, metals and metal oxides in particular (Sabella et al., 2014), and today – together with the oxidative stress mechanism - is considered the best paradigm to explain the enhanced toxicity of the metal-based nanomaterials. DLS and UV-Vis analyses of studied AgNPs showed that BPEI-AgNPs were stable in the FETAX medium, but Cit-AgNPs agglomerated and settled rapidly during the first minutes after suspension preparation (Table 1, Figures 1 and S2). Different stabilizing agents (e.g., citrate) and polymer coatings are used to increase the AgNPs dispersability and colloidal stability due to the charge and steric repulsion forces (Fabrega et al., 2011; Tolaymat et al., 2010). It has been shown that citrate-stabilized AgNPs were more unstable than polymer-coated particles in chloride-containing medium since the citrate is weakly bound to the surface of the particles (Tejamaya et al., 2012) resulting in the formation of insoluble silver-chlorocomplexes and precipitation (Groh et al., 2015; Levard et al., 2013). In our work, the solubility of surface functionalized AgNPs in FETAX medium has been estimated by ICP-OES and comparatively by UV-Vis absorption spectroscopy that has been used successfully in several published papers on AgNPs (Zook et al., 2011; Ivask et al., 2014c). It can be noted that the solubility of the studied AgNPs was low (2–4%) and is in line with the data obtained in many other papers using different model organisms and cell cultures, and thus involving the use of different test media (Ivask et al., 2014a, 2014c; Kaosaar et al., 2016).

Considering the evidence on comparable AgNPs solubility and the extremely different results coming from the embryotoxicity screening, we can conclude that the main biological responses determined by the exposure to the Cit- and BPEI-AgNPs did not depend upon the extracellularly dissolved Ag^+, but were mainly the consequence of the specific physico-chemical behavior imparted to the NPs by the surface functional molecules. This result is in agreement with data obtained in zebrafish embryos

where none of the phenotypic defects observed in AgNPs treatment were noted in the Ag^+-treated embryos (Asharani et al., 2008).

It is worthy of attention that in our model system, contrary to Ag^+, no effects were evident in embryos exposed to Cit-AgNPs, even at the highest test concentrations, neither in term of mortality nor in term of malformations. Of course these results may be affected by the Cit-AgNPs aggregation and sedimentation in FETAX medium, which likely reduced the amount of the nanosized particles and the NM surface area available for biological interactions. It has to be taken into account that large amounts of Cit-AgNPs aggregates were accumulated into the intestine (Figure 9), without inducing embryotoxicity or histological alterations, supporting the conclusion that the tested concentrations of Cit-AgNPs were not toxic. This result is in line with those obtained in zebrafish embryos by Osborne et al. (2013), who found that coating AgNPs with citrate significantly decreased toxicity. On the other hand, at the same concentrations at which Cit-AgNPs are completely ineffective, the BPEI-coated AgNPs are extremely embryotoxic (96 h LC50 = 0.385 mg/L; 96 h EC50 = 0.240 mg/L). LC50s ranging from 0.0346 to 250 mg/L were reported in different fish species (Cho et al., 2013), and were dependent on AgNP size, coating agent, developmental stages and exposure duration. In zebrafish embryos, uncoated 10 nm AgNPs induced a lower embryotoxicity with a 120 h LC50 value of 13.5 mg/L (Bar-Ilan et al., 2009), while BSA and starch coated AgNPs of 5-20 nm display a LC50 value of 25.5 mg/L.

Although these effective concentrations are higher than predicted environmental concentrations of 0.09–2.63 ng/L (Gottschalk et al., 2009), it is noteworthy that the reported LC50 and EC50 for Ag^+ and BPEI-AgNPs in *Xenopus* embryos are comparable to levels in heavily polluted freshwater systems, where Ag concentrations up to 0.260 mg/L were measured (Kashiwada et al., 2012).
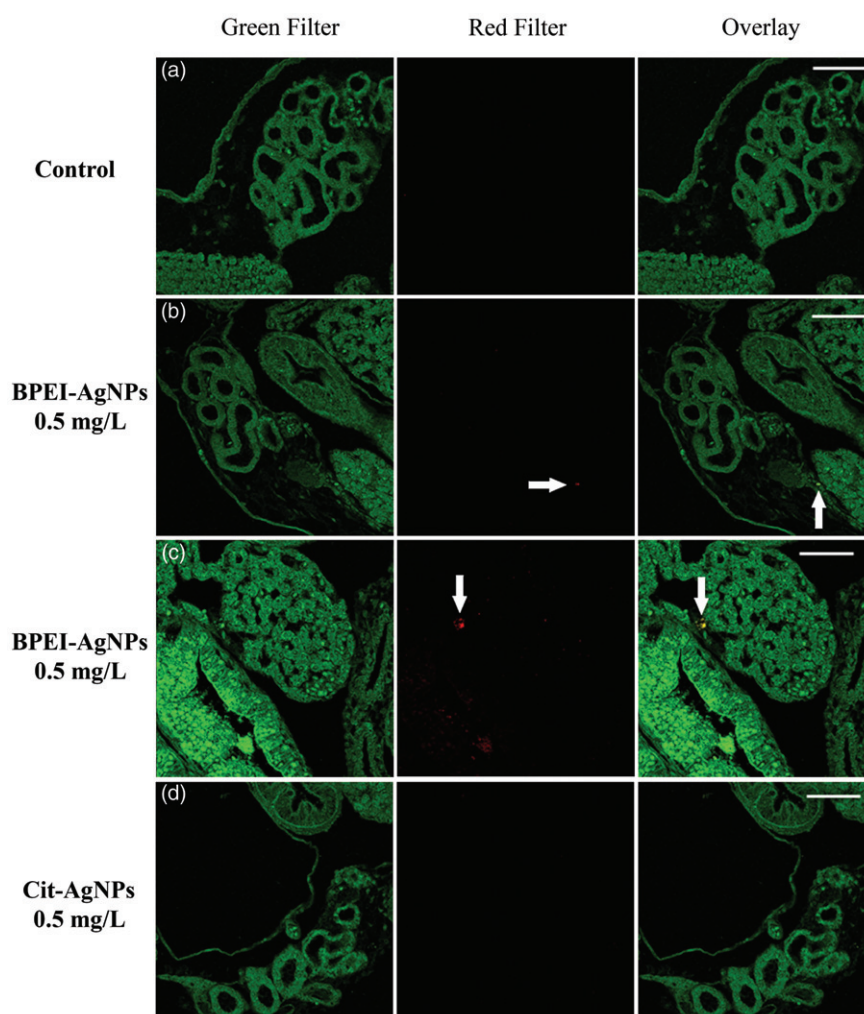
Green Filter	Red Filter	Overlay

Figure 9. Two-photon excitation confocal microscopy images taken at the level of pronephros and liver of stage 46 *X. laevis* larvae. (a) Control pronephros; (b and c) 0.5 mg Ag/L BPEI-AgNPs-treated pronephros and liver respectively; (d) 0.5 mg Ag/L Cit-AgNPs treated pronephros. NP signal is clearly visible in the red channel (middle column, arrow). In the green channel (left column), autofluorescence is visible. The right column is a superposition of the images obtained in the two channels, where the colocalization of the two signals indicated by the arrows corresponds to the presence of NPs. Scale bar = 100 μm.

Our results clearly indicate that the coating agent plays a crucial role in delivering different degrees of AgNPs toxicity and, to the best of our knowledge, the present is the first work reporting that a NM, i.e., the BPEI-coated AgNPs, may be considered a teratogenic hazard, having a TI = 1.6.

AgNPs ingestion and bio-interactions at the intestinal barrier level

The most appreciable abnormalities have been recorded at the abdominal level of the embryos where severe edemas coupled with irregular gut coiling were characteristic of the BPEI-AgNPs treated embryos. This observation is in agreement with the microscopic analyses, showing most of the histopathological lesions and the NPs luminescence signal at the same level (Figures 6 and 8). It is also consistent with the results obtained from exposing embryos to BPEI-AgNPs from stage 39 to stage 46, after the stomodeum opening, when embryos freely swallow materials from the water column. The exposure during this developmental window produced up to almost 100% malformed embryos, similarly to the exposure throughout the whole FETAX test (stage 8–46) (Figure 5). This clearly supports the hypothesis that (1) ingestion is the main exposure route to AgNPs, and (2) since BPEI-AgNPs were mapped in secondary target organs (i.e., pronephros and liver),

the translocation through the intestinal barrier with the consequent ending up in the blood stream is the main uptake mechanism. Previous work has demonstrated that aquatic organisms, like *Daphnia magna* and zebrafish, are mainly exposed to NMs through ingestion (Osborne et al., 2015; Santo et al., 2014; Xiao et al., 2015) and also in *X. laevis* the intestine was the most affected organ after exposure to metal oxide NPs (Bacchetta et al., 2012; Bacchetta et al., 2014; Bonfanti et al., 2015). After exposure of adult zebrafish to 20 nm and 110 nm Cit-AgNPs, (Osborne et al., 2015) observed that gills and intestine were the main affected organs, and the histopathological lesions occurred in correspondence to these high Ag-accumulating sites. Our TPE results suggest that the positively charged BPEI-coated AgNPs are more prone to interact with the cell membranes, to be internalized by the epithelial cells lining the gut and to be translocated in non-target organs. This particular NP behavior can be conferred by either the positive surface charge, which permits the electrostatic interactions with the negatively charged surface of the outer cell membranes (Jain et al., 2010) or the presence of the BPEI, which may carry NPs through the cell compartments. Indeed, one reason why BPEI-coated AgNPs can exert their specific teratogenic action in *Xenopus* embryos may reside in the specific ability of PEI – a cationic dispersant – to deliver materials to cells by avoiding the acidic lysosomal pathway. The PEI transfection capacity is indeed

dependent on the specific ability to produce osmotic swelling and rupture of the endosomes, with the consequent release of the vector into the cytoplasm (Akinc et al., 2005). The same mechanism can be shared by the BPEI-coated AgNPs, that can be released inside the enterocytes after having being ingested and internalized by endocytosis, making the NP surface free for oxidative dissolution and the consequent Ag^+-mediated oxidative damage to proteins, lipids and nucleic acids (Le Ouay & Stellacci, 2015). In the nematode *C. elegans* exposed to Cit-AgNPs and $AgNO_3$, it has been recently demonstrated that the AgNPs *in vivo* toxicity – but not that of $AgNO_3$ – is crucially driven by particle uptake by early endosomes, since endocytosis-deficient mutants and worms exposed to chloropromazine – a clathrin-mediated endocytosis inhibitor – were less sensitive than wild-types (Maurer et al., 2016). Moreover, organ-specific and size-dependent AgNPs toxicity has been shown in zebrafish, where the smaller NPs were more prone to be retained at the basolateral level of the intestinal epithelial cells and are able to disrupt the Na^+/K^+ ATPase pump (Osborne et al., 2015). Taken together, the aforementioned data sustain the idea that the 10 nm BPEI-AgNPs may specifically target the *Xenopus* developing intestine, penetrating enterocytes through endocytosis and inducing cell toxicity after endosomal disruption. Of course this hypothesis requires further experimental evidences.

AgNPs effects on early embryogenesis: relevance of NPs surface properties and implications for reprotox safety assessment

A second possible mechanism of BPEI-AgNPs tissue interaction and teratogenicity should be taken into consideration. After exposure to BPEI-AgNPs during embryo stages 8–28, *Xenopus* larvae finally displayed significantly high malformation percentages (Figure 5). This indicates that during segmentation, gastrulation and early organogenesis – including neurulation – when embryos are still surrounded by the fertilization envelope, NPs significantly interact and affect embryo structures. From our results, it is clear that BPEI-AgNPs are effectively adsorbed by the fertilization envelope (Figure 4(b)), although no clear evidence of particle penetration inside the embryo tissues has been achieved from this study. No NPs, in fact, have been mapped inside the central nervous system and or somites. On the contrary, as shown in Figure 4(b), the NPs adsorbed onto the fertilization coating turned it brownish and sticky, with the consequence of a delayed embryo hatching. Although no appreciable malformations can be detected soon after hatching in BPEI-AgNPs exposed embryos, this contact might have influenced molecular or physiological events during early developmental stages, since significant malformations appeared during the later stages. Of course, this aspect is worthy of further investigation, but is coherent with the findings of Ong et al. (2014), who reported that NPs are able to affect zebrafish hatching by interacting with the ZHE1 hatching enzyme. In this latter paper, where the effective NPs concentrations were in the range 10-100 nm, it was also underlined that the effects were mediated by the NPs themselves rather than the corresponding dissolved metal ions, further supporting our findings that the teratogenic hazard posed by the positively-charged BPEI-AgNPs derived from the peculiar nano-bio-interaction. Moreover, in our study the BPEI-AgNPs were effective at concentrations well below 0.5 mg Ag/L. Together these observations point out that surface coating and charge of AgNPs, even at low concentrations, may contribute to modulation of the effects on the very sensitive early embryogenetic phases.

The earliest developmental stages have been suggested to be the much more sensitive ones by Browning et al. (2013), who

demonstrated that the phenotypes obtained after zebrafish treatment with AgNPs strictly depend on NP size and embryonic developmental stages of exposure. They concluded by suggesting that AgNPs can potentially enable target-specific studies and therapy for embryo development.

Developmental toxicity is one of the priority aspects to be addressed to guarantee NM safety. In mammals, of course, the placenta represents an extremely important biological barrier able to prevent or modulate the access and effects of xenobiotics to the fetus. Pietroiusti et al. (2013) reviewed the effects of different NMs on the placental barrier, indicating that some NPs may both cross and damage placental and fetal tissues. Nevertheless, by using inert fluorescent polystyrene particles of different sizes, it has been demonstrated that up to 500 nm NPs were taken up by the mouse placenta and can even cross it, but the issue of NM translocation and cytotoxic effects on placental barrier and fetus is far from well understood. In a recent paper, Austin et al. (2016) observed that 10 nm citrate-coated AgNPs intravenously injected in pregnant mice preferentially ended up in maternal liver, spleen and visceral yolk sac, and although potential effects on embryo growth were arguable, the NP uptake by fetus was negligible. These studies, in parallel with our findings on the potential teratogenic hazard of the positively-charged BPEI-coated AgNPs highlight the need to further explore the role of particle size and coating in determining the fate and toxicity of AgNPs during development, to finally address both the safety and the potential biomedical applications of Ag-based engineered NMs.

Conclusions

This is the first report on AgNPs effects on amphibian development. The focus was on very small (10 nm) particles either positively charged – BPEI-coated – or negatively charged – citrate-coated. Due to the coating molecule, the Cit-AgNPs were innocuous to embryos, likely as a consequence of both particle agglomeration and diminished capability to cross the epithelial barriers. The positively charged BPEI-coated AgNPs induced severe effects on embryo development, posing a teratogenic hazard, with NPs interacting with and disrupting embryo tissues, intestine in particular. Indications of an enhanced ability to cross the intestinal epithelium and reach non-target organs have been obtained. Additional adverse developmental toxicity outcomes may also derive from the bio-interaction with the early embryo stages. These are likely the consequence of the peculiar physico-chemical properties conferred by the BPEI surface coating. The effects of the BPEI-AgNPs are worthy of further investigation to better understand the cellular and molecular mechanisms behind their action.

References

Akinc A, Thomas M, Klibanov AM, Langer R. 2005. Exploring poly-ethylenimine-mediated DNA transfection and the proton sponge hypothesis. J Gene Med 7:657–63.

American Society for Testing and Materials (ASTM). 1998. Standard guide for conducting the Frog Embryo Teratogenesis Assay-Xenopus (FETAX) E-1439–E1498.

Asharani PV, Lian Wu Y, Gong Z, Valiyaveettil S. 2008. Toxicity of silver nanoparticles in zebrafish models. Nanotechnology 19:255102

Austin CA, Hinkley GK, Mishra AR, Zhang Q, Umbreit TH, Betz MW, et al. 2016. Distribution and accumulation of 10 nm silver nano-particles in maternal tissues and visceral yolk sac of pregnant mice, and a potential effect on embryo growth. Nanotoxicology 10:654–61.

Bacchetta R, Moschini E, Santo N, Fascio U, Del Giacco L, Freddi S, et al. 2014. Evidence and uptake routes for Zinc oxide nanoparticles through the gastrointestinal barrier in *Xenopus laevis*. Nanotoxicology 8:728–44.

Bacchetta R, Santo N, Fascio U, Moschini E, Freddi S, Chirico G, et al. 2012. Nano-sized CuO, TiO₂ and ZnO affect *Xenopus laevis* development. Nanotoxicology 6:381–98.

Bantle JA, Finch RA, Fort DJ, Stover EL, Hull M, Kumsher-King M, Gaudet-Hull AM. 1999. Phase III interlaboratory study of FETAX. Part 3. FETAX validation using 12 compounds with and without an exogenous metabolic activation system. J Appl Toxicol 19:447–72.

Bar-Ilan O, Albrecht RM, Fako VE, Furgeson DY. 2009. Toxicity assessments of multisized gold and silver nanoparticles in zebrafish embryos. Small 5:1897–910.

Benn TM, Westerhoff P. 2008. Nanoparticle silver released into water from commercially available sock fabrics. Environ Sci Technol 42:4133–9.

Bondarenko O, Juganson K, Ivask A, Kasemets K, Mortimer M, Kahru A. 2013. Toxicity of Ag, CuO and ZnO nanoparticles to selected environmentally relevant test organisms and mamma-lian cells in vitro: a critical review. Arch Toxicol 87:1181–200.

Bonfanti P, Colombo A, Orsi F, Nizzetto I, Andrioletti M, Bacchetta R, et al. 2004. Comparative teratogenicity of Chlorpyrifos and Malathion on *Xenopus laevis* development. Aquat Toxicol 70:189–200.

Bonfanti P, Moschini E, Saibene M, Bacchetta R, Rettighieri L, Calabri L, et al. 2015. Do nanoparticle physico-chemical proper-ties and developmental exposure window influence nano ZnO embryotoxicity in *Xenopus laevis*? Int J Environ Res Public Health 12:8828–48.

Browning LM, Lee KJ, Nallathamby PD, Xu XH. 2013. Silver nano-particles incite size- and dose-dependent developmental phe-notypes and nanotoxicity in zebrafish embryos. Chem Res Toxicol 26:1503–13.

Caccia M, Sironi L, Collini M, Chirico G, Zanoni I, Granucci F. 2008. Image filtering for two-photon deep imaging of lymphonodes. Eur Biophys J 37:979–87.

Chae JP, Park MS, Hwang YS, Min BH, Kim SH, Lee HS, Park MJ. 2015. Evaluation of developmental toxicity and teratogenicity of diclofenac using Xenopus embryos. Chemosphere 120:52–8.

Cho JG, Kim KT, Ryu TK, Lee J, Kim JE, Kim J, et al. 2013. Stepwise embryonic toxicity of silver nanoparticles on *Oryzias latipes*. Biomed Res Int 2013:494671.

Dawson DA, Bantle JA. 1987. Development of a reconstituted water medium and preliminary validation of the frog embryo teratogenesis assay–Xenopus (FETAX). J Appl Toxicol 7:237–44.

Fabrega J, Luoma SN, Tyler CR, Galloway TS, Lead JR. 2011. Silver nanoparticles: behaviour and effects in the aquatic environ-ment. Environ Int 37:517–31.

Finney DJ. 1971. Statisical logic in the monitoring of reactions to therapeutic drugs. Methods Inf Med 10:237–45.

Fort DJ, Paul RR. 2002. Enhancing the predictive validity of Frog Embryo Teratogenesis Assay–Xenopus (FETAX). J Appl Toxicol 22:185–91.

Geranio L, Heuberger M, Nowack B. 2009. The behavior of silver nanotextiles during washing. Environ Sci Technol 43:8113–18.

Gottschalk F, Sonderer T, Scholz RW, Nowack B. 2009. Modeled environmental concentrations of engineered nanomaterials (TiO₂, ZnO, Ag, CNT, Fullerenes) for different regions. Environ Sci Technol 43:9216–22.

Gottschalk F, Kost E, Nowack B. 2013. Engineered nanomaterials in water and soils: a risk quantification based on probabilistic exposure and effect modeling. Environ Toxicol Chem 32:1278–87.

Groh KJ, Dalkvist T, Piccapietra F, Behra R, Suter MJ, Schirmer K. 2015. Critical influence of chloride ions on silver ion-mediated acute toxicity of silver nanoparticles to zebrafish embryos. Nanotoxicology 9:81–91.

Hadrup N, Lam HR. 2014. Oral toxicity of silver ions, silver nano-particles and colloidal silver-a review. Regul Toxicol Pharmacol 68:1–7.

He X, Aker WG, Fu PP, Hwang H-M. 2015. Toxicity of engineered metal oxide nanomaterials mediated by nano-bio-eco-interac-tions: a review and perspective. Environ Sci Nano 2:564–82.

Ivask A, Elbadawy A, Kaweeteerawat C, Boren D, Fischer H, Ji Z, et al. 2014a. Toxicity mechanisms in *Escherichia coli* vary for silver nanoparticles and differ from ionic silver. ACS Nano 8:374–86.

Ivask A, Juganson K, Bondarenko O, Mortimer M, Aruoja V, Kasemets K, et al. 2014b. Mechanisms of toxic action of Ag, ZnO and CuO nanoparticles to selected ecotoxicological test organisms and mammalian cells in vitro: a comparative review. PLoS One 9:e102108.

Ivask A, Kurvet I, Kasemets K, Blinova I, Aruoja V, Suppi S, et al. 2014c. Size-dependent toxicity of silver nanoparticles to bac-teria, yeast, algae, crustaceans and mammalian cells in vitro. In: A. Quigg, ed. PLoS One. San Francisco, USA.

Jain K, Kesharwani P, Gupta U, Jain NK. 2010. Dendrimer toxicity: let's meet the challenge. Int J Pharm 394:122–42.

Kaegi R, Sinnet B, Zuleeg S, Hagendorfer H, Mueller E, Vonbank R, et al. 2010. Release of silver nanoparticles from outdoor facades. Environ Pollut 158:2900–5.

Kaosaar S, Kahru A, Mantecca P, Kasemets K. 2016. Profiling of the toxicity mechanisms of coated and uncoated silver nanopar-ticles to yeast *Saccharomyces cerevisiae* BY4741 using a set of its 9 single-gene deletion mutants defective in oxidative stress response, cell wall or membrane integrity and endocytosis. Toxicol in Vitro 35:149–62.

Kasemets K, Suppi S, Kunnis-Beres K, Kahru A. 2013. Toxicity of CuO nanoparticles to yeast *Saccharomyces cerevisiae* BY4741 wild-type and its nine isogenic single-gene deletion mutants. Chem Res Toxicol 26:356–67.

Kashiwada S, Ariza ME, Kawaguchi T, Nakagame Y, Jayasinghe BS, Gärtner K, et al. 2012. Silver nanocolloids disrupt medaka embryogenesis through vital gene expressions. Environ Sci Technol 46:6278–87.

Kim J, Kim S, Lee S. 2011. Differentiation of the toxicities of silver nanoparticles and silver ions to the Japanese medaka (*Oryzias latipes*) and the cladoceran Daphnia magna. Nanotoxicology 5:208–14.

Kim S, Ryu DY. 2013. Silver nanoparticle-induced oxidative stress, genotoxicity and apoptosis in cultured cells and animal tissues. J Appl Toxicol 33:78–89.

Le Ouay B, Stellacci F. 2015. Antibacterial activity of silver nanoparticles: a surface science insight. Nano Today 10: 339–54.

Lee KJ, Browning LM, Nallathamby PD, Desai T, Cherukui PK, Xu XHN. 2012. In vivo quantitative study of sized-dependent transport and toxicity of single silver nanoparticles using zebrafish embryos. Chem Res Toxicol 25:1029–46.

Levard C, Mitra S, Yang T, Jew AD, Badireddy AR, Lowry GV, Brown GE Jr. 2013. Effect of chloride on the dissolution rate of silver nanoparticles and toxicity to E. coli. Environ Sci Technol 47:5738–45.

Lubick N. 2008. Nanosilver toxicity: ions, nanoparticles-or both? Environ Sci Technol 42:8617.

Ma H, Williams PL, Diamond SA. 2013. Ecotoxicity of manufactured ZnO nanoparticles-a review. Environ Pollut 172:76–85.

Massarsky A, Dupuis L, Taylor J, Eisa-Beygi S, Strek L, Trudeau VL, Moon TW. 2013. Assessment of nanosilver toxicity during zebrafish (Danio rerio) development. Chemosphere 92:59–66.

Maurer LL, Yang X, Schindler AJ, Taggart RK, Jiang C, Hsu-Kim H, et al. 2016. Intracellular trafficking pathways in silver nanoparticle uptake and toxicity in Caenorhabditis elegans. Nanotoxicology 10:831–5.

Misra SK, Dybowska A, Berhanu D, Luoma SN, Valsami-Jones E. 2012. The complexity of nanoparticle dissolution and its importance in nanotoxicological studies. Sci Total Environ 438:225–32.

Nations S, Wages M, Cañas JE, Maul J, Theodorakis C, Cobb GP. 2011. Acute effects of Fe2O3, TiO2, ZnO and CuO nanomaterials on Xenopus laevis. Chemosphere 83:1053–61.

Navarro E, Piccapietra F, Wagner B, Marconi F, Kaegi R, Odzak N, et al. 2008. Toxicity of silver nanoparticles to Chlamydomonas reinhardtii. Environ Sci Technol 42:8959–64.

Nieuwkoop PD, Faber J. 1956. Normal table of Xenopus laevis (Daudin). Amsterdam: North Holland Publishing Co.

Ong KJ, Zhao X, Thistle ME, Maccormack TJ, Clark RJ, Ma G, et al. 2014. Mechanistic insights into the effect of nanoparticles on zebrafish hatch. Nanotoxicology 8:295–304.

Osborne OJ, Johnston BD, Moger J, Balousha M, Lead JR, Kudoh T, Tyler CR. 2013. Effects of particle size and coating on nanoscale Ag and TiO(2) exposure in zebrafish (Danio rerio) embryos. Nanotoxicology 7:1315–24.

Osborne OJ, Lin S, Chang CH, Ji Z, Yu X, Wang X, et al. 2015. Organ-specific and size-dependent Ag nanoparticle toxicity in gills and intestines of adult Zebrafish. ACS Nano 9:9573–84.

Pietroiusti A, Campagnolo L, Fadeel B. 2013. Interactions of engineered nanoparticles with organs protected by internal biological barriers. Small 9:1557–72.

Powers CM, Levin ED, Seidler FJ, Slotkin TA. 2011. Silver exposure in developing zebrafish produces persistent synaptic and behavioral changes. Neurotoxicol Teratol 33:329–32.

Sabella S, Carney RP, Brunetti V, Malvindi MA, Al-Juffali N, Vecchio G, et al. 2014. A general mechanism for intracellular toxicity of metal-containing nanoparticles. Nanoscale 6:7052–61.

Santo N, Fascio U, Torres F, Guazzoni N, Tremolada P, Bettinetti R, et al. 2014. Toxic effects and ultrastructural damages to Daphnia magna of two differently sized ZnO nanoparticles: does size matter? Water Res 53:339–50.

Scown TM, Santos EM, Johnston BD, Gaiser B, Baalousha M, Mitov S, et al. 2010. Effects of aqueous exposure to silver nanoparticles of different sizes in rainbow trout. Toxicol Sci 115:521–34.

Singh RP, Ramarao P. 2012. Cellular uptake, intracellular trafficking and cytotoxicity of silver nanoparticles. Toxicol Lett 213:249–59.

Tejamaya M, Romer I, Merrifield RC, Lead JR. 2012. Stability of citrate, PVP, and PEG coated silver nanoparticles in ecotoxicology media. Environ Sci Technol 46:7011–17.

Tolaymat TM, El Badawy AM, Genaidy A, Scheckel KG, Luxton TP, Suidan M. 2010. An evidence-based environmental perspective of manufactured silver nanoparticle in syntheses and applications: a systematic review and critical appraisal of peer-reviewed scientific papers. Sci Total Environ 408:999–1006.

Van Aerle R, Lange A, Moorhouse A, Paszkiewicz K, Ball K, Johnston BD, et al. 2013. Molecular mechanisms of toxicity of silver nanoparticles in zebrafish embryos. Environ Sci Technol 47:8005–14.

Vance ME, Kuiken T, Vejerano EP, Mcginnis SP, Hochella MF, Rejeski D, Hull MS. 2015. Nanotechnology in the real world: redeveloping the nanomaterial consumer products inventory. Beilstein J Nanotechnol 6:1769–80.

Volker C, Kampken I, Boedicker C, Oehlmann J, Oetken M. 2015. Toxicity of silver nanoparticles and ionic silver: comparison of adverse effects and potential toxicity mechanisms in the freshwater clam Sphaerium corneum. Nanotoxicology 9:677–85.

Williams JR, Rayburn JR, Cline GR, Sauterer R, Friedman M. 2015. Effect of allyl isothiocyanate on developmental toxicity in exposed Xenopus laevis embryos. Toxicol Rep 2:222–7.

Xiao Y, Vijver MG, Chen G, Peijnenburg WJ. 2015. Toxicity and accumulation of Cu and ZnO nanoparticles in Daphnia magna. Environ Sci Technol 49:4657–64.

Xiu ZM, Zhang QB, Puppala HL, Colvin VL, Alvarez PJ. 2012. Negligible particle-specific antibacterial activity of silver nanoparticles. Nano Lett 12:4271–5.

Yang X, Gondikas AP, Marinakos SM, Auffan M, Liu J, Hsu-Kim H, Meyer JN. 2012. Mechanism of silver nanoparticle toxicity is dependent on dissolved silver and surface coating in Caenorhabditis elegans. Environ Sci Technol 46:1119–27.

Zhao CM, Wang WX. 2012. Importance of surface coatings and soluble silver in silver nanoparticles toxicity to Daphnia magna. Nanotoxicology 6:361–70.

Zook JM, Long SE, Cleveland D, Geronimo CL, Maccuspie RI. 2011. Measuring silver nanoparticle dissolution in complex biological and environmental matrices using UV-visible absorbance. Anal Bioanal Chem 401:1993–2002.

A glyphosate micro-emulsion formulation displays teratogenicity in *Xenopus laevis*

Patrizia Bonfanti[a,*], M. Saibene[a], R. Bacchetta[b], P. Mantecca[a], A. Colombo[a]

[a] Department of Earth and Environmental Sciences, Research Centre POLARIS, University of Milano-Bicocca, 1, Piazza della Scienza, 20126 Milan, Italy
[b] Department of Environmental Science and Policy, University of Milan, 26, Via Celoria, 20133 Milan, Italy

ARTICLE INFO

ABSTRACT

Glyphosate is the active ingredient in broad-spectrum herbicide formulations used in agriculture, domestic area and aquatic weed control worldwide. Its market is growing steadily concurrently with the cultivation of gly-phosate-tolerant transgenic crops and emergence of weeds less sensitive to glyphosate. Ephemeral and lentic waters near to agricultural lands, representing favorite habitats for amphibian reproduction and early life-stage development, may thus be contaminated by glyphosate based herbicides (GBHs) residues. Previous studies on larval anuran species highlighted increased mortality and growth effects after exposure to different GBHs in comparison to glyphosate itself, mainly because of the surfactants such as polyethoxylated tallow amine present in the formulations.

Nevertheless, these conclusions are not completely fulfilled when the early development, characterized by primary organogenesis events, is considered.

In this study, we compare the embryotoxicity of Roundup® Power 2.0, a new GBH formulation currently authorized in Italy, with that of technical grade glyphosate using the Frog Embryo Teratogenesis Assay–*Xenopus* (FETAX). Our results evidenced that glyphosate was not embryolethal and only at the highest concentration (50 mg a.e./L) caused edemas. Conversely, Roundup® Power 2.0 exhibited a 96 h LC50 of 24.78 mg a.e./L and a 96 h EC50 of 7.8 mg a.e./L. A Teratogenic Index of 3.4 was derived, pointing out the high teratogenic potential of the Roundup® Power 2.0.

Specific concentration-dependent abnormal phenotypes, such as craniofacial alterations, microphthalmia, narrow eyes and forebrain regionalization defects were evidenced by gross malformation screening and histo-pathological analysis. These phenotypes are coherent with those evidenced in *Xenopus laevis* embryos injected with glyphosate, allowing us to hypothesize that the teratogenicity observed for Roundup® Power 2.0 may be related to the improved efficacy in delivering glyphosate to cells, guaranteed by the specific surfactant for-mulation. In conclusion, the differences in GBH formulations should be carefully considered by the authorities, since sub-lethal and/or long-term effects (e.g. teratogenicity) can be significantly modulated by the active in-gredient salt type and concentration of the adjuvants. Finally, the mechanistic toxicity of glyphosate and GBHs are worthy of further research.

1. Introduction

Pesticide contamination of surface and groundwater is well documented worldwide and constitutes a major issue that gives rise to concerns from local to global scale. Due to their direct application on the soil, pesticides or some of their residues may reach the aquatic environment through direct run-off and leaching.

According to the 2016 Italian National report by ISPRA (ISPRA, 2016) 21.3% of the surface waters monitoring points have pesticide concentrations beyond the Environmental Standard Quality limits.

Herbicides including glyphosate and its metabolite AMPA exceed these limits in the 25.2% and 52.2% of the monitored sites respectively. European Glyphosate Environmental Information Sources (EGEIS, 1993–2009) have documented a similar glyphosate contamination across the whole European Union. Such a widespread contamination derives from the fact that glyphosate is the active ingredient of a high number of different broad spectrum herbicides. The applications of these Glyphosate Based Herbicides (GBHs) are measured in gross ton-nage mainly during cultivation of genetically modified plants (i.e. soybean, canola, sugarbeet and cotton), engineered to tolerate

glyphosate (Saunders and Pezeshki, 2015; Duke and Powles, 2008; Cerdeira and Duke, 2006). Although glyphosate has a short half-life (2–14 days) and high affinity for soil particles, background concentrations between 10 and 40.8 μg acid equivalents (a.e.)/L are nonetheless detectable in surface waters (Battaglin et al., 2009; Byer et al., 2008; Struger et al., 2008). Peruzzo et al. (2008) detected glyphosate concentrations ranging from 0.1 to 0.7 mg/L in Pampean rivers near to transgenic soybean cultivation areas and Edwards et al. (1980) found a concentration of 5.2 mg/L in watershed samples in a runoff study. This level of contamination could be reached temporarily in ephemeral and lentic waters, where contaminants may accumulate without substantial dilution. The presence of high concentrations of herbicides in these habitats, that are favorite by amphibians for their breeding and early life-stage development, has been pointed to be one of the causes of the global amphibian decline (Collins, 2010).

The many GBH formulations differ each other for the content of active ingredient, the form of G salt, the identity and concentration of the surfactant. Glyphosate targets 5-enolpyruvylshikimate-3-phosphate synthase enzyme, which is involved in the metabolism of aromatic amino acids in plants and some microorganisms (Rubin et al., 1982). Since this biochemical pathway does not exist in Vertebrates, glyphosate is generally considered low toxic to non-target organisms (Williams et al., 2012). Indeed, the extensive literature on glyphosate and GBH comparative toxicity points out detrimental effects only of GBHs on freshwater organisms such as microbial communities and planktonic algae (Bonnet et al., 2007; Pérez et al., 2011) as well as fish (Modesto and Martinez, 2010; Glusczak et al., 2011; Hued et al., 2012; Menezes et al., 2011) and most notably amphibians (Relyea, 2005; Govindarajulu, 2008; Mann et al., 2009). In particular, different GBHs formulations (i.e. Roundup® Original, WeatherMax, Ultramax, Transorb, Biactive) previously studied on various amphibian species highlighted mortality or growth effects during larval development in comparison to the sole active ingredient (Mann and Bidwell, 1999; Edginton et al., 2004; Howe et al., 2004; Relyea and Jones, 2009; Williams and Semlitsch, 2010; Fuentes et al., 2011). This discrepancy has been attributed mainly to the presence of surfactants in GBH formulations, which are supposed to be key factors in toxicity also in other aquatic organisms (Folmar et al., 1979; Giesy et al., 2000; Tsui and Chu, 2003). Glyphosate formulations containing polyethoxylated tallow amine (POEA) are generally more toxics to amphibian larvae than other formulations making use of other surfactants from the alkoxylated alkyl amine family (Howe et al., 2004; Relyea, 2005; Govindarajulu, 2008; Fuentes et al., 2011; Lajmanovich et al., 2011).

Nevertheless, these conclusions are not completely fulfilled when the early development is considered. Perkins et al. (2000) using the Frog Embryo Teratogenesis Assay–*Xenopus* (FETAX) test evaluated the toxicity of two glyphosate formulations (Roundup® and Rodeo®), both containing glyphosate isopropylamine (IPA) salt and the surfactant POEA only in Roundup®. They concluded that formulation with POEA was embryolethal with a 96 h LC50 of 9.3 mg a.e./L and that this toxicity was attributable to the surfactant, since Rodeo® was toxic only at very high concentrations (96 h LC50 7.29 gr a.e./L). Surprisingly no increment of malformations was observed in embryos exposed to sublethal concentrations of GBHs and POEA itself. A subsequent investigation performed in *X. laevis* embryos by Paganelli et al. (2010), evidenced that sublethal doses of Roundup® Classic (corresponding to 72 mg a.e/L) caused malformations at tadpole stages, such as shortening of the trunk, cephalic reduction, microphthalmy, cyclopia, and craniofacial malformations. Paganelli observed the same phenotypes also in embryos injected with glyphosate alone, suggesting that glyphosate itself was able to induce specific malformations, some of these referable to the alteration of the retinoic acid signaling pathway. These results undermine the idea of a safe glyphosate, although its toxicity was only evinced in the presence of the surfactant. In a more recent study, also Wagner et al. (2016) describe effects of another GBH formulation, Roundup® UltraMax, on *Xenopus* viscerocranial skeleton

development with a 96 h EC50 of 37.35 mg active ingredient/L (corresponding to 27.64 mg a.e./L: conversion factor for glyphosate IPA salt 0.74, Giesy et al., 2000). This glyphosate formulation contains glyphosate IPA salt and an ether amine ethoxylate as surfactant.

Since a large number of studies indicates that differences in toxicity between different formulations of Roundup® may be largely attributable to the type of surfactant, there is a need to extend the investigations to new generation GBHs containing novel surfactants, especially during embryonic development.

In this study, we compare the embryotoxicity of Roundup® Power 2.0 (RU-PW) (Monsanto Italia S.p.A.), a relatively new GBH formulation, with that of technical grade glyphosate. RU-PW is a mixture of glyphosate in form of potassium salt, smaller than IPA salt and then characterized by a rapid assimilation, and an ethoxylated ether alkyl ammine described as an effective surfactant with high affinity for the cuticle waxes. The embryotoxicity was assessed using FETAX (ASTM, 1998), a standardized approach to screen teratogenic potential of environmental contaminants during early developmental stages and organogenesis of *Xenopus laevis* (Bantle et al., 1999; Bonfanti et al., 2004; Bonfanti et al., 2015; Williams et al., 2015; Colombo et al., 2017).

In addition to the median lethal concentration (LC50), we wanted to extrapolate the median concentration inducing malformations (EC50) and the teratogenicity index (TI), these latter poorly investigated previously, but imperative for assessing the risk in non-target species. Moreover, we performed a histological analysis on embryos at the end of the test, comparing the possible pathological fields with those from controls.

2. Materials and methods

2.1. Chemicals

All analytical-grade reagents, human chorionic gonadotropin (HCG), 3-amino-benzoic acid ethyl ester (MS222), salts for FETAX solution, technical grade *N*-(Phosphonomethyl)glycine (Glyphosate CAS Number: 1071-83-6), were purchased from Sigma-Aldrich S.r.l., Italy. The commercial formulation of glyphosate considered in this study was Roundup® Power 2.0 (Monsanto Italia S.P.A., commercially purchased), indicated in this work as RU-PW. RU-PW has been approved for 5 years in Italy (3/20/2013 to 12/31/2017) and was formulated with a guarantee of 360 g glyphosate acid equivalent (a.e.) per liter present as the potassium salt (CAS RN 70901-12-1). Six percent by volume of the RU-PW formulation consisted of ethoxylated ether alkyl ammine (CAS RN 68478-96-6) and 58.5% water and other ingredients not specified by the producer.

2.2. Roundup® Power 2.0 solutions

To evaluate the emulsion properties of RU-PW, the hydrodynamic diameter of the commercial formulation (without dilution) was measured by a Zetasizer Nano ZS (Malvern Instrument, UK) with prior shaking. DLS analysis revealed that RU-PW is characterized by microemulsion made of micelles of about 4 μm in diameter (for results see Supplementary materials S1).

Primary stock solution of RU-PW was prepared at nominal concentration of 100 mg/L, calculated as nominal concentrations of a.e. glyphosate, using FETAX solution and subsequently stirred for 15 min. The control FETAX solution composition in mg/L was NaCl 625, NaHCO3 96, KCl 30, CaCl2 15, CaSO4-2H2O 60, and MgSO4 70, pH 7.5–8.5 (Dawson and Bantle, 1987).

2.3. Animals

Adult *X. laevis* were purchased from Centre de Ressources Biologiques *Xénopes* (Université de Rennes 1, Rennes Cedex), housed in aquariums with dechlorinated tap water at a 22 ± 2 °C and alternating

12-h light/dark cycles. The animals were fed a semi-synthetic diet (Mucedola S.r.L., Settimo Milanese, Italy) three times a week.

2.4. Frog Embryo Teratogenesis Assay-Xenopus (FETAX)

Embryotoxicity tests were conducted according to the standard guide for the Frog Embryo Teratogenesis Assay –*Xenopus* (FETAX) (ASTM, 1998) with minor modification.

2.4.1. Breeding and embryo collection

Embryos were obtained as previously described (Bonfanti et al., 2015). Briefly, to obtain natural breeding, pairs of adult *X. laevis* previously injected with HCG into the dorsal lymph sac (females: 300 IU; males: 150 IU), were placed in false-bottom breeding tanks filled with well-aerated FETAX solution. Amplexus normally ensued within 2–6 h, and the egg fertilization occurred from 9 to 12 h after injection. After breeding, adults were removed, embryos collected and the jelly coat was removed by swirling the embryos for 1–2 min in a 2.25% L-cysteine solution (pH 8.1).

2.4.2. Treatment groups

An initial range finding test has been set up for RU-PW in the range of 1–100 mg a.e./L to identify the best approximation of the 96 h LC50 and EC50 for definitive testing. In order to compare the embryotoxic effects of RU-PW and pure glyphosate, at least three replicate definitive tests in the same experimental conditions were performed. Each test was conducted using embryos from a different male/female pair of *X. laevis* (n = 4 for RU-PW, in this case the additional test was performed for control and concentrations of 5, 7.5 and 20 mg a.e./L, and n = 3 for glyphosate). Normally-cleaved embryos at the midblastula stage (Stage 8), 5 h post-fertilization (hpf) (Nieuwkoop and Faber, 1956), were selected for testing and groups of 25 embryos from each male/female pair were randomly placed in covered 6.0 cm Petri dishes containing 10 mL of control or test solution. Three replicate dishes were used for each test concentration (RU-PW 1–25 mg a.e./L and pure glyphosate 7.5–50 mg/L freshly prepared in FETAX solution), while for control group four replicate dishes were used.

Control (not exposed) embryos were incubated in standard FETAX medium. Since the acidic nature of glyphosate changed pH value of the FETAX solution at the highest RU-PW concentration tested (100 mg a.e./L), a group of embryos was exposed to FETAX solution adjusted to the lowest pH measured (pH 6.8) with addition of HCl.

All of the Petri dishes were incubated in a thermostatic chamber at 23 ± 0.5 °C until the end of the test (96 hpf). Exposure solutions were changed daily, and dead embryos were recorded and removed.

2.4.3. Data collection and statistical analysis

At the end of the assay, surviving embryos of each experimental group were anaesthetized with MS-222 at 100 mg/L and screened for single morphological abnormalities by examining each embryo under a dissecting microscope (Zeiss, Germany). Surviving normal embryos were formalin fixed to estimate the growth retardation by measuring head–tail length with the digitizing software AxioVision.

The data were tested for homogeneity and normality. When these assumptions were met, one-way analysis of variance (ANOVA) was performed; otherwise, the non-parametric Kruskal–Wallis test was applied. The significance level was set at $p < 0.05$. The incidence of specific malformations was investigated by chi-square method, using Yates's correction for continuity ($\chi 2$ test) or Fisher's exact tests (FE test). Mortality and malformation percentages were used to calculate the 96 h LC50 (concentration causing 50% lethality) and 96 h EC50 (concentration inducing teratogenesis in 50% of surviving embryos) for each experimental group. These values were obtained following the elaboration of the lethality and malformation percentages by the Probit analysis (Finney, 1971), using the U.S. EPA Probit Analysis Program, Version 1.5. The Teratogenic Index (TI), useful in estimating the

teratogenic risk associated with the tested compounds, is represented by the LC_{50}/EC_{50} ratio (ASTM, 1998).

2.5. Morphological analysis of stage 46 embryos

2.5.1. Whole mount cartilage staining

To clearly observe the cartilage structures, randomly selected stage 46 control and treated embryos (n = 15 for each experimental group) were fixed in 10% buffered formalin overnight at room temperature, bleached and stained overnight with Alcian Blue 8GX and then cleared in a mixture of benzyl alcohol:ethanol 70%:glycerine (1:2:2). The cartilage has resulted stained in blue while skin and the other embryo tissues have become almost transparent. Each embryo was examined under a dissecting microscope (Zeiss, Germany) equipped with digitizing software AxioVision.

2.5.2. Histopathological analysis

For light microscopy analyses, stage 46 embryos (n = 15 for each experimental group) were randomly selected, fixed in Bouin's solution and processed for paraffin embedding. The samples were transversely cut from eye to proctodeum into serial sections 6 μm thick, then mounted on glass slides and stained with hematoxylin and eosin (H&E). The sections were finally examined by a Zeiss Axioplan light microscope, equipped with an Axiocam MRc5 digital camera. Ten specimens for each experimental group were histologically screened.

3. Results

3.1. Comparative embryotoxicity of Roundup® Power 2.0 and glyphosate

In the initial range finding test, we found that exposure to 100, 50 and 30 mg a.e./L of RU-PW affected severely the survival rates during FETAX test, causing the death of 100% of the embryos within 24, 48 and 72 hpf respectively (Fig. 1). At the concentration of RU-PW 25 mg a.e./L, the mortality occurred significantly only at the end of exposure reaching values close to 50%. The calculated 96 hpf LC50 for RU-PW was indeed 24.78 mg a.e./L (Table 1).

Instead, at the end of exposure in the range of concentrations 1–22.5 mg a.e./L the mortality rate stood at values comparable to those of control groups (Fig. 2a). Concurrently, the malformation rate increased in a concentration dependent manner with a sharp trend. The threshold effect appeared at 5 mg a.e./L of RU-PW, and at 20 mg a.e./L, in spite of a low mortality, the malformation rate was 100% (Fig. 2a).

The median 96 h EC50 for RU-PW was 7.28 mg a.e./L and Teratogenic Index (TI) value calculated as the ratio LC50/EC50 was 3.4 (Table 1). According to ASTM guidelines (1998), TI values greater than 1.5 indicate increasing developmental hazard and TI values greater than 3.0 indicate concern. Since TI value for RU-PW is greater than 3, we can attribute to this compound a high teratogenic hazard.

In contrast to the formulation of RU-PW, glyphosate did not result embryolethal at any of the concentrations tested and a significant increase in the incidence of malformations was recorded only at 50 mg/L (Fig. 2b). Comparing the malformation incidence between RU-PW and glyphosate, we observed that the rate of malformed embryos exposed to glyphosate 50 mg/L (17.78%) is comparable to the rate recorded in embryos exposed to a concentration 10 times lower of RU-PW (15.28%). Since glyphosate was not embryolethal and was only slightly teratogenic in the range of concentrations tested, it was not possible to calculate LC50 and EC50 values (Table 1).

As last FETAX endpoint, we measured the head-tail length of embryos. Significant growth inhibition was observed after exposure to RU-PW starting from 5 mg a.e./L compared to the unexposed control group (Fig. 3). No significant reduction in length was observed in embryos exposed to glyphosate (data not shown).
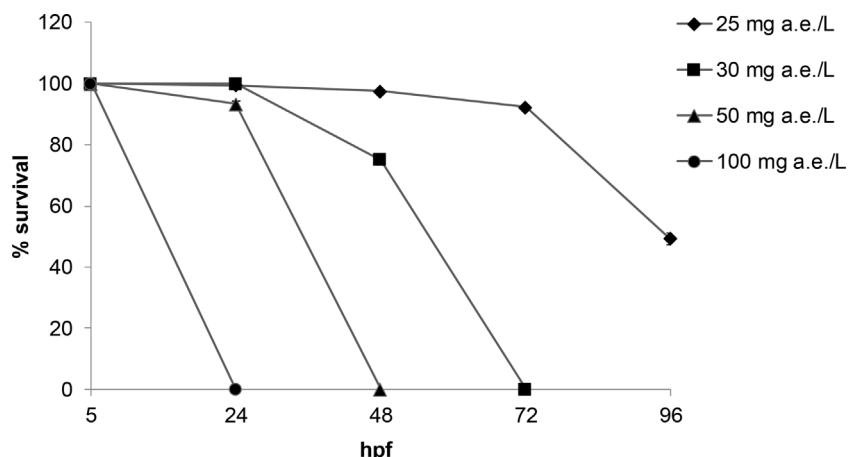
Table 1
Comparative toxicity of Roundup® Power 2.0 and pure glyphosate in 96 hpf *Xenopus laevis* embryos during FETAX.

Treatment	LC$_{50}$ [a]	EC$_{50}$ [b]	TI [c]
Roundup	24.78	7.8	3.4
	(24.54–25.04)	(4.24–8.62)	
Glyphosate	n.d.	n.d.	n.d.

LC$_{50}$ and EC$_{50}$ were determined by US EPA Probit Analysis Program (version 1.5, with 95% confidence interval in parenthesis) and are expressed on an acid equivalent basis in mg/L.

[a] LC$_{50}$ = Median lethal concentration.
[b] EC$_{50}$ = Median teratogenic concentration.
[c] TI = Teratogenic index (LC$_{50}$/EC$_{50}$).

3.2. Morphological analysis of stage 46 embryos

3.2.1. Gross malformations

In order to describe malformations related to RU-PW and glyphosate exposure, stage 46 embryos were observed at the dissection microscope and each malformation quantitatively scored on a standard score sheet and tallied according to the ASTM International Guide (ASTM, 1998). Only the recurrent and not those sporadic malformations were reported in Table 2. In comparison to the normal morphology observed in control embryos, the multiple malformations registered in RU-PW exposed embryos appear in a concentration dependent manner starting from 1 mg a.e./L where gut miscoiling and cardiac edema had a significant incidence (Table 2a). Miscoiling of the gut included different degrees of deviation from the normal arrangement in a spiral pattern of the gastrointestinal tract, which ranged from a looser coiled or few looped to a sigmoid or an almost straight tube. Cardiac edema appeared as swollen

fluid filled area in the cardiac region. On the contrary, in glyphosate exposed embryos, the only malformation resulted to be statistically significant was the cardiac edema at 30 and 50 mg/L (Table 2b).

Starting from RU-PW 5 mg a.e./L, the most common induced phenotypes included, besides the uncorrected gut coiling and cardiac edema, facial and abdominal edemas, craniofacial anomalies such as small, narrowed and flattened head with rounded brow and prominent oral sucker, and eyes defects such as oval shape, monolateral or bilateral microphthalmia and narrowing (Table 2a; Fig. 4). The large edemas that characterize the embryos exposed to RU-PW 7.5 and 10 mg a.e./L were reduced at the higher concentrations leaving the place to epidermal blisters (Fig. 4).

The craniofacial anomalies consisted mainly in a size concentration dependent reduction of head region, accompanied by a decrease of the distance between eyes and by a truncation of the anterior dorsal part (Figs. 4 and 5).

Paying attention to the brain, the loss of delineated structures in the forebrain was observed in embryos exposed to RU-PW 20 mg a.e./L where the telencephalon with olfactory bulbs and diencephalon, clearly visible in control embryos, were indistinguishable (Fig. 5, lower panel). Moreover, in lateral views, treated embryos showed an abnormal sliding and folding of the forebrain toward the rostral region in comparison to the control. Likewise, the eyes were located in a more dorsal and rostral region. In contrast, midbrain and hindbrain seemed to remain fairly delineated also in RU-PW embryos. This altered phenotype is well evident in the histological sections (Fig. 7).

3.2.2. Whole mount cartilage staining

To better characterize the anomalies of the cephalic region, the cartilages were stained with Alcian blue (Fig. 6).
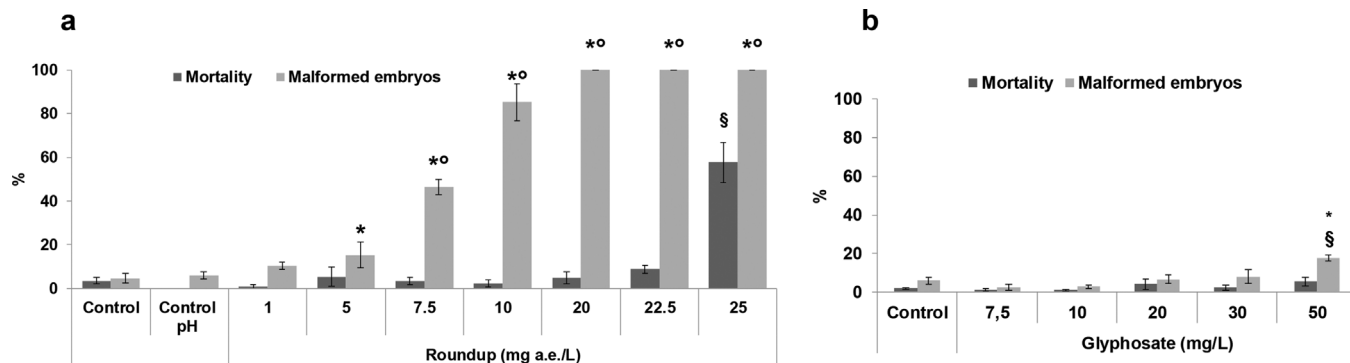

Fig. 2. Comparative embryotoxicity of Roundup® Power 2.0 and glyphosate, evaluated by FETAX. Mortality and malformation rates in 96 hpf embryos after exposure to RU-PW 1–25 mg a.e./L (a) and 7.5–50 mg/L glyphosate (b). Control pH group was exposed to FETAX solution with the pH adjusted to 6.8 value (see materials and methods). All values are given as mean ± SE of three independent assays. (*) statistically different from control, (°) malformation and (§) mortality rates statistically different from those registered at the lower concentrations. ($p < 0.01$, ANOVA + Fisher LSD Method).
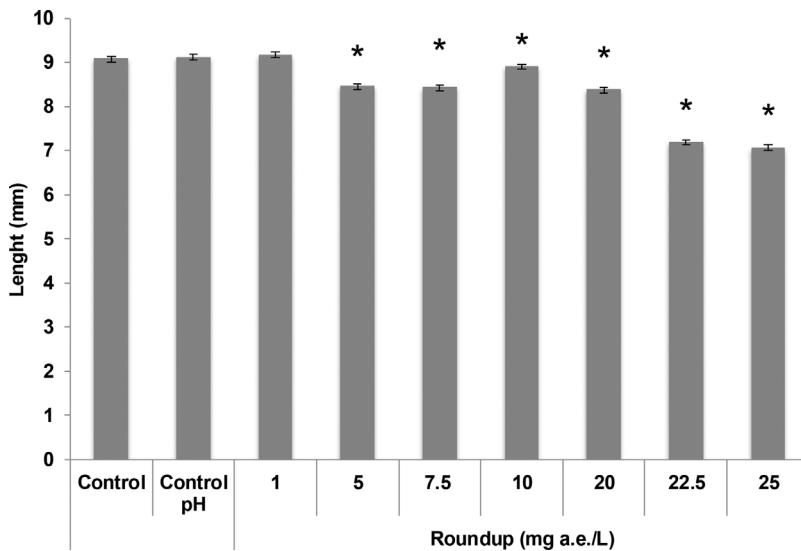
Fig. 3. Head-tail length of stage 46 embryos. Error bar represents ± SE of the mean length of embryos at the end of Roundup® Power 2.0 FETAX experiments. (*) indicates significant differences compared with controls (*p* < *0.01*, ANOVA + Fisher LSD Method).

The analysis at the dissection microscope of control embryos showed the organization of the cartilaginous elements derived from cranial neural crest cells that, after detachment from mid-hindbrain region of neural tube, have colonized the branchial arches (Fig. 6). In particular, Meckel's and palatoquadrate cartilages, constituting the lower and upper jaw elements respectively, are evident as well as ceratohyal cartilages and gill basket (Fig. 6, upper panel). Moreover, the ethmoid-trabecular cartilage and the cartilage supporting the otic vesicles are visible in lateral view (Fig. 6, lower panel). RU-PW treatment interferes with development of cranial cartilage structures in concentration dependent manner, up to almost complete disappearance of upper and lower jaws in embryos exposed to 20 mg a.e./L. Only some sketches of ceratohyal remain detectable.

3.2.3. Histopathological analysis

In order to supplement the gross morphological observations, serial transverse E&E stained histological sections were performed in 46 stage embryos and examined with a light microscope (Fig. 7).

In control embryos, section passing through olfactory bulbs (Fig. 7, line A) showed the pharynx cavity bordered by cartilaginous structures

Table 2
Pattern of malformations in *Xenopus laevis* embryos exposed to Roundup® Power 2.0 and pure Glyphosate.

a	Control	Control pH 6.8	Roundup® Power 2.0 (mg a.e./L)						
			1	5	7.5	10	20	22.5	25
Total embryos	**521**	**220**	**224**	**300**	**303**	**225**	**304**	**228**	**172**
Living embryos	**503**	**220**	**222**	**283**	**293**	**220**	**289**	**208**	**78**
Severe	3 (0.6)	1 (0.5)	2 (0.9)	2 (0.7)	3 (1.0)	1 (0.5)	4 (1.4)	13 (6.3)*	5 (6.4)*
Gut miscoiling	12 (2.4)	8 (3.6)	17 (7.7)*	27 (9.5)*	98 (33.4)*	153 (69.5)*	262 (90.7)*	195 (93.8)*	73 (93.6)*
Edema Multiple	2 (0.4)		1 (0.5)	2 (0.7)	30 (10.2)*	218 (99.1)*	152 (52.6)*	111 (53.4)*	23 (29.5)*
Cardiac	2 (0.4)	2 (0.9)	6 (2.7)*	1 (0.4)	5 (1.7)	22 (10.0)*	61 (21.1)*	35 (16.8)*	4 (5.2)*
Abdominal	1 (0.2)		3 (1.4)		8 (2.7)*	36 (16.4)*	23 (8.0)*		22 (28.2)*
Facial	2 (0.4)	1 (0.5)	3 (1.4)		15 (5.1)*	18 (8.2)*	4 (1.4)	38 (18.3)*	36 (46.2)*
Blisters							25 (8.7)*	44 (21.2)*	15 (19.2)*
Craniofacial defects	8 (1.6)	6 (2.7)	8 (3.6)	25 (8.8)*	76 (25.9)*	149 (67.7)*	242 (83.7)*	194 (93.3)*	72 (92.3)*
Eye defects	8 (1.6)	2 (0.9)	6 (2.7)	9 (3.2)	36 (12.3)*	81 (36.8)*	263 (91.0)*	195 (93.8)*	61 (78.2)*
Hemorrhage		1 (0.5)			7 (2.4)*	31 (14.1)*	29 (10.0)*	20 (9.6)*	17 (21.8)*

b	Control	Glyphosate (mg/L)				
		7.5	10	20	30	50
Total embryos	**228**	**226**	**226**	**225**	**219**	**225**
Living embryos	**224**	**224**	**224**	**216**	**214**	**213**
Severe					2 (0.89)	
Gut miscoiling	7 (3.13)		2 (0.89)	7 (3.13)	5 (2.23)	7 (3.13)
Edema Multiple	3 (1.34)		1 (0.45)	1 (0.45)		
Cardiac			1 (0.45)	7 (3.13)	9 (4.02)*	32 (14.3)*
Abdominal	1 (0.45)				1 (0.45)	
Facial						1 (0.45)
Blisters	1 (0.45)					1 (0.45)
Craniofacial defects	2 (0.89)		2 (0.89)	1 (0.45)		2 (0.89)
Eye defects	4 (1.78)		2 (0.89)	1 (0.45)		3 (1.4)
Hemorrhage			1 (0.45)			1 (0.45)

Percentages based on number of malformations/number of those living.
Bold was used to differentiate malformation incidence from total number of embryos used and from living embryos.
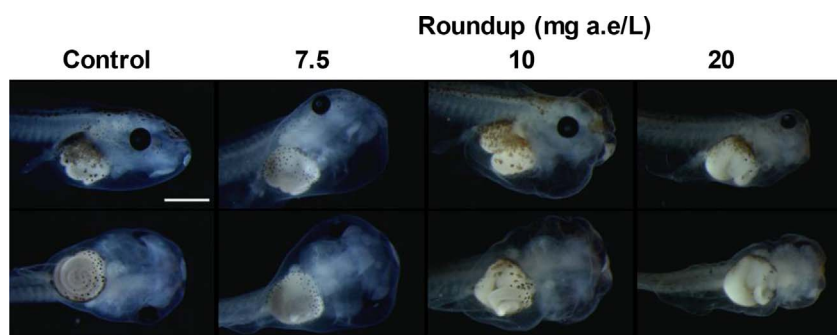 * chi square test: p < 0.001 vs Control.

Fig. 4. Lateral (upper panel) and ventral (lower panel) views of representative *X. laevis* embryos at 96 hpf exposed to Roundup® Power 2.0 (mg a.e./L). In comparison to control phenotype, exposed embryos were severely affected by edemas, gut miscoiling and alteration in shape and size of head structures. Scale bar = 500 μm.
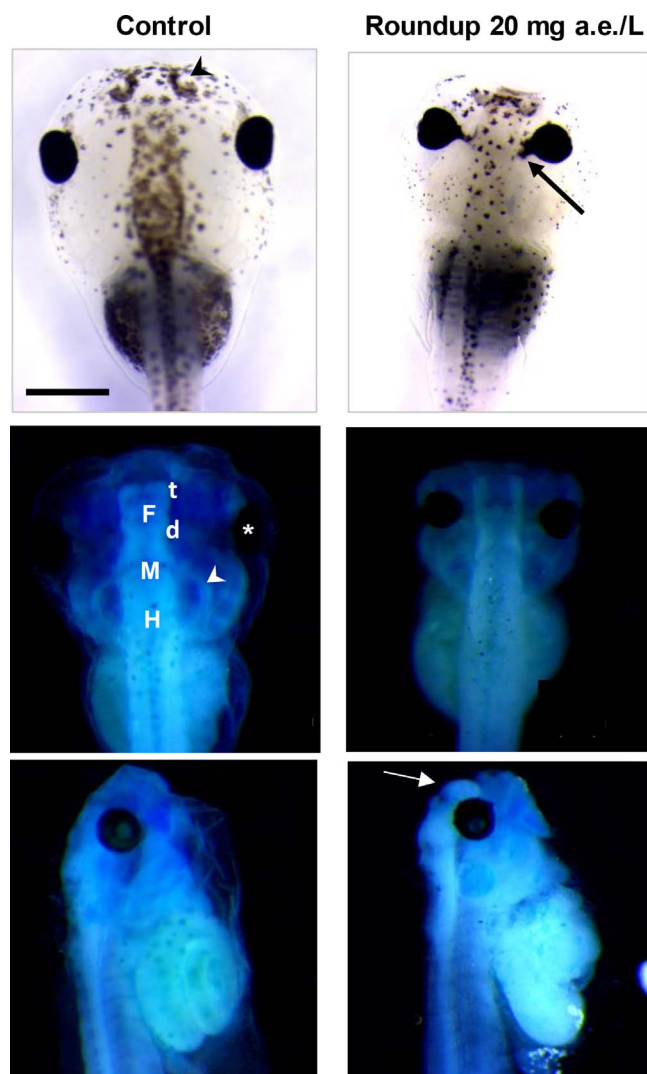

Fig. 5. Representative dorsal (upper, middle panels) and lateral (lower panel) views of cephalic region of *X. laevis* embryos at 96 hpf. Embryos exposed to Roundup® Power 2.0 20 mg a.e./L show eye abnormal phenotype such as microphthalmia and eyes narrowing towards the midline of the body (upper panel). The eyes are located close to the brain and the optic tract is covered by pigment (black arrow, upper panel). In control embryos, a clear delineation of the telencephalic (t) and diencephalic (d) portions of the forebrain (F) as well as the midbrain (M) and hindbrain (H) are evident (middle panel). The treatment seems to prevent the regionalization of the forebrain (telencephalon with olfactory bulbs and diencephalon are indistinguishable, middle panel) and caused its folding and sliding forward (white arrow, lower panel). (*) eye; (white arrowhead) otocyst. Scale bar = 500 μm.

and levator mandibular muscle fibers well organized. In sheer contrast, treated embryos showed a concentration dependent damage of craniofacial cartilages and associated muscles arrangement that culminate

with an unarticulated and reduced mouth opening. Furthermore, the treatment with the highest concentration of RU-PW altered the morphology of the telencephalon, which lacks of the paired olfactory bulbs.

In section passing through eye level (Fig. 7, line B), control embryos showed differentiated eyes characterized by *tapetum nigrum*, retina and crystalline lens well apart from diencephalon. Moreover, the velar plate occupied the pharynx cavity ventrally. In treated embryos, the abovementioned structures were progressively affected showing a range of phenotypes from mild to severe in relation to dose. In particular, the eyes appeared to be modified in shape, close to the neural tube and showed a disorganization of the retina multipolar cell layers at RU-PW 10 and 20 mg a.e./L (Fig. 8).

In section passing through rhombencephalon and otic vesicles (Fig. 7, line C), control embryos were characterized by the notochord and parachordal cartilages and by velar plate that divides the pharynx into two lateral branchial cavities. Ventrally, the three-chambered heart was well evident. In RU-PW treated embryos, velar plate and branchial chamber phenotype were progressively damaged. The treatment did not hinder the formation of the three cardiac chambers, but the atria have appeared more widened and the ventricular myocardial wall seemed thinner and provided by few trabeculae, especially in embryos exposed to 20 mg a.e./L. In addition, the cardiac region of all treated embryos is affected by the presence of edema. Cross-sections of control embryos at abdominal level (Fig. 7, line D) show the appearance of the first intestinal loops and near liver, pancreas and stomach. In the dorsal side, the nothocord, bordered by somitic musculature and the spinal cord are well evident. In embryos exposed to RU-PW 7.5 and 10 mg a.e./L, the abdominal region presents mild changes in organ distribution. More severe injuries are evident in embryos treated with 20 mg a.e./L, where morphology and localization of primitive organs are affected and the intestinal tract is still characterized by abundant vitelline platelets and by almost complete closure. In addition, only few pronephric tubules can be seen and somitic musculature, surrounding notochord and spinal cord, is poorly organized.

4. Discussion

The present study was planned to investigate the response of *X. laevis* embryos to a relatively new formulation of Roundup (Roundup® Power 2.0), currently authorized in Italy (http://www.fitosanitari.salute.gov.it/fitosanitariwsWeb_new/FitosanitariServlet), and for which no toxicological data are available so far.

Since very few data relate to GBHs exposure during early development, the FETAX test was used to follow the early phases of *X. laevis* development, when important morphogenetic movements and primary organogenesis occur. As shown in previous studies, FETAX is a reliable and sensitive test to detect developmental toxicants, in particular pesticides toward which *X. laevis* embryos were often found to be highly sensitive (Bonfanti et al., 2004; Colombo et al., 2005; Di Renzo et al., 2011).

Unlike other Roundup formulations (Roundup® Original, Vision® and Roundup® UltraMax) previously tested in *X. laevis* embryos (Perkins
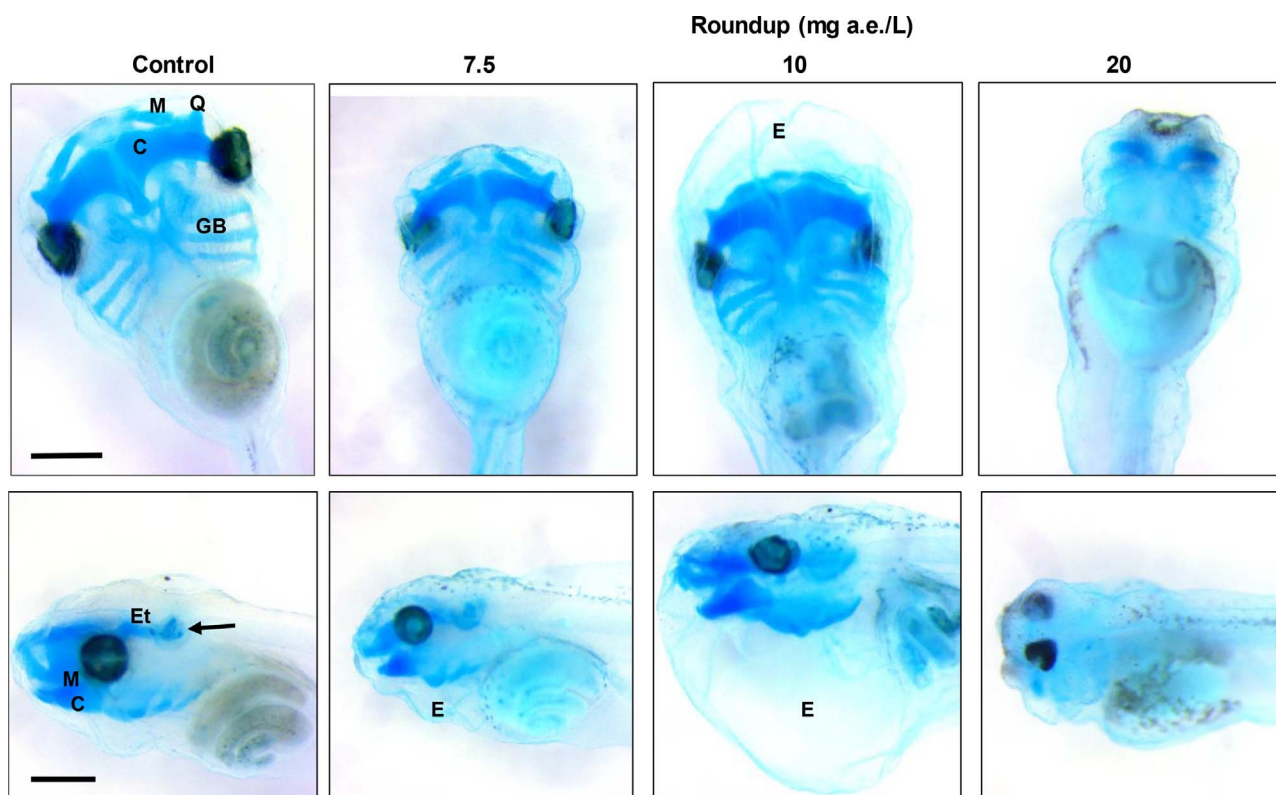
Roundup (mg a.e./L)

Fig. 6. Representative chondrocranial alterations resulting from Roundup treatment of *X. laevis* embryos at 96 hpf. In control embryos, Meckel's (M) and palatoquadrate (Q) cartilages derived from the first branchial arch, the ceratohyal (C) cartilages derived from the second branchial arch and the gill basket (GB) derived from the more posterior arches are well evident (upper panel, ventral view). In lateral view (lower panel), ethmoid-trabecular cartilage (Et) and the cartilage supporting the otic vesicles (arrow) can be observed. In comparison to control, RU-PW treatment caused a progressive reduction until the almost complete disappearance of the cartilaginous elements in embryos exposed to Roundup® Power 2.0 20 mg a.e./L. E = edema. Scale bars 500 μm.

et al., 2000; Edginton et al., 2004; Wagner et al., 2016), RU-PW contains glyphosate potassium salt instead of IPA salt, and a little percentage of a particular ethoxylated ether alkyl amine surfactant, declared as having high affinity with leaf cuticle waxes.

Beside lethality, a high incidence of malformations during early development is an important issue to be considered in amphibian decline because it can impair the success of metamorphosis and increase the natural population losses due to predation, competition and parasitism (Collins, 2010).

The main finding of this study is that RU-PW has a TI of 3.4 and thus is to be classified as highly teratogenic according to the ASTM guide (1998). This is the first time that a teratogenic potential is reported for a GBH, because other formulations tested during embryonic development (i.e. Roundup® Ultramax) were reported to have a TI < 1.5, although concentration dependent increments in malformation rates were evidenced both for *X. laevis* and *Discoglossus pictus* embryos (Wagner et al., 2016).

On the contrary, glyphosate did not show any embryolethality and only at the highest concentration (50 mg a.e./L) embryos showed diffused edemas statistically different from controls. The difference between the toxicity observed with our commercial formulation compared to the glyphosate is in agreement with most studies previously performed in amphibians and other aquatic organisms. In one of the first Roundup® acute toxicity studies performed on four aquatic invertebrate and four fish species, Folmar et al. (1979) had already evidenced that the toxicity of the surfactant POEA was similar to those of Roundup® formulation, while technical grade glyphosate was considerably less toxic. Perkins et al. (2000) confirmed these findings in *X. laevis* embryos, demonstrating that Rodeo®, a commercial surfactant free-formulation, was 575 times less toxic than Roundup® with POEA. Similarly, studies in different anuran larvae established that surfactants

appear to be primary responsible for the acute toxicity of GBH formulations (Mann and Bidwell, 1999; Howe et al., 2004).

Unfortunately, in this work we did not have the chance to test the surfactant toxicity because not commercially available and, to the best of our knowledge, there were not previous toxicity test for a comparison. Nevertheless, based on 96 h LC50 values reported in previous FETAX studies, we can state that RU-PW is not as lethal (96 h LC50 24.78 mg a.e./L) as other GBH formulations for *X. laevis* embryos. In detail, it results less toxic than Roundup® original (96 h LC50 9.3 mg a.e./L) of 2.66 times (Perkins et al., 2000), than Vision (considering 96 h LC50 7.9 mg a.e./L obtained at pH 7.5) of 3.14 (Edginton et al., 2004) and than Roundup® Ultramax (96 h LC50 19.36 mg a.e./L) of 1.3 (Wagner et al., 2016). Assuming that the embryolethality is caused mainly by the surfactant, we can hypothesize that the lower embryotoxicity of RU-PW is due to the type of surfactant added as well as to its lower percentage content (6% by volume versus 15% of POEA in Roundup® Original and Vision® and 7.5 wt% of ether amine ethoxylate in Roundup® Ultramax). However, the amounts of surfactant calculated in all the above-mentioned GBH solutions at the concentrations corresponding to the respective LC50 values are comparable (about 4 μL/L). This indicates that the reduced embryolethality of RU-PW is related to the lower surfactant percentage rather than to the kind of surfactant present in the formulation. At the highest tested concentration (100 mg a.e./L), the embryotoxicity was so severe as to prevent embryonic development already after 24 hpf, likely being the result of alterations in lipid composition and fluidity of cell membranes and subsequent loss of osmotic stability caused by the surfactant (Cardellini and Ometto, 2001).

On the other hand, sublethal RU-PW concentrations induced dose dependent teratogenic effects (96 h EC50 7.8 mg a.e./L) with phenotypes including abnormal gut coiling, craniofacial and eye defects
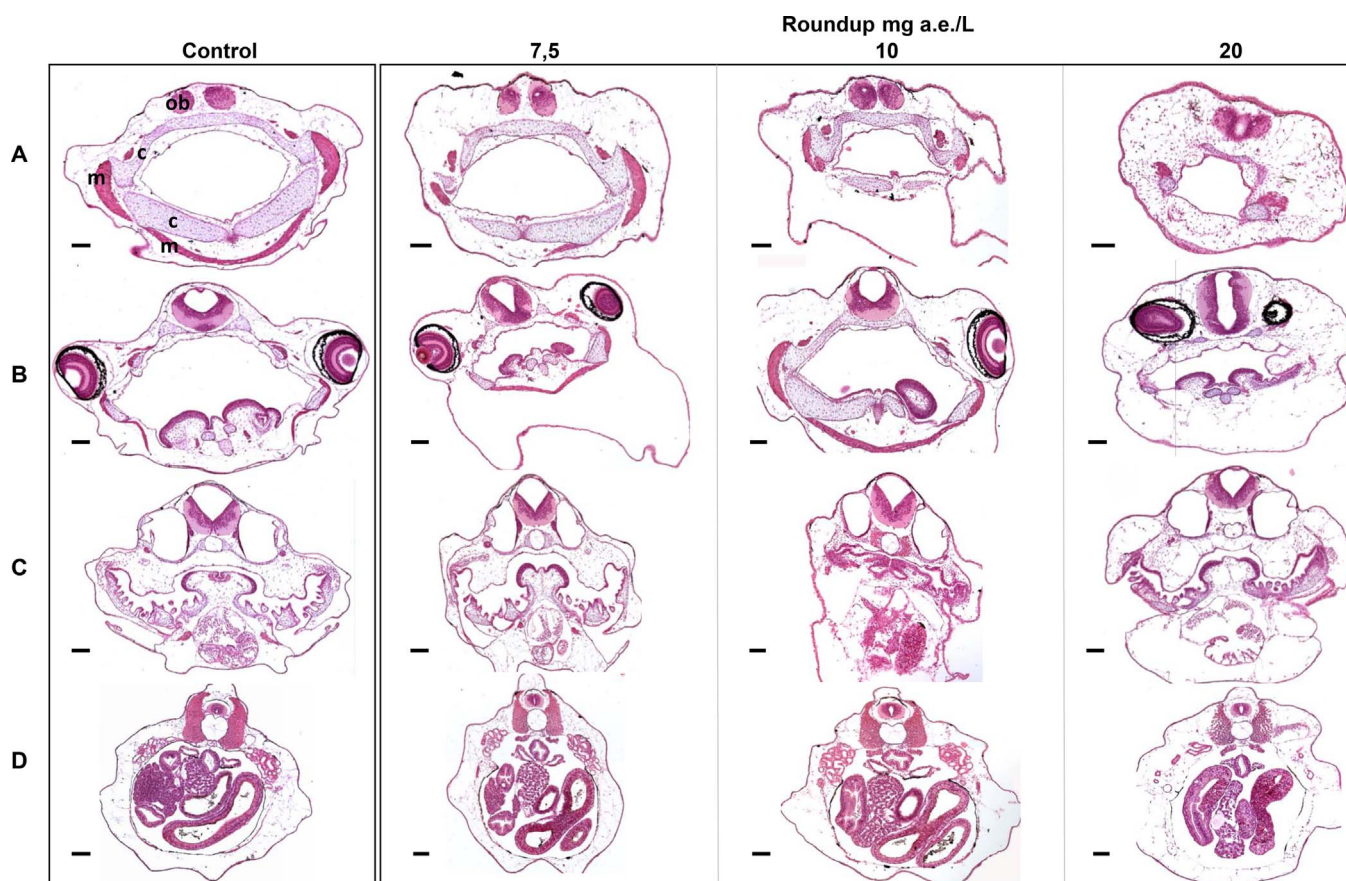
Fig. 7. Histological transversal sections of stage 46 *X. laevis* embryos at level of olfactory bulbs (line A), eyes (line B), rhombencephalon (line C), abdominal region (line D). Note the altered morphology and localization of primitive organs in the treated embryos compared to control. ob = olfactory bulbs; c = cartilage; m = muscle. Scale bar = 100 μm.

starting from 5 mg a.e./L. Moreover, at 10 mg a.e./L cardiac, abdominal and multiple edemas in almost all surviving embryos were detected. While improper gut coiling, edemas and ocular abnormalities (reduced size and oval shape) were previously described as malformations occurring in *X. laevis* embryos exposed to different non-ionic surfactants, which however have a TI < 2.0 (Presutti et al., 1994; Mann and Bidwell, 2000), cephalic and chondrocranial alterations are relevant to GBH exposure during early development (Paganelli et al., 2010; Wagner et al., 2016). Since stage 46 *X. laevis* embryos, developing after injection of pure glyphosate at 2-cell stage, displayed the same phenotypes of GBH exposed embryos, Paganelli et al. (2010) conclude that glyphosate and not the adjuvant could be responsible for the onset of these malformations. In the same paper, they argued that glyphosate itself causes an increase of endogenous retinoic acid activity, consistent with the observed decrease of sonic hedgehog (*shh*) signalling from the

embryonic dorsal midline, especially from the prechordal mesoderm, with the inhibition of *otx2* expression and with the disruption of cephalic neural crest development. The narrowing of the eyes towards the midline of the embryos, the loss of olfactory bulbs and the forebrain regionalization we observed in our samples are similar to the holoprosencephalic syndrome cited by Paganelli, coherent with inhibition of anterior *shh* signalling and reduced *otx2* domain, which impair the brain separation into two hemispheres, the eye field subdivision and the craniofacial development.

In the light of the above discussed, we hypothesize that the RU-PW malformations induced in *X. laevis* embryos can be attributed only minimally to the surfactant, while a significant contribution to the appearance of specific phenotypes is given by the active ingredient glyphosate.

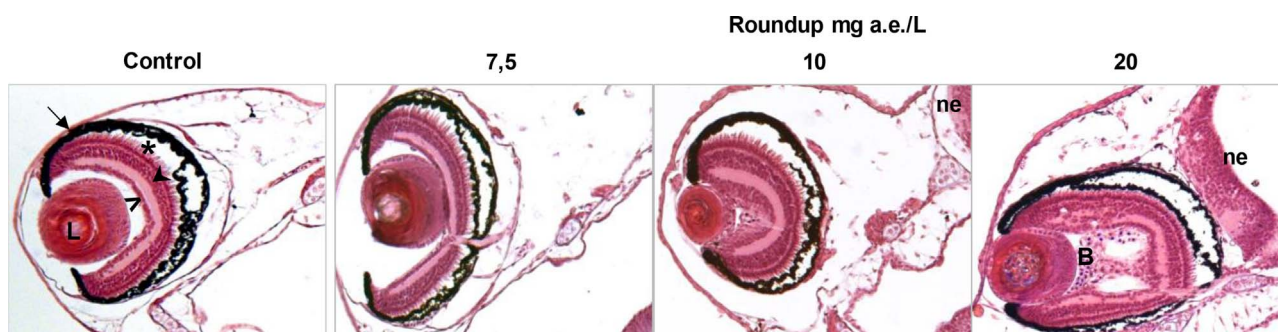Since in our study glyphosate does not display teratogenicity, the

Fig. 8. Representative transverse sections of eyes at higher magnification. In Roundup® Power 2.0 treated embryos, a disorganisation of retina layers is evident at 10 and 20 mg a.e./L, worsened by the presence of haemorrhagic areas (B) in 20 mg a.e./L. Note the closeness of eye to neural epithelium (ne). (→) pigmented layer of the retina; (*) fotoreceptor layer; (◄) bipolar cell layer; (>) multipolar cell layer; (L) lens.

teratogenic potential of RU-PW observed for the first time in formulation with this brand can be related to the typology of its characteristic components. In particular, the smaller size of glyphosate potassium salt associated with a high-affinity adjuvant for cuticle waxes, as highlighted in data sheet, may be the reason for more efficient glyphosate penetration through biological barriers of non-target organisms. This hypothesis is supported by the DLS results which have shown that the RU-PW formulation consists of a micro-emulsion, being constituted by micelles with hydrodynamic diameter of about 4 µm, a feature that facilitates their interaction with cells.

Also a recent zebrafish early development study supports the idea that glyphosate itself is a developmental toxicant, being able to induce cephalic and eye reductions and to exert neurotoxicity with loss of brain ventricle delineation comparable to those of commercial formulation Roundup® classic (Roy et al., 2016a). Moreover, in an additional study Roy et al. (2016b) demonstrated cardiotoxicity of glyphosate in zebrafish embryos, which recalls the malformations to cardiac chambers appreciated in our histological sections of 20 mg a.e./L exposed embryos, evidencing another developmental target of glyphosate.

To the best of our knowledge, the mechanism underlying retinoic acid signalling disruption by glyphosate has not yet been elucidated, although the CYP26 enzyme, essential for the catabolism and homeostasis of retinoic acid during development, is suspected of being a good candidate. In fact, several cytochrome P450 members resulted to be targets of glyphosate. For example, hepatic level of cytochrome P-450 and monooxygenase activities in the rat are decreased by glyphosate (Hietanen et al., 1983). Moreover, activity and mRNA levels of aromatase, a CYP450 that converts testosterone to estrogen, are disrupted by exposure to glyphosate in human cell lines (Richard et al., 2005; Gasnier et al., 2009). In amphibians, a study showed gonadal abnormalities in *Rana pipiens* tadpoles chronically exposed to environmentally relevant concentrations of glyphosate formulations, even if they were related in part to disruption of thyroid hormone signalling (Howe et al., 2004).

In addition to CYP26, it would be interesting to explore if other mechanisms of action of glyphosate and GBH, well documented in amphibian and fish larvae, could contribute to the onset of observed toxic effects on *Xenopus* embryos. As suggested by numerous studies, oxidative stress is one of the mechanisms of glyphosate toxicity (Annett et al., 2014). In different larval anuran species, including *Xenopus*, glyphosate exposure can cause alteration in the activity of antioxidant enzymes such as glutathione S-transferase (GST) and glutathione reductase (Lajmanovich et al., 2011; Güngördü, 2013). The unregulated generation of reactive oxygen species (ROS) derived by the unbalance of antioxidant systems can initiate oxidative damage to nucleic acids, lipids, and proteins compromising cellular integrity and inducing apoptosis. Since apoptosis has a crucial role in a variety of morphogenetic events during development, its increase may compromise normal development. The link between the appearance of malformations and apoptosis caused by ROS abundance was highlighted in zebrafish embryos where glyphosate exposure caused an inhibitory effect of carbonic anhydrase enzyme (Sulukan et al., 2017). Moreover, although glyphosate is not classified as an acetylcholinesterase (AChE) inhibitor, some studies have reported that exposure to GBH causes inhibition of this enzyme activity in aquatic organisms (Lajmanovich et al., 2011; Modesto and Martinez, 2010; Sandrini et al., 2013). On the contrary, glyphosate caused an increase in AChE activity in tadpoles of three different anuran species, of which *Xenopus laevis* resulted the most sensitive (Güngördü, 2013). Since it has been demonstrated that AChE is required for normal muscle and neuron development in fish and amphibians (Behra et al., 2002; Bonfanti et al., 2004), the alteration of its activity may be a contributing factor to the teratogenic effects induced by RU-PW.

Considering that RU-PW has a low embryolethality and a high teratogenic potential in *Xenopus* embryos, it would be important to evaluate its impact on wildlife anuran embryonic development. It has been shown that amphibians have variable sensitivity to GBHs depending on the species and stages of development (Howe et al., 2004; Fuentes et al., 2011). Even if larval stages are more susceptible to GBHs than embryos mainly because of surfactant action on gills epithelia (Wagner et al., 2016), a teratogenic effect during morphogenetic process of embryonic development could lead to larvae unable to eat and to accomplish the delicate phase of metamorphosis, with long-term effects on species survival.

As the 96 h EC 50 value of 7.8 mg a.e./L is much higher than the background values measured in surface water, the RU-PW application does not seem to pose any apparent risk. However, it is important to consider that this value approaches the expected environmental concentrations (EECs) in worst-case scenarios, that as reported by Wagner et al. (2013) can reach up to 7.6 mg active ingredient/L. Considering that, land area treated with GBHs rose rapidly, with the consequent appearance of weed phenotype less sensitive to glyphosate, the rate and the number of applications continue to increase (Benbrook, 2016). Therefore, concentrations as high as EECs could easily be reached in lentic and ephemeral waters close to agricultural areas, where amphibians prefer to breed. Unfortunately, there is a lack of accurate monitoring data on these waters, necessary for an adequate risk assessment (Battaglin et al., 2009). It should also be noted that near the agricultural areas, lentic and ephemeral waters become collectors of pesticide mixtures, which could synergistically affect amphibian development. It has been shown for example that triazole fungicides interfere with RA pathway, causing craniofacial malformations in *Xenopus* embryos similar to those induced by GBHs (Di Renzo et al., 2011).

Another important consideration is that FETAX constitutes an efficient development toxicity alert test, not only to evaluate environmental toxicants for potential effects on amphibian populations, but also to predict human teratogens with a 75% accuracy (Fort and Robbin, 2002). RU-PW teratogenic potential is manifested with specific malformations, which appear recurrent when exposure to different GBHs occurs during amphibian early developmental stages, even though at different concentrations depending on the type of formulation. As mentioned above, the onset of these specific malformations was correlated with the increase of RA, a known morphogen involved in morphogenetic processes common to all Vertebrates (Paganelli et al., 2010). It would be important to expand the knowledge on these mechanistic aspects even during the development of mammals to assess whether or not a risk for human embryo development exists following chronic or accidental exposure during pregnancy. This is even more important since it has been shown that glyphosate can cross the placenta (Poulsen et al., 2009).

5. Conclusion

In the present study, we have characterized for the first time the teratogenic hazard of a commercial GBH. Although not embryolethal, RU-PW induced a dose-dependent increase of craniofacial and eye malformations on *Xenopus* embryos from a concentration of 5 mg a.e./L and marked neural defects at 20 mg a.e./L. In addition, this study has highlighted that slight differences in GBH formulation, in terms of active ingredient and surfactant, can modulate sub-lethal and/or long-term effects (e.g. teratogenicity) and thus should be carefully considered by the authorities. Finally, further research concerning mechanistic toxicity of glyphosate and GBHs are needed.

Acknowledgments

Appendix A. Supplementary data

Supplementary data associated with this article can be found, in the online version, at https://doi.org/10.1016/j.aquatox.2017.12.007.

References

American Society for Testing and Materials (ASTM), 1998. Standard Guide for Conducting the Frog Embryo Teratogenesis Assay-Xenopus (FETAX). pp. E1439–E1498.

Annett, R., Habibi, H.R., Hontela, A., 2014. Impact of glyphosate and glyphosate-based herbicides on the freshwater environment. J. Appl. Toxicol. 34, 458–479. http://dx.doi.org/10.1002/jat.2997.

Bantle, J.A., Finch, R.A., Fort, D.J., Stover, E.L., Hull, M., Kumsher-King, M., Gaudet-Hull, A.M., 1999. Phase III interlaboratory study of FETAX. Part 3. FETAX validation using 12 compounds with and without an exogenous metabolic activation system. J. Appl. Toxicol. 19, 447–472.

Battaglin, W.A., Rice, K.C., Focazio, M.J., Salmons, S., Barry, R.X., 2009. The occurrence of glyphosate, atrazine, and other pesticides in vernal pools and adjacent streams in Washington, DC, Maryland, Iowa, and Wyoming, 2005–2006. Environ. Monit. Assess. 155, 281–307. http://dx.doi.org/10.1007/s10661-008-0435-y.

Behra, M., Cousin, X., Bertrand, C., Vonesch, J.L., Biellmann, D., Chatonnet, A., Strähle, U., 2002. Acetylcholinesterase is required for neuronal and muscular development in the zebrafish embryo. Nat. Neurosci. 5 (2), 111–118. http://dx.doi.org/10.1038/nn788.

Benbrook, C., 2016. Trends in glyphosate herbicide use in the United States and globally. Environ. Sci. Eur. 28, 3. http://dx.doi.org/10.1186/s12302-016-0070-0.

Bonfanti, P., Colombo, A., Orsi, F., Nizzetto, I., Andrioletti, M., Bacchetta, R., Mantecca, P., Fascio, U., Vailati, G., Vismara, C., 2004. Comparative teratogenicity of Chlorpyrifos and Malathion on Xenopus laevis development. Aquat. Toxicol. 70, 189–200. http://dx.doi.org/10.1016/j.aquatox.2004.09.007.

Bonfanti, P., Moschini, E., Saibene, M., Bacchetta, R., Rettighieri, L., Calabri, L., Colombo, A., Mantecca, P., 2015. Do nanoparticle physico-chemical properties and developmental exposure window influence nano ZnO embryotoxicity in Xenopus laevis? Int. J. Environ. Res. Public Health 12, 8828–8848. http://dx.doi.org/10.3390/ijerph120808828.

Bonnet, J.L., Bonnemoy, F., Dusser, M., Bohatier, J., 2007. Assessment of the potential toxicity of herbicides and their degradation products to nontarget cells using two microorganisms, the bacteria Vibrio fischeri and the ciliate Tetrahymena pyriformis. Environ. Toxicol. 22 (1), 78–91.

Byer, J.D., Struger, J., Klawunn, P., Todd, A., Sverko, E., 2008. Low cost monitoring of glyphosate in surface waters using the ELISA method: an evaluation. Environ. Sci. Technol. 42, 6052–6057.

Cardellini, P., Ometto, L., 2001. Teratogenic and toxic effects of alcohol ethoxylate and alcohol ethoxy sulfate surfactants on Xenopus laevis embryos and tadpoles. Ecotoxicol. Environ. Saf. 48, 170–177. http://dx.doi.org/10.1006/eesa.2000.2005.

Cerdeira, A.L., Duke, S.O., 2006. The current status and environmental impacts of glyphosate-resistant crops: a review. J. Environ. Qual. 35 (5), 1633–1658. http://dx.doi.org/10.2134/jeq2005.0378.

Collins, J.P., 2010. Amphibian decline and extinction: what we know and what we need to learn. Dis. Aquat. Org. 92, 93–99. http://dx.doi.org/10.3354/dao02307.

Colombo, A., Orsi, F., Bonfanti, P., 2005. Exposure to the organophosphorus pesticide chlorpyrifos inhibits acetylcholinesterase activity and affects muscular integrity in Xenopus laevis larvae. Chemosphere 61 (11), 1665–1671.

Colombo, A., Saibene, M., Moschini, E., Bonfanti, P., Collini, M., Kasemets, K., Mantecca, P., 2017. Teratogenic hazard of BPEI-coated silver nanoparticles to Xenopus laevis. Nanotoxicology 11 (3), 405–418. http://dx.doi.org/10.1080/17435390.2017.1309703.

Dawson, D.A., Bantle, J.A., 1987. Development of a reconstituted water medium and preliminary validation of the frog embryo teratogenesis assay-Xenopus (FETAX). J. Appl. Toxicol. 7, 237–244.

Di Renzo, F., Bacchetta, R., Sangiorgio, L., Bizzo, A., Menegola, E., 2011. The agro-chemical fungicide triadimefon induces abnormalities in Xenopus laevis embryos. Reprod. Toxicol. 31, 486–493. http://dx.doi.org/10.1016/j.reprotox.2011.01.003.

Duke, S.O., Powles, S.B., 2008. Glyphosate: a once-in-a-century herbicide. Pest. Manag. Sci. 64, 319–325. http://dx.doi.org/10.1002/ps.1518.

EGEIS, 2009. EGEIS-European Glyphosate Environmental Information Sources which Summarized Surface and Groundwater Monitoring Data from 1993 to 2009. http://www.egeis.org/.

Edginton, A.N., Sheridan, P.M., Stephenson, G.R., Thompson, D.G., Boermans, H.J., 2004. Comparative effects of pH and Vision® herbicide on two life stages of four anuran amphibian species. Environ. Toxicol. Chem. 23 (4), 815–822.

Edwards, W.M., Triplett Jr., G.B., Kramer, R.M., 1980. A watershed study of glyphosate transport in runoff. J. Environ. Qual. 9, 661–665.

Finney, D.J., 1971. Statisical logic in the monitoring of reactions to therapeutic drugs. Methods Inf. Med. 10, 237–245.

Folmar, L.C., Sanders, H.O., Julin, A.M., 1979. Toxicity of the herbicide glyphosate and several of its formulations to fish and aquatic invertebrates. Arch. Environ. Contam. Toxicol. 8, 269–278.

Fort, D.J., Robbin, R.P., 2002. Enhancing the predictive validity of frog embryo teratogenesis assay – Xenopus (FETAX). J. Appl. Toxicol. 22, 185–191. http://dx.doi.org/10.1002/jat.848.

Fuentes, L., Moore, L.J., Rodgers, J.H., Bowerman, W.W., Yarrow, G.K., Chao, W.Y., 2011. Comparative toxicity of two glyphosate formulations (original formulation of Roundup® and Roundup Weathermax®) to six north american larval anurans. Environ. Toxicol. Chem. 30 (12), 2756–2761. http://dx.doi.org/10.1002/etc.670.

Güngördü, A., 2013. Comparative toxicity of methidathion and glyphosate on early life stages of three amphibian species: pelophylax ridibundus, Pseudepidalea viridis, and Xenopus laevis. Aquat. Toxicol. 140–141 (2013), 220–228. http://dx.doi.org/10.1016/j.aquatox.2013.06.012.

Gasnier, C., Dumont, C., Benachour, N., Clair, E., Chagnon, M.C., Séralini, G.E., 2009. Glyphosate-based herbicides are toxic and endocrine disruptors in human cell lines. Toxicology 262, 184–191.

Giesy, J.P., Dobson, S., Solomon, K.R., 2000. Ecotoxicological risk assessment for Roundup® herbicide. Rev. Environ. Contam. Toxicol. 167, 35–120.

Glusczak, L., Loro, V.L., Pretto, A., Moraes, B.S., Raabe, A., Duarte, M.F., da Fonseca, M.B., de Menezes, C.C., Valladao, D.M.D., 2011. Acute exposure to glyphosate herbicide affects oxidative parameters in Piava (Leporinus obtusidens). Arch. Environ. Contam. Toxicol. 61, 624–630. http://dx.doi.org/10.1007/s00244-011-9652-4.

Govindarajulu, P.P., 2008. Literature Review of Impacts of Glyphosate Herbicide on Amphibians: What Risks can the Silvicultural Use of This Herbicide Pose for Amphibians. Ph.D. Victoria B.C., Wildlife Report n. R-28. Ministry of Environment.

Hietanen, E., Linnainmaa, K., Vainio, H. l., 1983. Effects of phenoxyherbicides and glyphosate on the hepatic and intestinal biotransformation activities in the rat. Acta Pharmacol. Toxicol. 53 (2), 103–112.

Howe, C.M., Berrill, M., Pauli, B.D., Helbing, C.C., Werry, K., Veldhoen, N., 2004. Toxicity of glyphosate-based pesticides to four North American frog species. Environ. Toxicol. Chem. 23, 1928–1938.

Hued, A.C., Oberhofer, S., Bistoni, M.D., 2012. Exposure to a commercial glyphosate formulation (Roundup®) alters normal gill and liver histology and affects male sexual activity of Jenynsia multidentata (Anablepidae, Cyprinodontiformes). Arch. Environ. Contam. Toxicol. 62 (1), 107–117. http://dx.doi.org/10.1007/s00244-011-9686-7.

ISPRA, 2016. Rapporto Nazionale Pesticidi Nelle Acque. Dati 2013–2014. http://www.isprambiente.gov.it/files/pubblicazioni/rapporti/rapporto-244/Rapporto_244_2016.pdf.

Lajmanovich, R.C., Attademo, A.M., Peltzer, P.M., Celina, M.J., Cabagna, M.C., 2011. Toxicity of herbicide formulations with glyphosate on Rhinella arenarum (Anura: bufonidae) tadpoles: b-esterases and glutathione S-transferase inhibitors. Arch. Environ. Contam. Toxicol. 60, 681–689. http://dx.doi.org/10.1007/s00244-010-9578-2.

Mann, R.M., Bidwell, J.R., 1999. The toxicity of glyphosate and several glyphosate formulations to four species of southwestern australian frogs. Arch. Environ. Contam. Toxicol. 36, 193–199.

Mann, R.M., Bidwell, J.R., 2000. Application of the FETAX protocol to assess the developmental toxicity of nonylphenol ethoxylate to Xenopus laevis and two Australian frogs. Aquat. Toxicol. 51, 19–29.

Mann, R.M., Hyne, R.V., Choung, C.B., Wilson, S.P., 2009. Amphibians and agricultural chemicals: review of the risks in a complex environment. Environ. Pollut. 157, 2903–2927. http://dx.doi.org/10.1016/j.envpol.2009.05.015.

Menezes, C.C., Fonseca, M.B., Loro, V.L., Santi, A., Cattaneo, R., Clasen, B., Pretto, A., Morsch, V.M., 2011. Roundup effects on oxidative stress parameters and recovery pattern of Rhamdia quelen. Arch. Environ. Contam. Toxicol. 60, 665–671. http://dx.doi.org/10.1007/s00244-010-9574-6.

Modesto, K.A., Martinez, C.B., 2010. Roundup causes oxidative stress in liver and inhibits acetylcholinesterase in muscle and brain of the fish Prochilodus lineatus. Chemosphere 78, 294–299. http://dx.doi.org/10.1016/j.chemosphere.2009.10.047.

Nieuwkoop, P.D., Faber, J., 1956. Normal Table of Xenopus laevis (Daudin). North Holland Publishing Co., Amsterdam.

Pérez, G.L., Vera, M.S., Miranda, L.A., 2011. Effects of herbicide glyphosate and Glyphosate-Based formulations on aquatic ecosystems. In: Kortekamp, Andreas (Ed.), Herbicides and Environment, pp. 343–368. http://dx.doi.org/10.5772/12877.

Paganelli, A., Gnazzo, V., Acosta, H., Lopez, S.L., Carrasco, A.E., 2010. Glyphosate-based Herbicides produce teratogenic effects on vertebrates by impairing retinoic acid signaling. Chem. Res. Toxicol. 23, 1586–1595. http://dx.doi.org/10.1021/tx1001749.

Perkins, P.J., Boermans, H.J., Stephenson, G.R., 2000. Toxicity of glyphosate and triclopyr using the frog embryo teratogenesis assay – Xenopus. Environ. Toxicol. Chem. 19, 940–945.

Peruzzo, P.J., Porta, A.A., Ronco, A.E., 2008. Levels of glyphosate in surface waters, sediments and soils associated with direct sowing soybean cultivation in North Pampasic region of Argentina. Environ. Pollut. 156 (1), 61–66. http://dx.doi.org/10.1016/j.envpol.2008.01.015.

Poulsen, M.S., Rytting, E., Mose, T., Knudsen, L.E., 2009. Modeling placental transport: correlation of in vitro BeWo cell permeability and ex vivo human placental perfusion. Toxicol. In Vitro 23, 1380–1386. http://dx.doi.org/10.1016/j.tiv.2009.07.028.

Presutti, C., Vismara, C., Camatini, M., Bernardini, G., 1994. Ecotoxicological effects of a nonionic detergent (Triton DF-16) assayed by modFETAX. Bull. Environ. Contam. Toxicol. 53, 405–411.

Relyea, R.A., Jones, D.K., 2009. The toxicity of Roundup Original MAX® to 13 species of larval amphibians. Environ. Toxicol. Chem. 28, 2004–2008. http://dx.doi.org/10.1897/09-021.1.

Relyea, R.A., 2005. The lethal impact of Roundup on aquatic and terrestrial amphibians. Ecol. Appl. 15, 1118–1124.

Richard, S., Moslemi, S., Sipahutar, H., Benachour, N., Seralini, G.E., 2005. Differential effects of glyphosate and roundup on human placental cells and aromatase. Environ. Health Perspect. 113 (6), 716–720.

Roy, N.M., Carneiro, B., Ochs, J., 2016a. Glyphosate induces neurotoxicity in zebrafish. Environ. Toxicol. Pharmacol. 42 (45–54). http://dx.doi.org/10.1016/j.etap.2016.01.003.

Roy, N.M., Ochs, J., Zambrzycka, E., Anderson, A., 2016b. Glyphosate induces

cardiovascular toxicity in *Danio rerio*. Environ. Toxicol. Pharmacol. 46, 292–300. http://dx.doi.org/10.1016/j.etap.2016.08.010.

Rubin, J.L., Gaines, C.G., Jenson, R.A., 1982. Enzymological basis for herbicidal action of glyphosate. Plant Physiol. 70, 833–839.

Sandrini, J.Z., Rola, R.C., Lopes, F.M., Buffon, H.F., Freitas, M.M., Martins, C., de, M., da Rosa, C.E., 2013. Effects of glyphosate on cholinesterase activity of the mussel *Perna perna* and the fish *Danio rerio* and *Jenynsia multidentata*: in vitro studies. Aquat. Toxicol. 130–131, 171–173. http://dx.doi.org/10.1016/j.aquatox.2013.01.006.

Saunders, L.E., Pezeshki, R., 2015. Glyphosate in runoff waters and in the root-zone. Toxics 3, 462–480. http://dx.doi.org/10.3390/toxics3040462.

Struger, J., Thompson, D., Staznik, B., Martin, P., McDaniel, T., Marvin, C., 2008. Occurrence of glyphosate in surface waters of Southern Ontario. Bull. Environ. Contam. Toxicol. 80, 378–384. http://dx.doi.org/10.1007/s00128-008-9373-1.

Sulukan, E., Köktürk, M., Ceylan, H., Beydemir, Ş., Işik, M., Atamanalp, M., Ceyhun, S.B., 2017. An approach to clarify the effect mechanism of glyphosate on body malformations during embryonic development of zebrafish (*Daino rerio*). Chemosphere 180, 77–85. http://dx.doi.org/10.1016/j.chemosphere.2017.04.018.

Tsui, M.T., Chu, L.M., 2003. Aquatic toxicity of glyphosate based formulations: comparison between different organisms and the effects of environmental factors. Chemosphere 52, 1189–1197. http://dx.doi.org/10.1016/S0045-6535(03)00306-0.

Wagner, N., Reichenbecher, W., Teichmann, H., Tappeser, B., Lotters, S., 2013. Questions concerning the potential impact of glyphosate-based herbicides on amphibians. Environ. Toxicol. Chem. 32 (8), 1688–1700. http://dx.doi.org/10.1002/etc.2268.

Wagner, N., Müller, H., Viertel, B., 2016. Effects of a commonly used glyphosate-based herbicide formulation on early developmental stages of two anuran species. Environ. Sci. Pollut. Res. http://dx.doi.org/10.1007/s11356-016-7927-z.

Williams, B.K., Semlitsch, R.D., 2010. Larval responses of three midwestern anurans to chronic, low-dose exposures of four herbicides. Arch. Environ. Contam. Toxicol. 58, 819–827. http://dx.doi.org/10.1007/s00244-009-9390-z.

Williams, A.L., Watson, R.E., Desesso, J.M., 2012. Developmental and reproductive outcomes in humans and animals after glyphosate exposure: a critical analysis. J. Toxicol. Environ. Health B: Crit. Rev. 15, 39–96.

Williams, J.R., Rayburn, J.R., Cline, G.R., Sauterer, R., Friedman, M., 2015. Effect of allyl isothiocyanate on developmental toxicity in exposed *Xenopus laevis* embryos. Toxicol. Rep. 2, 222–227. http://dx.doi.org/10.1016/j.toxrep.2014.12.005.